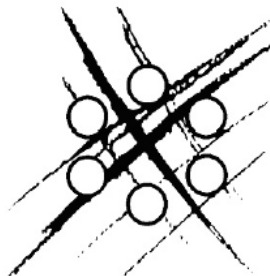


## USER DOCUMENTATION :

### Validation Report for TrioCFD v1.9.2



Code Version	Date	Code manager	Authors
v1.9.2	June 13, 2023	 F. BUFFA	TrioCFD Team
<b>DES/ISAS/DM2S CEA SACLAY 91191 GIF-SUR-YVETTE CEDEX</b>		<i>Input file : validation_report_TrioCFD.tex</i> <i>Software : TrioCFD</i>	
		DES/ISAS/DM2S/STMF/LMSF/UD	

## Contents

<b>Contents</b>	<b>2</b>
<b>List of Figures</b>	<b>8</b>
<b>List of Tables</b>	<b>12</b>
<b>I Introduction</b>	<b>13</b>
<b>II Methodology for building the validation report</b>	<b>15</b>
<b>1 Introduction</b>	<b>16</b>
1.1 Inventory and sort . . . . .	16
1.2 Development of a new PRM template . . . . .	17
1.3 Running with v1.9.2 and L <sup>A</sup> T <sub>E</sub> X files . . . . .	17
<b>2 Overview of new PRM template</b>	<b>17</b>
2.1 Old PRM syntax . . . . .	18
2.2 New PRM syntax . . . . .	19
General improvements . . . . .	19
Modification of Python script . . . . .	20
<b>3 L<sup>A</sup>T<sub>E</sub>X files and report generation</b>	<b>23</b>
3.1 L <sup>A</sup> T <sub>E</sub> X files . . . . .	23
3.2 New shell script for gathering all .tex files . . . . .	24
3.3 Enhancement . . . . .	24
<b>III Laminar Flow</b>	<b>24</b>
<b>1 Poiseuille flow 2D with VDF and VEF meshes</b>	<b>26</b>
1.1 Purpose . . . . .	26
1.2 Problem Description . . . . .	26
Geometry . . . . .	26
Initial Conditions and Boundary Conditions . . . . .	27
Fluid Properties . . . . .	27
Flow Physics . . . . .	27
1.3 Case Setup . . . . .	27
Grid . . . . .	27
Model Options . . . . .	28
Other Options (calculation) . . . . .	28
1.4 Results . . . . .	28
Validation Specific Informations . . . . .	28

---

Plot Data . . . . .	29
1.5 Conclusion . . . . .	30
1.6 Data Files . . . . .	30
test . . . . .	30
<b>2 2D Lid driven cavity test</b>	<b>32</b>
2.1 Purpose . . . . .	32
2.2 Problem Description . . . . .	32
Geometry . . . . .	32
Initial Conditions and Boundary Conditions . . . . .	32
Fluid Properties . . . . .	32
Flow Physics . . . . .	32
2.3 Case Setup . . . . .	32
Grid . . . . .	32
Other Options (calculation) . . . . .	33
2.4 Results . . . . .	34
Validation Specific Informations . . . . .	34
Plot Data . . . . .	34
2.5 Conclusion . . . . .	36
2.6 References . . . . .	36
2.7 Data Files . . . . .	36
defilante . . . . .	36
<b>3 Cylinder in Laminar Cross Flow</b>	<b>39</b>
3.1 Purpose . . . . .	39
3.2 Problem Description . . . . .	39
Geometry . . . . .	39
Initial Conditions and Boundary Conditions . . . . .	39
Fluid Properties . . . . .	40
Flow Physics . . . . .	40
3.3 Case Setup . . . . .	40
Grid . . . . .	40
Model Options . . . . .	41
Other Options (calculation) . . . . .	41
3.4 Results . . . . .	41
Validation Specific Informations . . . . .	41
Plot Data . . . . .	42
3.5 Conclusion . . . . .	46
3.6 References . . . . .	46
3.7 Data Files . . . . .	47
test . . . . .	47
<b>IV Thermal Laminar Flow</b>	<b>48</b>
<b>1 Convection Vahl Davis</b>	<b>50</b>
1.1 Purpose . . . . .	50
1.2 Problem Description . . . . .	50
Geometry . . . . .	50
Initial Conditions and Boundary Conditions . . . . .	50
Fluid Properties . . . . .	50
Flow Physics . . . . .	51
1.3 Case Setup . . . . .	51
Grid . . . . .	51
Model Options . . . . .	52
Other Options (calculation) . . . . .	53

---

1.4	Results . . . . .	53
	Validation Specific Informations . . . . .	53
	Plot Data . . . . .	54
1.5	Conclusion . . . . .	59
1.6	References . . . . .	59
1.7	Data Files . . . . .	60
	test . . . . .	60
<b>2</b>	<b>Oscillatory convection flow</b>	<b>63</b>
2.1	Purpose . . . . .	63
2.2	Problem Description . . . . .	63
	Geometry . . . . .	63
	Initial Conditions and Boundary Conditions . . . . .	63
	Fluid Properties . . . . .	64
	Flow Physics . . . . .	64
2.3	Case Setup . . . . .	64
	Grid . . . . .	64
	Model Options . . . . .	65
	Other Options (calculation) . . . . .	65
2.4	Results . . . . .	65
	Validation Specific Informations . . . . .	65
	Plot Data . . . . .	66
2.5	Conclusion . . . . .	69
2.6	References . . . . .	69
2.7	Data Files . . . . .	69
	test . . . . .	69
<b>V</b>	<b>Turbulent Flow</b>	<b>71</b>
<b>1</b>	<b>Turbulent flow in a 2D diffuser with the <math>k - \epsilon</math> model</b>	<b>73</b>
1.1	Purpose . . . . .	73
1.2	Problem Description . . . . .	73
	Geometry . . . . .	73
	Initial Conditions and Boundary Conditions . . . . .	74
	Fluid Properties . . . . .	74
	Flow Physics . . . . .	74
1.3	Case Setup . . . . .	74
	Grid . . . . .	74
	Model Options . . . . .	75
	Other Options (calculation) . . . . .	75
1.4	Results . . . . .	75
	Validation Specific Informations . . . . .	75
	Plot Data . . . . .	76
1.5	Conclusion . . . . .	82
1.6	References . . . . .	82
1.7	Data Files . . . . .	83
	Calcul . . . . .	83
<b>2</b>	<b>Mixing length in 2D and 3D VEF-plane channel</b>	<b>86</b>
2.1	Purpose . . . . .	86
2.2	Problem Description . . . . .	86
	Geometry . . . . .	86
	Initial Conditions and Boundary Conditions . . . . .	86
	Fluid Properties . . . . .	86
2.3	Case Setup . . . . .	86

---

Grid . . . . .	86
Model Options . . . . .	89
Other Options (calculation) . . . . .	89
2.4 Results . . . . .	89
Validation Specific Informations . . . . .	89
Plot Data . . . . .	91
2.5 Conclusion . . . . .	98
2.6 References . . . . .	98
2.7 Data Files . . . . .	98
2D . . . . .	98
3D . . . . .	100
3D_keps . . . . .	102
<b>VI Thermal Turbulent Flow</b>	<b>104</b>
1 <b>Turbulent flow inside a double-periodic plane channel with heated walls</b>	<b>106</b>
1.1 Purpose . . . . .	106
1.2 Problem Description . . . . .	106
Geometry . . . . .	106
Initial Conditions and Boundary Conditions . . . . .	106
Fluid Properties . . . . .	107
Flow Physics . . . . .	107
1.3 Case Setup . . . . .	107
Grid . . . . .	107
Model Options . . . . .	108
Other Options (calculation) . . . . .	108
1.4 Results . . . . .	108
Validation Specific Informations . . . . .	108
Plot Data . . . . .	109
1.5 Conclusion . . . . .	113
1.6 References . . . . .	113
1.7 Data Files . . . . .	113
Canal_plan_bi_periodique_M1 . . . . .	113
<b>VII Two-phase Flows with Front-Tracking</b>	<b>116</b>
1 <b>Oscillation of a bubble</b>	<b>118</b>
1.1 Purpose . . . . .	118
1.2 Problem Description . . . . .	118
Geometry . . . . .	119
Initial Conditions and Boundary Conditions . . . . .	120
Fluid Properties . . . . .	120
1.3 Case Setup . . . . .	121
Grid . . . . .	121
Model Options . . . . .	121
Other Options (calculation) . . . . .	122
1.4 Results . . . . .	122
Validation Specific Informations . . . . .	122
Plot Data . . . . .	123
1.5 Conclusion . . . . .	131
1.6 References . . . . .	131
1.7 Data Files . . . . .	131
FTD_Oscillation_Bulle_3D_VDF . . . . .	131
FTD_Oscillation_Bulle_3D_VDF . . . . .	134

---

<b>2 Drop hanged at the ceiling</b>	<b>138</b>
2.1 Purpose . . . . .	138
2.2 Problem Description . . . . .	138
Geometry . . . . .	141
Initial Conditions and Boundary Conditions . . . . .	141
Fluid Properties . . . . .	141
2.3 Case Setup . . . . .	141
Grid . . . . .	141
Model Options . . . . .	141
2.4 Results . . . . .	142
Validation Specific Informations . . . . .	142
Plot Data . . . . .	142
2.5 Conclusion . . . . .	158
2.6 Data Files . . . . .	159
goutte . . . . .	159
goutte . . . . .	161
 <b>VIII Fluid-structure interactions with ALE</b>	 <b>164</b>
<b>1 Single-phase flow around a vibrating cylindrical tube</b>	<b>166</b>
1.1 Purpose . . . . .	166
1.2 Problem Description . . . . .	166
Geometry . . . . .	166
Initial Conditions and Boundary Conditions . . . . .	167
Fluid Properties . . . . .	167
1.3 Case Setup . . . . .	167
Grid . . . . .	167
Model Options . . . . .	168
1.4 Results . . . . .	168
Validation Specific Informations . . . . .	168
Plot Data . . . . .	168
1.5 Conclusion . . . . .	172
1.6 References . . . . .	172
1.7 Data Files . . . . .	172
TwoCylinders . . . . .	172
 <b>2 Hydrodynamic interaction of two cylinders subjected to small oscillations</b>	 <b>175</b>
2.1 Purpose . . . . .	175
2.2 Problem Description . . . . .	175
Geometry . . . . .	175
Initial Conditions and Boundary Conditions . . . . .	176
Fluid Properties . . . . .	176
2.3 Case Setup . . . . .	176
Grid . . . . .	176
Model Options . . . . .	176
2.4 Results . . . . .	176
Validation Specific Informations . . . . .	176
Plot Data . . . . .	177
2.5 Conclusion . . . . .	181
2.6 References . . . . .	181
2.7 Data Files . . . . .	182
TwoOscillatingCylinders . . . . .	182
 <b>3 Vibrations of a cylinder in a square tube bundle immersed in a viscous fluid</b>	 <b>184</b>
3.1 Purpose . . . . .	184

3.2	Problem Description . . . . .	184
	Geometry . . . . .	185
	Initial Conditions and Boundary Conditions . . . . .	185
	Fluid Properties . . . . .	185
3.3	Case Setup . . . . .	185
	Grid . . . . .	186
	Model Options . . . . .	188
3.4	Results . . . . .	188
	Validation Specific Informations . . . . .	188
	Plot Data . . . . .	189
3.5	Conclusion . . . . .	196
3.6	References . . . . .	196
3.7	Data Files . . . . .	196
	DIVA . . . . .	196
<b>IX</b>	<b>Conclusion</b>	<b>198</b>
<b>Annexe A:</b>	<b>List of TrioCFD PRM files</b>	<b>200</b>

## List of Figures

II.2.1	Original PRM syntax version - Parameters part . . . . .	18
II.2.2	Original PRM syntax version - Generated introduction . . . . .	18
II.2.3	Original PRM syntax version - Chapter part . . . . .	19
II.2.4	Original PRM syntax version - Generated chapter . . . . .	19
III.1.1	Geometry: Dimensions and domain overview . . . . .	26
III.1.2	VDF Mesh . . . . .	27
III.1.3	VEF Mesh . . . . .	28
III.1.4	Transverse velocity profile . . . . .	29
III.2.1	MESH . . . . .	33
III.2.2	VITESSE_X SOM . . . . .	33
III.2.3	Evolution of residue . . . . .	34
III.2.4	Velocity along line $x=0.5$ . . . . .	35
III.2.5	Velocity along line $y=0.5$ . . . . .	35
III.3.1	Geometry . . . . .	39
III.3.2	Mesh overview . . . . .	40
III.3.3	Zoom of the vicinity of the cylinder . . . . .	41
III.3.4	Pressure fields at $t = 90s$ . . . . .	42
III.3.5	Velocity vectors at $t = 90s$ . . . . .	43
III.3.6	Pressure course at the cylinder surface at $y = \pm 0.5d$ with a Muscl convection scheme . . . . .	43
III.3.7	Pressure course at the cylinder surface at $y = \pm 0.5d$ with an EF_stab ( $\alpha = 0.2$ ) convection scheme . . . . .	44
III.3.8	Zoom of the pressure evolution at the cylinder surface (Muscl) . . . . .	44
III.3.9	Zoom of the pressure evolution at the cylinder surface (EF_stab with alpha = 0.2) . . . . .	45
III.3.10	Comparison of the mean pressure distribution along the cylinder surface with different convection and time schemes . . . . .	46
IV.1.1	2D VDF Mesh . . . . .	51
IV.1.2	2D coarse VEF Mesh . . . . .	52
IV.1.3	2D fine VEF Mesh . . . . .	52
IV.1.4	Temperature evolution of two points inside the domain . . . . .	54
IV.1.5	Temperature and velocity fields at steady state (refine mesh) . . . . .	55
IV.1.6	Comparison of convection schemes for the Temperature ( $y = 0.5$ ) . . . . .	55
IV.1.7	Comparison of convection schemes for the Temperature ( $x = 0.5$ ) . . . . .	56
IV.1.8	Comparison of convection schemes for the velocity v ( $y = 0.5$ ) . . . . .	56
IV.1.9	Comparison of convection schemes for the velocity u ( $x = 0.5$ ) . . . . .	56
IV.1.10	Comparison of the probe types for an EF_stab convection scheme in the VEF case (velocities at $y = 0.5$ ) . . . . .	57
IV.1.11	Comparison of the probe types for an EF_stab convection scheme in the VEF case (velocities at $x = 0.5$ ) . . . . .	57
IV.2.1	Dimensions of the domain and boundary conditions for temperature equation. . . . .	63
IV.2.2	VDF Mesh . . . . .	65

*LIST OF FIGURES*

---

IV.2.3	VEF Mesh . . . . .	65
IV.2.4	Velocity vectors at t = 800s for VEF mesh (Muscl) . . . . .	67
IV.2.5	y-component of the velocity along the x-axis at y = 0.5m, and t = 800s . . . . .	67
IV.2.6	Temperature profile along x axis: y = 0.5m . . . . .	68
IV.2.7	Time evolution of the velocity (Muscl scheme) . . . . .	68
V.1.1	Diffuser geometry . . . . .	73
V.1.2	Periodic box: mesh 1 (1104 cells) . . . . .	74
V.1.3	Periodic box: mesh 2 (440 cells) . . . . .	75
V.1.4	Diffuser Mesh (36644 cells) . . . . .	75
V.1.5	Mesh 1 computations convergence: friction velocity evolution . . . . .	77
V.1.6	Mesh 2 computations convergence: friction velocity evolution . . . . .	77
V.1.7	Pressure field in the diffuser, Legend . . . . .	78
V.1.8	Pressure field in the diffuser, mesh1. . . . .	78
V.1.9	Pressure field in the diffuser, mesh2. . . . .	78
V.1.10	Velocity field in the diffuser, Legend. . . . .	78
V.1.11	Velocity field in the diffuser, mesh 1. . . . .	79
V.1.12	Velocity field in the diffuser, mesh 2. . . . .	79
V.1.13	Y+ field in the diffuser, Legend. . . . .	79
V.1.14	Y+ field in the diffuser, mesh1. . . . .	79
V.1.15	Y+ field in the diffuser, mesh2. . . . .	79
V.1.16	Longitudinal velocity profile at x=6 . . . . .	80
V.1.17	Longitudinal velocity profile at x=17 . . . . .	80
V.1.18	Longitudinal velocity profile at x=20 . . . . .	81
V.1.19	Longitudinal velocity profile at x=27 . . . . .	81
V.1.20	Longitudinal velocity profile at x=34 . . . . .	82
V.2.1	3 x 6 in 2D geometry . . . . .	87
V.2.2	3 x 41 in 2D geometry . . . . .	87
V.2.3	3 x 6 x 3 in 3D geometry . . . . .	88
V.2.4	3 x 41 x 6 in 3D geometry . . . . .	89
V.2.5	Velocity profile . . . . .	92
V.2.6	Velocity profile U+ . . . . .	92
V.2.7	Turbulent viscosity . . . . .	92
V.2.8	Velocity profile . . . . .	93
V.2.9	Velocity profile U+ . . . . .	94
V.2.10	Turbulent viscosity . . . . .	94
V.2.11	Velocity profile . . . . .	95
V.2.12	Velocity profile U+ . . . . .	96
V.2.13	Turbulent viscosity . . . . .	96
V.2.14	Velocity profile comparison with keps . . . . .	97
V.2.15	Velocity profile U+ comparison with keps . . . . .	97
V.2.16	Turbulent viscosity comparison with keps . . . . .	98
VI.1.1	Geometry . . . . .	106
VI.1.2	Mesh M1 . . . . .	107
VI.1.3	Mesh M1_tetraedrise . . . . .	108
VI.1.4	Mean axial velocity profiles for different stretch factors . . . . .	110
VI.1.5	Comparison with mesh M1_tetraedrise . . . . .	110
VI.1.6	Explanations of M1 result : contribution of transverse velocity . . . . .	110
VI.1.7	Deviations of transverse velocity V . . . . .	111
VI.1.8	Deviations of transverse velocity W . . . . .	111
VI.1.9	Mean temperature profiles for different stretch factors . . . . .	112
VI.1.10	Comparison with mesh M1_tetraedrise . . . . .	112
VII.1.1	Geometry . . . . .	120

## LIST OF FIGURES

---

VII.1.2	Illustration of the Eulerien and Lagrangien mesh for 61x61x61 hexaedra . . . . .	121
VII.1.3	Cas_01 : M2 : Bubble in a square box : oscillations of the interface . . . . .	121
VII.1.4	Interfacial area between air and water . . . . .	123
VII.1.5	Interfacial area between air and water . . . . .	123
VII.1.6	Interfacial area between air and water . . . . .	124
VII.1.7	Interfacial area between air and water- comparaison of case 1 and case 2 . . . . .	124
VII.1.8	Mesh convergence : frequency error and time calculation - This curve is not updated when we regenerate the validation sheet . . . . .	125
VII.1.9	Pressure difference between the inner and outer fluid . . . . .	125
VII.1.10	Pressure difference between the inner and outer fluid - comparaison of case 1 and case 2 . . . . .	126
VII.1.11	Damping of oscillation with different numirical schemes - This curve is not updated when we regenerate the validation sheet . . . . .	127
VII.1.12	Damping of oscillation with different numirical shemes after reduction of remeshing - This curve is not updated when we regenerate the validation sheet . . . . .	127
VII.1.13	Comparison of the results given by the two temporal schemes Euler and Runge Kutta 3 - This curve is not updated when we regenerate the validation sheet . . . . .	128
VII.1.14	Limit Time step for stability at the interface - This curve is not updated when we regenerate the validation sheet . . . . .	129
VII.1.15	Limit Time step for stability at the interface - This curve is not updated when we regenerate the validation sheet . . . . .	129
VII.1.16	Initial interface . . . . .	130
VII.1.17	Bubble interface at t=0.002s . . . . .	130
VII.1.18	Bubble interface at t=0.004s . . . . .	130
VII.1.19	Bubble interface at t=0.006s . . . . .	130
VII.1.20	Bubble interface at t=0.008s . . . . .	130
VII.1.21	Bubble interface at t=0.01s . . . . .	130
VII.1.22	Bubble interface at t=0.012s . . . . .	131
VII.1.23	Bubble interface at t=0.014s . . . . .	131
VII.2.1	Profiles of the drop : theoretical data for different amount of water and a contact angle between the tangential curve at the drop close to the wall of 1 radian. . . . .	139
VII.2.2	Profiles of the drop : theoretical data for different amount of water and a contact angle between the tangential curve at the drop close to the wall of 1.5 radian. . . . .	139
VII.2.3	Profiles of the drop : theoretical data for different amount of water and a contact angle between the tangential curve at the drop close to the wall of 2 radian. . . . .	140
VII.2.4	Profiles of the drop : theoretical data for different amount of water and a contact angle between the tangential curve at the drop close to the wall of 2.5 radian. . . . .	140
VII.2.5	Profiles of the drop : theoretical data for different amount of water and a contact angle between the tangential curve at the drop close to the wall of 3 radian. . . . .	140
VII.2.6	Drop hanged at the top of the box with a contact angle of 1.5 radian - t=0s . . . . .	143
VII.2.7	Drop hanged at the top of the box with a contact angle of 1.5 radian - t=0.01s . . . . .	143
VII.2.8	Drop hanged at the top of the box with a contact angle of 1.5 radian - t=0.05s . . . . .	144
VII.2.9	Drop hanged at the top of the box with a contact angle of 1.5 radian - t=0.1s . . . . .	144
VII.2.10	Drop hanged at the top of the box with a contact angle of 1.5 radian - t=0.15s . . . . .	145
VII.2.11	Drop hanged at the top of the box with a contact angle of 1.5 radian - t=0.2s . . . . .	145
VII.2.12	Drop hanged at the top of the box with a contact angle of 1.5 radian - t=0.35s . . . . .	146
VII.2.13	Drop hanged at the top of the box with a contact angle of 1.5 radian - t=0.5s . . . . .	146
VII.2.14	Drop hanged at the top of the box with a contact angle of 1.5 radian - t=0.75s . . . . .	147
VII.2.15	Drop hanged at the top of the box with a contact angle of 1.5 radian - t=1s . . . . .	147
VII.2.16	Drop hanged at the top of the box with a contact angle of 1.5 radian - t=1.5s . . . . .	148
VII.2.17	Drop hanged at the top of the box with a contact angle of 1.5 radian - t=2s . . . . .	148
VII.2.18	Drop hanged at the top of the box with a contact angle of 1.5 radian - t=2.5s . . . . .	149
VII.2.19	Drop hanged at the top of the box with a contact angle of 1.5 radian - t=3s . . . . .	149
VII.2.20	Profils 1.5 radians . . . . .	150
VII.2.21	Drop hanged at the top of the box with a contact angle of 2.5 radian - t=0s . . . . .	151
VII.2.22	Drop hanged at the top of the box with a contact angle of 2.5 radian - t=0.01s . . . . .	151

---

*LIST OF FIGURES*

---

VII.2.23 Drop hanged at the top of the box with a contact angle of 2.5 radian - t=0.05s . . . . .	152
VII.2.24 Drop hanged at the top of the box with a contact angle of 2.5 radian - t=0.1s . . . . .	152
VII.2.25 Drop hanged at the top of the box with a contact angle of 2.5 radian - t=0.15s . . . . .	153
VII.2.26 Drop hanged at the top of the box with a contact angle of 2.5 radian - t=0.2s . . . . .	153
VII.2.27 Drop hanged at the top of the box with a contact angle of 2.5 radian - t=0.35s . . . . .	154
VII.2.28 Drop hanged at the top of the box with a contact angle of 2.5 radian - t=0.5s . . . . .	154
VII.2.29 Drop hanged at the top of the box with a contact angle of 2.5 radian - t=0.75s . . . . .	155
VII.2.30 Drop hanged at the top of the box with a contact angle of 2.5 radian - t=1s . . . . .	155
VII.2.31 Drop hanged at the top of the box with a contact angle of 2.5 radian - t=1.25s . . . . .	156
VII.2.32 Drop hanged at the top of the box with a contact angle of 2.5 radian - t=1.5s . . . . .	156
VII.2.33 Drop hanged at the top of the box with a contact angle of 2.5 radian - t=1.75s . . . . .	157
VII.2.34 Drop hanged at the top of the box with a contact angle of 2.5 radian - t=2s . . . . .	157
VII.2.35 Profils 2.5 radians . . . . .	158
VIII.1.1 The domain . . . . .	166
VIII.1.2 Mesh . . . . .	167
VIII.1.3 Force per unit length of cylinder . . . . .	169
VIII.1.4 TrioCFD PRESSION SOM . . . . .	170
VIII.1.5 TrioCFD VITESSE_magnitude SOM . . . . .	171
VIII.1.6 TrioCFD Mesh velocity SOM . . . . .	171
VIII.1.7 TrioCFD Total displacement of the mesh SOM . . . . .	172
VIII.2.1 The domain . . . . .	175
VIII.2.2 Force per unit length of cylinder . . . . .	177
VIII.2.3 TrioCFD PRESSION SOM . . . . .	179
VIII.2.4 TrioCFD VITESSE_magnitude SOM . . . . .	180
VIII.2.5 TrioCFD Mesh velocity SOM . . . . .	181
VIII.3.1 DIVA geometry . . . . .	185
VIII.3.2 Mesh_1 . . . . .	186
VIII.3.3 Mesh_2 . . . . .	187
VIII.3.4 Mesh_3 . . . . .	187
VIII.3.5 Force per unit length of cylinder . . . . .	189
VIII.3.6 TrioCFD Mesh_1 PRESSION SOM . . . . .	193
VIII.3.7 TrioCFD Mesh_1 VITESSE_magnitude SOM . . . . .	193
VIII.3.8 TrioCFD Mesh_2 PRESSION SOM . . . . .	194
VIII.3.9 TrioCFD Mesh_2 VITESSE_magnitude SOM . . . . .	194
VIII.3.10 TrioCFD Mesh_3 PRESSION SOM . . . . .	195
VIII.3.11 TrioCFD Mesh_3 VITESSE_magnitude SOM . . . . .	195

---

## List of Tables

I.0.1	Type of flow investigated to each Part.	15
II.1.1	List of folders of <b>TrioCFD</b> test cases.	16
II.1.2	Computer characteristics for running the test cases database.	17
II.2.1	New blocks of instructions in PRM file: content (left) and corresponding keywords (right) in English or French.	20
II.2.2	Keywords that can be used in block <b>Parameters</b> for PRM files.	21
II.2.3	List of keywords for the <b>Problem description</b> block.	22
II.2.4	List of keywords for the <b>Case Setup</b> block.	22
II.3.1	<b>LATEX</b> files of this report.	23
III.1.1	Physical properties	27
III.1.2	Performance Chart	29
III.2.1	Performance Chart	34
III.2.2	CPU informations for new and reference solutions	36
III.3.1	Physical properties of the fictitious fluid	40
III.3.2	Performance Chart	42
III.3.3	Comparison of Strouhal numbers	45
IV.1.1	Physical properties	51
IV.1.2	Performance Chart	54
IV.1.3	Summary of values from literature	57
IV.1.4	Results for $\text{Max}(u^*)$	58
IV.1.5	Results for $\text{Max}(v^*)$	58
IV.1.6	Relative errors for $\text{Max}(u^*)$ : $\text{ERR}[\text{Max}(v^*)]$ in %	59
IV.1.7	Relative errors for $\text{Max}(v^*)$ : $\text{ERR}[\text{Max}(v^*)]$ in %	59
IV.2.1	Physical properties	64
IV.2.2	Performance Chart	66
IV.2.3	Oscillation frequency	68
V.1.1	Physical properties	74
V.1.2	Performance Chart	76
V.2.1	Performance Chart	91
V.2.2	2D - $Re_b = 10000$	91
V.2.3	2D - $Re_b = 10^5$	93
V.2.4	3D - $Re_b = 100\ 000$	95
VI.1.1	Performance Chart	109
VI.1.2	Nusselt Calculation	113

VII.1.1	Analytic values for validation . . . . .	119
VII.1.2	Physical parameters of fluids . . . . .	120
VII.1.3	Performance Chart . . . . .	122
VII.2.1	Performance Chart . . . . .	142
VIII.1.1	Meshes properties . . . . .	168
VIII.1.2	Performance Chart . . . . .	168
VIII.1.3	Added mass and damping coefficients . . . . .	170
VIII.2.1	Performance Chart . . . . .	177
VIII.2.2	Added mass and damping coefficients . . . . .	179
VIII.3.1	Meshes properties . . . . .	188
VIII.3.2	Performance Chart . . . . .	189
VIII.3.3	Added mass coefficients for the Center cylinder . . . . .	190
VIII.3.4	Added damping coefficients for the Center cylinder . . . . .	190
VIII.3.5	Added mass coefficients for the Nord cylinder . . . . .	190
VIII.3.6	Added damping coefficients for the Nord cylinder . . . . .	191
VIII.3.7	Added mass coefficients for the Sud cylinder . . . . .	191
VIII.3.8	Added damping coefficients for the Sud cylinder . . . . .	191
VIII.3.9	Added mass coefficients for the Est cylinder . . . . .	191
VIII.3.10	Added damping coefficients for the Est cylinder . . . . .	192
VIII.3.11	Added mass coefficients for the West cylinder . . . . .	192
VIII.3.12	Added damping coefficients for the West cylinder . . . . .	192

# I. Introduction

THE TrioCFD database contains currently around 160 test cases of validation which are called in this document “validation sheets”. The present report is the result of an inventory work of the most important of these validation sheets to know (non exhaustive list): What type of flow do they simulate? What is the degree of maturity of each validation? What sort of comparison do they exhibit? and so on ...

This validation report has several objectives:

- Help users to identify application areas of TrioCFD code;
- Give users examples of modeling (TrioCFD keywords and boundary conditions) on specific cases;
- Inform users of changes/improvements on the code validation;
- Make an inventory of the code validation for each delivered version;
- Account for physical and/or numerical impacts observed resulting from implementation, corrections or modifications of test cases that have been made between each version;
- Update the validation status of the code.

In previous versions of TrioCFD, each validation sheet has been written by different authors who used their own approach. In order to improve the readability of this report, the content of all these validation sheets has been harmonized by using identical titles and same general organization. For this purpose, a new PRM template has been updated since TrioCFD v1.8.2. The update has required modifying the Python script and revising all PRM files with the same content. More precisely, new tags have been added and new keywords must be used by authors when writing the PRM file. Details about this new PRM template and keywords are presented in Part II. This new template will be helpful for future versions of this document when a specific study using TrioCFD will lead to write a new PRM sheet or to update an old one. The Part II will also describe the methodology for making this report.

Moreover, until now, all validation sheets were placed in various folders of the TrioCFD package. Hence, some of them could not be found quickly by users who had to browse all directories. This report gathers in one single document some of these sheets classified according the type of flow or physics investigated. The selected test cases are representative of five subdomains summarized in Table I.0.1 and successively presented for flows of increasing complexity: “Laminar flow” (Part III), “Thermal laminar flow” (Part IV), “Turbulent flow” (Part V), “Thermal turbulent flow” (Part VI), “Front Tracking” (Part VII) and “Arbitrary Lagrangian-Eulerian Method” (Part VIII). The first four parts gather the test cases for single phase flow, coupled or not with turbulence and thermal modeling. The last part is dedicated to two-phase flows with interface tracking. Finally Part IX concludes this report and perspectives will be sketched.

---

Parts	Type of flows
Part III	Laminar Flow
Part IV	Thermal Laminar Flow
Part V	Turbulent Flow
Part VI	Thermal Turbulent Flow
Part VII	Two-phase Flows with Front Tracking
Part VIII	ALE method for fluid/structure interactions

---

Table I.0.1: Type of flow investigated to each Part.

The sheets appearing in those parts are selected because they separately simulate a particular flow well-known in the CFD literature, such as the “*Poiseuille flow*” and “*lid-driven cavity flow*” which are two examples of “Laminar Flows”. For “Thermal Laminar Flows” the “*Vahl Davis convection flow*” is a standard test case. Other sheets were selected because they compare **TrioCFD** with other CFD results using alternative academic or commercial codes (e.g. **Fluent** or other benchmarks) such as “*OBI diffuser*” (Turbulent flow). When available and representative of flows, experimental data measured on facility tests were included for comparisons and appear on the graphs (e.g. “*Thermal stratification flow in a plenum*”). The number of tests presented in this report will be gradually increased at each new version release of **TrioCFD**. For example, the eighth part which concerns the modeling of the fluid/structure interactions with the ALE method has been added since the last delivery

## II. Methodology for building the validation report

### II.1

#### Introduction

**I**N this chapter, the three-stage methodology to build this report is developed as following: 1) inventory and sort of the TrioCFD database ; 2) development of a new PRM template ; 3) running the v1.9.2 of TrioCFD and description of L<sup>A</sup>T<sub>E</sub>X files. In this first section we present a summary of those three stages before giving accurate instructions and commands in next sections.

#### 1.1 Inventory and sort

Currently, the TrioCFD database contains 198 validation reports archived in different folders (see Table II.1.1). First, an important inventory work was carried out to sort the test cases for targeting quickly the use of TrioCFD in different CFD configurations. The inventory resulted in a single table with plenty information (LibreOffice format), where the test cases are classified into several subdomains of fluid flows. In this document, some of them have been selected and detailed because 1) they are well-known in the literature, 2) they present comparisons with other academic or commercial CFD codes and 3) they present comparisons with experimental data.

Validation reports for a given TrioCFD module are located in  
`./share/Validation/Rapports_automatiques/{nameOfTheModule}` as shown in the table below.

Module folder in <code>./share/Validation/Rapports_automatiques</code>	Comments
<code>Criterie_Entrainement_Gaz</code>	Gaz Entrainement
<code>Fluid_Structure_Interaction</code>	ALE method
<code>Multiphase/CMFD</code>	reports for Two phase mixing
<code>Multiphase/Front_tracking_discontinu</code>	reports for Front-tracking module
<code>Multiphase/Front_tracking_IJK</code>	reports for Front-tracking IJK module
<code>P1NCPORT</code>	P1NCPORT module
<code>Rayonnement</code>	Radiation
<code>Schema_Euler_Implicite_Stationnaire</code>	Steady state implicit Euler scheme
<code>Sensitivity_analysis</code>	Sensitivity analysis for NS
<code>Turbulence</code>	Turbulence models (LES and RANS)
<code>validation</code>	Files validating several modules

Table II.1.1: List of folders of TrioCFD test cases.

Some of them can run only with TRUST (laminar and thermal laminar problems) but the choice was made to keep them in TrioCFD. They are grouped here in accordance with the themes structuring this present validation report (Laminar Flow, Thermal Laminar Flow,...) In addition the summary table of all these validation sheets is present in the appendix **Annexe A: List of TrioCFD PRM files** of this report.

## 1.2 Development of a new PRM template

For each datafile of test cases, the PDF file is generated by running a bash script (command `Run_fiche`) which acts on a PRM file. A PRM file is a set of specific instructions for interfacing the L<sup>A</sup>T<sub>E</sub>X commands with the TrioCFD results post-processed with `Gnuplot` or `Visit`. As its content differs following the test cases, the generated PDF reports may be structured differently, making them hard to read and to understand. Consequently, a new PRM template has been implemented in the present report to harmonize their content for a more homogeneous rendering. Differences between the old and new versions of the PRM template are detailed in Section 2.2. All validation sheets of this report have been revised and enhanced by taking into account the new PRM template.

## 1.3 Running with v1.9.2 and L<sup>A</sup>T<sub>E</sub>X files

All validation test case datafiles have been run with the version 1.9.2 of TrioCFD for checking the achievement of computations. The validation database has been launched on *URUK* and *PEGASI2*. The characteristics of these computers are given in Table II.1.2.

For each validation sheet, the full documentation is automatically generated via the `Run_fiche` procedure. Finally, all selected sheets are gathered in one single document. Precisions will be given on the L<sup>A</sup>T<sub>E</sub>X files in Section 3.

COMPUTER	OPERATING SYSTEM	COMPILER
uruk@intra.cea.fr		
PC Linux Intel(R) Xeon(R) Gold 5218R CPU @ 2.10GHz 2 CPU - 20 physical cores per CPU	LINUX Ubuntu 20 Kernel 5.4.0-147	GCC9.4.0 MPICH 3.3.2
pegasi2@intra.cea.fr		
PC Linux Intel(R) Xeon(R) Gold 5120 CPU @2.20GHz 2 CPU - 14 physical cores per CPU	CentOS 7.9.2009 Kernel 3.10.0-1160.90.1.el7	GCC4.8.5 MPICH3.2

Table II.1.2: Computer characteristics for running the test cases database.

## II.2

## Overview of new PRM template

The PRM files are written in a specific template more user-friendly as described in the following. The PRM sheet is then read by Python scripts which convert it to L<sup>A</sup>T<sub>E</sub>X files.

For a better readability, an enhanced rendering and uniformity of this document, a new PRM template has been implemented. This new template provides a skeleton of the main items one should find in a CFD study. By browsing it, the user will immediately know the system geometry, the physical models, the boundary conditions, the numerical methods and other unavoidable details. Each validation sheet included in this document has been revised and improved with this new PRM template. For some test cases, the physical content has been enriched with an extended analysis and discussion. In subsection 2.1, we remind the

structure of an old PRM syntax (until version v1.8.1). The new syntax available since version v1.8.2 is then detail in subsection 2.2.

## 2.1 Old PRM syntax

In the previous versions of **TrioCFD**, the formalism of a PRM was left to the hand of the writer of the file. The general structure was made up of a first part called **Parameters**. Then the writer could define as many chapters as he wanted via the keyword *Chapter*. The titles of the chapters were left to the discretion of the editor. The methodology for writing the PRM as well as the keywords are explained in the [PRM syntax](#) section after launching "trust-index".

In order to better understand the old structure, we will take the example of the PRM present in Chapter III.3 of this report on a Cylinder in Laminar Cross Flow. The first keyword *Parameters* was structured as follows:

```
Parameters {
    Title "Cir Cyl Re100" % PRM title
    Description "Oscillating flow behind a circular cylinder perpendicular to the flow." % PRM Description
    VersionTrio_U "1.6.1" % Trio-CFD used to establish de TestCase
    ParametersTrio_U Type of problem: 2D laminar hydraulic_problem % definition of different physical and numerical models
    ParametersTrio_U Discretization: VEFPreP1B % used in the modeling
    ParametersTrio_U Time scheme: Euler Explicit for VDF and VEF
    ParametersTrio_U Momentum convection scheme: EF_stab with alpha = 0.2 or Muscl
    ParametersTrio_U Solving of equations: Navier_Stokes_standard

    # Reference " $[1]$ Chabard J.P., Lalanne P., Metivet B., Projet N3S de Mecanique des fluides. Cahier de Validation 2D. EDF/DER HE-41/88.08 1988. "
    # Reference " $[2]$ Braza P., Chassang P., H. Ha Minh, Numerical study and physical analysis of pressure and velocity fields in the near wake of a circular cylinder. J. Fluid Mech. 165, 79-130, 1986 "

    TestCase EI/Muscl test % Name of generated TestCase with .data file
    TestCase EI/EF_stab02 test

    Author "E. MOREAU (S. VANDROUX)" % Writer(s) of the Test Case and the PRM
    IncludeData 2 % Number of TestCase generated
}
```

Figure II.2.1: Original PRM syntax version - Parameters part

This part generates the first section of the PRM pdf entiteled *1. Introduction* as follows:

<p><b>2 TESTS DESCRIPTION</b></p> <hr/> <p>Cir Cyl Re100</p> <p><b>1 Introduction</b></p> <p>Validation made by : E. MOREAU (S. VANDROUX). Report generated 25/06/2020.</p> <p><b>1.1 Description</b> Oscillating flow behind a circular cylinder perpendicular to the flow.</p> <p><b>1.2 Parameters TRUST</b></p> <ul style="list-style-type: none"> <li>• Version TRUST : 1.6.1</li> <li>• Binary: /export/home/jd249769/TRIO_CFD/deposits_git/trioefd-code/TrioCFD.opt (built on TRUST v/export/home/jd249769/TRIO_CFD/deposits_git/trioefd-code/validation/share/Validation/Rapports au)</li> <li>• Type of problem: 2D laminar hydraulic_problem</li> </ul>	<ul style="list-style-type: none"> <li>• Discretization: VEFPreP1B</li> <li>• Time scheme: Euler Explicit for VDF and VEF</li> <li>• Momentum convection scheme: EF_stab with alpha = 0.2 or Muscl</li> <li>• Solving of equations: Navier_Stokes_standard</li> </ul> <p><b>1.3 Test cases</b></p> <ul style="list-style-type: none"> <li>• EI/Muscl/test.data :</li> <li>• EI/EF_stab02/test.data :</li> </ul> <p><b>1.4 References :</b></p> <ul style="list-style-type: none"> <li>• [1] Chabard J.P., Lalanne P., Metivet B., Projet N3S de Mecanique des fluides. Cahier de Validation 2D. EDF/DER HE-41/88.08 1988.</li> <li>• [2] Braza P., Chassang P., H. Ha Minh, Numerical study and physical analysis of pressure and velocity fields in the near wake of a circular cylinder. J. Fluid Mech. 165, 79-130, 1986</li> </ul>
---	--

Figure II.2.2: Original PRM syntax version - Generated introduction

After this first part, chapters can be freely added via the keyword *Chapter{ ... }* as follows:

```

Chapter {
    Title "Tests Description"                                % Chapter title
    #
    Description "Hydraulic initial conditions; quiescent fluid U = V = 0 m/s"           % chapter redaction
    Description "Hydraulic boundary condition;"          % chapter redaction
    Description "$bullet$ The velocity is fixed in order to obtain U = 0.03937m/s in such a kind that Re =  $Ud/\nu$  = 100 "
    Description "$bullet$ CERCLE paroi_fixe"
    Description "$bullet$ PAROI1 symetrie"
    Description "$bullet$ PAROI2 symetrie"
    Description "$bullet$ SORTIE frontiere_ouverte_pression_imposee Champ_Front_Uniforme 1 0.0 "
    Description "$bullet$ SORTIE frontiere_ouverte_vitesse_imposee Champ_Front_Uniforme 2 0.03937 0.0 "
    Description "% \underline{Validated model:}\underline{Validation with:}\underline{Calculation N3S of Chabard [1] and experiments of Braza et al. [2]}% use of pure latex commands"
    Description "- No-slip at the wall "
    Description "- 2D channel "
    Description "- Disturbance of a laminar flow "
    Description "% "
    Description "% \underline{Validation with:}\underline{Calculation N3S of Chabard [1] and experiments of Braza et al. [2]}% use of pure latex commands"
    #
    Figure {
        Title "Geometry"                                     % insertion of a figure png
        Description "In the following scheme, L = 0.635m ; W = 0.1524m and d = 0.0254m "          % figure title -> new subsection creation
        Width 14cm                                         % Text preceding the figure
        picture geometry.png                               % figure dimensions
    }
    #
    visu {
        Title "Mesh overview"                            % insertion of a visu extract from lata
        Description " Mesh build with Gmsh: 9668 elements "          % visu title -> new subsection creation
        Width 14cm                                         % Text preceding the visu
        mesh EI/Muscl/test.lata dom                      % figure dimensions and resizing
    }
    #
    properties Geometry {
        Table {
            Title "Physical properties"                  % insertion of a table
            Description ""                                % table title -> new subsection creation
            nb_columns 1                                 % Text preceding the table
            label Value
            line {
                legend "$\rho$ (kg/m3)"             % table header
                file propertiesGeometry.dat
                nb_columns_file 3
                columns ($1)
            }
            line {
                legend "$\mu$ (N/m2/s)"             % table header
                file propertiesGeometry.dat
                nb_columns_file 3
                columns ($2)
            }
            line {
                legend "Re"                            % table header
                file propertiesGeometry.dat
                nb_columns_file 3
                columns ($3)
            }
        }
    }
}

```

Figure II.2.3: Original PRM syntax version - Chapter part

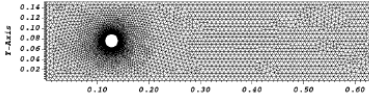
This part generates the second section of the PRM pdf entiteled *2. Tests Description* as follows:

## 2 Tests Description

Hydraulic initial conditions: quiescent fluid U = V = 0 m/s  
 Hydraulic boundary condition:  
 • The velocity is fixed in order to obtain U = 0.03937m/s in such a kind that Re =  $Ud/\nu$  = 100  
 • CERCLE paroi\_fixe  
 • PAROI1 symetrie  
 • PAROI2 symetrie  
 • SORTIE frontiere\_ouverte\_pression\_imposee Champ\_Front\_Uniforme 1 0.0  
 • SORTIE frontiere\_ouverte\_vitesse\_imposee Champ\_Front\_Uniforme 2 0.03937 0.0  
 Validated model:  
 - No-slip at the wall  
 - 2D channel  
 - Disturbance of a laminar flow  
Validation with: Calculations N3S of Chabard [1] and experiments of Braza et al. [2]

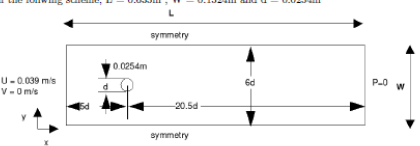
## 2.2 Mesh overview

Mesh build with Gmsh: 9668 elements



## 2.1 Geometry

In the following scheme, L = 0.635m ; W = 0.1524m and d = 0.0254m



## 2.3 Physical properties

	Value
$\rho$ (kg/m <sup>3</sup> )	1.33
$\mu$ (N/m <sup>2</sup> /s)	1e-05
Re	100.0

Figure II.2.4: Original PRM syntax version - Generated chapter

## 2.2 New PRM syntax

### General improvements

Improvements have been made to the `Run_fiche` procedure (managed by TRUST code) and a new tag, `newvalidTrio`, has been created to activate the new formalism. Some modifications have been made in

this new version for the generation of the L<sup>A</sup>T<sub>E</sub>X file from the PRM file, without affecting the syntax of the PRM. Thus, the PRM still includes the first block of instructions entitled **Parameters** (see Section 2.1) which is followed by several blocks of instructions entitled by new tags (or keywords). Those new keywords are listed in Section 2.2. The tag **Chapter** appearing in previous versions is removed and replaced by many other tags. An additional improvement concerns the “headers and footers” of PDF files. In earlier versions, the left header stated the number and title of last section whereas the left footer stated the test name. Now, the name is put on the left header, the left footer is empty and the right footer still states the page number. That modification was necessary for the concatenation of L<sup>A</sup>T<sub>E</sub>X files into one single document and facilitates the readability.

### Modification of Python script

As seen in section 2.1, adding a new figure, **visu**, or **table** automatically created a new subsection. The title of that subsection is the same as the figure name (respectively **visu** or **table**). Therefore, too many irrelevant subsections were created and the title was used as a caption for figures. In this work, the Python scripts have been modified so that the title fields of figures (resp. **visu** and **tables**) now correspond to the caption and their creation no longer generates a subsection.

CONTENT OF NEW PRM file	KEYWORDS OF NEW PRM SYNTAX	
	English	French
<b>1. Purpose</b>	<code>purpose</code>	<code>objectif</code>
<b>2. Problem description</b>	<code>pb_description</code>	
2.1 Geometry	<code>geometry</code>	<code>geometrie</code>
2.2 Initial and boundary conditions	<code>icbc</code>	<code>cicl</code>
2.3 Fluid properties	<code>fluidprop</code>	<code>propfluide</code>
2.4 Flow Physics	<code>flowphy</code>	<code>phyecou</code>
<b>3. Case Setup</b>	<code>casesetup</code>	<code>description_cas</code>
3.1 Grid	<code>grid</code>	<code>maillage</code>
3.2 Model options	<code>model_options</code>	<code>options_modele</code>
3.3 Other options (calculations)	<code>other_options</code>	<code>autres_options</code>
<b>4. Results</b>	<code>results</code>	<code>resultats</code>
3.1 Specific information	<code>none</code>	
3.2 Data plots	<code>none</code>	
<b>5. Conclusion</b>	<code>conclusion</code>	
<b>6. References</b>	<code>Reference in block Parameters</code>	
<b>7. Datafile</b>	<code>TestCase in block Parameters (if followed by \*)</code>	

Table II.2.1: New blocks of instructions in PRM file: content (left) and corresponding keywords (right) in English or French.

Moreover, the PRM is now interpreted line by line in order to allow better positioning of the figures in the validation sheet. Previously, the **Description** fields were all displayed together at the start of a section/subsection and the figures afterwards. The Python script has been enhanced with the use of double dictionary to write, in the generated L<sup>A</sup>T<sub>E</sub>X file, the fields in the same order as that of the PRM. It is therefore now possible to alternate the **Description**, **Figure**, **Visu** or **Table** fields and their order will be reproduced in the .tex file.

In addition to these modifications, a new PRM syntax has been implemented in order to present an identical content for all validation sheets: now seven sections define all of them. Those sections are listed in Table II.2.1 (left part). When writing one PRM file, a new section corresponds to a new block of instructions which must be declared by its corresponding keyword. The list of keywords is presented in Table II.2.1 (right

part). All instructions inside the block must be enclosed by braces: e.g `objectif {...}`, `pb_description {...}`, `maillage {...}` and so on, where “...” means several instructions on several lines.

Let us remind that in the old PRM syntax, the unique keyword `Chapter` was defined as many times as necessary for defining a new block of instructions. In particular, the number and name of Sections were chosen by the authors (see Section 2.1) and the final rendering was different from one sheet to another. With the new syntax, the blocks of instructions follow the first one called `Parameters`. The second block of instructions is `objective {}`, the third one is `pb_description {...}`, and so on until `conclusion {...}`. The block `Parameters` already existed in previous PRM version but minor modifications have been brought. The commands are listed in Table II.2.2 and an example of use is presented in Alg. 2.1. The first one, `newvalidTrio`, is mandatory because this new flag indicates the new PRM template. `TestCase` and `ParametersTrio_U` can be used multiple times in the block.

Keywords	Use
<code>newvalidTrio</code>	Required keyword to activate the new syntax
<code>Title</code>	Defines title of the validation sheet
<code>VersionTrio_U</code>	First version of TrioCFD that performed validation
<code>ParametersTrio_U</code>	Comments that appear in Section 4.1 of the validation sheet
<code>Reference</code>	References cited in the validation sheet
<code>TestCase</code>	List of test cases run by TrioCFD and included in the validation sheet
<code>Author</code>	First authors who carried out this validation
<code>IncludeData</code>	Command for including the entry datafile of TrioCFD
<code>Description</code>	available in initial formalism, is no longer taken into account.

Table II.2.2: Keywords that can be used in block `Parameters` for PRM files.

---

**Algorithm 2.1** One example of block `Parameters` (for brevity, few instructions are replaced by “...”).

---

```
Parameters {
    newvalidTrio
    Title "Turbulent flow inside a double-periodic plane channel with heated walls"
    TestCase "Incompressible/Canal_plan_bi_periodique_M1" "Canal_plan_bi_periodique_M1.data" /**
    TestCase "Incompressible/Canal_plan_bi_periodique_M10" "Canal_plan_bi_periodique_M10.data"
    TestCase "Incompressible/Canal_plan_bi_periodique_M100" "Canal_plan_bi_periodique_M100.data"

    TestCase "Incompressible/Canal_plan_bi_periodique_M1_tetraedrise" ...
    TestCase "Incompressible/Canal_plan_bi_periodique_Mibis_tetraedrise" ...

    ParametersTrio_U "Bi-periodic plane channel in X and Z"
    ParametersTrio_U "Convection scheme = EF_stab"
    ParametersTrio_U "k-$\backslash varepsilon$ modelling of turbulence"
    ParametersTrio_U "Wall law = loi_standard_hydr ..."
    ParametersTrio_U "Heat transfer with imposed temperatures"
    ParametersTrio_U "No-slip at the wall"
    Reference "$[1]$ Stanislav N. Danov, Norio Arai and Stuart ..."
    Author "FOURNIER C"
    IncludeData 2
}
```

---

The keyword `Description`, available in the initial formalism, is no longer taken into account.

In the old formalism, `Chapter` block was defined as many time as necessary with title chosen by the writer of the validation sheet (see Chapter II.1). With this new formalism, predefined blocks can be used after the

block **Parameters**.

**The second block** is **Purpose** which can be activated by the keyword **purpose** or **objectif**. In the PDF file, the section **Purpose** is then created provided that the author wants to fill it up. It explains which models will be validated in the sheet and what sort of results (numerical, analytical, ...) **TrioCFD** will be compared with.

**The third block** is **Problem description** which can be activated by the keyword **pb\_description**. The section named **Problem description** is then created. In this block, 4 sub-blocks are available for creating 4 subsections which describe the geometry of the physical domain defined to model the phenomenon, the initial and boundary conditions used in the modeling, the fluid properties and the flow physics. They can be activated with the following keywords:

Keyword	Subsection number	Subsection title
<b>geometry</b> or <b>geometrie</b>	2.1	Geometry
<b>icbc</b> or <b>cicl</b>	2.2	Initial Conditions and Boundary Conditions
<b>fluidprop</b> or <b>propfluide</b>	2.3	Fluid Properties
<b>flowphy</b> or <b>phyecou</b>	2.4	Flow Physics

Table II.2.3: List of keywords for the **Problem description** block.

**The fourth block** entitled **Case Setup** block and activable by the keyword **casesetup** or **description\_cas** has 3 available subsections which can be defined by:

Keyword	Subsection number	Subsection title
<b>grid_mesh</b> or <b>maillage</b>	3.1	Grid
<b>model_options</b> or <b>options_modele</b>	3.2	Model Options
<b>other_options</b> or <b>autres_options</b>	3.3	Other Options (calculation)

Table II.2.4: List of keywords for the **Case Setup** block.

**The fifth block** is an overview of the results of interest from the validation sheet. This block entitled **Results** and activable by the keyword **results** or **resultats** is composed of two subsections. No keyword needed to activate those subsections and the Results block definition is sufficient to create them.

The first, named **Validation Specific Informations** is automatically generated and groups the fields **VersionTrio\_U** and **ParametersTrio\_U** defined in the **Parameters** block. The performance table for each test case is automatically inserted at the end of this subsection.

The second subsection, entitled **Plot Data** is generated by reading line by line the keywords **Description**, **Figure**, **Visu** or **Table** defined by the author in the block. Respecting this order allows an easier writing and reading of the PRM file.

The **last block** named Conclusion defined by the keyword conclusion has no subsection and is filled by line-by-line reading of the PRM like the other blocks. Here is an assessment of the validation status of the sheet.

The **two last sections** of the validation sheet, **References** and **Data Files**, are automatically generated respectively from keywords Reference and TestCase inside the Parameters block.

Four instructions can be used inside all blocks and sub-blocks: Description, Figure, Visu and Table that can be repeated as many times as necessary and in the desired writing order.

## II.3

# L<sup>A</sup>T<sub>E</sub>X files and report generation

The procedure for generating this report is flexible and automated. As a matter of fact, each author can work independently on each validation sheet with the new PRM template (Section 2.2). Moreover, all parts of this document are written in several L<sup>A</sup>T<sub>E</sub>X files with clear names (Section 3.1). A new one can easily be added. Finally a shell script automates the following tasks: gathering all L<sup>A</sup>T<sub>E</sub>X files, cleaning all sheets texfiles (Section 3.2) and making one single PDF document.

### 3.1 L<sup>A</sup>T<sub>E</sub>X files

The main L<sup>A</sup>T<sub>E</sub>X file of this report is named validation\_report\_TrioCFD.tex. The file contains the standard instructions \documentclass, \usepackage, \begin{document} and \end{document}. The eight parts of this report are written in eight separated L<sup>A</sup>T<sub>E</sub>X files (see their names in Tab. II.3.1). Those files are included in the main with the command \input{} (e.g. \input{./part1-introduction.tex}).

L <sup>A</sup> T <sub>E</sub> X file	Comment
validation_report_TrioCFD.tex	Main file
part1-introduction.tex	File included
part2-methodology.tex	id
part3-laminar.tex	id
part4-thermallaminar.tex	id
part5-turbulent.tex	id
part6-thermalturbulent.tex	id
part7-FT.tex	id
part8-conclusion.tex	id

Table II.3.1: L<sup>A</sup>T<sub>E</sub>X files of this report.

The validation sheets are also included in the main by the same command. All of them are placed inside the folder ./fiches containing subfolders of all test cases e.g. Poiseuille\_flow\_2D\_VDF\_VEF, Cir\_Cyl\_Re100, OBI\_diffuser\_VEF\_k\_eps, and so on ... Inside them, the L<sup>A</sup>T<sub>E</sub>X file of each validation sheet is called fic.tex which can be found in the directory ./build/.tmp/. For instance, instruction for including the validation sheet of “Lid driven cavity flow” is:

\input{./fiches/Lid\_driven\_cavity/build/.tmp/fic.tex}. All these `fic.tex` files were generated by Python scripts reading the PRM template.

### 3.2 New shell script for gathering all .tex files

The folder `archives` and all subfolders of test cases are created by `generer_rapport_valid.sh`. For all test cases, the first task of this shell script is to copy the `build` directory of TrioCFD results in corresponding subfolders. The second task is to clean each `fic.tex` file in order to be included in the main L<sup>A</sup>T<sub>E</sub>X file. Finally the instruction `pdflatex validation_report_TrioCFD.tex` compiles and generates the PDF file.

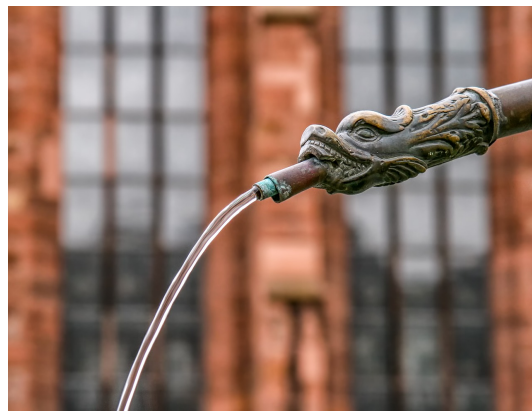
### 3.3 Enhancement

For future versions of this document, the shell script will be enhanced. Currently, adding a new sheet to the report is carried out manually in the shell script. It would be more comfortable to automate the procedure by copying all PRM files which contains the keyword `newvalidTrio`, copy the build directory and do a loop inside the shell script.

### III. Laminar Flow

**I**N this third part of the document, the test cases with laminar flows are considered. Let us remind that a flow is laminar when the viscous forces dominates the inertial ones. This competition is characterized by the Reynolds number ( $Re$ ) which is non-dimensional and defined as  $Re = LU_0/\nu$ , where  $L$  is a characteristic linear dimension,  $\nu$  is the kinematic viscosity and  $U_0$  a characteristic velocity of the system. A flow characterized by a Reynolds number under a critical value of 2000 (approximately) is considered as laminar. Beyond this value, the flow is considered as turbulent. The validation cases of turbulent flows will be considered in Part V of this document. In what follows, three academic cases are detailed:

- Poiseuille flow
- Lid driven cavity flow
- Cylinder in laminar Cross Flow for  $Re = 100$



## Poiseuille flow 2D with VDF and VEF meshes

### 1.1 Purpose

The purpose is to validate the incompressible laminar module of TrioCFD on the well-known analytical solution of Poiseuille flow in a plane channel. Thirteen test cases of Poiseuille flow exist in the TrioCFD database (poiseuille\_3D, Poiseuille\_flow\_2D\_VDF\_VEF, PoiseuilleInOut2DVDFVEF\_prismes, PoiseuilleInOut2DVDFVEF, PoiseuilleInOutVDFVEF, Poiseuilleperio2D, and so on ...). Here we present the test corresponding to the Poiseuille\_flow\_2D\_VDF\_VEF, for which the analytical solution writes:

$$V_x(H) = -\frac{1}{2}H^2 + 0.125$$

when a pressure drop is applied at inlet and outlet.

Validation made by : E.MOREAU (V.BARTHEL).  
Report generated 09/06/2023.

### 1.2 Problem Description

#### Geometry

The geometry is a two-dimensional plane channel of dimensions  $H = 0.5\text{m}$  and  $L = 1\text{m}$  (see Figure)

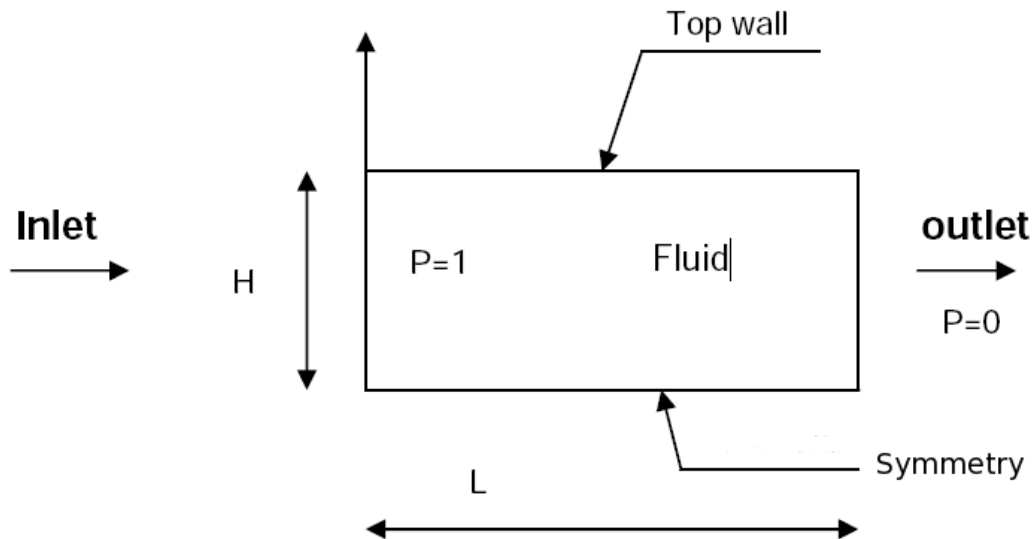


Figure III.1.1: Geometry: Dimensions and domain overview

### Initial Conditions and Boundary Conditions

At the beginning of the simulation, the fluid is at rest  $V_x = 0$  inside a rectangular domain where the top boundary is a fixed wall, the lower boundary is a symmetry condition and two different values of pressure are applied at the left and the right boundaries. The initial and boundary conditions are summarized below:

- Initial conditions:  $V_x = 0$
- Hydraulic boundary conditions:
  - INLET pressure imposed:  $P = 1$  bar
  - OUTLET pressure imposed:  $P = 0$  bar
  - Top wall: fixed wall
  - Symmetry: symmetry

### Fluid Properties

The fluid used in this test is fictive. The two parameters of the model are the dynamic viscosity  $\mu$  and the density  $\rho$ . Their values are summarized in Table 1.

	Value
$\mu$ ( $N/m^2/s$ )	1.0
$\rho$ ( $kg/m^3$ )	1.0

Table III.1.1: Physical properties

### Flow Physics

At the steady state, the profile of the  $V_x$  component must fit the analytical solution (parabolic profile) with a maximum velocity for  $H = 0$  and 0 for  $H = 0.5$ .

## 1.3 Case Setup

### Grid

The calculations are carried out by using two meshes: the first mesh in VDF and the second one in VEF. For the VDF mesh, the 2D grid is composed of 200 cells ( $20 \times 10$ ) and for the VEF mesh, the grid is composed of 400 cells ( $20 \times 10 \times 2$ ). Both meshes are presented on Fig. 2 (VDF) and Fig. 3 (VEF).

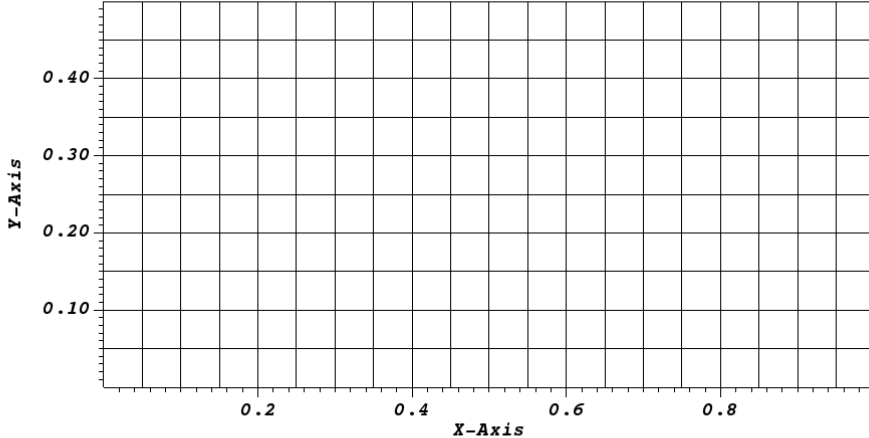


Figure III.1.2: VDF Mesh

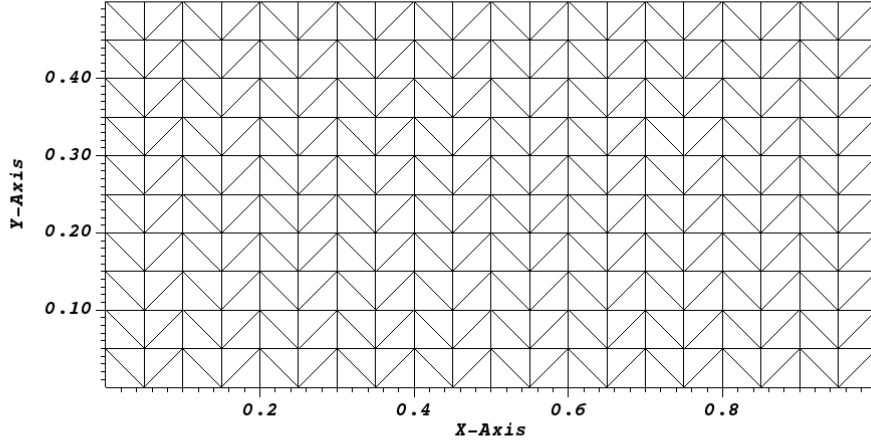


Figure III.1.3: VEF Mesh

## Model Options

The case modeled here being a laminar hydraulic problem in 2D, the equations solved are those of standard Navier-Stokes.

## Other Options (calculation)

The numerical results are compared with the analytical solution for five spatial discretization schemes implemented in TrioCFD: 'Amont' and 'Quick' for 'VDF' and 'Amont', 'Muscl' and 'stab' for VEF.

## 1.4 Results

### Validation Specific Informations

- Version TRUST : 1.6.1
- Type of probem: 2D hydraulic
- Discretization: VEFPreP1B and VDF
- Time scheme: Explicit Euler
- VDF convection scheme: Quick or Amont
- VEFPreP1B convection scheme: Muscl or Amont or EF\_stab ( $\alpha = 1$ )
- Turbulence model: none
- Type of boundary condition: inlet ; outlet
- Equations being solved: Navier\_Stokes\_standard
- Master Test case: poiseuille.data
- Location: /validation/share/Validation/Rapports\_automatiques/Validant/Fini/Poiseuille\_flow\_2D\_VDF\_VEF
- Generated Test cases :
  - VDF/Amont/test.data :
  - VDF/Quick/test.data :
  - VEF/Amont/test.data :

→ VEF/Muscl/test.data :

→ VEF/EF\_stab/test.data :

- Performance Chart :

	host	system	Total CPU Time	CPU time/step	number of cell
VDF/Amont/test	uruk	Linux	2.55087	0.000817659	200
VDF/Quick/test	uruk	Linux	2.60075	0.00083301	200
VEF/Amont/test	uruk	Linux	46.3224	0.00194965	400
VEF/Muscl/test	uruk	Linux	48.0028	0.00201914	400
VEF/EF_stab/test	uruk	Linux	49.4425	0.00207962	400
Total			148.919		

Table III.1.2: Performance Chart

### Plot Data

- Transitory calculation time: about 2s of physical time (transitory calculation until a stationnary flow is reached).
- Average time step:  $6.2 \cdot 10^{-4}$ s in VDF and  $7.8 \cdot 10^{-5}$ s in VEFPreP1B.

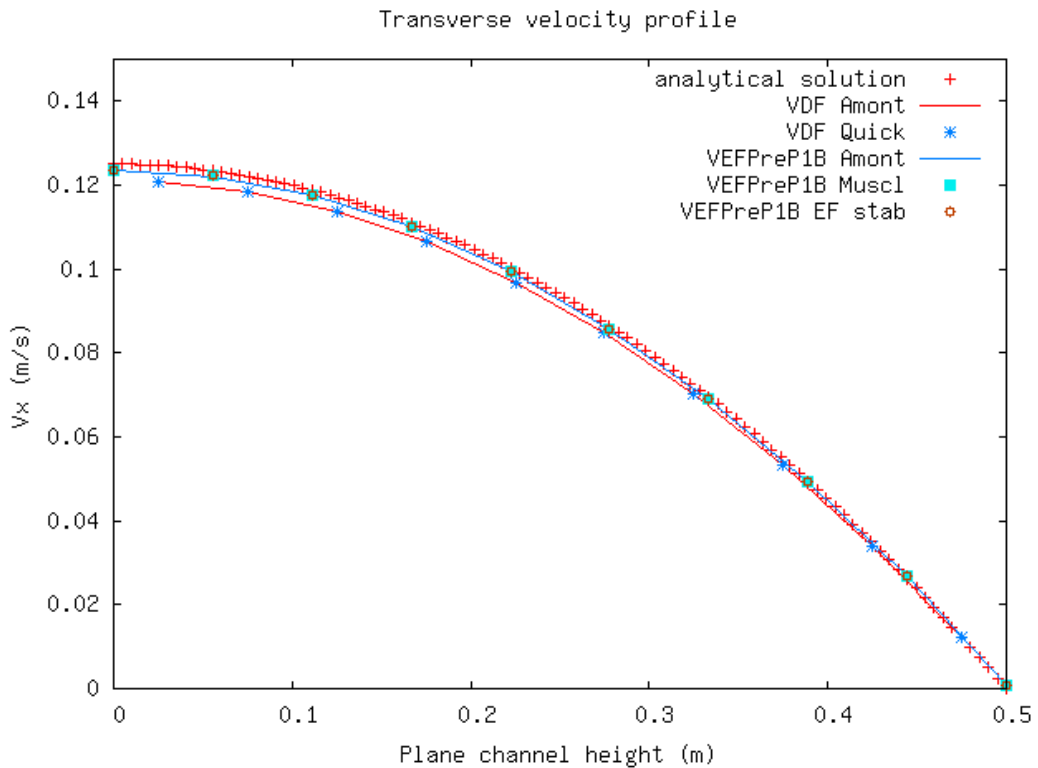


Figure III.1.4: Transverse velocity profile

## 1.5 Conclusion

In VEFPreP1B discretization (greatest refinement), the analytical solution is well-fitted with TrioCFD, in particular with the EF\_stab scheme. The simulations give slightly different results in VDF discretization (less than 3%).

- **Recommendations for users**

The VEFPreP1B discretization associated to an EF\_stab scheme gives the best results on the whole domain.

## 1.6 Data Files

test

```
# Hydraulique 2D : Poiseuille 2D #
# uc=DP/L/8.=0.125 m/s #
# Or a cause de la premiere et derniere demi maille #
# On trouve uc=0.125/0.95=0.131 #
dimension 2
Pb_hydraulique pb
Domaine dom
Mailler dom
{
    Pave Entree
    {
        Origine 0. 0.
        Nombre_de_Noeuds 21 11
        Longueurs 1 0.5
    }
    {
        bord Entree X = 0. 0. <= Y <= 0.5
        bord Haut Y = 0.5 0. <= X <= 1.0
        bord Bas Y = 0. 0. <= X <= 1.0
        bord Sortie X = 1.0 0. <= Y <= 0.5
    }
}
# VDF dis #
VDF dis
Schema_Euler_explicode sch
Read sch
{
    tinit 0
    tmax 5000.
    dt_min 0.0001
    dt_max 1.0
    dt_impr 0.0001
    dt_sauv 100
    seuil_statio 1.e-8
}
Champ_Uniforme gravite
Read gravite 2 0 0
Associate pb dom
Associate pb sch
Discretize pb dis
Read pb
{
    fluide_incompressible {
        mu Champ_Uniforme 1 1.
        rho Champ_Uniforme 1 1.
    }
    Navier_Stokes_standard
```

```

{
  solveur_pression GCP {
    precond ssor { omega 1.650000 }
    seuil 1.000000e-16
    impr
  }
  convection { amont }
  diffusion { }
  conditions_initiales {
    vitesse Champ_Uniforme 2 0. 0.
  }
  boundary_conditions {
    Haut paroi_fixe
    Bas symetrie
    Entrée frontiere_ouverte_pression_imposee Champ_Front_Uniforme 1 1.
    Sortie frontiere_ouverte_pression_imposee Champ_Front_Uniforme 1 0.
  }
}
Postraitemt
{
  format lata
  Sondes
  {
    seg_P pression periode 0.1 segment 10 0 0.25 1 0.25
    seg_U1 vitesse periode 0.1 segment 10 0.5 0.025 0.5 0.475
    sonde_pression pression periode 0.1 points 1 0.5 0.425
    sonde_vitesse vitesse periode 0.1 points 1 0.5 0.425
  }
  Champs dt_post 1.0
  {
    pression elem
    pression som
    vitesse elem
    vitesse som
  }
}
Solve pb
Fin
Fin

```

## 2D Lid driven cavity test

### 2.1 Purpose

The purpose is to check a new time scheme implementation with the 'implicit\_steady' solver using a dual time step in order to reach faster the steady state solution. The new time scheme 'Implicit\_Euler\_steady\_scheme' can be seen as a modification of the 'Euler\_Implicit' option (i.e. implicit solver) but with a time step varying inside the domain. The velocity profiles that are obtained with those two time schemes of TrioCFD are superimposed with the Fluent solution and the solutions of references [1] and [2].

Validation made by : MA PUSCAS.  
Report generated 10/06/2023.

### 2.2 Problem Description

The lid-driven cavity test is a well-known benchmark test for checking the incompressible Navier-Stokes solvers in laminar condition.

#### Geometry

The cavity is a two-dimensional square of size 1m.

#### Initial Conditions and Boundary Conditions

At initial time, the fluid is at rest inside the cavity (i.e.  $\mathbf{V} = \mathbf{0}$ ). The upper horizontal wall has a non zero  $x$ -velocity whereas the 'no-slip boundary condition' is imposed for the three other walls (i.e. the lower horizontal wall and the two vertical ones).

#### Fluid Properties

Only two parameters are involved in the simulation: the density  $\rho = 1$  and the dynamic viscosity  $\mu = 0.01$ .

#### Flow Physics

Under the combined influence of the moving upper horizontal wall and the fluid viscosity, the fluid starts to flow inside the cavity. The direction of rotation is clockwise. When the steady state is reached, the  $V_x$  and  $V_y$  profiles are compared with the reference solutions.

### 2.3 Case Setup

#### Grid

The mesh is presented on Fig. 1 (with Visit).

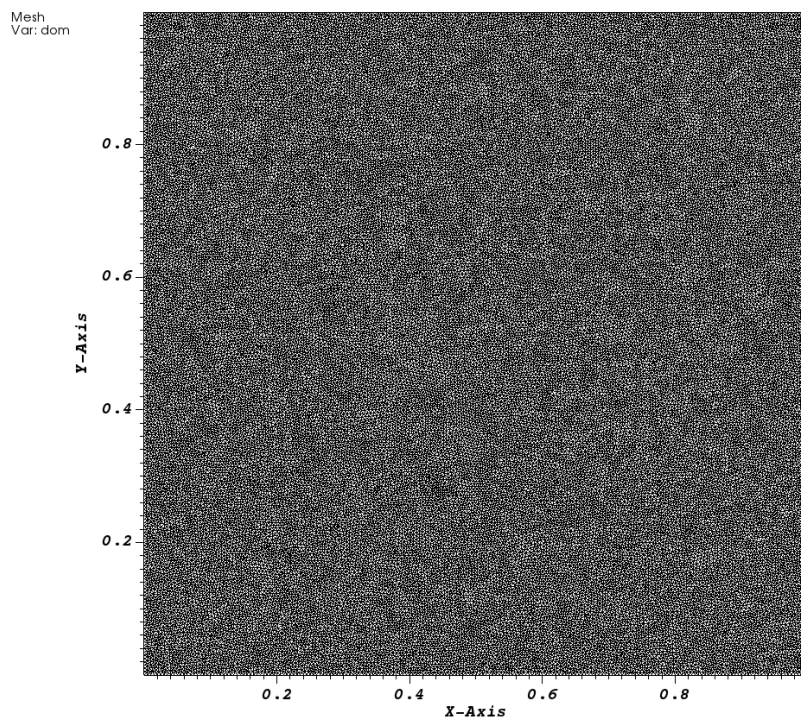


Figure III.2.1: MESH

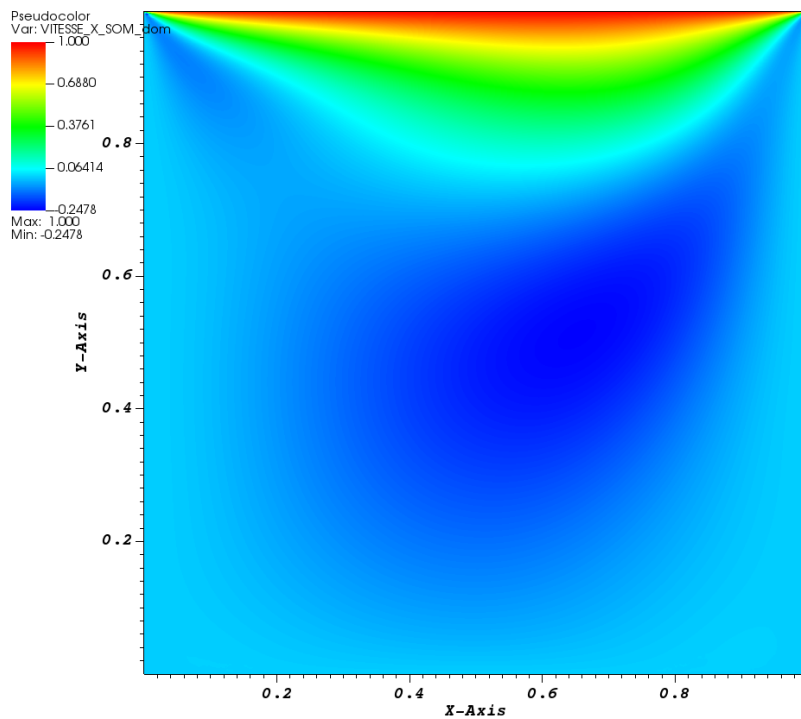


Figure III.2.2: VITESSE\_X SOM

### Other Options (calculation)

TrioCFD is run with the numerical options that are summarized in Section 4.1.

---

## 2.4 Results

### Validation Specific Informations

- Version TRUST : 1.7.3
- Type of problem: Steady Navier-Stokes
- Discretizations: VEFPreP1B
- Type of meshes: Triangles
- Pressure solver: GCP with SSOR preconditioneur
- Time scheme: Implicit\_Euler\_steady\_scheme with Solveur implicit\_steady
- Convection scheme: amont
- Generated Test cases :
  - Steady/defilante.data : /\*jdd en annexe\*/
- Performance Chart :

	host	system	Total CPU Time	CPU time/step	number of cell
Steady/defilante	uruk	Linux	44656.2	127.006	105724

Table III.2.1: Performance Chart

### Plot Data

- Convergence

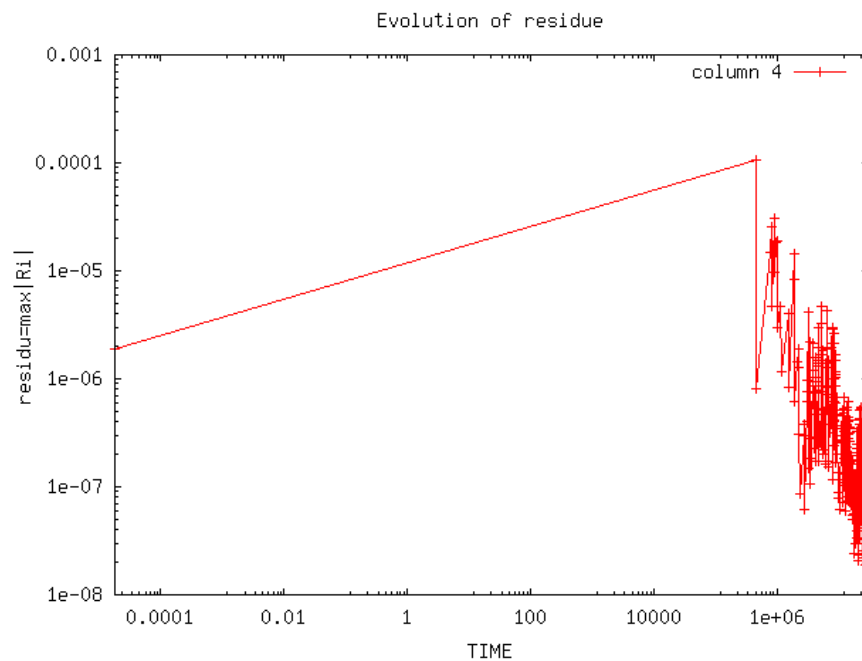


Figure III.2.3: Evolution of residue

- $V_x$ - and  $V_y$ -profiles

The  $V_x$ - and  $V_y$ -profiles are plotted respectively with respect to the  $y$ - and  $x$ -positions on Figs. 4 and 5. Here after the 'reference solution TrioCFD' is the 'Euler\_Implicit' solution.

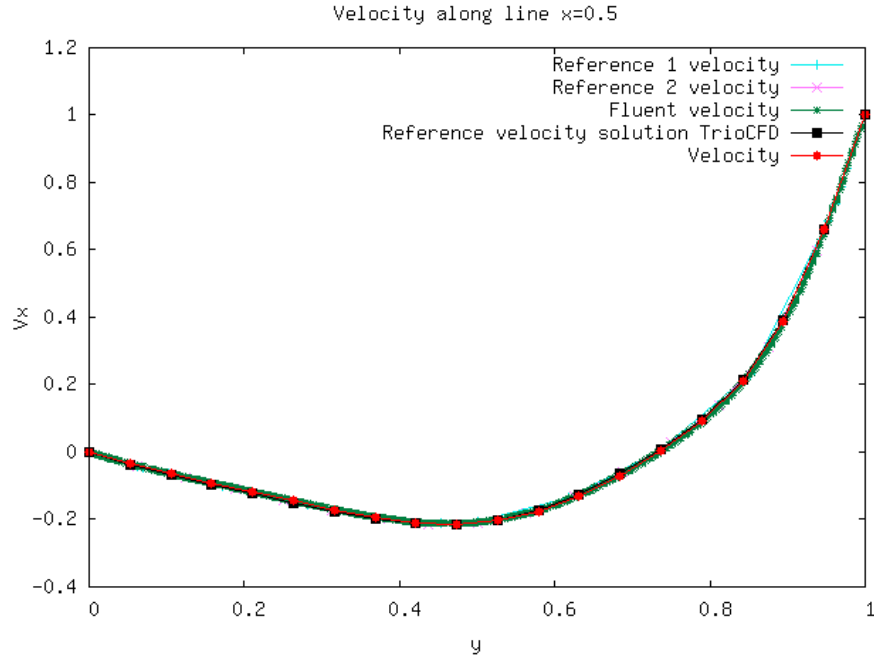


Figure III.2.4: Velocity along line  $x=0.5$

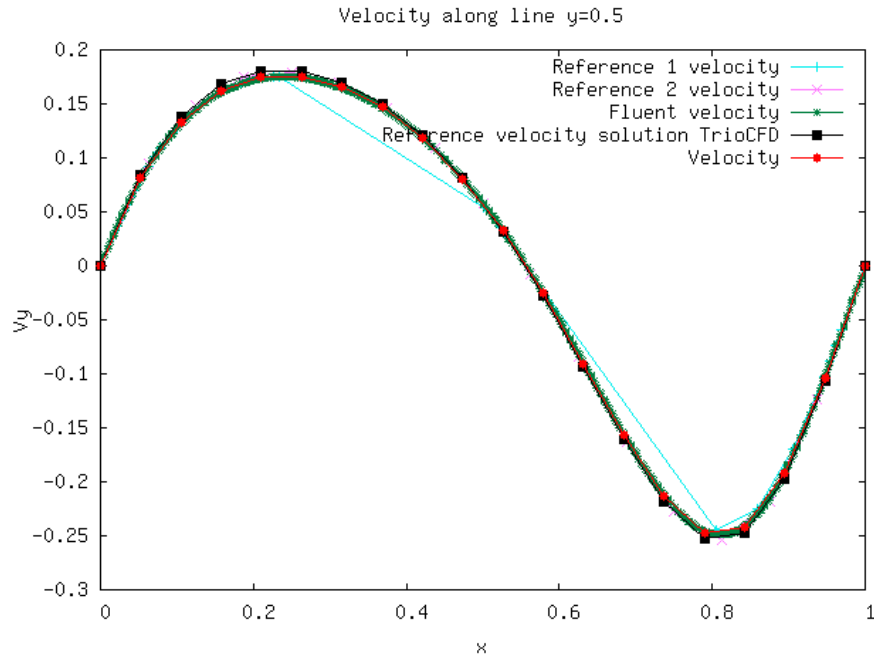


Figure III.2.5: Velocity along line  $y=0.5$

- CPU table

	nb_iter
New time scheme	350
Reference solution	3202

Table III.2.2: CPU informations for new and reference solutions

## 2.5 Conclusion

The time scheme option 'Implicit\_Euler\_steady\_scheme' of TrioCFD reproduces the steady state solution that is obtained with the original time scheme 'Euler\_Implicit' but by considerably decreasing the number of time steps required for the transient phase. The both TrioCFD solutions are in perfect agreement with the Fluent solution and with the solutions from two references of the literature. For this test case, the CPU times (in seconds) were equal to 1) 42269s for the 'Euler\_Implicit' scheme, 2) 6241s for the 'Implicit\_Euler\_steady\_scheme', and 5196s for Fluent.

## 2.6 References

- 1 U. Ghia, and K. N. Ghia, and C. Shin, 'High-Re solutions for incompressible flow using the Navier-Stokes equations and a multigrid method', Journal of Computational Physics, 48, pp. 387-411, 1982.
- 2 C. H. Marchi, and R. Suero, and L. K. Araki, 'The lid-driven square cavity flow: numerical solution with a 1024 x 1024 grid', Journal of the Brazilian Society of Mechanical Sciences and Engineering, 3:186–198, 2009.

## 2.7 Data Files

### defilante

```
# Hydraulique 2D : Paroi defilante #
# PARALLEL OK 5 #
dimension 2
Pb_Hydraulique pb
Domaine dom
# BEGIN MESH #
Lire_MED {
    domain dom
    file square.med
}
# END MESH #
# BEGIN PARTITION
Partition dom
{
    Partitionneur metis { Nb_parts 4 }
    Larg_joint 2
    Nom_Zones DOM
}
End
END PARTITION #
# BEGIN SCATTER
Scatter DOM.Zones dom
END SCATTER #
VEFpreP1b dis
Implicit_Euler_steady_scheme sch
Read sch
```

```

{
  tinit 0.
    nb_pas_dt_max 350
  dt_min 1.e-16
  dt_max 1.e+06
  dt_impr 0.01
  dt_sauv 1.e+06
  seuil_statio 1.e-8
  facsec 1
  steady_security_facteur 10
  steady_global_dt 1
  Solveur implicit_steady {
    solveur gmres { diag seuil 1.e-13 controle_residu 1 nb_it_max 3 }
}
}
Associate pb dom
Associate pb sch
Discretize pb dis
Read pb
{
  fluide_incompressible {
    gravite champ_uniforme 2 0 -9.81
    mu Champ_Uniforme 1 0.01
    rho Champ_Uniforme 1 1.
  }
  Navier_Stokes_standard
{
  solveur_pression GCP {
    precond ssor { omega 1.500000 }
    seuil 1.000000e-16
  }
  convection { amont }
  diffusion { }
  initial_conditions {
    vitesse Champ_Uniforme 2 0. 0.
  }
  boundary_conditions {
    Upper paroi_defilante Champ_Front_Uniforme 2 1. 0.
    Lower paroi_fixe
    Outlet paroi_fixe
    Inlet paroi_fixe
  }
}
Post_processing
{
  Probes
{
  sonde_pression_1 pression periode 1.e+06 segment 10 0. 0. 1 0.
  sonde_pression_2 pression periode 1.e+06 segment 10 0. 0.5 1 0.5
  sonde_pression_3 pression periode 1.e+06 segment 10 0. 1 1 1
  sonde_pression_4 pression periode 1.e+06 segment 10 0.5 0. 0.5 1
  sonde_vitesse_x_1 vitessex periode 1.e+06 segment 10 0. 0. 1 0.
  sonde_vitesse_x_2 vitessex periode 1.e+06 segment 10 0. 0.5 1 0.5
  sonde_vitesse_x_3 vitessex periode 1.e+06 segment 10 0. 1 1 1
  sonde_vitesse_x_4 vitessex periode 1.e+06 segment 20 0.5 0. 0.5 1
  sonde_vitesse_y_1 vitessey periode 1.e+06 segment 10 0. 0. 1 0.
  sonde_vitesse_y_2 vitessey periode 1.e+06 segment 20 0. 0.5 1 0.5
  sonde_vitesse_y_3 vitessey periode 1.e+06 segment 10 0. 1 1 1
  sonde_vitesse_y_4 vitessey periode 1.e+06 segment 10 0.5 0. 0.5 1
}
}
Format lata

```

```
fields dt_post 1.e+06
{
    pression elem
    pression som
    vitesse elem
    vitesse som
}
sauvegarde_simple binaire Cas.sauv
}
Solve pb
End
End
```

## Cylinder in Laminar Cross Flow

### 3.1 Purpose

The purpose of the validation is to compare numerical values of an oscillating flow behind a circular cylinder perpendicular to the flow with those obtained by calculations and experiments.

#### Validated model:

- No-slip wall
- 2D channel
- Disturbance of a laminar flow

Validation with: Calculations N3S of Chabard [1] and experiments of Braza et al. [2]

Validation made by : E. MOREAU (S. VANDROUX).

Report generated 09/06/2023.

### 3.2 Problem Description

In order to observe the disturbances generated by a circular obstacle in an initially laminar flow, we define here a rectangular channel having at mid-height a hole which will correspond to the obstacle. The geometric dimensions of these different elements are given below as well as the conditions necessary for the establishment of the initial laminar flow at the beginning of the transient.

#### Geometry

In the following scheme,  $L = 0.635\text{m}$  ;  $W = 0.1524\text{m}$  and  $d = 0.0254\text{m}$

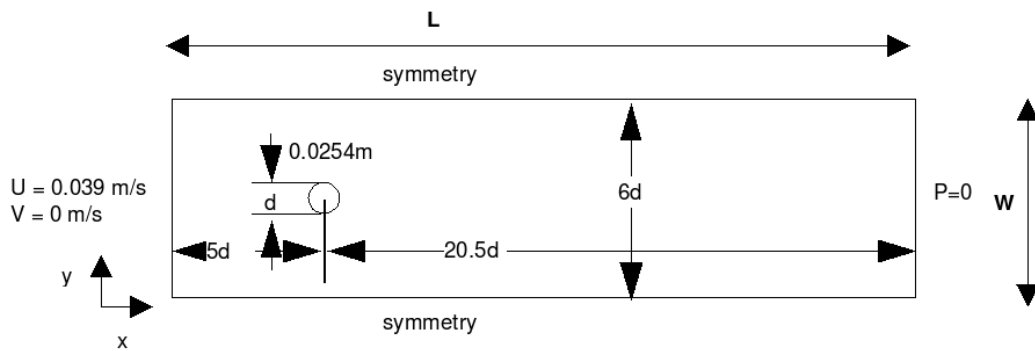


Figure III.3.1: Geometry

#### Initial Conditions and Boundary Conditions

Hydraulic initial conditions: quiescent fluid  $U = V = 0 \text{ m/s}$

Hydraulic boundary condition:

- The X-velocity is imposed in order to obtain  $U = 0.03937\text{m/s}$  so that  $\text{Re} = Ud/\nu = 100$

- CERCLE : paroi\_fixe
- PAROI1 : symetrie
- PAROI2 : symetrie
- SORTIE : frontiere\_ouverte\_pression\_imposee Champ\_Front\_Uniforme 1 0.0
- SORTIE : frontiere\_ouverte\_vitesse\_imposee Champ\_Front\_Uniforme 2 0.03937 0.0

## Fluid Properties

The fluid used in this test is fictive with the following properties :

	Value
$\rho$ ( $\text{kg}/\text{m}^3$ )	1.33
$\mu$ ( $\text{N}/\text{m}^2/\text{s}$ )	1e-05
Re	100.0

Table III.3.1: Physical properties of the fictitious fluid

## Flow Physics

At the beginning of the transient, fluid flow is completely laminar with the Reynolds number equal to 100. In view of the characteristics defined for the fluid, this flow will be quickly disturbed by the obstacle present in the mid-height of the channel.

### 3.3 Case Setup

#### Grid

The mesh was built with gmesh and has 9668 elements. It is a tetraedric mesh, homogeneous over most of the domain with a refinement around the central obstacle in order to capture the formation of the boundary layer around the cylinder induced by the adverse pressure gradient. This refinement will optimize the recirculation phenomena around the cylinder and reveal the development of turbulence in an initially laminar flow.

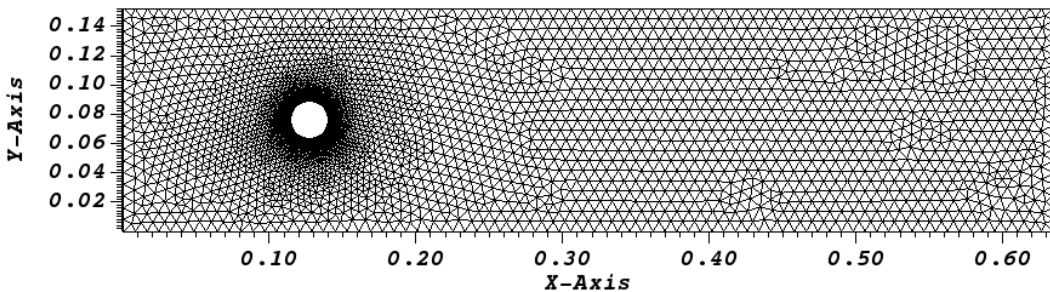


Figure III.3.2: Mesh overview

Triangle layer with 200 points around the circle

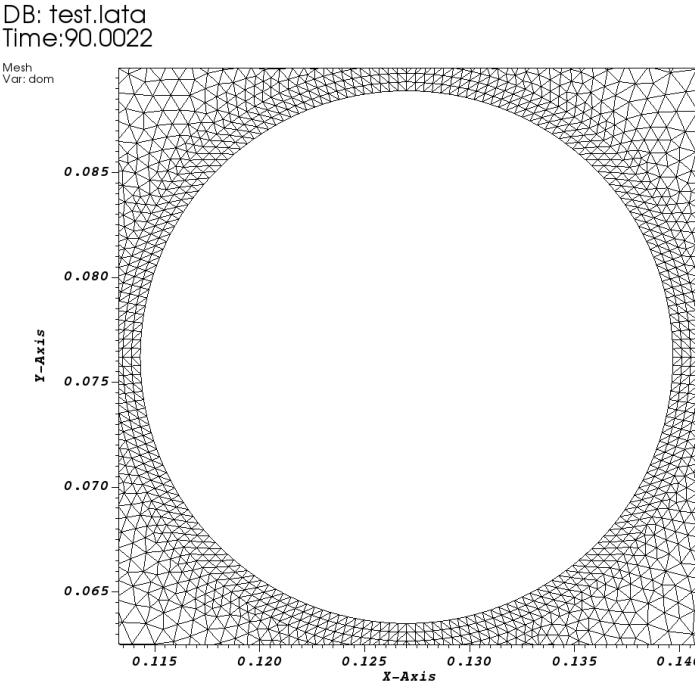


Figure III.3.3: Zoom of the vicinity of the cylinder

### Model Options

- The case modeled here being a laminar hydraulic problem, the equations solved are those of standard Navier-Stokes.
- Momentum convection scheme: EF\_stab with  $\alpha = 0.2$  or Muscl.
- Diffusion scheme: default

### Other Options (calculation)

- The time scheme defined in this test case is the Explicit Euler with implicit diffusion. Indeed, **the Euler implicit scheme is not recommended** because, as the calculation presents oscillations, the value of the facsec coefficient must remain small. The calculation time is then increased instead of being improved.
- The pressure variable to be employed in the data file is not 'Pression' but 'Pression\_Pa', that gives the pressure in Pa.

## 3.4 Results

### Validation Specific Informations

- Version TRUST : 1.6.1
- Type of problem: 2D laminar hydraulic\_problem
- Discretization: VEFPreP1B
- Time scheme: Explicit Euler for VDF and VEF
- Momentum convection scheme: EF\_stab with  $\alpha = 0.2$  or Muscl
- Solving of equations: Navier\_Stokes\_standard
- Master Test case: cc\_re100.data

- Location: validation/share/Validation/Rapports\_automatiques/Validant/Fini/Cir\_Cyl\_Re100
- Generated Test cases :
  - EI/Muscl/test.data :
  - EI/EF\_stab02/test.data :
- Performance Chart :

	host	system	Total CPU Time	CPU time/step	number of cell
EI/Muscl/test	uruk	Linux	9940.07	0.294513	9668
EI/EF_stab02/test	uruk	Linux	9584.9	0.281117	9668
Total			19525		

Table III.3.2: Performance Chart

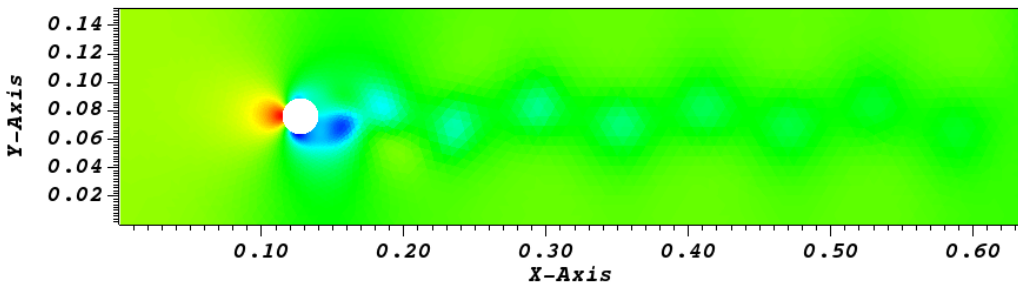
## Plot Data

The temporal pressure evolution at two probes located on the cylinder surface ( $y = -0.5d$  and  $y = +0.5d$ ) is shown in the following figure for each convection scheme. The simulations have been performed up to 90s of physical time in order to get sufficient cycles allowing the calculation of a frequency.

### • Von Karman vortices

When a viscous Newtonian fluid flows around a cylinder, the latter is subjected to forces from the surrounding fluid and complex Reynolds number-dependent phenomena appear. Near the surface of the cylinder wall in contact with the flow, a thin layer of viscous fluid (boundary layer) forms. In this, a speed gradient is established due to viscous stresses which are not negligible. The closer the fluid is to the wall, the more braked, the speed being zero at the surface of the cylinder to satisfy the condition grip. This redistribution in the velocity field leads to a diffusion of the momentum, either by a viscous mechanism or by turbulent movements induced by vortex detachment.

At a specific point, the friction is canceled out and the boundary layer lifts off the wall; this is the point of separation. This separation is not due to the singularity in the geometry, as it would have been the case for a square cylinder, but to the fact that the boundary layer develops in the presence of a pressure gradient that we can observe in the following figure in the pressure field of the domain.

Figure III.3.4: Pressure fields at  $t = 90s$ 

When this pressure gradient is large enough, the speed fluid particles will decrease until they become zero then negative and the separation of the boundary layer occurs.

Behind the cylinder, we can see the development of Karman vortex street caused by a vortex shedding. The characteristics of the fictitious fluid examined here as well as the Reynolds number were established in this academic test case in order to reveal these instabilities.

The boundary layer fluid reaches the detachment area around  $\pm \frac{\pi}{2}$  and when its kinetic energy is insufficient to pass further downstream of the cylinder where the pressure is greater, the fluid tends to take off thus generating a recirculation vortex. This vortex, after reaching a certain size, detaches itself from the layer limit and is convected in the wake. The downstream flow then takes shape of a vortex path and the boundary layer peels off from the cylinder wall.

The wake of the flow will be different depending on the Reynolds number. For  $Re = 100$ , which will correspond to the case modeled here, the wake of the flow becomes asymmetric and unstable. This gives rise to the phenomenon of vortex detachment: vortices form on each side of the cylinder and are alternately convected in the wake forming a street of laminar vortices, called Von Karman vortices. This detachment is done periodically and two-dimensional, that is to say that the detachment does not take place in the transverse direction (Williamson [3]).

We can observe the establishment of this type of vortex in the figure below.

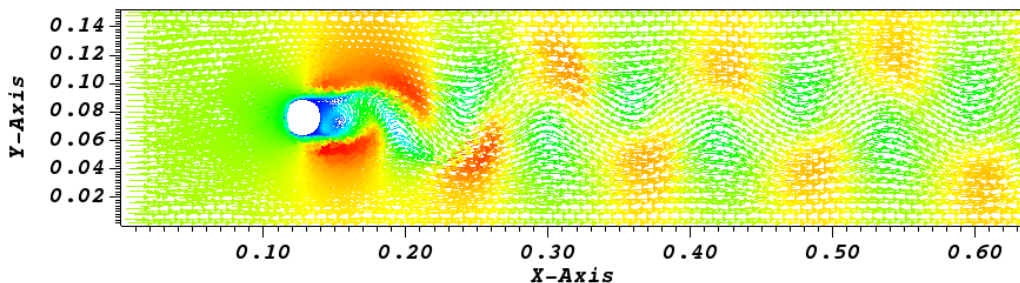


Figure III.3.5: Velocity vectors at  $t = 90s$

- **Pressure evolution at the cylinder surface**

It can be seen that the time of stabilization of the oscillations is of about 40s. From this instant, an oscillation frequency can be determined.

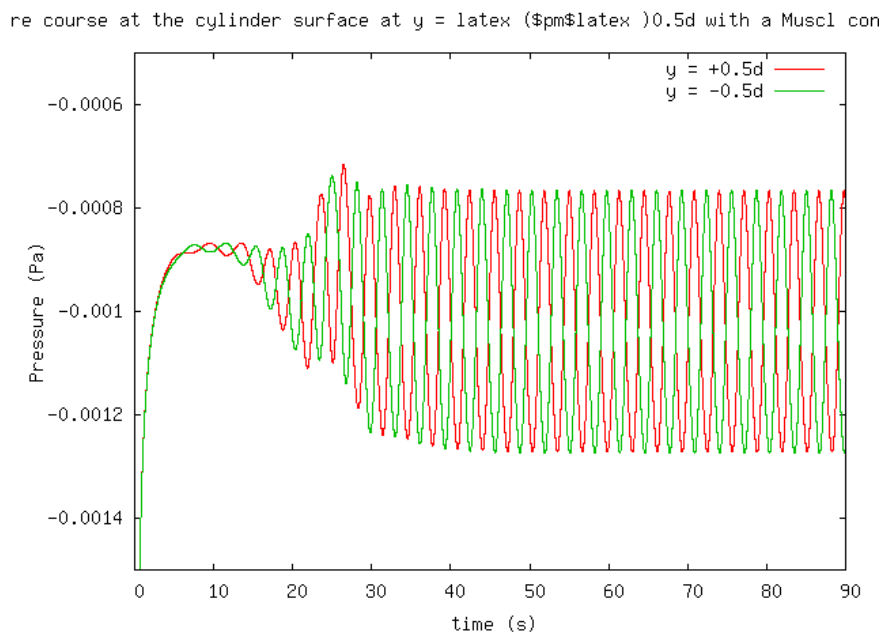


Figure III.3.6: Pressure course at the cylinder surface at  $y = \pm 0.5d$  with a Muscl convection scheme

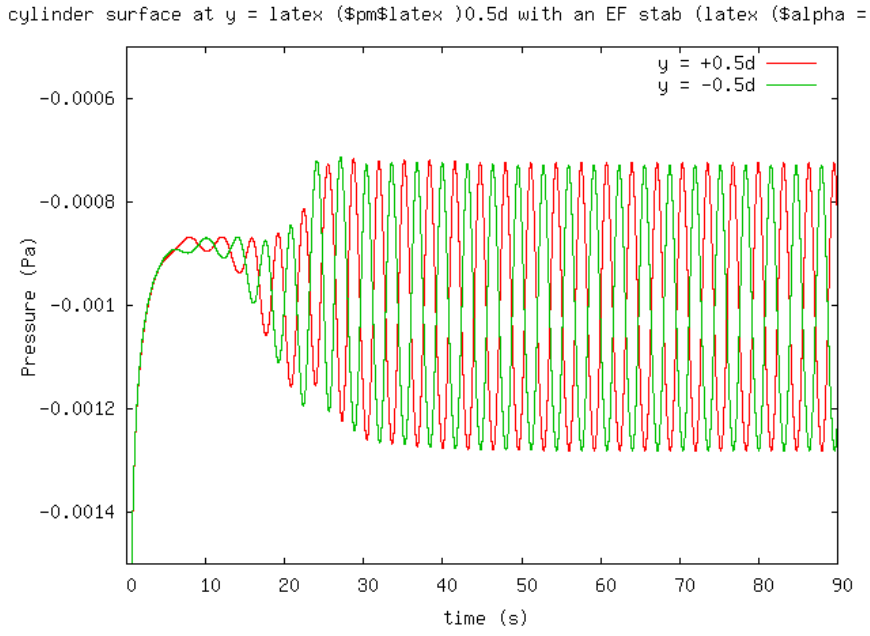


Figure III.7: Pressure course at the cylinder surface at  $y = \pm 0.5d$  with an EF\_stab ( $\alpha = 0.2$ ) convection scheme

The two following figures represent a zoom of the two previous figures from 40 up to 50s. We can notice that oscillations are well established in this time range.

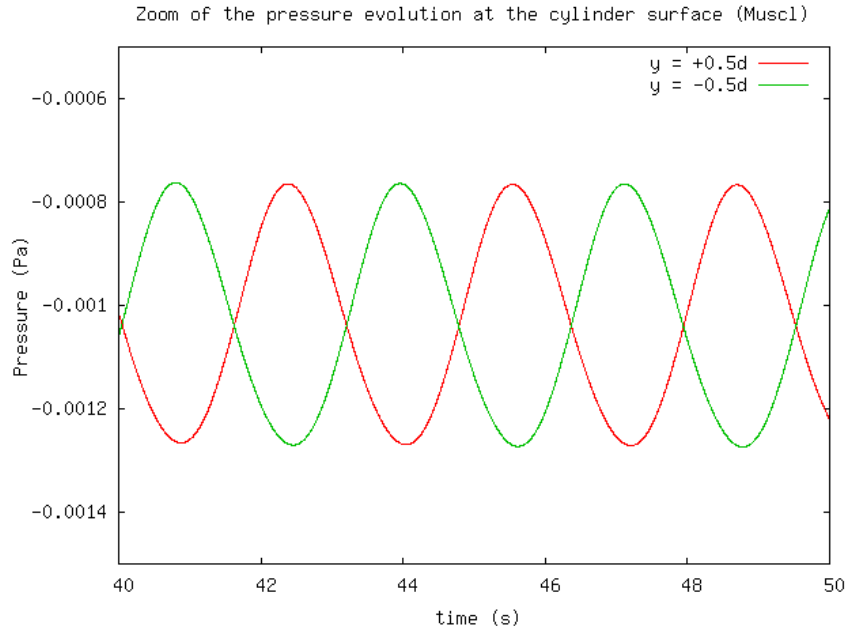


Figure III.8: Zoom of the pressure evolution at the cylinder surface (Muscl)

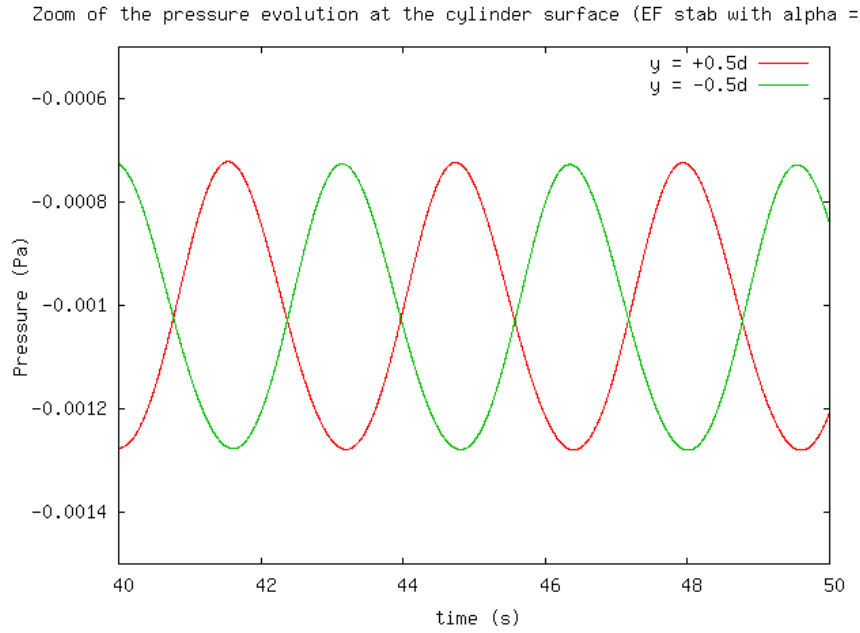


Figure III.3.9: Zoom of the pressure evolution at the cylinder surface (EF\_stab with alpha = 0.2)

#### • Comparison of Strouhal numbers

The temporal pressure evolution in the media allows the determination of the Strouhal number  $S_t$  defined as  $S_t = \frac{f \cdot d}{U}$ , where  $f$  stands for the vortices emission frequency,  $U$  the undisturbed velocity (in our case the inlet velocity), and  $d$  the cylinder diameter. We can in this way compare the simulation values with those of Tritton and Roshko collected by Chabard [1].

	Frequency (Hz)	Strouhal Number	Error % (Tritton)	Error % (Roshko)
Tritton	0.243	0.157	0	6
Roshko	0.259	0.167	6	0
Muscl	0.316	0.204	23.096	18.198
EF_stab ( $\alpha = 0.2$ )	0.313	0.202	22.13	17.17

Table III.3.3: Comparison of Strouhal numbers

Variations in the Strouhal number are associated with changes in the flow structure as described by Blevins [4]. For flow around a circular cylinder at  $Re \sim 40 - 3 \times 10^7$ , Williamson [5], Roshko [6] and Schewe [7] observed experimentally that the Strouhal number is close to the value 0.2.

In the case we are modeling here, the value of the Reynolds number is included in this interval ( $Re = 100$ ) and we note that the Strouhal number obtained numerically is equal to 0.2 to  $10^{-3}$ .

#### • Mean Pressure

The distribution of the mean pressure along the cylinder surface (averaged from 40s up to 90s) is shown and compared to values of N3S [1] and Braza [2]

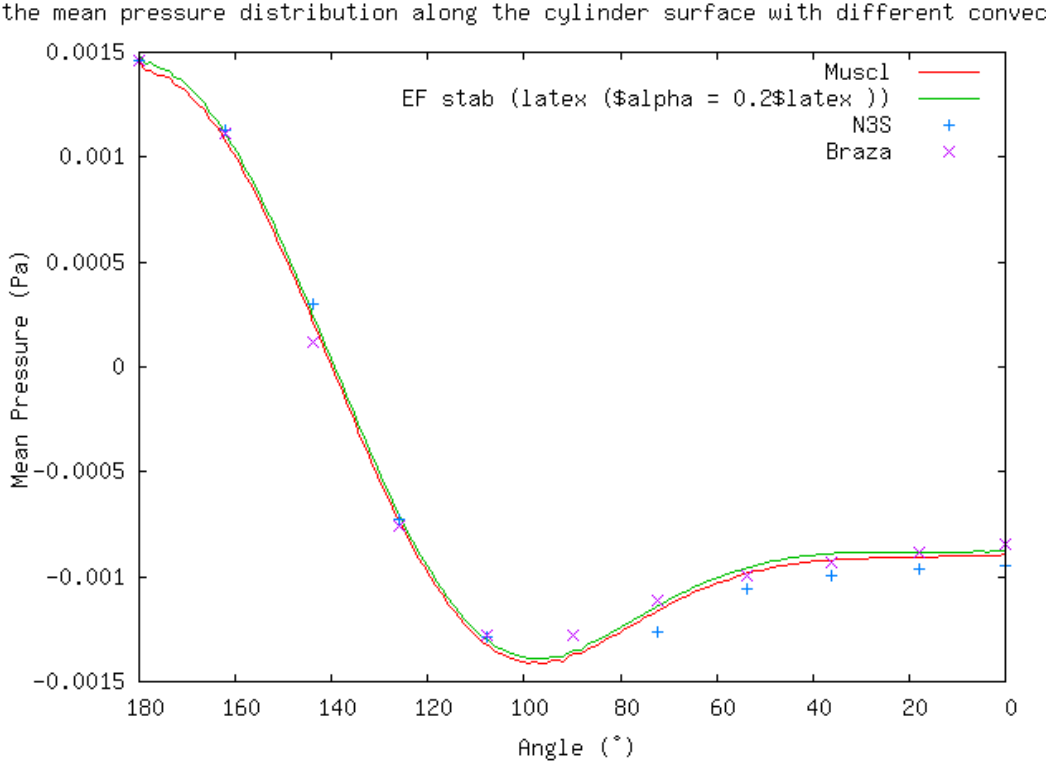


Figure III.3.10: Comparison of the mean pressure distribution along the cylinder surface with different convection and time schemes

### 3.5 Conclusion

The computation of this test with TrioCFD is satisfactory with a good agreement between calculated results with others numerical results by Chabard [1] and experimental results described by Braza [2].

The calculation ends normally without any particular numerical troubles.

This simulation enables the validation of laminar calculations with Trio-CFD of an oscillating flow behind a cylinder with isothermal fluid and VEF grids.

### 3.6 References

- [1] Chabard J.P, Lalanne P., Metivet B., Projet N3S de Mecanique des fluides. Cahier de Validation 2D. EDF/DER HE-41/88.08 1988.
- [2] Braza P., Chassaing P., H. Ha Minh, Numerical study and physical analysis of pressure and velocity fields in the near wake of a circular cylinder. *J. Fluid Mech.* 165, 79-130, 1986
- [3] Williamson C. H. K., Oblique and parallel modes of vortex shedding in the wake of a circular cylinder at low reynolds number. *J. of Fluid Mech.* 31(11), 3165-3168, 1988
- [4] Blevins R.D., *Flow-Induced Vibration*, deuxieme edition, 1990
- [5] Williamson C. H. K., Oblique and parallel modes of vortex shedding in the wake of a circular cylinder at low reynolds number. *J. of Fluid Mech.* 31(11), 3165-3168, 1988
- [6] Roshko A., Experiments on the flow past a circular cylinder at very high reynolds number. *J. of Fluid Mech.* 10 (3), 345-356, 1961

- [7] Schewe G., On the force fluctuations acting on a circular cylinder in crossflow from subcritical up to transcritical reynolds numbers. J. of Fluid Mech., 133, 265-285, 1995

### 3.7 Data Files

**test**

```
# Hydraulique 2D laminaire schema centre #
dimension 2
Pb_hydraulique pb
Domaine dom
# Read_file dom Cir_Cyl.geom #
Read_file dom ../../geometry.geom
VEFPreP1B dis
Schema_Euler_Explicite sch
Read sch
{
  tinit 0.0
  tmax 90.0
  dt_min 1.e-6
  dt_max 1.e-1
  dt_impr 0.1
  dt_sauv 10.0
  seuil_statio 1.e-8
    facsec 1.
    diffusion_ implicite 1
}
#
# nu = mu/rho = 7.518e-6
# Reynolds 100
#
Associate pb dom
Associate pb sch
Discretize pb dis
  imprimer_flux dom { CERCLE }
Read pb
{
  fluide_incompressible {
    mu Champ_Uniforme 1 1.00e-5
    rho Champ_Uniforme 1 1.33
  }
  Navier_Stokes_standard
  {
    solveur_pression Gcp { precond ssor { omega 1.6 }
      seuil 1.e-9
      impr
    }
    convection { muscl }
    diffusion { }
    conditions_initiales
    {
      vitesse Champ_Uniforme 2 0. 0.
    }
    boundary_conditions
    {
      CERCLE paroi_fixe
      PAROI1 symetrie
      PAROI2 symetrie
      SORTIE frontiere_ouverte_pression_imposee
        Champ_Front_Uniforme 1 0.0
    }
  }
}
```

```

ENTREE frontiere_ouverte_vitesse_imposee
    Champ_front_Uniforme 2 0.03937 0.0
}
}

Postraitemet
{
    Definition_champs {
        Pmoy Moyenne {
            t_deb 40 t_fin 89 source refChamp { Pb_champ pb Pression_Pa }
        }
    }
    Sondes
    {
        sonde_pression pression periode 1.e-6 points 4 0.1142 0.0762
                                         0.1398 0.0762
                                         0.1270 0.0890
                                         0.1270 0.0634
        sonde_Pmoy1 Pmoy Periode 10 Circle 150 0.127 0.0762 0.0127 180 0
        sonde_Pmoy2 nodes Pmoy Periode 10 Circle 150 0.127 0.0762 0.0127 180 0
        sonde_Pmoy3 grav Pmoy Periode 10 Circle 150 0.127 0.0762 0.0127 180 0
    }
    Format lata
        Champs dt_post 30.0
    {
        pression som
            Pression_Pa elem
        vitesse som
        vitesse elem
    }
}
}

Solve pb
End
    sonde_Pmoy Pmoy Periode 10.5 Circle 150 0. 0. 0.0127 0 180
    reprise formatte ./sauv/circ_cyl_100_pb.sauv
    imprimer_flux dom { CERCLE }
    Cholesky { impr }
    Gcp { precond ssor { omega 1.5 }
          seuil 1.e-14
          impr
    }
    GCP_ssor { omega 1.65 seuil 1.e-6 impr }
}

```

## IV. Thermal Laminar Flow

COMPARED to the previous part, the phenomena considered here will involve thermal aspects and, in particular, the flow is still laminar.

The first validation sheet of this category corresponds to the **Vahl Davis** benchmark, which is one of the most known test case for checking the coupling between the convective and thermal phenomena. The second one **Oscillatory convection flow** is very similar to the Vahl Davis test case but this time, the cavity and therefore the flow are no longer symmetrical.



## Convection Vahl Davis

### 1.1 Purpose

The Vahl Davis benchmark is one of the well known test case for checking the coupling between flow and thermics in laminar condition. The coupling between the Navier-Stokes equations and the temperature one is carried out with the Boussinesq approximation.

The validations are presented for three meshes: the first one for the VDF discretization and the two other for the VEF discretization (one coarse and another one fine).

Validation made by : E. MOREAU (S. VANDROUX).  
Report generated 09/06/2023.

### 1.2 Problem Description

#### Geometry

The geometry is a square domain of dimensions 1mx1m.

#### Initial Conditions and Boundary Conditions

The initial and boundary conditions must be imposed for temperature equations and fluid flow equations:

- For temperature equation, Dirichlet boundary conditions are applied on the vertical walls  $T(x=0)=300.5\text{K}$ ,  $T(x=1)=299.5\text{K}$  and zero flux on the two other boundaries (horizontal walls). As initial condition, a temperature gradient is imposed such as:  $T = -x + 300.5$  (in K).
- For fluid flow equations, the initial condition is a uniform velocity  $\mathbf{V} = \mathbf{0}$  m/s and no-slip boundary conditions (walls) are applied on all boundaries.

#### Fluid Properties

In the incompressible Navier-Stokes model, the parameters in the equation of impulsion balance equation are the dynamic viscosity  $\mu$ , the density  $\rho$  and the thermal expansion coefficient  $\beta_{th}$ . In the temperature equation, the parameters are the thermal conductivity and the specific heat  $C_p$ . For physical problem involving a coupling between fluid flow and thermics, a dimensionless number, the Rayleigh is defined such as:  $Ra = \frac{g\beta_{th}}{\nu D}(T_{\Gamma_1} - T_{\Gamma_3})H^3$  where  $\nu$  is the kinematic viscosity,  $D$  is thermal diffusivity and  $H$  is the domain size. The values of those parameters are summarized in Table 1.

	Value
$\rho$ ( $\text{kg}/\text{m}^3$ )	1186.78
$\mu$ ( $\text{N}/\text{m}^2/\text{s}$ )	-1.0
$\lambda$ ( $\text{W}/\text{m}/\text{K}$ )	1.0
$C_p$ ( $\text{J}/\text{kg}/\text{K}$ )	0.71
$\beta_{th}$	1.0
$Ra$	-1000000.0

Table IV.1.1: Physical properties

## Flow Physics

A fluid, initially at rest inside a square box is heated at the left vertical wall and cooled at the right vertical wall. Under the influence of combined effects of the temperature gradient and the gravity, the fluid begins to turn inside the box. The velocity is upward at the left wall and downward at the right.

### 1.3 Case Setup

#### Grid

The simulations with TrioCFD are run for three two-dimensional meshes: the first one for the VDF discretization and the two other ones for the VEF discretization (one coarse and another one fine). The VDF mesh, presented on Fig. 1 is composed of 4761 square cells for an area of 1m by 1m. The VEF meshes are respectively composed of 1444 triangular cells, (coarse mesh obtained with option Trianguler\_H) and 6084 triangular cells (fine mesh, obtained with option Trianguler\_H) for the same area. They are both presented on Figs. 1 and 2.

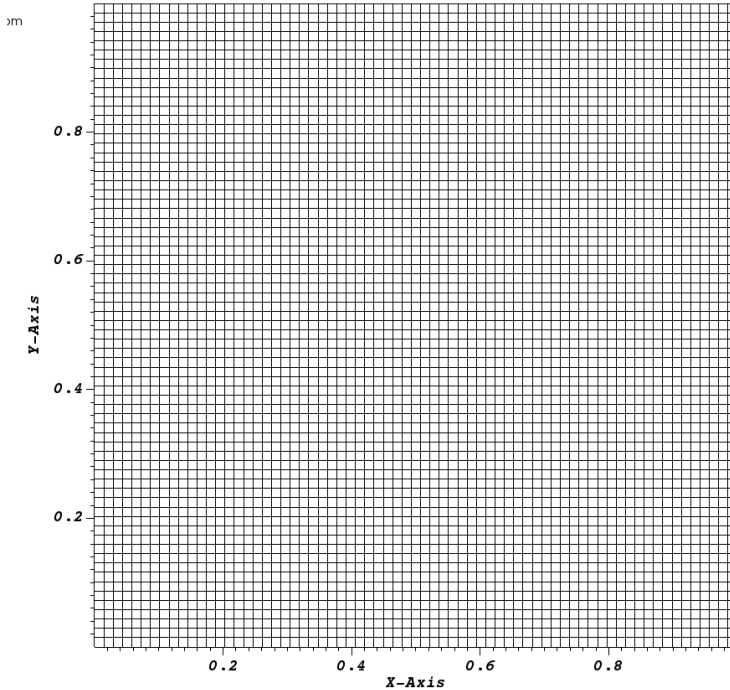


Figure IV.1.1: 2D VDF Mesh

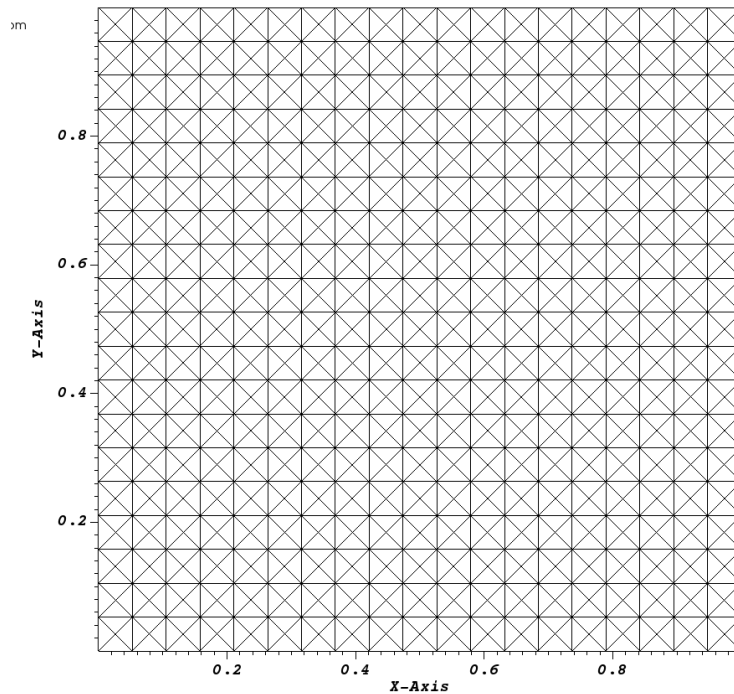


Figure IV.1.2: 2D coarse VEF Mesh

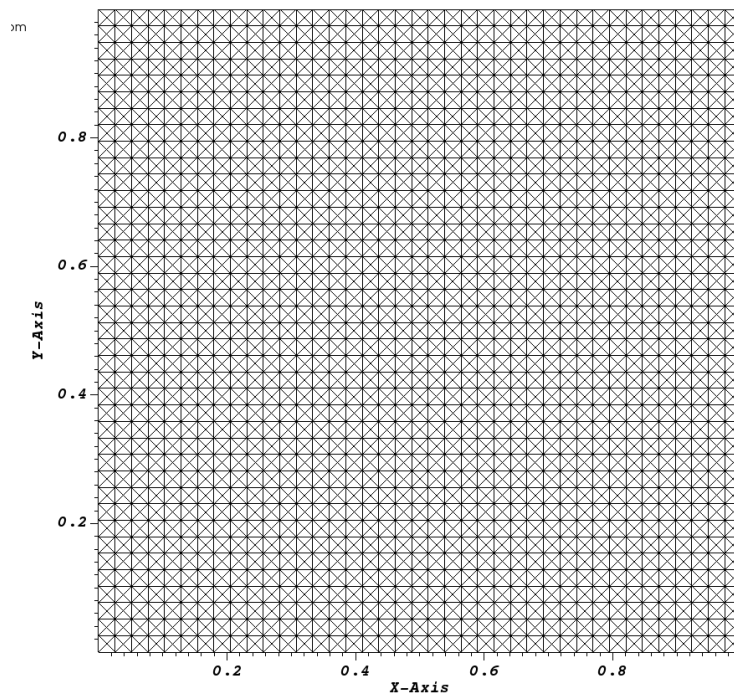


Figure IV.1.3: 2D fine VEF Mesh

## Model Options

The gravity is downward.

## Other Options (calculation)

TrioCFD simulations are performed with several numerical options for the VDF and VEF discretization. When plotting the temperature and velocity profiles, several curves will be presented, each one of them corresponding to the options 'Amont' or 'Quick' for VDF and 'Muscl', 'Amont', 'EF\_stab' (alpha=1) and 'EF\_stab (alpha=0.2)' for VEF (for each mesh Coarse/Fine). The options are summarized in section 4.1.

## 1.4 Results

### Validation Specific Informations

- Version TRUST : 1.6.1
- Dimension: 2D
- Discretization: VEFPreP1B or VDF
- Time scheme: Euler Explicite for VDF, and Euler Implicit for VEF
- Momentum convection scheme: EF\_stab, Muscl or Amont
- Temperature convection scheme: EF\_stab, Muscl or Amont
- Momentum diffusion scheme: Negligible
- Temperature diffusion scheme: Negligible
- Solving of equations: Navier\_Stokes\_standard and Convection\_Diffusion\_Temperature
- Master Test case: Vahl-Davis.data
- Location: /validation/share/Validation/Rapports\_automatiques/Validant/Fini/Convection\_Vahl\_Davis
- Generated Test cases :
  - VDF/Amont/test.data :
  - VDF/Quick/test.data :
  - VEF\_CoarseMesh/Amont/test.data :
  - VEF\_CoarseMesh/Muscl/test.data :
  - VEF\_CoarseMesh/EF\_stab/test.data :
  - VEF\_CoarseMesh/EF\_stab0.2/test.data :
  - VEF\_FineMesh/Amont/test.data :
  - VEF\_FineMesh/Muscl/test.data :
  - VEF\_FineMesh/EF\_stab/test.data :
  - VEF\_FineMesh/EF\_stab0.2/test.data :
- Performance Chart :

	host	system	Total CPU Time	CPU time/step	number of cell
VDF/Amont/test	uruk	Linux	57.1	0.0170007	4761
VDF/Quick/test	uruk	Linux	60.1081	0.0179816	4761
VEF_CoarseMesh/Amont/test	uruk	Linux	40.1178	0.0363841	1444
VEF_CoarseMesh/Muscl/test	uruk	Linux	52.9926	0.0373571	1444
VEF_CoarseMesh/EF_stab/test	uruk	Linux	49.0686	0.0372661	1444
VEF_CoarseMesh/EF_stab0.2/test	uruk	Linux	51.1278	0.0368132	1444

	host	system	Total CPU Time	CPU time/step	number of cell
VEF_FineMesh/Amont/test	uruk	Linux	656.109	0.174903	6084
VEF_FineMesh/Muscl/test	uruk	Linux	964.445	0.216041	6084
VEF_FineMesh/EF_stab/test	uruk	Linux	730.592	0.173775	6084
VEF_FineMesh/EF_stab0.2/test	uruk	Linux	873.142	0.199431	6084
Total			3534.8		

Table IV.1.2: Performance Chart

### Plot Data

The temperature evolution for two points inside the domain (point 1:  $x=0.5$ ,  $y=0.2$ ; point 2:  $x=0.2$ ,  $y=0.5$ ) shows that, after a few oscillations of weak magnitude (Fig. 4), the steady state is reached after about 60 seconds of physical time. Once the steady state is reached (see the temperature and velocity fields on Fig. 5), the velocity and temperature profiles are compared at  $x = 0.5\text{m}$  and  $y = 0.5\text{m}$  for various temporal schemes and convection schemes. The results are also presented for coarsed and refined mesh, and compared with values published in the literature.

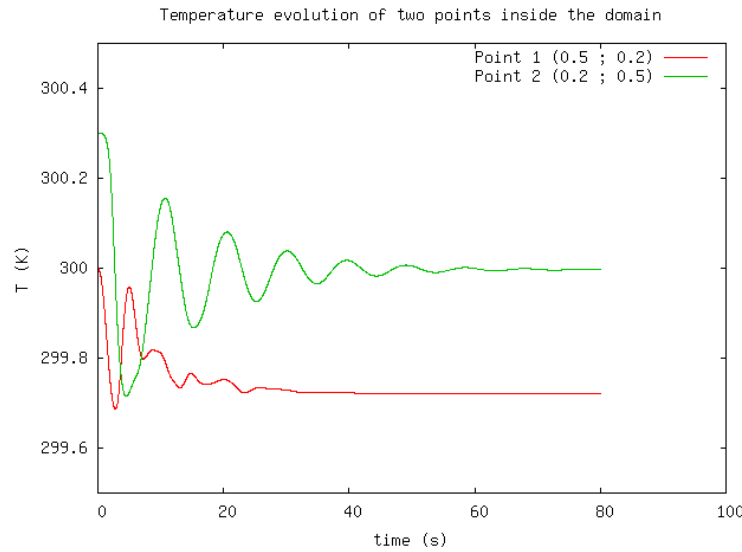


Figure IV.1.4: Temperature evolution of two points inside the domain

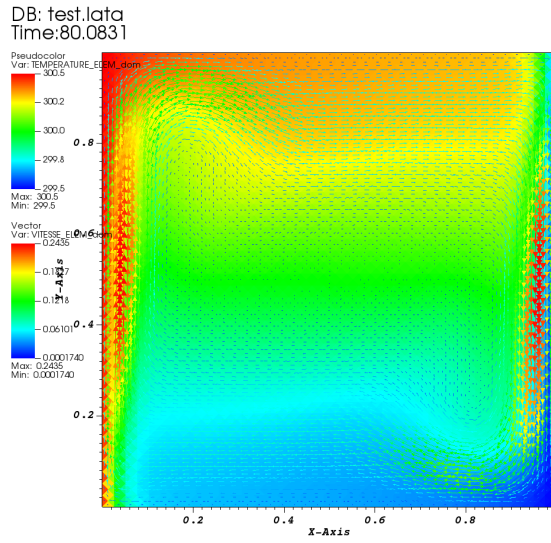


Figure IV.1.5: Temperature and velocity fields at steady state (refine mesh)

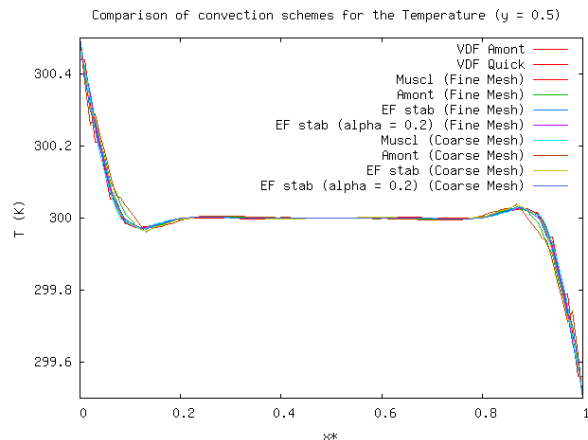


Figure IV.1.6: Comparison of convection schemes for the Temperature ( $y = 0.5$ )

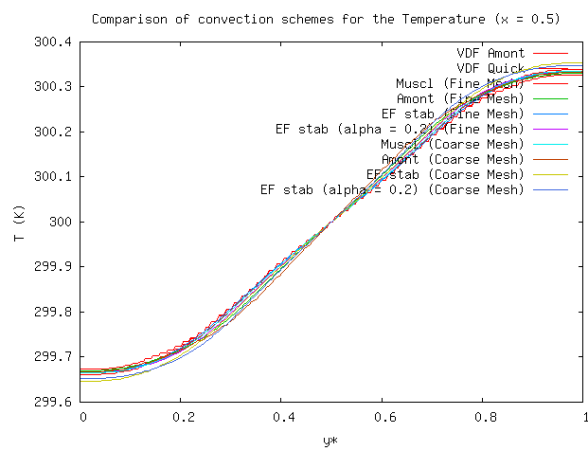
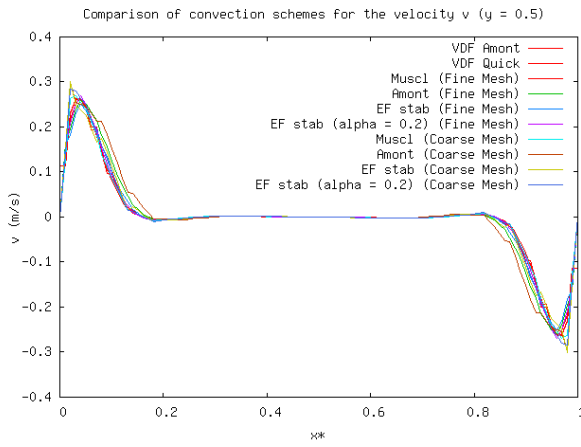
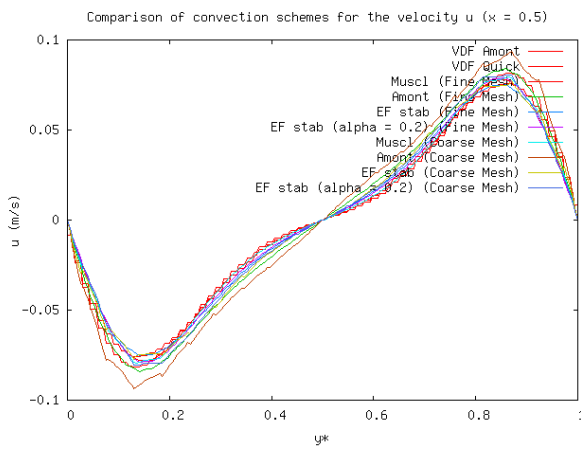


Figure IV.1.7: Comparison of convection schemes for the Temperature ( $x = 0.5$ )

The Amont, Muscl and EF\_stab ( $\alpha = 1$  and  $\alpha = 0.2$ ) convection schemes are used either for momentum or for energy equation.

Figure IV.1.8: Comparison of convection schemes for the velocity  $v$  ( $y = 0.5$ )Figure IV.1.9: Comparison of convection schemes for the velocity  $u$  ( $x = 0.5$ )

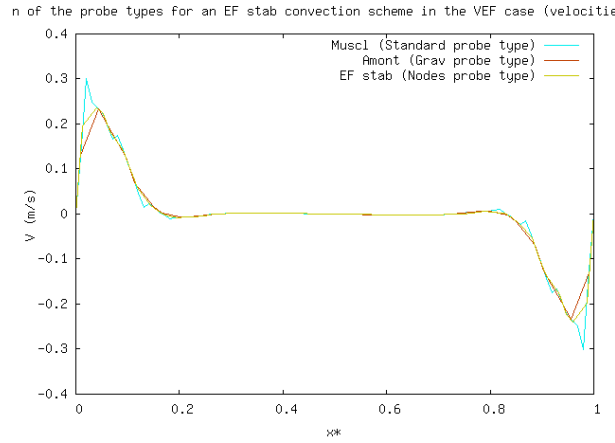


Figure IV.1.10: Comparison of the probe types for an EF\_stab convection scheme in the VEF case (velocities at  $y = 0.5$ )

Probe type: standard, grav or nodes.

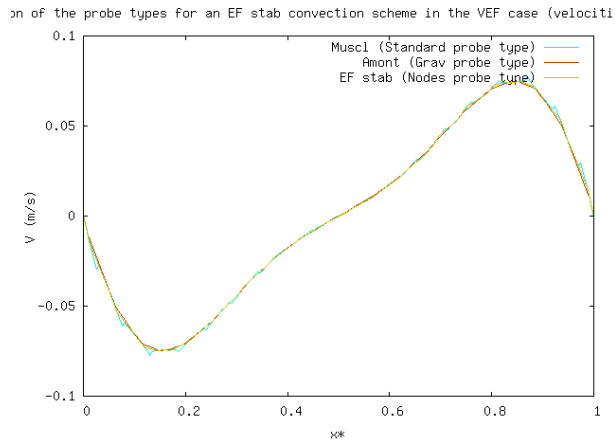


Figure IV.1.11: Comparison of the probe types for an EF\_stab convection scheme in the VEF case (velocities at  $x = 0.5$ )

#### • Comparison with values from the literature

The following values of  $u_x^*$  and  $u_u^*$  are given respectively for  $x = 0.5\text{m}$  and  $y = 0.5\text{m}$ , with:  
 $u^* = uL\sqrt{Ra \times Pr}$  ;  $v^* = vL\sqrt{Ra \times Pr}$  ;  $y^* = y/L$  ;  $x^* = x/L$

	Max( $u^*$ )	$y^*$	Max( $v^*$ )	$x^*$
Vahl Davis	64.63	0.85	216.36	0.03791
Gresho	64.593	0.888	220.64	0.0237
Winter	63.9	0.85	222	0.039

Table IV.1.3: Summary of values from literature

	Max(u*)	y*
VDF (Amont)	68.52998303	0.85929648
VDF (Quick)	63.81984039	0.85929648
VEF Coarse Mesh (Amont)	79.04809562	0.86934673
VEF Coarse Mesh (EF_stab)	65.00696018	0.86934673
VEF Coarse Mesh (EF_stab alpha = 0.2)	67.89840452	0.86432161
VEF Coarse Mesh (Muscl)	66.81241427	0.86432161
VEF Fine Mesh (Amont)	70.84465152	0.85929648
VEF Fine Mesh (EF_stab)	63.30202711	0.85929648
VEF Fine Mesh (EF_stab alpha = 0.2)	66.44112896	0.85929648
VEF Fine Mesh (Muscl)	65.79922487	0.85929648

Table IV.1.4: Results for Max(u\*)

	Max(v*)	x*
VDF (Amont)	222.35199978	0.03030303
VDF (Quick)	219.48033002	0.03030303
VEF Coarse Mesh (Amont)	251.44078604	0.02020202
VEF Coarse Mesh (EF_stab)	254.09465332	0.02020202
VEF Coarse Mesh (EF_stab alpha = 0.2)	239.22156619	0.02020202
VEF Coarse Mesh (Muscl)	226.68710722	0.03030303
VEF Fine Mesh (Amont)	218.44112707	0.04040404
VEF Fine Mesh (EF_stab)	211.85461139	0.04040404
VEF Fine Mesh (EF_stab alpha = 0.2)	226.40395826	0.04040404
VEF Fine Mesh (Muscl)	222.40342626	0.04040404

Table IV.1.5: Results for Max(v\*)

	Vahl-Davis	Gresho	Winter
VDF (Amont)	5.69091493	5.74490589	6.7561421
VDF (Quick)	1.25353491	1.19697121	0.1254454
VEF Coarse Mesh (Amont)	18.23964956	18.2864565	19.16313796
VEF Coarse Mesh (EF_stab)	0.57987665	0.63679363	1.70283333
VEF Coarse Mesh (EF_stab alpha = 0.2)	4.8136691	4.86816228	5.88880482
VEF Coarse Mesh (Muscl)	3.26648019	3.32185912	4.3590915
VEF Fine Mesh (Amont)	8.77222399	8.82445094	9.80264758
VEF Fine Mesh (EF_stab)	2.05473138	1.99862662	0.93579482
VEF Fine Mesh (EF_stab alpha = 0.2)	2.72591539	2.78160379	3.82463242
VEF Fine Mesh (Muscl)	1.77695843	1.83319009	2.88639399

Table IV.1.6: Relative errors for  $\text{Max}(u^*)$ :  $\text{ERR}[\text{Max}(v^*)]$  in %

	Vahl-Davis	Gresho	Winter
VDF (Amont)	2.69482612	0.76995025	0.15830745
VDF (Quick)	1.42169005	0.52559372	1.13498648
VEF Coarse Mesh (Amont)	13.95190756	12.24971753	11.70883472
VEF Coarse Mesh (EF_stab)	14.85062862	13.16621695	12.63098334
VEF Coarsev Mesh (EF_stab alpha = 0.2)	9.55664933	7.76751297	7.19900236
VEF Coarse Mesh (Muscl)	4.55566589	2.66760086	2.06765496
VEF Fine Mesh (Amont)	0.9527176	0.99658853	1.60309592
VEF Fine Mesh (EF_stab)	2.08235746	3.98177511	4.56999487
VEF Fine Mesh (EF_stab alpha = 0.2)	4.43629976	2.54587345	1.94517724
VEF Fine Mesh (Muscl)	2.71732606	0.79289527	0.1813939

Table IV.1.7: Relative errors for  $\text{Max}(v^*)$ :  $\text{ERR}[\text{Max}(v^*)]$  in %

## 1.5 Conclusion

- While the choice of the probe has no effect on the measured maximum velocity  $u$  ( $x = 0.5$ ), this is not the case for  $v$ . Indeed, as can be seen on the previous arrays, the values of  $x^*$  for which  $v^*$  is maximal, are located in a area where significant different values of velocities are observed. The use of probes which display the velocity value either at the gravity center of cells (probe grav) or at the cell nodes (probe node), can lead to smoother curves. The information about maximum velocity along the segment profile  $y=0.5$ , cannot be obtained very precisely. The curves are much smoother however with finer mesh.
- The different time schemes give approximatively the same results for a given set of convection schemes.
- The convection scheme does not influence a lot the temperature profile for  $y = 0.5$ . The influence of the coefficient scheme is more significant for  $x = 0.5$ .
- When using the different time schemes, the results obtained appear very closed from each other. There is no clearly visible difference.
- The amont scheme applied to the energy equation leads to higher extremum values of the velocities for  $x = 0.5$ .
- The temperature profiles are only little influenced by the different convection schemes.
- Regarding the relative errors, the arrays show clearly the influence of the mesh refinement on the results.

## Recommendations for users

Check the different profiles with different kinds of post processing probes, in order to ensure that the mesh is fine enough to perform a reliable calculation, especially where the velocity or temperature changes are steeps.

## 1.6 References

- P.M.GRESHO, C.D. UPSON, R.L. LEE. 'Finite Element Simulations of Thermally Induced Convection in an Enclosed Cavity'. Lawrence Livermore Laboratory Report UCID-18602 (March, 1980).

- G. de VAHL DAVIS. 'Natural Convection in a Square Cavity-A Benchmark Solution'. International Journal for Numerical Methods in Fluids , 3 , 249 - 264.
- K.H. WINTERS. 'A Numerical Study of Natural Convection in a Square Cavity'. United Kingdom Atomic Energy Authority, AERE-R9747 (August, 1980).

## 1.7 Data Files

test

```
# CAS VAHL DAVIS 2D #
dimension 2
Domaine dom
Mailler dom
{
Pave Cavite
{
    Origine 0. 0.
    Nombre_de_Noeuds 70 70
    Longueurs 1. 1.
}
{
    Bord bas      Y = 0.      0. <= X <= 1.
    Bord haut     Y = 1.      0. <= X <= 1.
    Bord gauche   X = 0.      0. <= Y <= 1.
    Bord droit    X = 1.      0. <= Y <= 1.
}
}
Pb_Thermohydraulique pb
VDF dis
Schema_Euler_Explicite sch
Read sch
{
tinit 0.
tmax 80.
dt_min 1.e-8
dt_max 1.e2
dt_impr 1e-1
dt_sauv 500.
seuil_statio 1.e-8
facsec 1.
}
Associate pb dom
Associate pb sch
Discretize pb dis
Read pb
{
fluide_incompressible {
    gravite champ_uniforme 2 0 -1. mu Champ_Uniforme 1 1.
    rho Champ_Uniforme 1 1186.78
    lambda Champ_Uniforme 1 1.
    Cp Champ_Uniforme 1 0.71
    beta_th Champ_Uniforme 1 1.
}
Navier_Stokes_standard
{
solveur_pression GCP
{
    precond ssor { omega 1.5 }
    seuil 1e-9
}
```

```

        }
    solveur_bar GCP
    {
        precond ssor { omega 1.5 }
        seuil 1e-9
    }
sources { Boussinesq_temperature { T0 300. } }
convection { Amont }
diffusion { }
conditions_initiales
{
    vitesse champ_uniforme 2 0. 0.
}
boundary_conditions
{
    haut     paroi_fixe
    bas      paroi_fixe
    gauche   paroi_fixe
    droit    paroi_fixe
}
}
Convection_Diffusion_Temperature
{
    conditions_initiales { Temperature Champ_Fonc_xyz dom 1 -1.*x+300.5 }
    convection { Amont }
    diffusion { }
    boundary_conditions
    {
        haut     paroi_adiabatique
        bas      paroi_adiabatique
        gauche   paroi_temperature_imposee Champ_Front_Uniforme 1 300.5
        droit    paroi_temperature_imposee Champ_Front_Uniforme 1 299.5
    }
}
Postraitemet
{
    format lata
    Sondes
    {
        sonde_temp0 temperature periode 0.001 segment 100
        0. 0.5 1. 0.5
        sonde_temp1 temperature periode 0.001 segment 200 0.5 0. 0.5 1.
        sonde_temppt0 temperature periode 0.01 Points 1 0.5 0.2
        sonde_temppt1 temperature periode 0.01 Points 1 0.2 0.5
        sonde_vit vitesse periode 0.1 Points 1 0.15 0.5
        sonde_vit0 vitesse periode 0.0001 segment 100 0. 0.5 1. 0.5
        sonde_vit1 vitesse periode 0.01 segment 200 0.5 0. 0.5 1.
        sonde_vit0_g grav vitesse periode 0.0001 segment 100 0. 0.5 1. 0.5
        sonde_vit1_g grav vitesse periode 0.01 segment 200 0.5 0. 0.5 1.
        sonde_vit0_n nodes vitesse periode 0.0001 segment 100 0. 0.5 1. 0.5
        sonde_vit1_n nodes vitesse periode 0.01 segment 200 0.5 0. 0.5 1.
    }
    Champs binaire dt_post 10
    {
        vitesse elem
        temperature elem
    }
}
Solve pb
End

```



## Oscillatory convection flow

### 2.1 Purpose

A two-dimensional 'oscillatory convection flow' is studied inside a rectangular heated cavity. The physical test is similar to the previous one, i.e. the 'Convection Vahl Davis' in laminar condition, but the cavity is now non-symmetric. The results are compared with the benchmark of Behnia et al. that is published in the book of reference [1]. The TrioCFD simulations run on VDF and VEF meshes for several options of the convection scheme.

Validation made by : E. MOREAU (S. VANDROUX).  
Report generated 09/06/2023.

### 2.2 Problem Description

#### Geometry

The test case geometry is a two-dimensional rectangular cavity of dimensions  $L=4m \times H=1m$  which is presented on Fig. 1 with the boundary conditions for temperature equation. On that figure the hot wall is on the left side and the cold wall is on the right side.

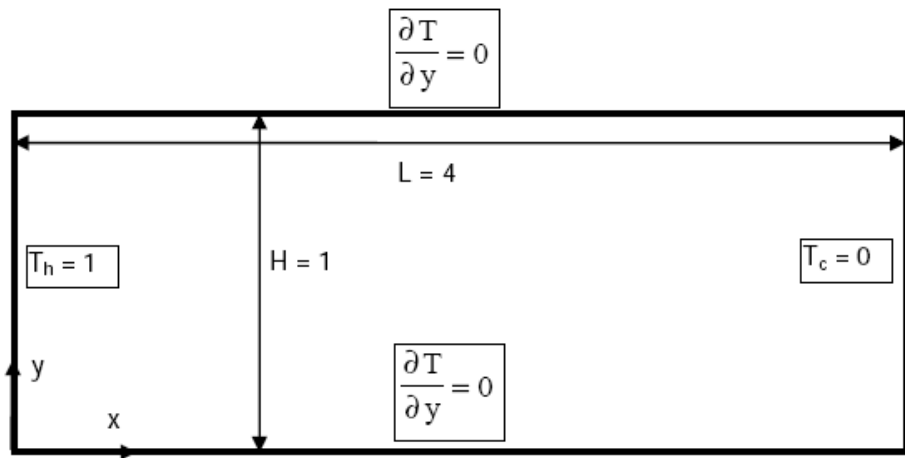


Figure IV.2.1: Dimensions of the domain and boundary conditions for temperature equation.

#### Initial Conditions and Boundary Conditions

The initial velocity is  $U = V = 0$  where  $U$  and  $V$  are respectively the x-component (horizontal) and the y-component (vertical) of the velocity. At  $t=0$ , a linear temperature is applied  $T(x) = 1 - x \frac{H}{L}$  in the horizontal

direction (zero Prandtl fluid). No-slip boundary conditions are applied for Navier-Stokes equations. For temperature equation, zero flux holds on horizontal walls and Dirichlet boundary conditions hold for vertical ones. The boundary conditions are summarized below with the TrioCFD keywords:

- Hydraulic boundary condition type: 'paroi\_fixe'
- The thermal boundary conditons types are as follow:
  - Y = 0 (bottom) and Y = 1 (top): 'Paroi\_adiabatique'
  - T = 1 K (hot side: left) and T = 0 (cold side: right)

The TrioCFD options for the thermal boundary conditions are (respectively for VDF and VEF):

- For VDF calculation:

```
ENTREE paroi_echange_externe_impose T_ext Champ_Front_Uniforme 1 1.00 H_imp
Champ_Front_Uniforme 1 1.e11
SORTIE paroi_echange_externe_impose T_ext Champ_Front_Uniforme 1 0.00 H_imp
Champ_Front_Uniforme 1 1.e11
```

- For VEF calculation:

```
ENTREE paroi_temperature_imposeee Champ_Front_Uniforme 1 1.00
SORTIE paroi_temperature_imposeee Champ_Front_Uniforme 1 0.00
```

## Fluid Properties

The physical parameters are set such as the Grashof number is equal to  $3.10^4$ . Hence, although the Prandtl number is equal to 200, the fluid may be considered as a zero Prandtl fluid because of a negligible thermal convection scheme. The values of parameters are given in Table 1, where  $\rho$  is the density,  $\mu$  is the dynamic viscosity,  $\lambda$  is the thermal conductivity,  $C_p$  is the specific heat and  $\beta_{th}$  is the thermal expansion coefficient.

	Value
$\rho$ (kg/m <sup>3</sup> )	1.18
$\mu$ (N/m <sup>2</sup> /s)	0.00062304
$\lambda$ (W/m/K)	0.00264
$C_p$ (J/kg/K)	1000.0
$\beta_{th}$	0.00341

Table IV.2.1: Physical properties

## Flow Physics

Under the influence of the temperature gradient and the Boussinesq approximation, the fluid starts swirling inside the rectangular cavity in the clockwise direction.

## 2.3 Case Setup

### Grid

The VDF and VEF meshes are presented on Figs 2 and 3. The VDF mesh contains 2500 cells which are generated with the 'Pave' option of TrioCFD.

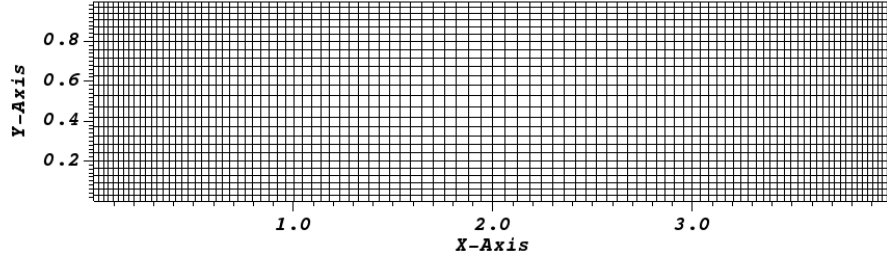


Figure IV.2.2: VDF Mesh

For VEF mesh contains 5040 triangular cells which are obtained with the 'triangular\_H' option of TrioCFD. An expansion has been applied with factors 1.02 along the x-axis, and 1.05 along the y-direction

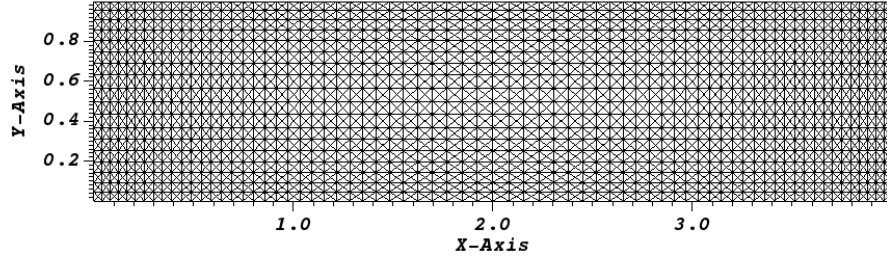


Figure IV.2.3: VEF Mesh

## Model Options

The gravity is downward.

## Other Options (calculation)

For the VDF scheme, the convection option is 'Quick' or 'Centre' and for the VEF scheme the convection option is 'Muscl', 'EF\_stab=0.2' and 'EF\_stab=1'. All other numerical options are summarized in Section 4.1.

## 2.4 Results

### Validation Specific Informations

- Version TRUST : 1.6.1
- Dimension: 2D
- Discretization: VDF / VEF
- Thermal hydraulic problem
- Momentum characteristic: Navier\_stokes\_standard
- Thermal characteristic: Source\_Boussinesq\_temperature
- Convection\_diffusion\_temperature not solved (analytical solution known)
- Time scheme: Euler explicite

- VDF Momentum convection scheme: Centre, Quick or Muscl
- VEF Momentum convection scheme: Muscl, EF\_stab or EF\_stab with alpha = 0.2
- VDF and VEF Temperature convection schemes: Negligible
- Type of fluid: incompressible
- Fluid boundary condition: adhesion on the wall
- Thermal boundary condition: imposed temperature and adiabatic walls
- Location: /validation/share/Validation/Rapports\_automatiques/Validant/Fini/Oscillating\_Flow
- Master Test case: test\_osc\_flow.data
- Generated Test cases :
  - VDF/Quick/test.data :
  - VDF/Centre/test.data :
  - VEF/Muscl/test.data :
  - VEF/EF\_stab/test.data :
  - VEF/EF\_stab02/test.data :
- Performance Chart :

	host	system	Total CPU Time	CPU time/step	number of cell
VDF/Quick/test	uruk	Linux	38.6082	0.00802455	2500
VDF/Centre/test	uruk	Linux	46.1016	0.00949475	2500
VEF/Muscl/test	uruk	Linux	3307.83	0.13387	5040
VEF/EF_stab/test	uruk	Linux	3103.26	0.127351	5040
VEF/EF_stab02/test	uruk	Linux	3098.52	0.125823	5040
Total			9594.32		

Table IV.2.2: Performance Chart

## Plot Data

### • Grashof number

As a consequence of a zero Prandtl fluid, the temperature field can be determined analytically as the time invariant of a pure conduction solution. Using the thermal boundary conditions shown above, this solution is given by the function  $T(x) = 1 - x \frac{H}{L}$ . The Grashof number (Gr) is defined by:

$$Gr = \frac{g\rho^2\beta\Delta TH^4}{L\mu^2}$$

Let us notice the presence of the factor  $H^4/L$  in the definition (and not  $L^3$ ) because the domain is rectangular. The desired value of the Grashof Number,  $3.10^4$ , is obtained by tuning the different parameters of its definition. The temperature scale  $\Delta T$  is expressed as  $\Delta T = (T_h - T_c) = 1K$  and the reference temperature is chosen such as  $T_0 = (T_h - T_c)/2 = 0.5K$ .

### • Velocity and temperature profiles

The velocity vectors are presented on Fig. 4 at the end of simulation. The profiles of the y-component of the velocity are plotted of Fig. 5 at the end of the simulation  $t = 800s$ . The profiles are presented for VDF and VEF along a horizontal profile for  $y=0.5$  (centre of the cavity) i.e.  $0 < x < 4$  and  $y=0.5$ . We can observe

that the three-cells structure of the vortices is calculated correctly for both discretization methods (VDF and VEF).

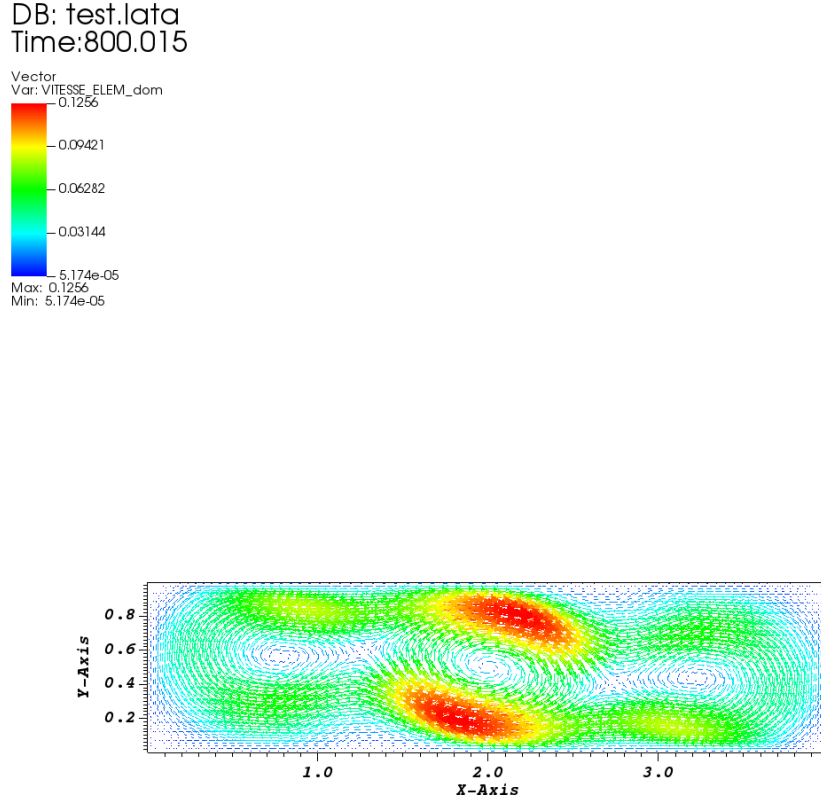


Figure IV.2.4: Velocity vectors at  $t = 800s$  for VEF mesh (Muscl)

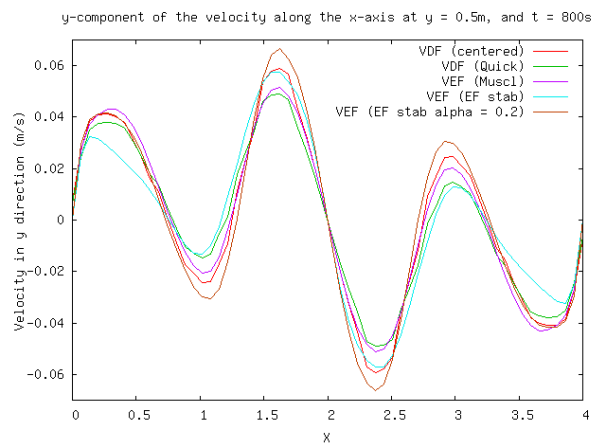
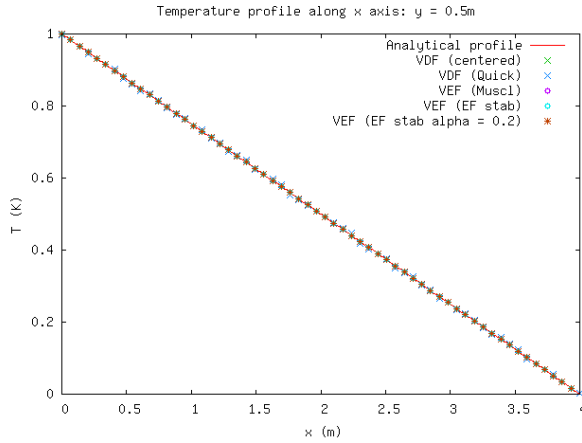


Figure IV.2.5: y-component of the velocity along the x-axis at  $y = 0.5m$ , and  $t = 800s$

All temperature profiles of TrioCFD, are superimposed to the analytical profile (see Fig. 6).

Figure IV.2.6: Temperature profile along x axis:  $y = 0.5\text{m}$ 

For a Grashof number equal to  $3.10^4$ , the flow is known to be periodic. In our case, the periodicity is well established near 300s (see Fig. 7). This time is the starting point for the calculation of the oscillation frequency.

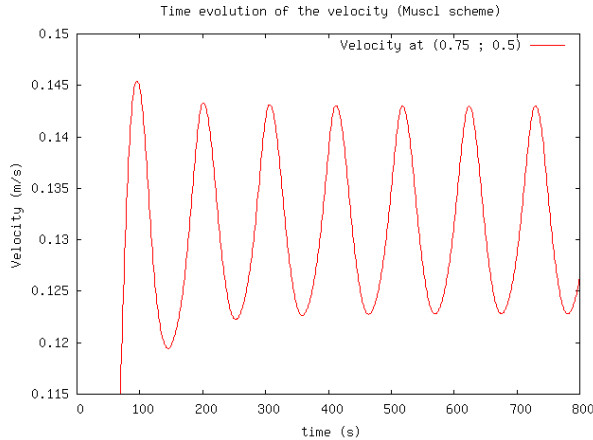


Figure IV.2.7: Time evolution of the velocity (Muscl scheme)

A comparison with the results of Behnia and Vahl Davis (in ref [1]) may be done for a non-dimensional frequency that is scaled with  $t_{ref} = H^2/\nu$ . The values of the five TrioCFD simulations are presented in Table 3, where the average frequencies are calculated in the range [300s; 800s].

	Period (s)	Non dimensional frequency	Relative error %
Behnia	105.98	17.87	0
VDF (Quick)	104.73	18.08	1.18
VDF (Centered)	106.74	17.74	0.7
VEF (Muscl)	105.75	17.91	0.22
VEF (EF_stab)	115.0	16.47	7.84
VEF (EF_stab alpha = 0.2)	108.75	17.42	2.54

Table IV.2.3: Oscillation frequency

## 2.5 Conclusion

The simulations validate the laminar fluid flow coupled with the temperature equation with Boussinesq approximation. The TrioCFD simulations are performed in 2D on VDF and VEF grids with several options of convective schemes. The results are in good agreement with those obtained by Behnia, except for the VEF scheme with the 'EF\_stab alpha=1' option. For other numerical schemes of TrioCFD, the relative errors vary from 0.22% for 'VEF/Muscl', up to 2.54% for VEF/'EF\_stab alpha = 0.2'.

- **Recommendations for users**

The results obtained with the 'EF\_stab' scheme are less good than the other ones. However the use of alpha=0.2 instead of alpha=1 improves the result significantly.

## 2.6 References

- [1] Numerical Simulation of Oscillatory Convection in Low-Pr Flow, Notes in Numerical Fluid Dynamics, A GAMM Workshop, Vol 27, Ed. Bernard ROUX, doi: 10.1007/978-3-322-87877-9, Publisher: Vieweg+Teubner Verlag, 365 p., 1990.

## 2.7 Data Files

**test**

```
# Thermohydraulique 2D VDF Boussinesq #
dimension 2
Pb_Thermohydraulique pb
Domaine dom
Mailler dom
{
    Pave Cavite
    {
        Origine 0. 0.
        Nombre_de_Noeuds 101 26
        Longueurs 4.0 1.0
        Facteurs 1.02 1.05
        Symx
        Symy
    }
    {
        Bord ENTREE X = 0. 0. <= Y <= 1.
        Bord HAUT Y = 1. 0. <= X <= 4.
        Bord BAS Y = 0. 0. <= X <= 4.
        Bord SORTIE X = 4. 0. <= Y <= 1.
    }
}
# AA #
VDF dis
Schema_Euler_Explicite sch
Read sch
{
    tinit 0.
    tmax 800.
    dt_min 0.0001
    dt_max 0.2
    dt_impr 0.001
    dt_sauv 100
```

```

seuil_statio 1.e-8
  facsec 1.0
}
# Pr = muCp/Lambda = 200 mais schema de convection therm negligible #
Associate pb dom
Associate pb sch
Discretize pb dis
Read pb
{
fluide_incompressible {
  gravite champ_uniforme 2 0 -9.81
  mu Champ_Uniforme 1 6.2304e-4
  rho Champ_Uniforme 1 1.18
  lambda Champ_Uniforme 1 2.64e-3
  Cp Champ_Uniforme 1 1000.
  beta_th Champ_Uniforme 1 3.41e-3
}
  Navier_Stokes_standard
{
  solveur_pression GCP { precond ssor { omega 1.5 } seuil 1.e-10 impr }
  convection { quick }
  diffusion { }
  sources { boussinesq_temperature { T0 0.5 } }
  conditions_initiales {
    vitesse Champ_Uniforme 2 0. 0.
  }
  boundary_conditions {
    HAUT paroi_fixe
    BAS paroi_fixe
    ENTREE paroi_fixe
    SORTIE paroi_fixe
  }
}
Convection_Diffusion_Temperature
{
  diffusion { negligable }
  convection { negligable }
  boundary_conditions {
    HAUT Paroi_adiabatique
    BAS Paroi_adiabatique
    ENTREE paroi_echange_externe_impose T_ext Champ_Front_Uniforme 1 1.00
    H_imp Champ_Front_Uniforme 1 1.e11
    SORTIE paroi_echange_externe_impose T_ext Champ_Front_Uniforme 1 0.00
    H_imp Champ_Front_Uniforme 1 1.e11
  }
  conditions_initiales { Temperature champ_fonc_xyz dom 1 1-x/4 }
}
Postraitemt
{
  Sondes
  {
    sonde_pression pression periode 1. points 1 2.00 0.5
    sonde_vitesse vitesse periode 1. points 5 0.75 0.5
      2.00 0.19
      2.00 0.5
      2.00 0.81
      3.25 0.5
    sonde_temp temperature periode 1. segment 60 0. 0.501 4. 0.501
      sonde_vite vitesse periode 1. segment 60 0. 0.501 4. 0.501
  }
}

```

```
Champs dt_post 400.0
{
    pression
    vitesse
}
format lata
Champs dt_post 400. { vitesse elem }
}
}
Solve pb
End
```

## V. Turbulent Flow

**I**N this fifth part of the document, the flow pattern changes completely compared to the two previous parts since here are considered turbulent flows. Let us remind that a flow is considered as turbulent when the Reynolds number is greater than 2000. This critical Reynolds number corresponds to the moment when the viscous forces are no longer strong enough to absorb the vortices. Fluid motion is characterized by chaotic changes in pressure and flow velocity. The flow has a whirlpool character at all points: eddies whose size, location and orientation vary constantly. Turbulent flows are therefore characterized by a very disordered appearance, behavior that is difficult to predict, and the existence of numerous space and time scales.

In this version of the report, two cases are studied:

- Turbulent flow in a 2D diffuser with the  $k - \epsilon$  model
- Mixing length in 2D and 3D VEF-plane channel

This part will be enriched in a following version with, in particular, a case in 3D.



## Turbulent flow in a 2D diffuser with the $k - \epsilon$ model

### 1.1 Purpose

This test case aims at validating TrioCFD for a turbulent flow inside a two-dimensional diffuser with the  $k - \epsilon$  model and wall functions. The validation are carried out by comparing experimental data and several computational profiles. Experimental results are taken from the ERCOFTAC experiment data base and the CFD profiles are obtained from Fluent and other publications that are listed below. For the test case, the diffuser mesh is generated with ICEM and a fictitious periodic rectangular box is used to provide boundary conditions for the main computational domain (the diffuser). Two different meshes are generated for the periodic box. The goal of the fictitious periodic box is to provide well established values of velocity and  $k - \epsilon$  at the inlet boundary conditions of the diffuser. There are two main computations with TrioCFD in this test case since there are two periodic boxes.

Validation made by : A.AUROUSSEAU (S.VANDROUX).

Report generated 09/06/2023.

### 1.2 Problem Description

#### Geometry

The diffuser geometry is presented on Fig. 1. All dimensions are expressed by a factor  $H$  which is equal to  $H = 1\text{m}$ .

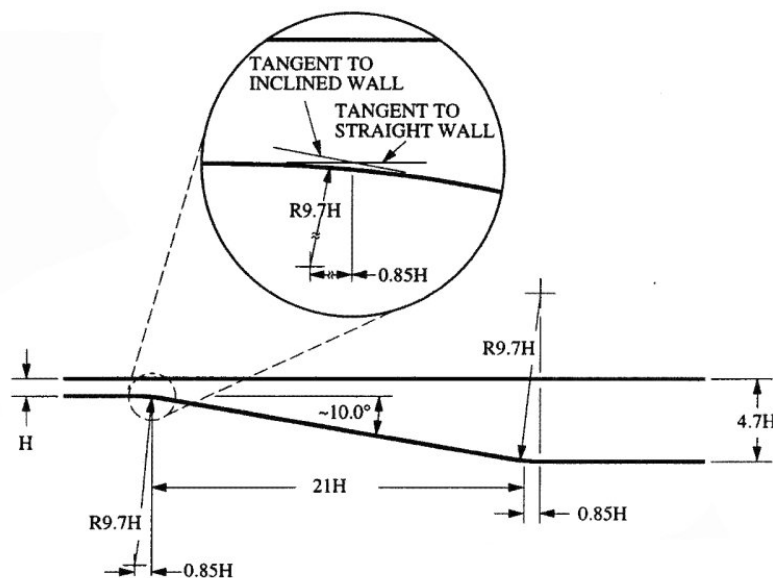


Figure V.1.1: Diffuser geometry.

## Initial Conditions and Boundary Conditions

- **Modeling: use of a periodic box**

A periodic rectangular box is introduced for computations on a fictitious periodic domain. That plane channel is used to generate an established velocity and  $k - \epsilon$  fields in order to be applied at the inlet of the diffuser (i.e. the main computational domain). Boundary conditions are imposed separately for the periodic box and the main computational domain. For the rectangular box, the periodicity is applied in the  $x$ -direction, and no-slip boundary conditions hold in the  $y$ -direction. For the diffuser, the values of the periodic box are applied for the  $k - \epsilon$  fields and the velocity at inlet and an uniform pressure is applied at outlet. All other boundaries are no-slip conditions. The numerical values of bulk velocity and outlet pressure are given below:

- Velocity inlet:  $U = 1$  m/s
- Outlet pressure:  $P = 0$

## Fluid Properties

Fluid domain: Fictitious fluid for which  $Re = 20000$ .

	Valeur
Fluid density $\rho$ (kg/m <sup>3</sup> )	5.7e-05
Fluid dynamic viscosity $\mu$ (Pa.s)	1.0

Table V.1.1: Physical properties

## Flow Physics

The objective is to validate the ' $k - \epsilon$  model' with wall function inside a diffuser.

### 1.3 Case Setup

#### Grid

Three meshes are presented: two for the periodic box and one additional for the diffuser. The fine mesh of periodic box is presented on Fig. 2 (1104 cells) and the coarse one is presented on Fig.3 (440 cells). For both meshes the dimensions are  $[-16, -11] \times [3.7, 4.7]$ . The diffuser mesh is presented on Fig. 4 where  $x$  varies between 0 and 20. For the actual dimension of the diffuser,  $x$  varies between  $[-11, 56]$ .

Mesh: Extruder en 3 of the inlet face of 3D ICEM mesh

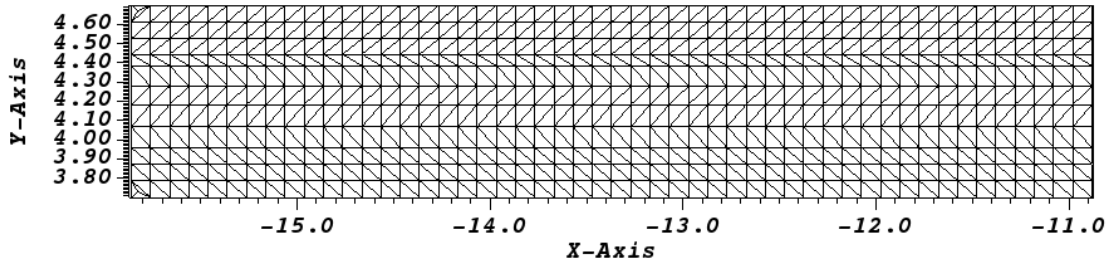


Figure V.1.2: Periodic box: mesh 1 (1104 cells)

Mesh: Extruder\_bord of the inlet face of 3D ICEM mesh

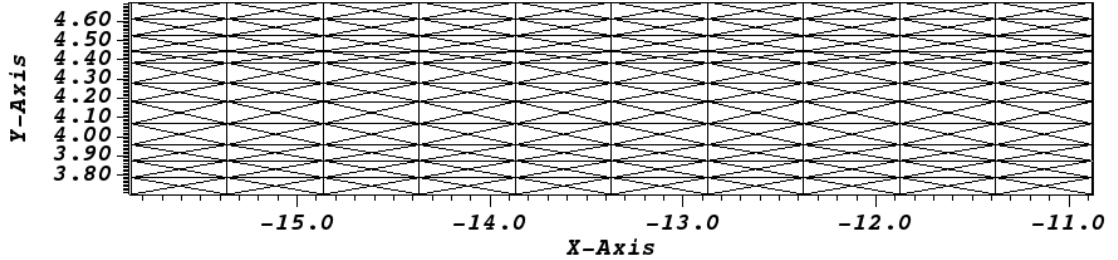


Figure V.1.3: Periodic box: mesh 2 (440 cells)

Mesh: 2D from 3D of ICEM mesh. This figure only shows the divergent part of the diffuser, but the actual domain lies between  $x=-10$  and  $x=56$ .

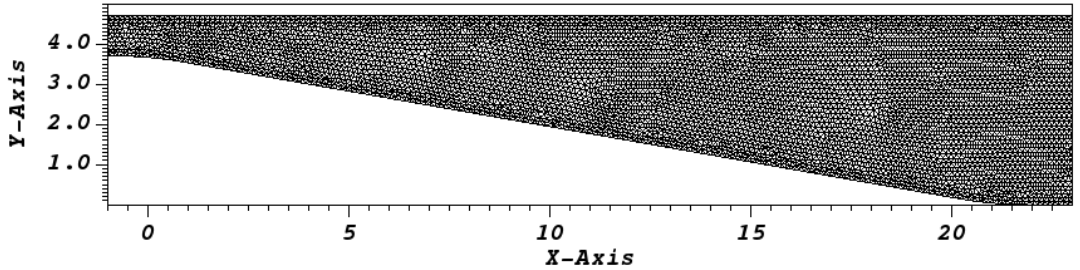


Figure V.1.4: Diffuser Mesh (36644 cells)

## Model Options

The Reichardt law is applied near the wall boundary and without gravity effect for this test.

## Other Options (calculation)

The 'EF\_stab' scheme is applied for convective terms with 'alpha=0.2'. The time scheme is implicit. All numerical options are summarized in Section 4.1.

## 1.4 Results

### Validation Specific Informations

- Version TRUST : 1.6.3
- Type of problem : Hydraulique\_Turbulent
- Diffusion scheme : Default{}
- Discretization : VEFPreP1B (ICEM mesh with prisms layer at walls). Two meshes for the periodic box have been generated: one with the extrudeBord keyword, the other one with extruder\_en3.
- Time scheme : Euler\_implicit - Solveur Implicit
- Solving of equations : Navier Stokes turbulent

- Convection : EF\_stab { alpha 0.2 }
- Turbulence model : k- $\epsilon$  model
- Wall law : turbulence\_paroi loi\_expert\_hydr { methode\_calcul\_face\_keps\_impose que\_les\_faces\_des\_elts\_dirichlet }, which is the default option for 3D calculations
- Type of boundary conditions : Periodic box: periodicity in the  $x$ -direction, walls in the  $y$ -direction. Main computation domain (diffuser): Velocity field and  $k - \epsilon$  field (from periodic box) for the inlet, outlet pressure, walls.
- Location : /validation/share/Validation/Rapports\_automatiques/Validant/Fini/OBI\_diffuser\_VEF\_k\_eps
- Master Test case : Calcul.data - Prepare\_extract.data - Prepare\_extrude.data
- Generated Test cases :
  - Calcul\_fin/Calcul.data : /\*see data set in the appendix\*/
  - Calcul\_gros/Calcul.data :
- Performance Chart :

	host	system	Total CPU Time	CPU time/step	number of cell
Calcul_fin/Calcul	uruk	Linux	8509.83	30.9175	36644
Calcul_gros/Calcul	uruk	Linux	8173.02	30.6927	36644
Total			16682.8		

Table V.1.2: Performance Chart

## Plot Data

The next two figures (Figs 5 and 6) show the computations convergence by plotting the evolution of friction velocity versus time for both periodic meshes. The two curves on both figures show the friction evolution in the periodic box computation (red curve) and in the main computation (green curve). The two domains are different so the friction velocity is computed on different surfaces, Reynolds numbers are different, and the ways the friction velocity is averaged are different too. That is why the values of  $U_\tau$  are different. For both meshes, the main computation reaches convergence after about 250s of physical time, and the periodic computation after 75s. The periodic computation stops around 200s since the convergence criteria (seuil\_statio) is met.

Main computation values are increased on purpose to allow plotting both curves on the same figure

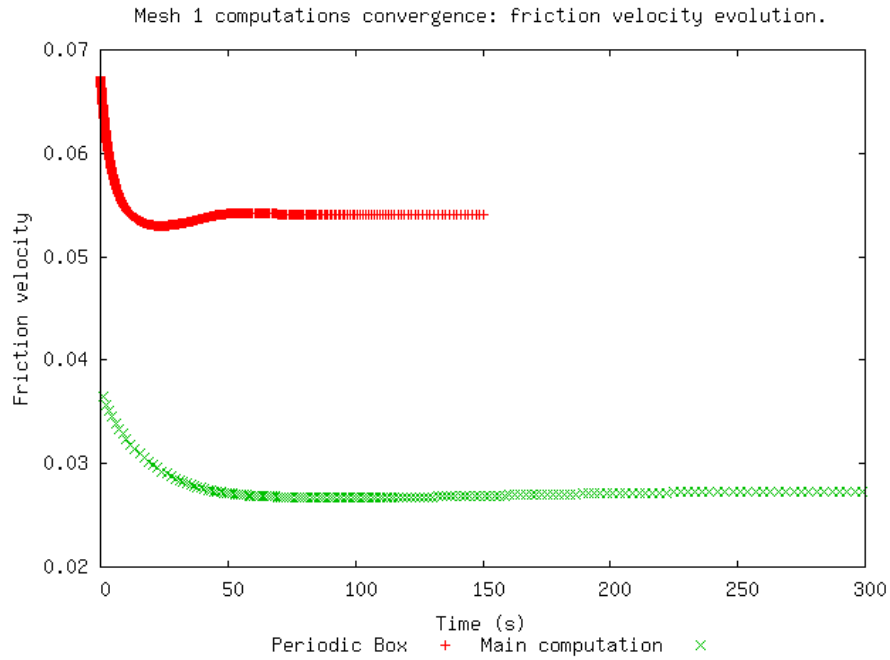


Figure V.1.5: Mesh 1 computations convergence: friction velocity evolution.

The convergence criteria on the periodic computation is met after 200s

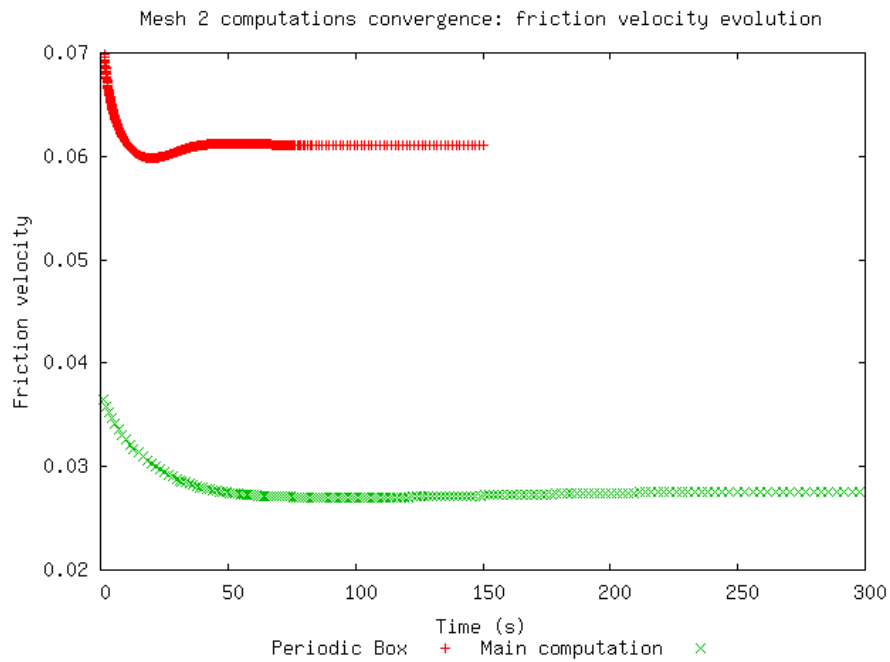


Figure V.1.6: Mesh 2 computations convergence: friction velocity evolution

- Fields of pressure, velocity and  $Y^+$

For each periodic mesh, the pressure field in the diffuser is presented on Figs. 8 and 9 (Fig. 7 is for the color scale) the velocity field in the diffuser is presented on Figs. 11 and 12 (Fig. 10 for the color scale). Finally the  $Y^+$  fields are presented on Figs. 14 and 15 (color scale on Fig. 13).

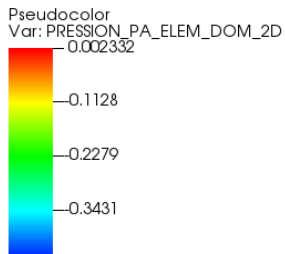


Figure V.1.7: Pressure field in the diffuser, Legend

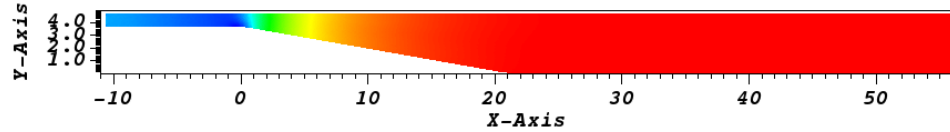


Figure V.1.8: Pressure field in the diffuser, mesh1.

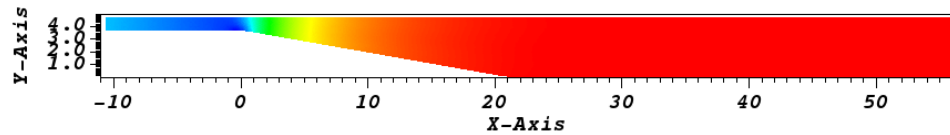


Figure V.1.9: Pressure field in the diffuser, mesh2.

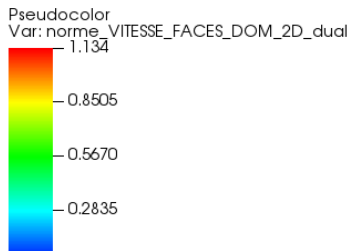


Figure V.1.10: Velocity field in the diffuser, Legend.

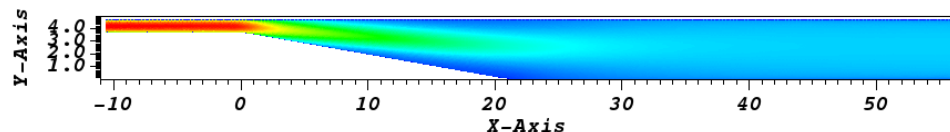


Figure V.1.11: Velocity field in the diffuser, mesh 1.

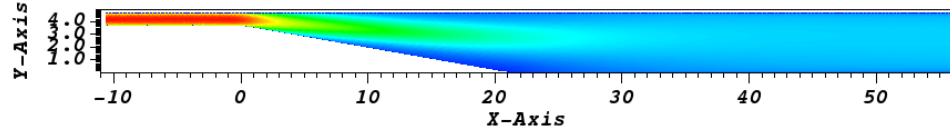
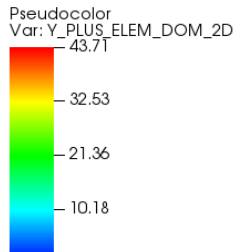
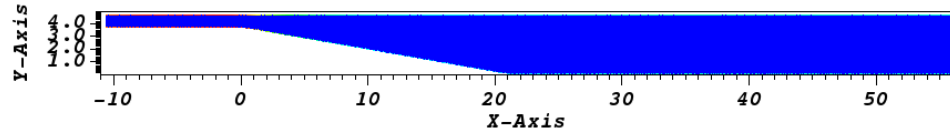
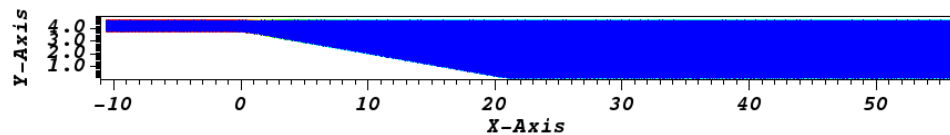
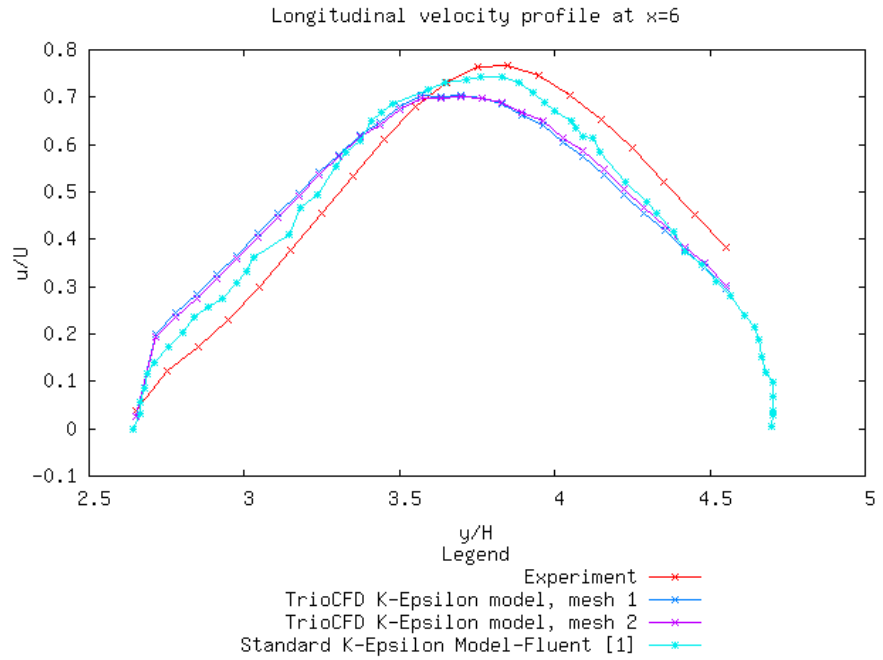
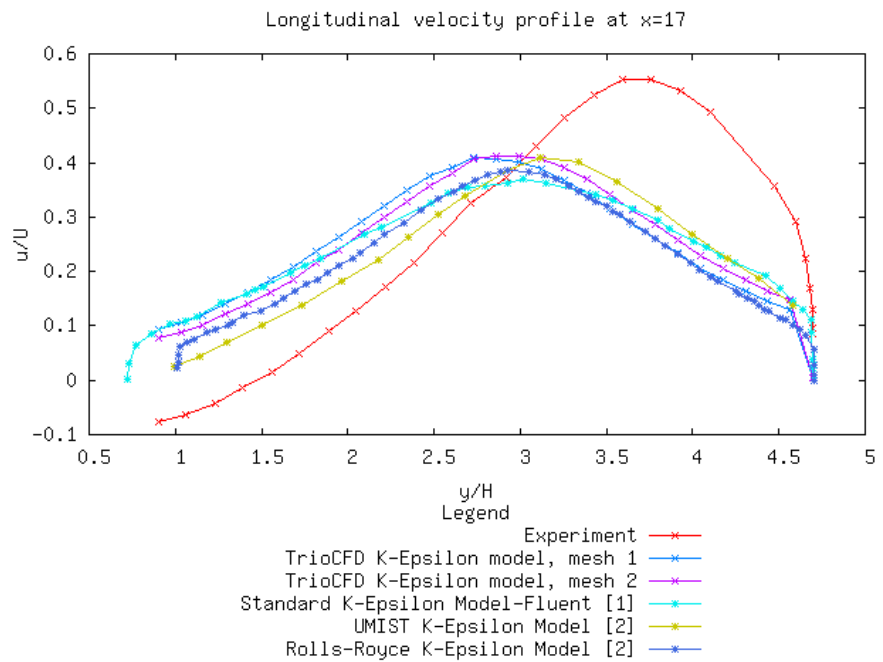


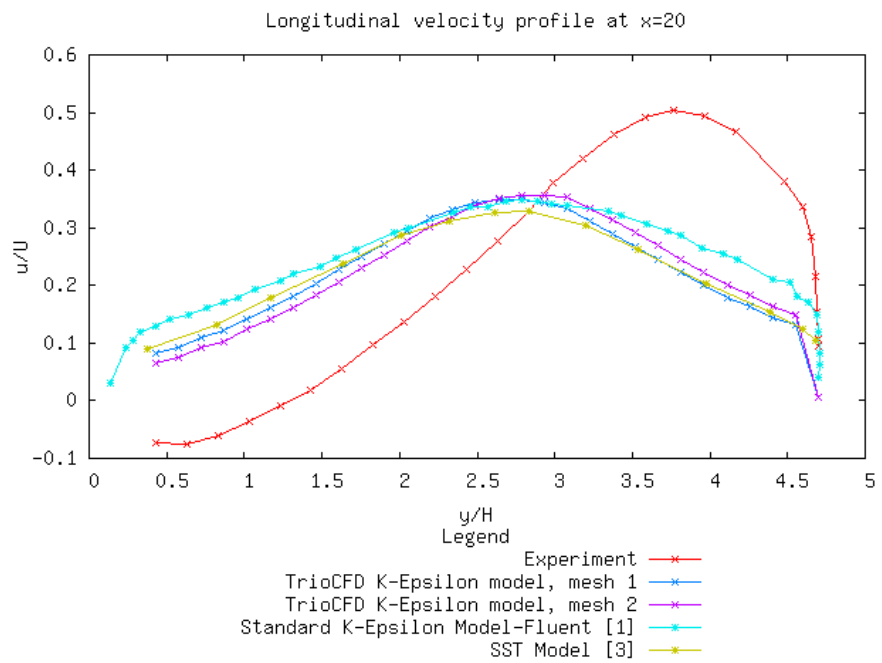
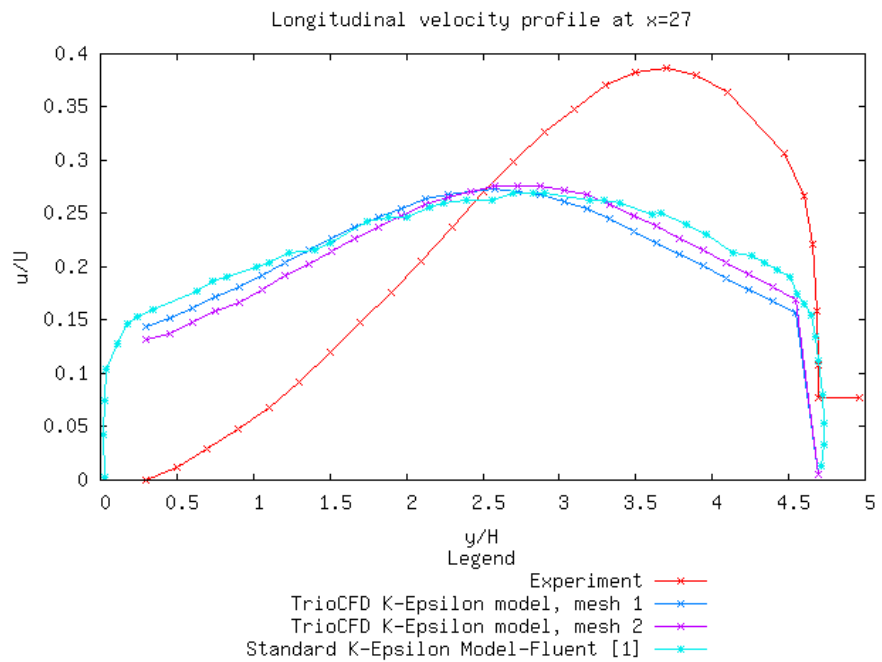
Figure V.1.12: Velocity field in the diffuser, mesh 2.

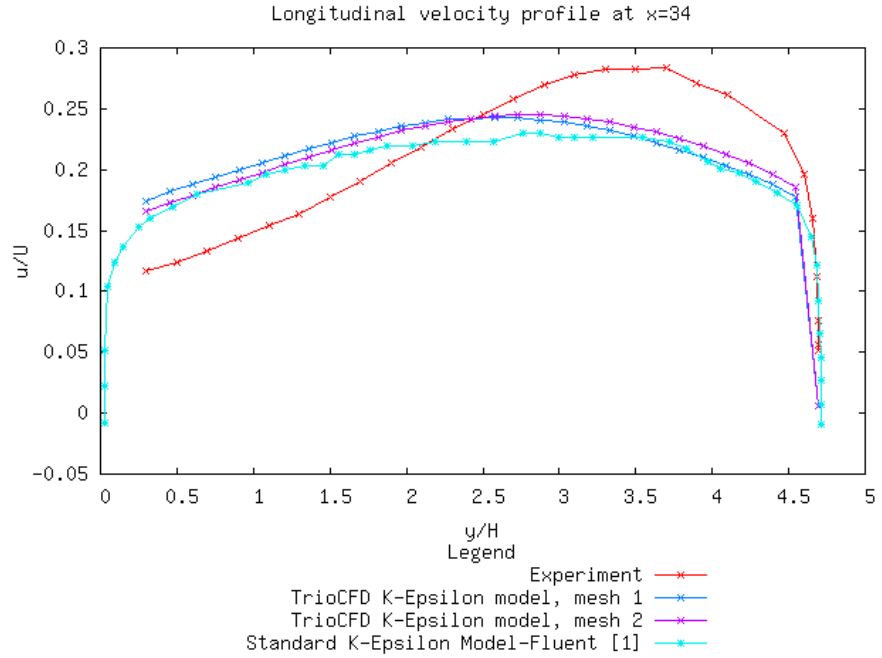
Figure V.1.13:  $Y^+$  field in the diffuser, Legend.Figure V.1.14:  $Y^+$  field in the diffuser, mesh1.Figure V.1.15:  $Y^+$  field in the diffuser, mesh2.

- Comparisons of TrioCFD profiles

The  $y$ -profiles of velocity are compared at several  $x$ -positions in the diffuser. The position  $x = 0$  corresponds to the point where the divergent part of the diffuser begins. The position  $x = 20$  is the end of the divergent part. Beyond this point, the domain is a plane channel. The  $y$ -profiles are presented for  $x = 6$  (Fig. 16),  $x = 17$  (Fig. 17),  $x = 20$  (Fig. 18),  $x = 27$  (Fig. 19) and  $x = 34$  (Fig. 20). For those graphs, the red curve is the experimental one and the cyan curve is the 'standard  $k - \epsilon$  model of Fluent'. The TrioCFD results are colored in blue (mesh 1) and magenta (mesh2).

Figure V.1.16: Longitudinal velocity profile at  $x=6$ Figure V.1.17: Longitudinal velocity profile at  $x=17$

Figure V.1.18: Longitudinal velocity profile at  $x=20$ Figure V.1.19: Longitudinal velocity profile at  $x=27$

Figure V.1.20: Longitudinal velocity profile at  $x=34$ 

## 1.5 Conclusion

- The pressure fields that are obtained by both meshes are similar. There is a low pressure zone at the beginning of the diffuser divergent part. The velocity fields are also similar in both computations. The divergent part of the diffuser is a low velocity zone.
- Comparisons of several  $y$ -profiles of velocity are carried out between 1) the  $k - \epsilon$  model of TrioCFD, 2) the 'Standard  $k - \epsilon$  model' of Fluent and 3) the experimental results from Ercoftac experiment. For few  $x$  values, other results are also available in the literature and used for comparisons.

At  $x=6$  (beginning of the divergent part), the profiles are relatively similar. The Fluent results are slightly closest to the experimental curve. This experimental profile is a little shifted toward larger  $y/H$  values. The computational curves are closest to the experimental one for that  $x$ -position. For other velocity profiles (larger  $x$  values: 17, 20, 27 and 34) all computational results are relatively similar but far from the experimental results. The experimental profiles are not symmetric, whereas the CFD profiles have a near symmetrical behavior.

- We note that the TrioCFD profiles are very close to each other, showing that the method used to generate the periodic mesh has a little influence on the final computation results. In conclusion, it is well-known that the  $k - \epsilon$  model of turbulence yields bad results for such a configuration, the TrioCFD results are not an exception and give similar results. A more promising  $k - \epsilon$  model, better suited for simulating this type of phenomenon will be proposed in a future version of this validation sheet.

## 1.6 References

- [1] A Comparative Study of Turbulence Models Performance for Turbulent Flow in a Planar Asymmetric Diffuser, Samy M. El-Behery and Mofreh H. Hamed. International Journal of Aerospace and Mechanical Engineering 5:2 2001.
- [2] Advanced Turbulence Modelling of Separated Flow in a Diffuser, D.D Apsley and M.A Leschziner. Flow, Turbulence and Combustion 63:81-112,1999.

- [3] Ten Years of Industrial Experience with the SST Turbulence Model, F.R Menter and M. Kuntz and R. Langtry. Turbulence, Heat and Mass Transfer 4. K. Hanjalic, Y. Nagano and M. Tummers (Editors), Begell House, Inc. 2003.

## 1.7 Data Files

### Calcul

```
# Hydraulique 3 #
# lance_test 3 ecart #
dimension 3
Domaine DOM_DOM
Read_unsupported_ASCII_file_from_ICEM DOM_DOM trio_DOM_geo.asc
Domaine DOM_2D
Extract_2D_from_3D DOM_DOM left DOM_2D
dimension 2
Pb_Hydraulique_Turbulent pb
VerifierCoin DOM_2D { }
Ecrire_fichier DOM_2D OBI_2D.geom
VEFPreP1B dis
Read dis { P0 P1 Changement_de_base_P1bulle 1 Modif_div_face_dirichlet 1 }
Schema_Euler_implicite sch
Read sch
{
  tinit 0.0
  tmax 600.
  dt_min 1.e-10
  dt_max 3.0
  dt_impr 1.0
  dt_sauv 1000.
  seuil_statio 1.e-8
  facsec 50.
  facsec_max 2000
  periode_sauvegarde_securite_en_heures 5
  solveur implicite
  {
    seuil_convergence_solveur 1.e-12
    solveur gmres { diag seuil 1.e-12 impr controle_residu 1 }
  }
}
Associate pb DOM_2D
Associate pb sch
Discretize pb dis
Read pb
{
  fluide_incompressible {
    mu Champ_Uniforme 1 5.7e-5
    rho Champ_Uniforme 1 1.
  }
  Navier_Stokes_Turbulent
  {
    solveur_pression Cholesky { }
    convection { EF_stab { alpha 0.2 } }
    diffusion { }
    conditions_initiales {
      vitesse Champ_Uniforme 2 1. 0.
    }
  }
  boundary_conditions
  {
    in frontiere_ouverte_vitesse_imposee champ_front_recyclage { pb_champ_evaluateur pb
  }
}
```

```

        moyenne_imposee connexion_approchee fichier FICHIER_V_PREPARE
        ampli_moyenne_imposee 2 1. 1.
        ampli_moyenne_recyclee 2 0. 0.
        ampli_fluctuation 2 0. 0. }
out      frontiere_ouverte_pression_imposee champ_front_Uniforme 1 0.
wall     paroi_fixe
}
modele_turbulence K_Epsilon
{
    Transport_K_Epsilon
    {
        convection { EF_stab { alpha 0.2 } }
        diffusion { }
        boundary_conditions
        {
            in frontiere_ouverte_K_eps_impose champ_front_recyclage { pb_champ_evaluate
                moyenne_imposee connexion_approchee fichier FICHIER_K_PREPARE
                ampli_moyenne_imposee 2 1. 1.
                ampli_moyenne_recyclee 2 0. 0.
                ampli_fluctuation 2 0. 0. }
            out frontiere_ouverte K_EPS_EXT Champ_Front_Uniforme 2 0.125e-2 0.492e-2
                wall paroi
            }
        conditions_initiales
        {
            k_Eps Champ_Uniforme 2 1.6e-7 1.6e-8
        }
    }
    turbulence_paroi loi_expert_hydr { methode_calcul_face_keps_impose que_les_faces_des_elt
    }
}
Traitement_particulier { Canal
{
    dt_impr_moy_spat 50.
}
}
Postraitemetn
{
    Sondes
    {
        sonde_V03 vitesse periode 0.01 segment 30   3. 3.25 3. 4.55
        sonde_V06 vitesse periode 0.01 segment 30   6. 2.65 6. 4.55
        sonde_V14 vitesse periode 0.01 segment 30  14. 1.50 14. 4.698
        sonde_V17 vitesse periode 0.01 segment 30  17. 0.90 17. 4.698
        sonde_V21 vitesse periode 0.01 segment 30  20. 0.43 20. 4.698
        sonde_V24 vitesse periode 0.01 segment 30  24. 0.30 24. 4.698
        sonde_V27 vitesse periode 0.01 segment 30  27. 0.30 27. 4.698
        sonde_V30 vitesse periode 0.01 segment 30  30. 0.30 30. 4.698
        sonde_V34 vitesse periode 0.01 segment 30  34. 0.30 34. 4.698
    }
}
Format lata
Champs binaire dt_post 100.
{
    pression_pa elem
    vitesse faces
    k elem
    eps elem
    viscosite_turbulente elem
    y_plus elem
}
}
```

```
Sauvegarde binaire OBI.sauv
}
Solve pb
End
```

## Mixing length in 2D and 3D VEF-plane channel

### 2.1 Purpose

The purpose is to validate one particular model of turbulence in TrioCFD, the 'mixing length' model. Comparisons are carried out in two and three dimensions with the analytical law of Reichardt [1] on several VEF meshes. The system is a plane channel in 2D and a parallelepipedal box in 3D, with periodic boundary conditions except in  $y$ -direction. The wall function of Reichardt is applied for the TrioCFD computations. The relative errors of the  $Re_\tau$  number are given for two values of the  $Re_b$  number, where the reference is obtained from the Dean's correlation. The comparisons are also carried out with TrioCFD simulations with the  $k - \epsilon$  model.

Validation made by : R. PAILLE.

Report generated 09/06/2023.

### 2.2 Problem Description

#### Geometry

The geometry is a two-dimensional plane channel of dimensions  $L_y = h = 2$ ,  $L_x = 0.2$  or  $0.8$ . For three-dimensional simulations, the geometry is a parallelepipedal box of same dimensions with  $L_z = L_x$ .

#### Initial Conditions and Boundary Conditions

A non-null velocity  $U_x=10$  is initialized inside the domain. Periodic boundary conditions are applied in  $x$ - and  $z$ -directions and no-slip boundary conditions are applied on top and bottom  $y$ -walls. A source term is added in order to maintain a constant flow.

#### Fluid Properties

##### Incompressible case:

The fluid is incompressible of constant density  $\rho = 1$ . Two values of viscosity are used for simulations:  $\mu = 0.001$  or  $0.0001$  such as  $Re_b = (U_b l)/\nu = 10\ 000$  or  $100\ 000$  where  $l = 1$  is the half-height  $h/2$ .

### 2.3 Case Setup

#### Grid

Four VEF meshes are used for the simulations: two 2D meshes (Figs 1 and 2) with option 'trianguler\_fin' and two 3D meshes (Fig 3 and 4) with option 'tetraedriser\_homogene\_fin' (3D). The number of cells are  $N_y = 6 - 11 - 21 - 41$ , and  $N_x = N_z = 3$  with options 'trianguler\_fin' (2D) or 'tetraedriser\_homogene\_fin' (3D)

Canal\_perio { bord periox }

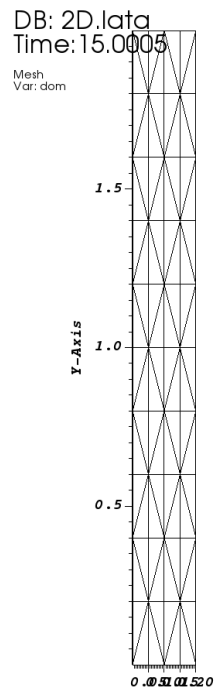


Figure V.2.1: 3 x 6 in 2D geometry

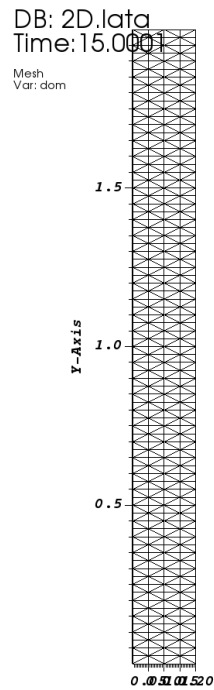
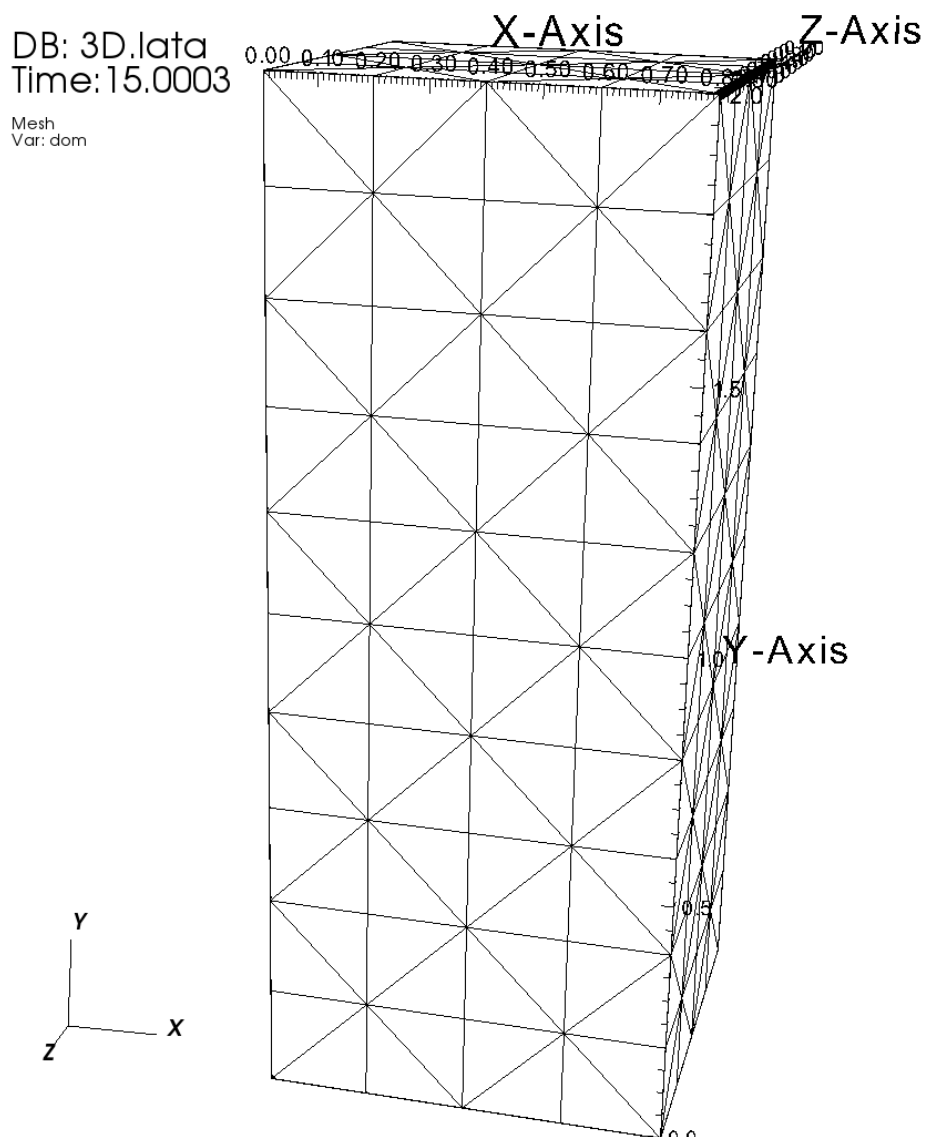


Figure V.2.2: 3 x 41 in 2D geometry

Figure V.2.3:  $3 \times 6 \times 3$  in 3D geometry

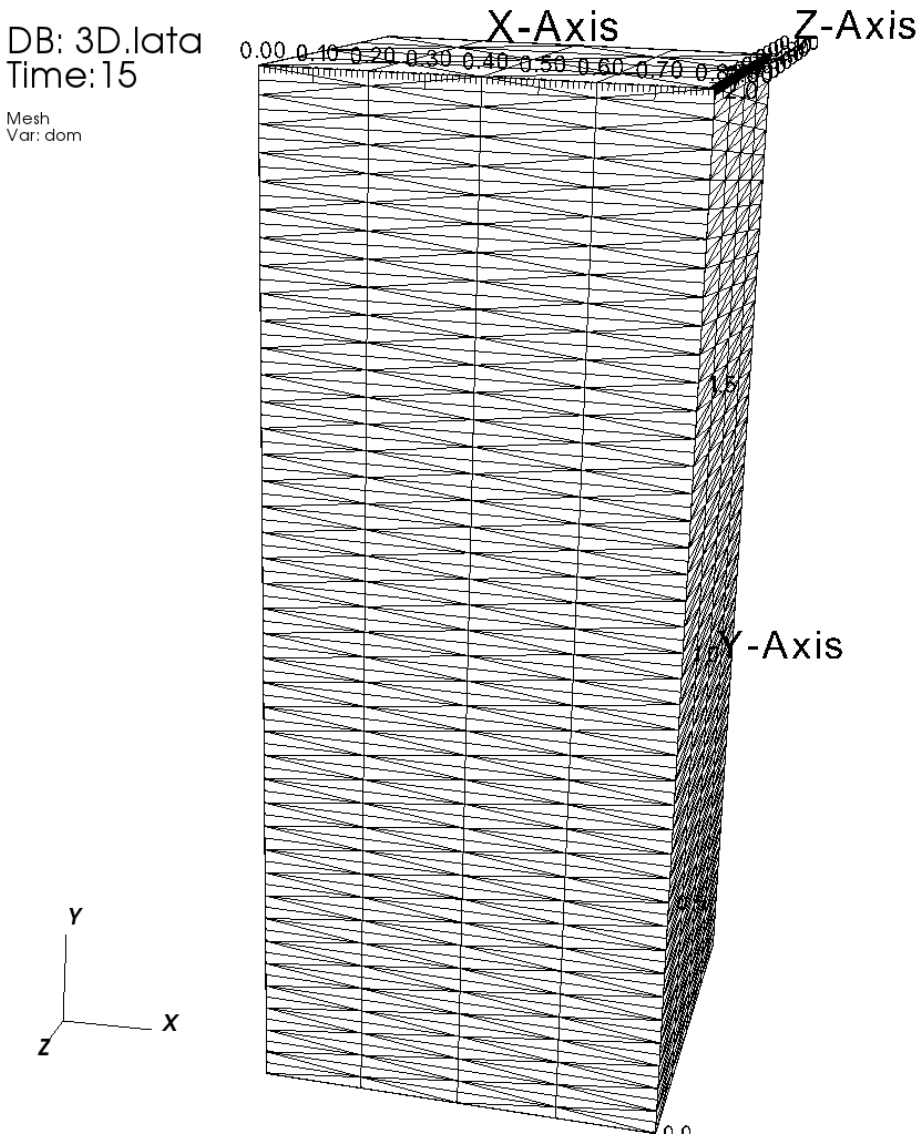


Figure V.2.4: 3 x 41 x 6 in 3D geometry

### Model Options

The 'mixing length' model of turbulence is applied inside a double-periodic plane channel. The flow is forced by adding a source term in the impulsion balance equation.

### Other Options (calculation)

The convection scheme is 'EF\_stab'. All other numerical options are summarized in section 4.1.

## 2.4 Results

### Validation Specific Informations

- Version TRUST : 1.5.5
- Type of problem : Hydraulique\_Turbulent

- Diffusion scheme : Default{}
- Discretization : VEFPreP1B
- Time scheme : Euler\_explícite (fac\_sec 0.9)
- Solving of equations : Navier Stokes turbulent with Modele\_turbulence Longueur\_melange
- Solving of equations : Turbulence\_paroi\_loi\_standard\_hydr (new ones)
- Convection : EF\_stab
- Turbulence model : Mixing Length (compared with k- $\epsilon$ )
- Type of boundary conditions : Periodicity in x (and z for 3D) direction, wall for y boundaries
- Location: /validation/share/Validation/Rapports\_automatiques/Validant/Fini/Mixing\_length\_VEF\_WF
- Master Test case: 2D.data - 3D.data - 3D\_keps.data
- Generated Test cases :
  - 2D\_100000\_11/2D.data :
  - 2D\_100000\_21/2D.data :
  - 2D\_100000\_41/2D.data :
  - 2D\_100000\_6/2D.data :
  - 2D\_10000\_11/2D.data :
  - 2D\_10000\_21/2D.data :
  - 2D\_10000\_41/2D.data :
  - 2D\_10000\_6/2D.data : /\*\*
  - 3D\_11/3D.data :
  - 3D\_21/3D.data :
  - 3D\_21\_keps/3D\_keps.data :
  - 3D\_41/3D.data :
  - 3D\_6/3D.data : /\*\*
  - 3D\_6\_keps/3D\_keps.data : /\*\*
- Performance Chart :

	host	system	Total CPU Time	CPU time/step	number of cell
2D_100000_11/2D	uruk	Linux	19.0181	0.000965311	160
2D_100000_21/2D	uruk	Linux	29.8542	0.00121955	320
2D_100000_41/2D	uruk	Linux	113.673	0.00256012	640
2D_100000_6/2D	uruk	Linux	22.0524	0.00116153	80
2D_10000_11/2D	uruk	Linux	32.9883	0.0014558	160
2D_10000_21/2D	uruk	Linux	40.3121	0.00138719	320
2D_10000_41/2D	uruk	Linux	131.991	0.00253369	640
2D_10000_6/2D	uruk	Linux	34.7054	0.00161957	80
3D_11/3D	uruk	Linux	138.88	0.00832625	1920
3D_21/3D	uruk	Linux	670.003	0.020684	3840
3D_21_keps/3D_keps	uruk	Linux	1262.72	0.0430123	3840

	host	system	Total CPU Time	CPU time/step	number of cell
3D_41/3D	uruk	Linux	22107.6	0.196102	7680
3D_6/3D	uruk	Linux	69.7508	0.00418008	960
3D_6_keps/3D_keps	uruk	Linux	127.163	0.00762297	960
Total			24800.7		

Table V.2.1: Performance Chart

### Plot Data

- **2D results for  $Re_b = 10^4$**

The  $Re_\tau$  number of TrioCFD is compared to the Dean's correlation ( $Re_\tau = 0.175(Re_b)^{7/8}$ ) for two values of  $Re_b$ . For 2D simulations the relative errors are given in Table 2 for  $Re_b = 10^4$  and Table 3 for  $Re_b = 10^5$ . For  $Re_b = 10^4$  the velocity profiles along the  $y$ -direction are presented on Fig. 5 for four values of  $N_y$  and the comparison with the Reichardt analytical solution (red line) is presented on a graph  $U+$  with respect to  $y+$  in logscale (Fig. 6). The  $y$ -profile of  $\nu_t$  is presented on Fig. 7.

	Ny	y+	$Re_\tau$	Relative error
Theoretical(*)		554.7		
6	56.0	559.9	0.9	
11	28.2	563.5	1.6	
21	14.1	564.1	1.7	
41	6.6	524.7	5.4	

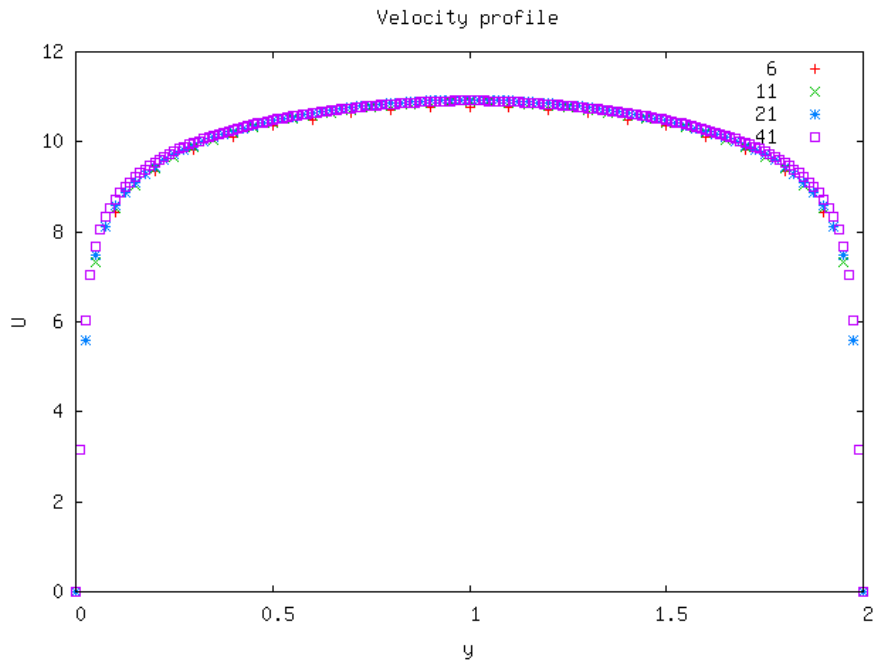
Table V.2.2: 2D -  $Re_b = 10000$ 

Figure V.2.5: Velocity profile

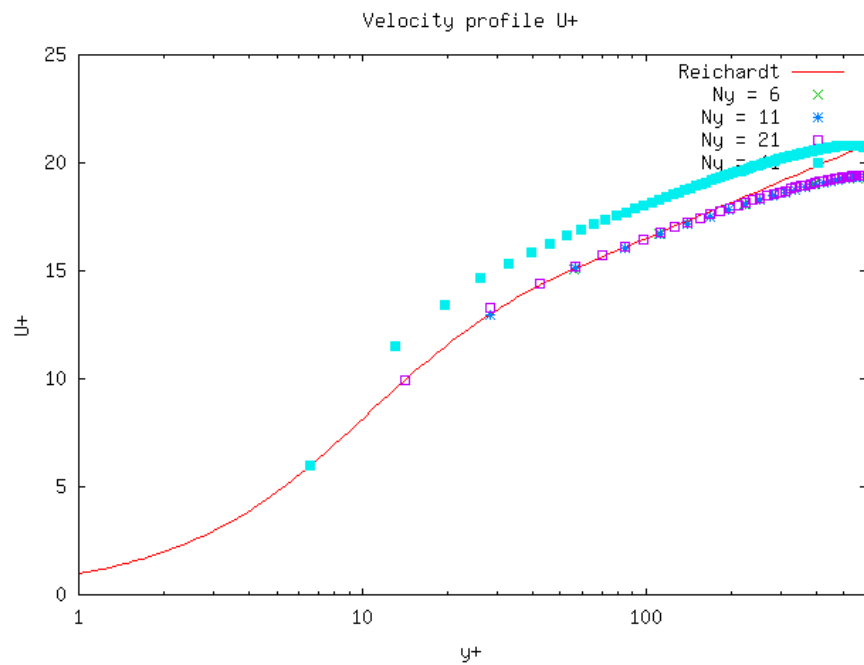
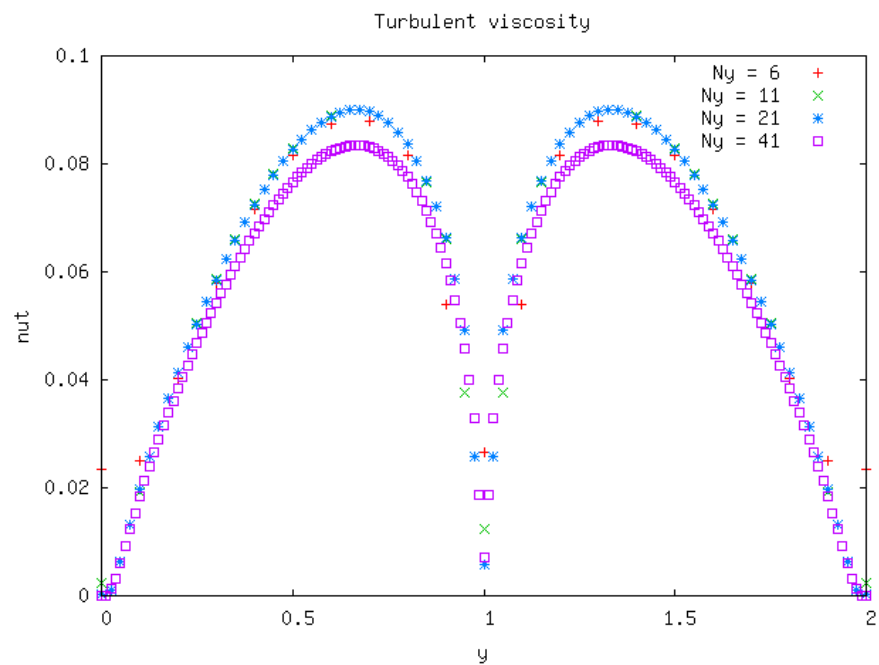
Figure V.2.6: Velocity profile  $U^+$ 

Figure V.2.7: Turbulent viscosity

- **2D results for  $Re_b = 10^5$**

For the two-dimensional simulation with  $Re_b = 10^5$ , the relative errors on the  $Re_\tau$  number (still compared to the Dean's correlation) are given in Table 3 and the same graphs are presented respectively on Fig. 8 for  $U$ , on Fig. 9 for  $U+$  and Fig. 10 for  $\nu_t$ . The Reichardt law is compared on Fig. 9.

	Ny	$y+$	$Re_\tau$	Relative error
Theoretical(*)			4159.4	
6	439.9	4399.4	5.8	
11	220.3	4406.4	5.9	
21	110.3	4413.0	6.1	
41	55.2	4414.8	6.1	

Table V.2.3: 2D -  $Re_b = 10^5$

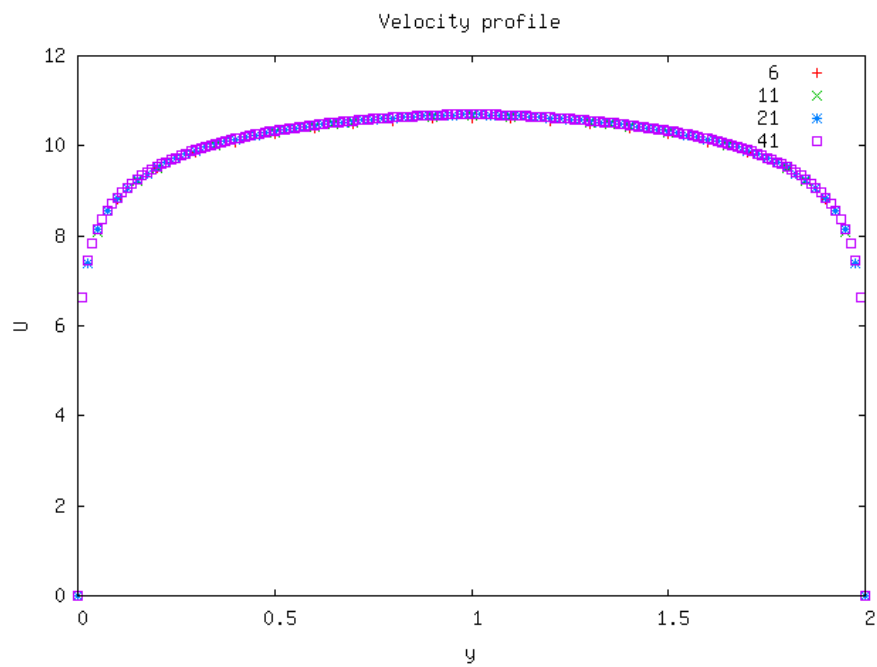


Figure V.2.8: Velocity profile

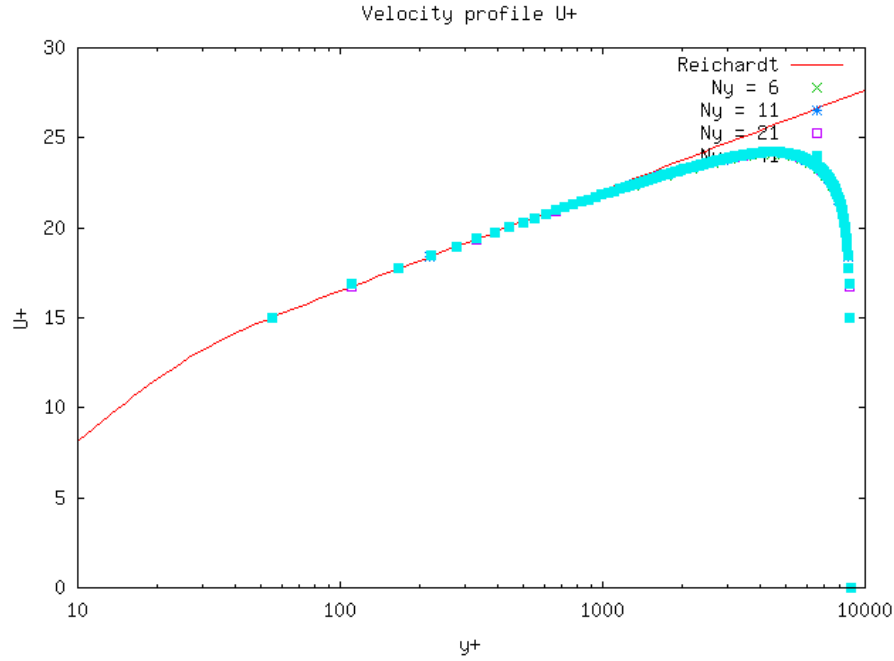
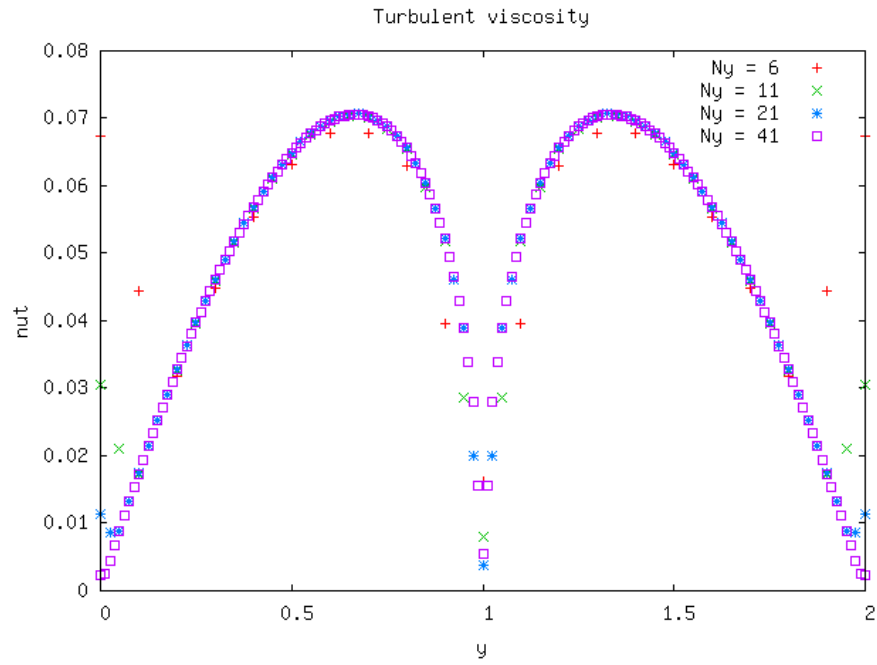
Figure V.2.9: Velocity profile  $U+$ 

Figure V.2.10: Turbulent viscosity

- **3D results for  $Re_b = 10^5$**

For 3D simulation, the relative errors are given in Table 4 for  $Re_b = 10^5$ . The profiles of  $U$ ,  $U+$  and  $\nu_t$  are presented on Figs 11, 12 and 13. For the same physical quantities, three additional graphs appear for comparing the TrioCFD profiles of 'Mixing length'-model and ' $k - \epsilon$ '-model for several meshes (Figs 14, 15 and 16).

Ny	y+	$Re_\tau$	Relative error
Theoretical(*)		4159.4	
6	313.1	4696.2	12.9
11	157.1	4711.6	13.3
21	77.4	4645.7	11.7
41	38.1	4571.4	9.9
6keps	286.2	4292.9	3.2
21keps	70.3	4215.4	1.3

Table V.2.4: 3D - Reb = 100 000

NB : The use of 'tetraedriser\_homogene mesh' for Ny=21 and k-eps model leads to higher relative error

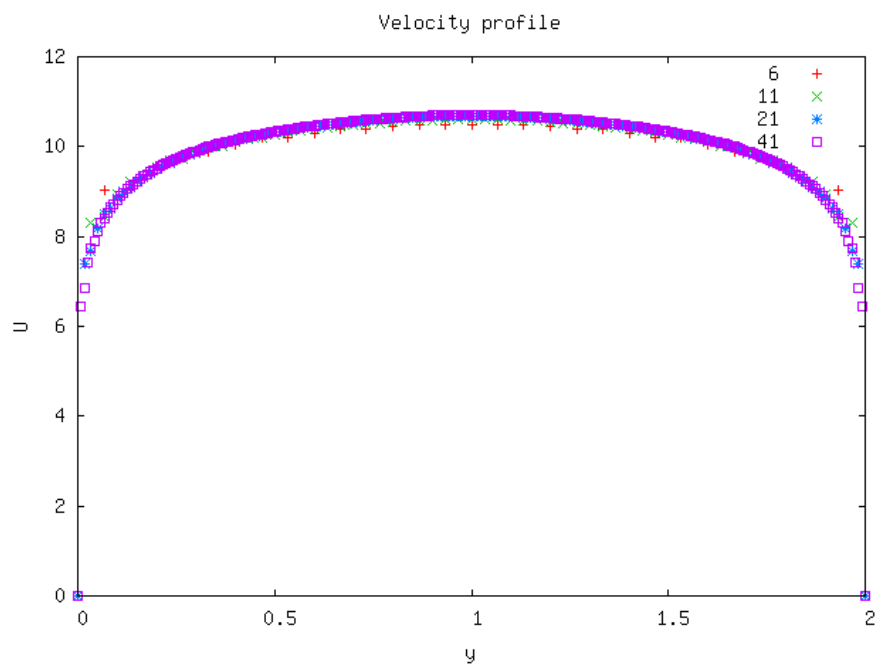


Figure V.2.11: Velocity profile

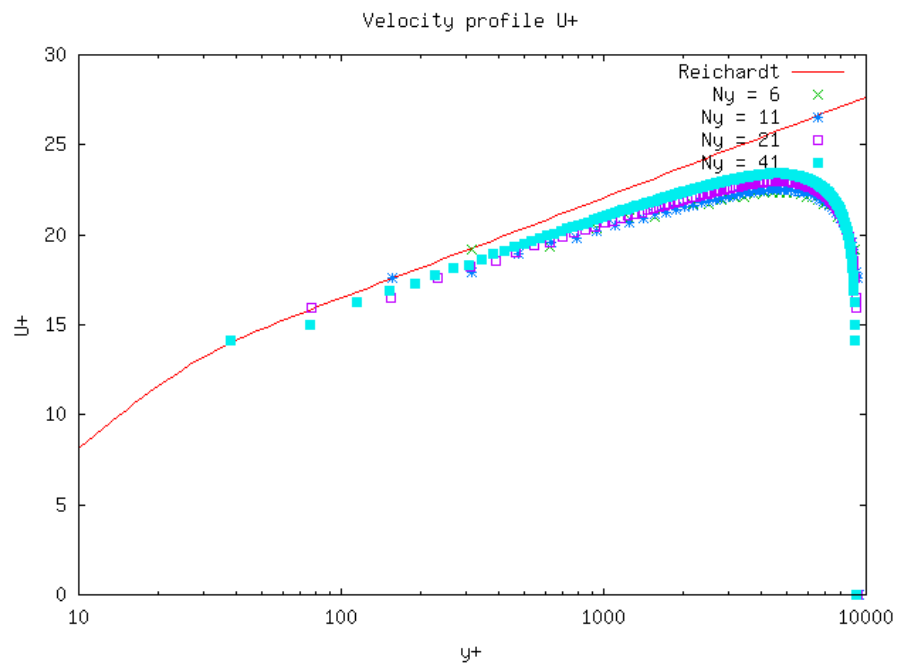
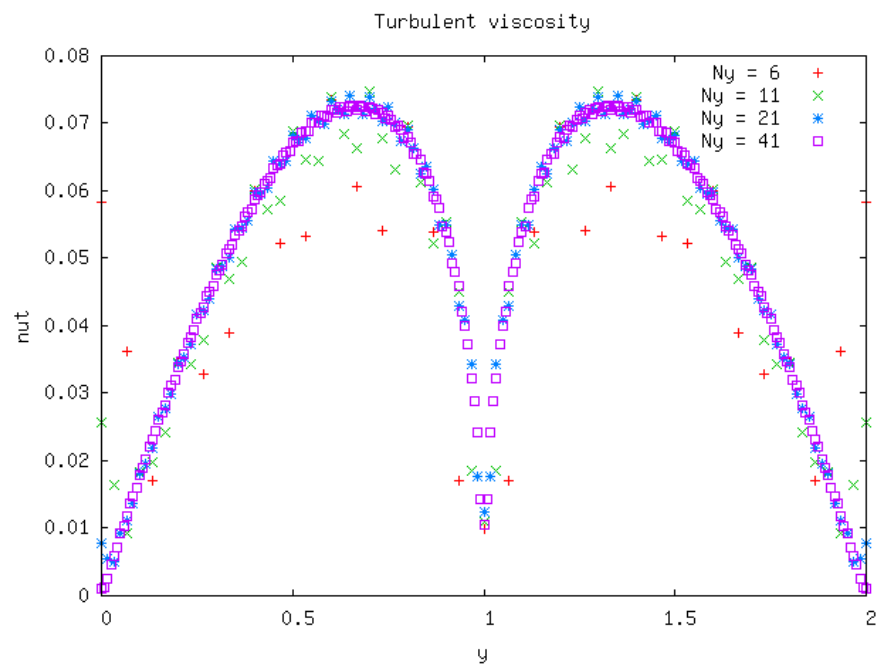
Figure V.2.12: Velocity profile  $U+$ 

Figure V.2.13: Turbulent viscosity

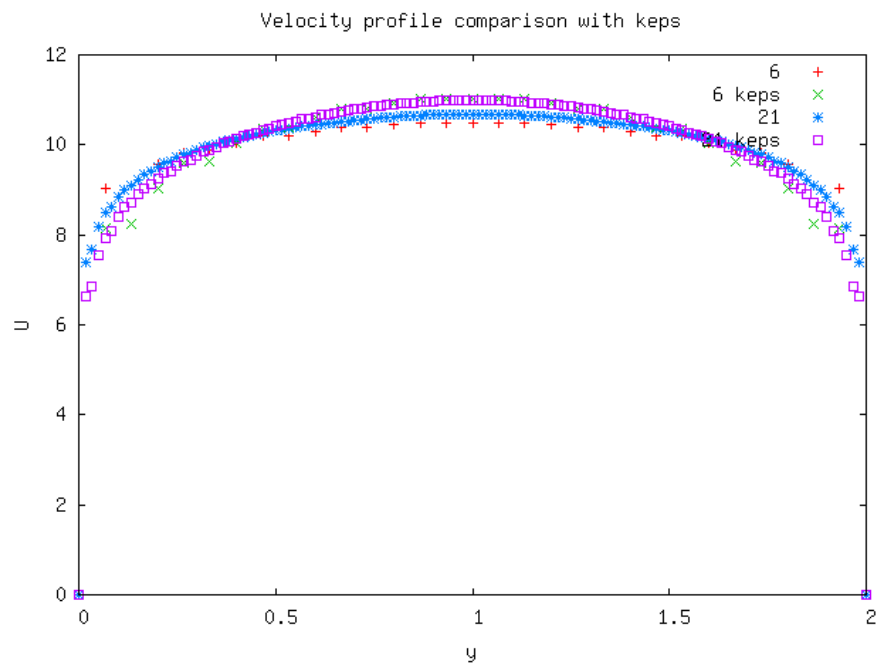
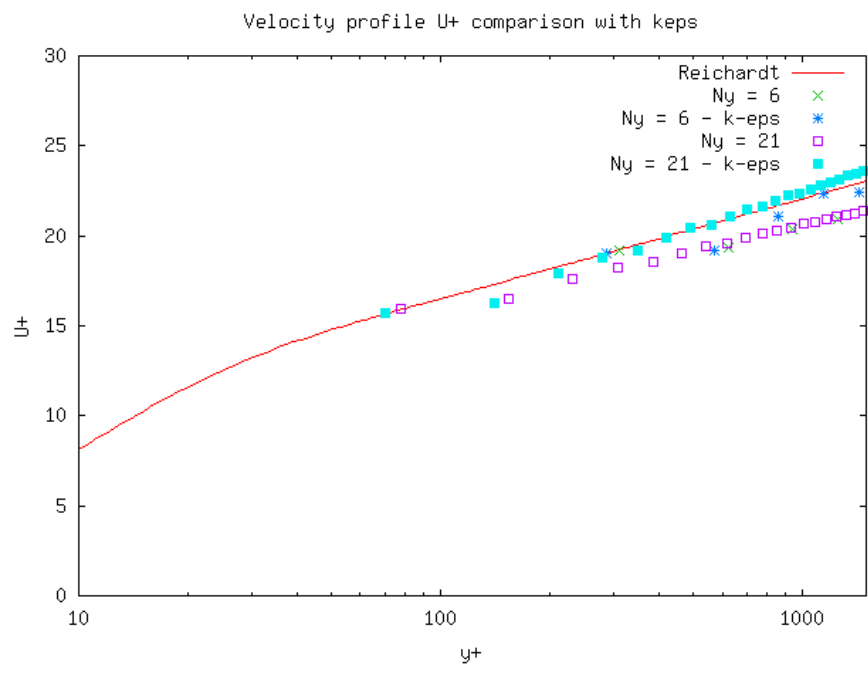


Figure V.2.14: Velocity profile comparison with keps

Figure V.2.15: Velocity profile  $U+$  comparison with keps

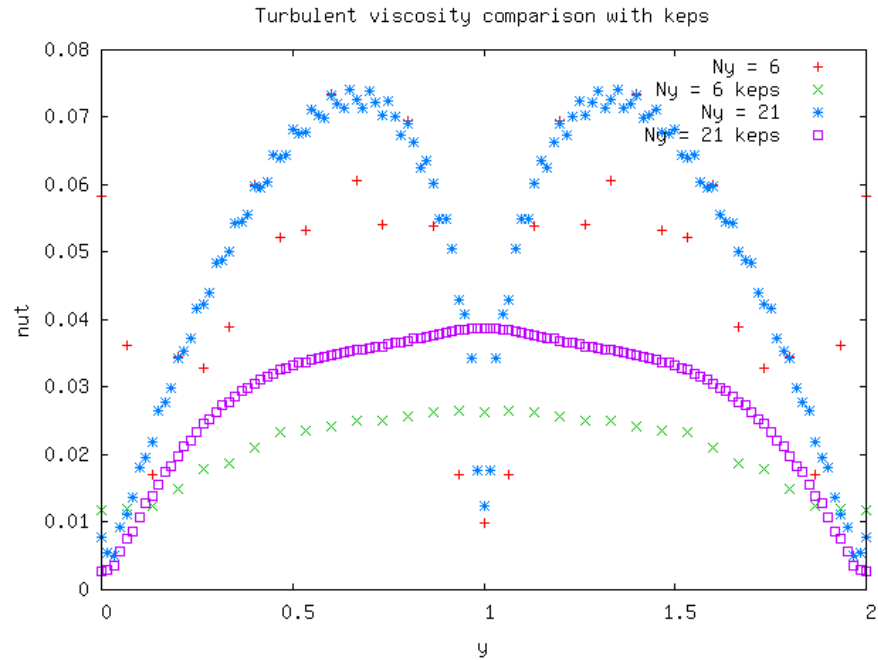


Figure V.2.16: Turbulent viscosity comparison with keps

## 2.5 Conclusion

With the 'Mixing length'-model, compared to the Dean's correlation, the 2D relative errors on  $Re_\tau$  is about 2% when  $Re_b = 10^4$  and 6% when  $Re_b = 10^5$ . For the 3D simulations with  $Re_b = 10^5$ , the relative error is about 10% with the 'Mixing length'-model whereas better results are obtained with the ' $k - \epsilon$ '-model (near 2%). Most of comparisons with the Reichardt analytical law are well-fitted except for the 2D case with  $N_y = 41$  and  $Re_b = 10^5$ .

## 2.6 References

- [1] Reichardt H. : Vollstaendige Darstellung der turbulenten Geschwindigkeitsverteilung in glatten Leitungen. ZAMM 31, 208-219 (1951)
- [2] <http://www.sla.maschinenbau.tu-darmstadt.de/lehre/tms/Turbulence-TUDarmstadt-Pt2-6.pdf>

## 2.7 Data Files

### 2D

```
# SIMULATION D UN CANAL PLAN 2D avec modele Longueur de melange #
# PARALLEL NOT postraitemet #
# Tests du modele Longueur de Melange et de la procedure de calcul du frottement parietal (Paro
dimension 2
Pb_Hydraulique_Turbulent pb
Domaine dom
# BEGIN MESH #
Mailler dom
{
Pave Cavite
}
```

```

        Origine 0. 0.
        Nombre_de_Noeuds 3 6
        Longueurs 0.2 2.
    }
{
    Bord periox   X = 0. 0. <= Y <= 2.
    Bord periox   X = 0.2 0. <= Y <= 2.
    Bord bas      Y = 0. 0. <= X <= 0.2
    Bord haut     Y = 2. 0. <= X <= 0.2
}
}
Trianguler_fin dom
# END MESH #
# BEGIN PARTITION
Partition dom
{
    Partitionneur tranche { tranches 1 2 }
    Larg_joint 2
    Nom_Zones DOM
    periodique 1 periox
}
End
END PARTITION #
# BEGIN MESH #
Distance_paroi dom 2 haut bas binaire
# END MESH #
# BEGIN SCATTER
Scatter DOM.Zones dom
END SCATTER #
VEFPreP1b dis
Schema_Euler_explicie sch
Read sch
{
    tinit 0.
    tmax 15.
    dt_min 1.e-7
    dt_max 1.e-3
    dt_start dt_calc
    dt_impr 0.1
    dt_sauv 10.
    seuil_statio 1.e-8
    facsec 0.9
}
Associate pb dom
Associate pb sch
Discretize pb dis
Read pb
{
    fluide_incompressible {
        mu Champ_Uniforme 1 0.001
        rho Champ_Uniforme 1 1
    }
    Navier_Stokes_Turbulent
    {
        solveur_pression GCP { precond ssor { omega 1.5 } seuil 1e-8 }
        convection { EF_stab { } }
        diffusion { }
        Sources { Canal_perio { bord periox } }
    }
    conditions_initiales
    {
        vitesse Champ_fonc_xyz dom 2 10. 0
    }
}

```

```

        }
    boundary_conditions
    {
        periox    periodique
        haut      paroi_fixe
        bas       paroi_fixe
    }
Modele_turbulence Longueur_Melange
{
    turbulence_paroi loi_standard_hydr dt_impr_ustar 10
    dmax 1000. fichier dom_Wall_length.xyz
}
Traitement_particulier { Canal
{
    dt_impr_moy_spat 5.
}
}
}
Postraitemetn
{
    Sondes
    {
        sonde_vit   vitesse periode 5. segment 50 0.05 0. 0.05 2.
        sonde_visu_turb viscosite_turbulente periode 5. segment 50 0.05 0. 0.05 2.
    }
format lata
Champs dt_post 10
{
    vitesse elem
    viscosite_turbulente elem
    pression elem
    y_plus elem
}
}
}
Solve pb
End

```

### 3D

```

# SIMULATION D UN CANAL PLAN 2D avec modele Longueur de melange #
# PARALLEL NOT postraitemetn #
# Tests du modele Longueur de Melange et de la procedure de calcul du frottement parietal (Par
dimension 3
Pb_Hydraulique_Turbulent pb
Domaine dom
# BEGIN MESH #
Mailler dom
{
Pave Cavite
{
    Origine 0. 0. 0.
    Nombre_de_Noeuds 3 6 3
    Longueurs 0.8 2. 0.8
}
{
    Bord periox X = 0. 0. <= Y <= 2. 0. <= Z <= 0.8
    Bord periox X = 0.8 0. <= Y <= 2. 0. <= Z <= 0.8
    Bord bas Y = 0. 0. <= X <= 0.8 0. <= Z <= 0.8
    Bord haut Y = 2. 0. <= X <= 0.8 0. <= Z <= 0.8
    Bord perioz Z = 0. 0. <= X <= 0.8 0. <= Y <= 2.
}

```

```

        Bord perioz    Z = 0.8 0. <= X <= 0.8 0. <= Y <= 2.
    }
}
Tetraedriser_homogene_fin dom
Corriger_frontiere_periodique { Domaine dom Bord periox }
Corriger_frontiere_periodique { Domaine dom Bord perioz }
# END MESH #
# BEGIN PARTITION
Partition dom
{
    Partitionneur_tranche { tranches 1 1 2 }
    Larg_joint 2
    Nom_Zones DOM
    periodique 2 periox perioz
}
End
END PARTITION #
# BEGIN MESH #
Distance_paroi dom 2 haut bas binaire
# END MESH #
# BEGIN SCATTER
Scatter DOM.Zones dom
END SCATTER #
VEFPreP1b dis
Schema_Euler_ex explicite sch
Read sch
{
    tinit 0.
    tmax 15.
    dt_min 1.e-7
    dt_max 1.e-3
    dt_start dt_calc
    dt_impr 1.
    dt_sauv 5.0
    seuil_statio 1.e-8
    facsec 0.9
}
Associate pb dom
Associate pb sch
Discretize pb dis
Read pb
{
    fluide_incompressible {
        mu Champ_Uniforme 1 0.0001
        rho Champ_Uniforme 1 1
    }
    Navier_Stokes_Turbulent
    {
        solveur_pression GCP { precond ssor { omega 1.5 } seuil 1e-8 }
        convection { EF_stab { } }
        diffusion { }
        Sources { Canal_perio { bord periox } }
    }
    conditions_initiales
    {
        vitesse Champ_fonc_xyz dom 3 10. 0. 0.
    }
    boundary_conditions
    {
        periox periodique
        perioz periodique
        haut paroi_fixe
    }
}

```

```

        bas      paroi_fixe
    }
Modele_turbulence Longueur_Melange
{
    turbulence_paroi loi_standard_hydr dt_impr_ustar 5.
    dmax 1000. fichier dom_Wall_length.xyz
}
Traitement_particulier { Canal
{
    dt_impr_moy_spat 5.
}
}
Postraitement
{
    Sondes
{
    sonde_vit vitesse periode 5. segment 50 0.05 0. 0.05 0.05 2. 0.05
    sonde_viscturb viscosite_turbulente periode 5. segment 50 0.05 0. 0.05
0.05 2. 0.05
}
format lata
Champs dt_post 10
{
    vitesse elem
    viscosite_turbulente elem
    pression elem
    y_plus elem
}
}
}
Solve pb
End

```

### 3D\_keps

```

# SIMULATION D UN CANAL PLAN 2D avec modele Longueur de melange #
# PARALLEL NOT postraitement #
# Tests du modele Longueur de Melange et de la procedure de calcul du frottement parietal (Paro
dimension 3
Pb_Hydraulique_Turbulent pb
Domaine dom
# BEGIN MESH #
Mailler dom
{
Pave Cavite
{
    Origine 0. 0. 0.
    Nombre_de_Noeuds 3 6 3
    Longueurs 0.8 2. 0.8
}
{
    Bord periox X = 0. 0. <= Y <= 2. 0. <= Z <= 0.8
    Bord periox X = 0.8 0. <= Y <= 2. 0. <= Z <= 0.8
    Bord bas Y = 0. 0. <= X <= 0.8 0. <= Z <= 0.8
    Bord haut Y = 2. 0. <= X <= 0.8 0. <= Z <= 0.8
    Bord perioz Z = 0. 0. <= X <= 0.8 0. <= Y <= 2.
    Bord perioz Z = 0.8 0. <= X <= 0.8 0. <= Y <= 2.
}
}
Tetraedriser_homogene_fin dom

```

```

Corriger_frontiere_periodique { Domaine dom Bord periox }
Corriger_frontiere_periodique { Domaine dom Bord perioz }
# END MESH #
# BEGIN PARTITION
Partition dom
{
    Partitionneur_tranche { tranches 1 1 2 }
    Larg_joint 2
    Nom_Zones DOM
    periodique 2 periox perioz
}
End
END PARTITION #
# BEGIN MESH #
Distance_paroi dom 2 haut bas binaire
# END MESH #
# BEGIN SCATTER
Scatter DOM.Zones dom
END SCATTER #
VEFPreP1b dis
Schema_Euler_explicie sch
Read sch
{
    tinit 0.
    tmax 15.
    dt_min 1.e-7
    dt_max 1.e-3
    dt_start dt_calc
    dt_impr 1.
    dt_sauv 5.0
    seuil_statio 1.e-8
    facsec 0.9
}
Associate pb dom
Associate pb sch
Discretize pb dis
Read pb
{
    fluide_incompressible {
        mu Champ_Uniforme 1 0.0001
        rho Champ_Uniforme 1 1
    }
    Navier_Stokes_Turbulent
    {
        solveur_pression GCP { precond ssor { omega 1.5 } seuil 1e-8 }
        convection { EF_stab { } }
        diffusion { }
        Sources { Canal_perio { bord periox } }
    }
    conditions_initiales
    {
        vitesse Champ_fonc_xyz dom 3 10. 0. 0.
    }
    boundary_conditions
    {
        periox periodique
        perioz periodique
        haut paroi_fixe
        bas paroi_fixe
    }
    modele_turbulence K_Epsilon {
        Transport_K_Epsilon
    }
}

```

```

{
    convection { EF_stab { } }
    diffusion { }
    boundary_conditions {
        periox    periodique
        perioz    periodique
        haut      paroi
        bas       paroi
    }
    conditions_initiales { k_eps Champ_Uniforme 2 0.45 0.075 }
}
turbulence_paroi loi_standard_hydr dt_impr_ustar 5.
}
Traitement_particulier { Canal
{
    dt_impr_moy_spat 5.
}
}
Postraitemet
{
    Sondes
    {
        sonde_vit   vitesse periode 5. segment 50 0.05 0. 0.05 0.05 2. 0.05
        sonde_viscturb viscosite_turbulente periode 5. segment 50 0.05 0. 0.05
0.05 2. 0.05
    }
    format lata
    Champs dt_post 10
    {
        vitesse elem
        viscosite_turbulente elem
        pression elem
        y_plus elem
    }
}
Solve pb
End

```

## VI. Thermal Turbulent Flow

**L**IKE for laminar flows, in this section, thermal aspects are added to turbulent flows. In this version of the report, two cases are studied:

- Thermal stratification flow in a plenum
- Turbulent flow inside a double-periodic plane channel with heated walls

These two cases both use  $k - \epsilon$  model for turbulence and 3D modeling.



## Turbulent flow inside a double-periodic plane channel with heated walls

### 1.1 Purpose

The purpose of this test case is to check TrioCFD on a thermal turbulent flow inside a double-periodic plane channel. The fluid is assumed to be Incompressible and the turbulence model is the  $k - \epsilon$  one. A temperature gradient is imposed at fixed walls where the Reichardt law function is applied. In this test, the effect of several meshes is compared. The validations are carried out between the Nusselt number computed by TrioCFD and an analytical expression that is derived in reference [1]. The comparisons are also presented for the mean velocity profile with the logarithmic law. Moreover, the mean temperature profile is compared to the linear law  $T^+ = PrY^+$  and the Kader's law. We remind the definitions of the Dean's correlation  $Re_\tau = 0.175 \cdot Re_{bulk}^{7/8}$  and the bulk Reynolds number  $Re_{bulk} = \frac{\rho(T_b) \cdot U_b \cdot (h/2)}{\mu(T_b)}$  where  $h$  is the distance between both walls and  $\rho$ ,  $\mu$  and  $U_b$  are the density, the dynamic viscosity and the bulk velocity.

Validation made by : FOURNIER C.

Report generated 09/06/2023.

### 1.2 Problem Description

#### Geometry

The geometry is a double-periodic plane channel of Dimensions :  $h = 4$  mm,  $L = 4$  mm,  $P = 2$  mm as sketched on Fig. 1.

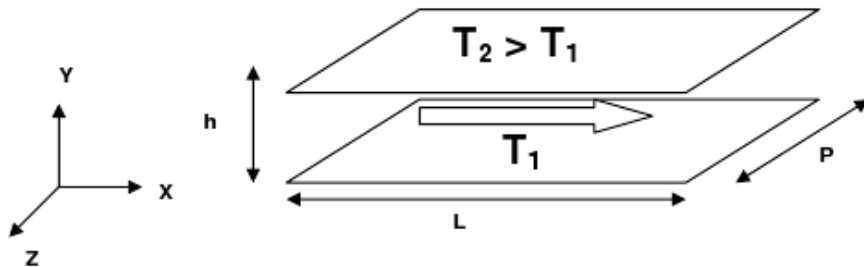


Figure VI.1.1: Geometry

#### Initial Conditions and Boundary Conditions

##### • Boundary conditions

For Navier-Stokes equations, periodic boundary conditions hold in  $x$ - and  $z$ -directions and a no-slip boundary condition is applied for both walls. For temperature equation, Dirichlet boundary conditions are applied on both walls. The walls temperatures are set such as  $\frac{T_2}{T_1} = 1.01$  where  $T_2$  and  $T_1$  are the temperatures of hot and cold walls respectively. For simulations, they are set equal to,  $T_2 = 680$  K and  $T_1 = 673$  K.

- **Initial conditions**

The flow initial condition imposes a uniform velocity equal to 80 m/s in the  $x$ -direction. For temperature, the initial condition is a linear profile between  $T_2$  and  $T_1$ .

## Fluid Properties

Inside the domain the fluid is Helium at 70 bars and 676 K with  $\rho = 3.824 \text{ kg/m}^3$ ,  $\mu = 3.475310^{-7} \text{ N/m}^2/\text{s}$ ,  $\lambda = 2.5638910^{-3} \text{ W/m/K}$ ,  $C_p = 5193 \text{ J/kg/K}$  and  $\beta_{th} = 0 \text{ K}^{-1}$ . The Reynold numbers are  $Re_{bulk} = 17605$  and  $Re_\tau = 908$ .

## Flow Physics

The flow is turbulent inside de double-periodic domain and heated with a temperature gradient between both walls.

### 1.3 Case Setup

#### Grid

3 meshes (tetrahedral elements) are made by stretching the mesh below, by a factor 1, 10 or 100 in X direction.

Number of cells : 2214

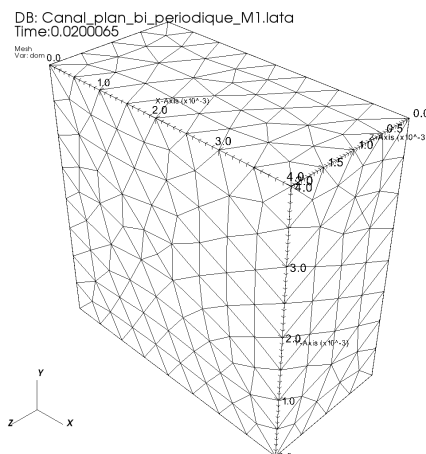


Figure VI.1.2: Mesh M1

2 meshes (tetrahedral elements) generated from cartesian hexahedral elements are used

Number of cells: mesh M1\_tetraedrise (drawn below) : 1536

Number of cells: mesh M1bis\_tetraedrise : 5184

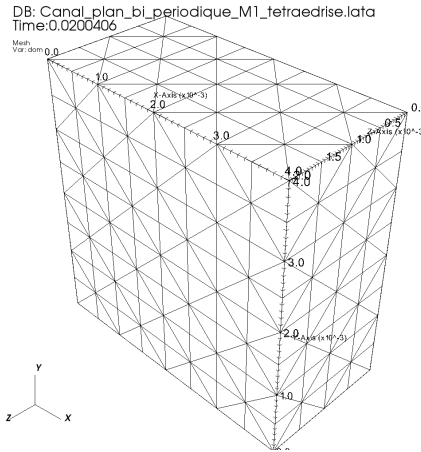


Figure VI.1.3: Mesh M1\_tetraedrise

## Model Options

The TrioCFD keywords are 'Pb\_Thermohydraulique\_Turbulent' with 'Fluide\_Incompressible' with constant properties. The turbulence models are taken into account by the keywords 'Navier\_Stokes\_Turbulent' with 'Modele\_Turbulence K\_Epsilon'. As the periodic and no-slip boundary conditions are considered, a force term is applied in the impulsion balance equation with the keyword 'Sources { Canal\_perio { bord Periox } }'. Finally for the temperature equation 'Convection\_Diffusion\_Temperature\_Turbulent', the keyword 'Modele\_Turbulence Prandtl' is used in the datafile. Finally the wall function is the Reichardt law with the option " loi standard hydr " (which is similar to 'loi expert hydr').

## Other Options (calculation)

The numerical options are 'Schema\_Euler\_Implicite - Solveur Implicite' with the 'EF\_stab' scheme for Navier-Stokes and temperature equation. For the latter 'EF\_stab { alpha 0.2 }'.

## 1.4 Results

### Validation Specific Informations

- Version TRUST :
- Bi-periodic plane channel in X and Z
- Convection scheme = EF\_stab
- k- $\varepsilon$  modelling of turbulence
- Wall law = loi\_standard\_hydr (similar to loi\_expert\_hydr { methode\_calcul\_face\_keps\_impose que\_les\_faces\_des\_elts\_dirichlet })
- Heat transfer with imposed temperatures
- No-slip at the wall
- Location: validation/share/Validation/Rapports\_automatiques/Validant/Fini/Channel\_T1\_T2\_incompressible
- Master Test Case: Canal\_plan.bi.periodique\_M1.data - Canal\_plan.bi.periodique\_M1\_tetraedrise.data

- Generated Test cases :

→ Incompressible/Canal\_plan\_bi\_periodique\_M1/Canal\_plan\_bi\_periodique\_M1.data : /\*\*/  
 → Incompressible/Canal\_plan\_bi\_periodique\_M10/Canal\_plan\_bi\_periodique\_M10.data :  
 → Incompressible/Canal\_plan\_bi\_periodique\_M100/Canal\_plan\_bi\_periodique\_M100.data :  
 → Incompressible/Canal\_plan\_bi\_periodique\_M1\_tetraedrise/Canal\_plan\_bi\_periodique\_M1\_tetraedrise.data :  
 → Incompressible/Canal\_plan\_bi\_periodique\_M1bis\_tetraedrise/Canal\_plan\_bi\_periodique\_M1bis\_tetraedrise.data :

- Performance Chart :

	host	system	Total CPU Time	CPU time/step	number of cell
M1	uruk	Linux	1115.86	0.377125	2214
M10	uruk	Linux	624.007	0.283499	2214
M100	uruk	Linux	814.565	0.251239	2214
M1_tetraedrise	uruk	Linux	407.555	0.949632	1536
M1bis_tetraedrise	uruk	Linux	2009.7	8.58665	5184
Total			4971.69		

Table VI.1.1: Performance Chart

## Plot Data

### • Velocity results

The mean axial velocity profiles at outlet ( $U^+ = U/U_\tau$ ;  $Y^+ = Y.U_\tau/\nu$ ) are compared to the wall function:  $U^+ = 1/0.415 \times \ln(Y^+) + 5.32$ . On Fig. 4 the comparisons are done for three meshes 'M1', 'M10' and 'M100'. For Fig. 5, the comparisons are done for 'M1' and 'M1 tetrahedrise'.

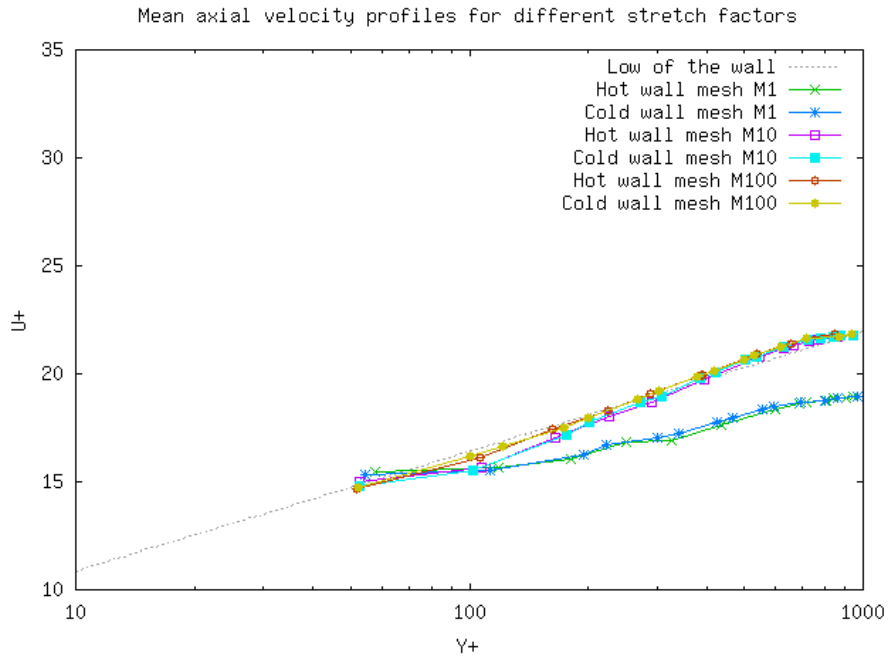


Figure VI.1.4: Mean axial velocity profiles for different stretch factors

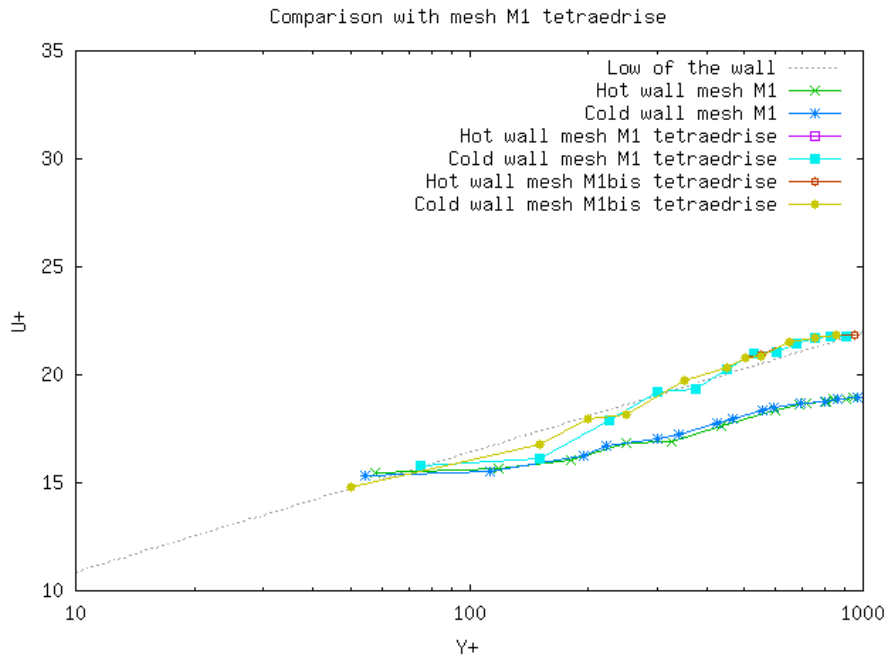
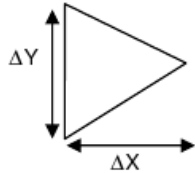


Figure VI.1.5: Comparison with mesh M1\_tetraedrise

	<b>Continuity equation :</b> $\operatorname{div}(U) = 0$ $\frac{\partial u}{\partial x} + \frac{\partial v}{\partial y} = 0$
	<b>In discretizing :</b> $\frac{\Delta u}{\Delta x} + \frac{\Delta v}{\Delta y} = 0$
	<b>Hypothesis :</b> $\begin{cases} \frac{\Delta y}{\Delta x} = \varepsilon = \frac{1}{\text{stretch factor}} \\ \Delta u \neq \infty \end{cases}$
	<b>Finally :</b> $\varepsilon \Delta u + \Delta v = 0 \Leftrightarrow \Delta v = -\varepsilon \Delta u$ $\Rightarrow \lim_{\text{stretch factor} \rightarrow \infty} (\Delta v) = \lim_{\varepsilon \rightarrow 0} (\Delta v) = 0$

When the stretch factor increases, the contribution of the deviation of transverse velocity decreases and the flow becomes one-dimensional.

Figure VI.1.6: Explanations of M1 result : contribution of transverse velocity

The deviations of transverse velocities  $V$  and  $W$  are respectively presented on Figs. 7 and 8. On those two figures, we can observe that the results obtained with the mesh M1 are not conclusive and can be interpreted as a non-negligible contribution of the deviation of transverse velocities. However the two other meshes M10 and M100 (made by stretching the mesh M1) and the meshes generated from cartesian hexahedral elements (M1\_tetraedrise and M1bis\_tetraedrise) give better results.

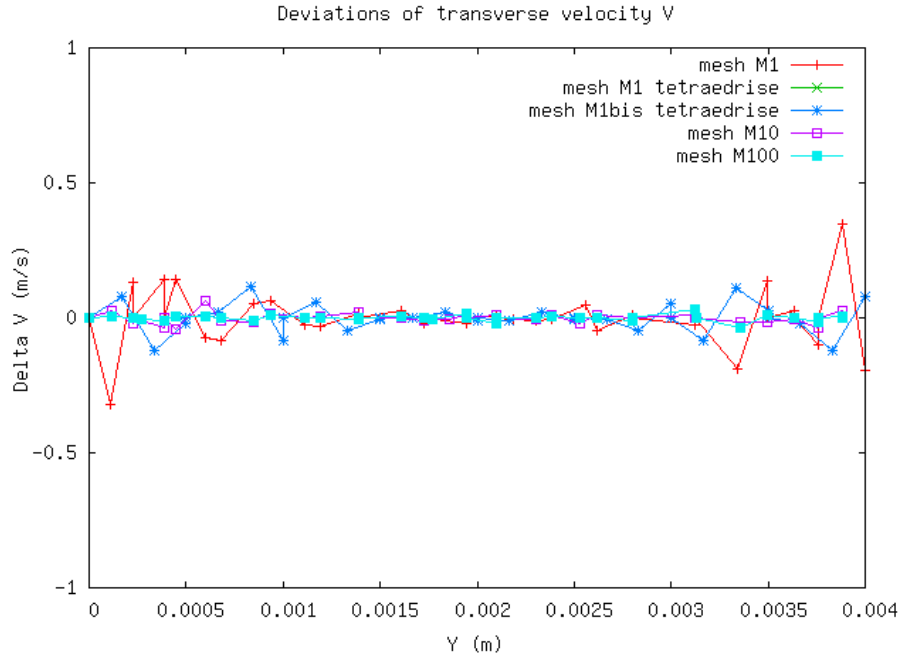


Figure VI.1.7: Deviations of transverse velocity V

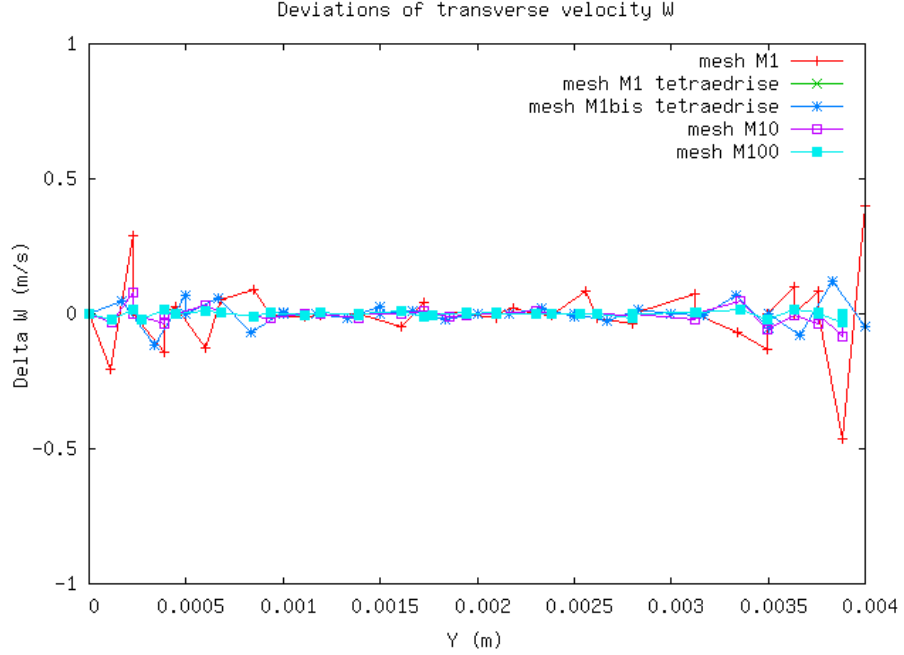


Figure VI.1.8: Deviations of transverse velocity W

- Temperature results

The mean temperature profiles at outlet ( $T^+ = T/T_\tau; T_\tau = \varphi/(\rho C_p U_\tau); Y^+ = YU_\tau/\nu$ ) are compared to the linear law  $T^+ = \text{Pr}Y^+$  and the Kader's law on Figs. 9 and 10. The Kader's law is defined by:  
 $T^+ = \text{Pr}Y^+\exp(-\Gamma) + [2.12 \ln(1+Y^+)+\beta(\text{Pr})]\exp(-1/\Gamma)$   
With  $\Gamma = 0.01(\text{Pr}Y^+)^4 / (1+5Y^+\text{Pr}^3)$  and  $\beta(\text{Pr}) = (3.85\text{Pr}^{1/3} - 1.3)^2 + 2.12 \ln(\text{Pr})$

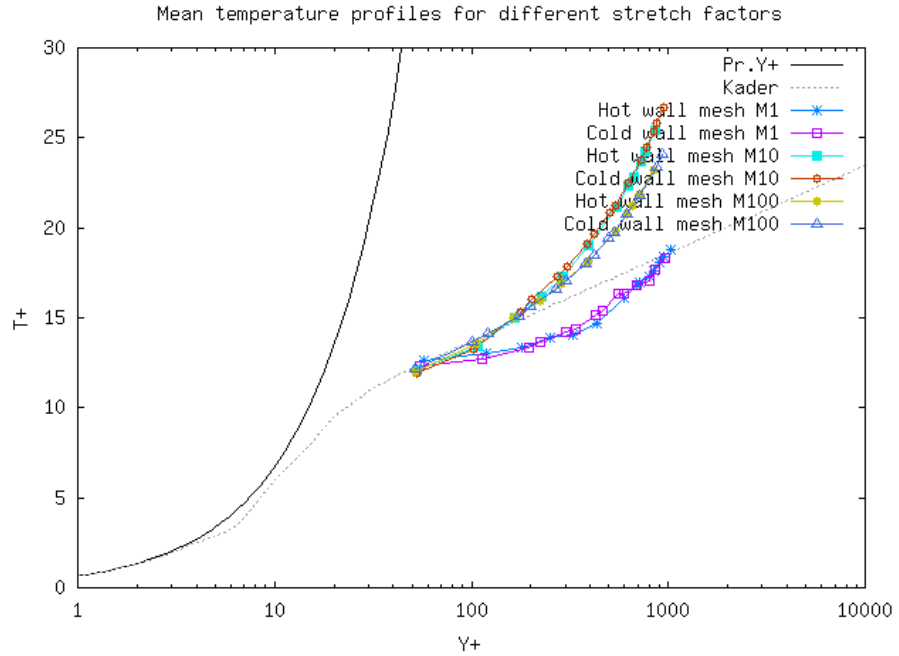


Figure VI.1.9: Mean temperature profiles for different stretch factors

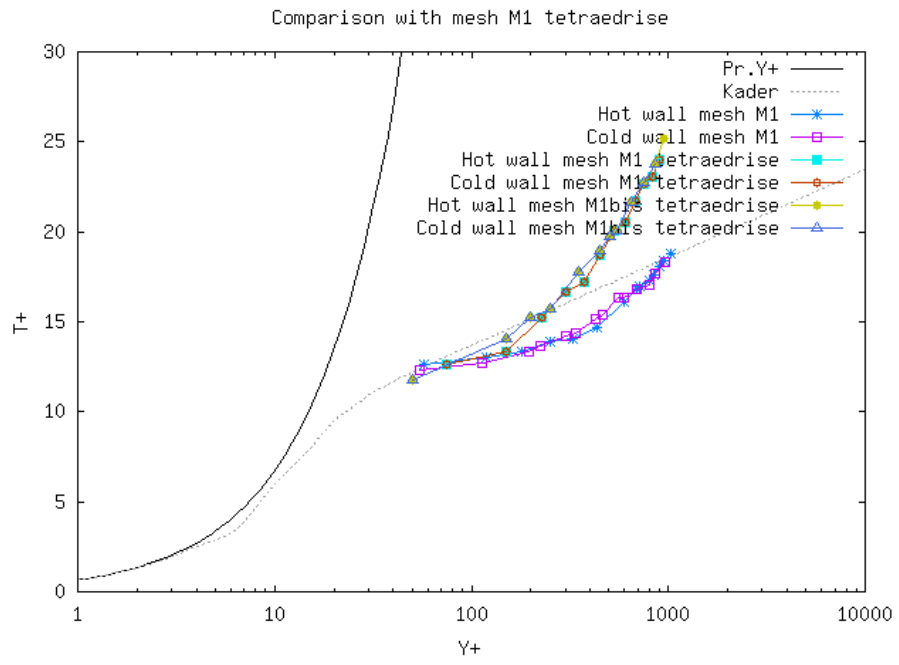


Figure VI.1.10: Comparison with mesh M1\_tetraedrise

- Nusselt Calculation

$$Nu = \frac{D_h \cdot \left( \frac{dT}{dy} \right)}{\Delta T}; D_h = \text{hydraulic diameter}$$

Classical correlations found in the literature (like the correlation of Colburn or Dittus Boelter) were derived in cases where the walls are subjected to an imposed flux or the same temperature. None of them seem

applicable in this case because both walls are subjected to different temperatures. In order to validate TrioCFD, we compare the results with numerical solutions corresponding to the convection in turbulent flow between parallel plates with unequal uniform temperature of reference [1]. The authors propose the following formulation for Nusselt number :

$$Nu_{Ref} = \frac{1}{4 * \int_0^1 \frac{dy^+}{1 + \frac{Pr}{Pr_t} \left( \frac{(u'v')^{++}}{1 - (u'v')^{++}} \right)}}$$

with  $(u'v')^{++} = -\rho \bar{u}'v'/\tau$ . We need an evaluation of the turbulent shear stress to calculate the Nusselt number numerically. In reference [1], the author uses a correlation based on a experimental data for a round tube and supposed to be valid for a flow between parallel plates. This correlation writes:

$$(u'v')^{++} = \left( \left[ 0.7 \left( \frac{y^+}{10} \right)^3 \right]^{-8/7} + \left[ \exp \left( \frac{-1}{0.436y^+} \right) - \frac{1}{0.436Re_\tau} \left( 1 + \frac{6.95y^+}{Re_\tau} \right) \right]^{-8/7} \right)^{-7/8}$$

In our case,  $Pr = 0.667$ ,  $Pr_t = 0.9$ ,  $Re_\tau = 908$  and  $Nu_{Ref} = 93$ . The TrioCFD Nusselt number and the relative errors are given in Table 2 where we observe that the TrioCFD results are very close to the analytical ones.

	$Nu_{TrioCFD}$	$\Delta Nu_{Ref}(\%)$
M1	145.67	56.63
M10	93.95	1.02
M100	102.05	9.73
M1_tetraedrise	101.84	9.51
M1bis_tetraedrise	99.98	7.51

Table VI.1.2: Nusselt Calculation

## 1.5 Conclusion

The thermal turbulent flow has been validated in this test case. The flow is considered inside a double-periodic plane channel with the ' $k - \epsilon$ ' model of turbulence. At fixed walls, the Reichardt law function is considered and a temperature gradient is applied. The temperature profiles were compared with the Kader's law and the linear one. Finally the Nusselt number that are computed by TrioCFD are close to those calculated in reference [1].

## 1.6 References

- [1] Stanislav N. Danov, Norio Arai and Stuart W. Churchill, Exact formulations and nearly exact numerical solutions for convection in turbulent flow between parallel plates, International Journal of Heat and Mass Transfer, Number 43, pp. 2767-2777, 2000.

## 1.7 Data Files

### Canal\_plan\_bi\_periodique\_M1

```
# SIMULATION D'UN CANAL PLAN 3D VEF EN THERMOHYDRAULIQUE INCOMPRESSIBLE #
dimension 3
Pb_Thermohydraulique_turbulent pb
Domaine dom
# BEGIN MESH #
Lire_Tgrid dom Canal_plan_bi_periodique_M1.msh
Transformer dom x y z
```

```

# END MESH #
# BEGIN PARTITION
Partition dom
{
    Partitionneur metis { Nb_parts 2 }
    Larg_joint 2
    Nom_Zones DOM
}
End
END PARTITION #
# BEGIN SCATTER
Scatter DOM.Zones dom
END SCATTER #
VEFPreP1B dis
Schema_Euler_implicite sch
Read sch
{
    tinit 0.
    tmax 0.02
    dt_min 1.e-10
    dt_max 1.e-1
    dt_impr 1.e-5
    dt_sauv 0.01
    seuil_statio 1.e-8
    facsec 10
    facsec_max 500
    Solveur
        Implicite
        {
            seuil_convergence_solveur 1.e-10
        }
}
Associate pb dom
Associate pb sch
Discretize pb dis
Read pb
{
    fluide_incompressible {
        gravite champ_uniforme 3 0 0 0
        mu Champ_Uniforme 1 3.4753e-5
        rho Champ_Uniforme 1 3.824
        lambda Champ_Uniforme 1 0.256389
        Cp Champ_Uniforme 1 5193.
        beta_th Champ_Uniforme 1 0.
    }
    Navier_Stokes_turbulent
    {
        solveur_pression GCP { precond ssor { omega 1.5 } seuil 1e-8 }
        convection { EF_stab { } }
        diffusion { }
        Sources { Canal_perio { bord Periox } }
        conditions_initiales { vitesse champ_uniforme 3 80. 0. 0. }
        boundary_conditions
        {
            Periox periodique
            Perioz periodique
            Bas Paroi_fixe
            Haut Paroi_fixe
        }
        Modele_turbulence K_Epsilon
    }
}

```

```

Transport_K_Epsilon
{
    convection { EF_stab { } }
                diffusion { }
                boundary_conditions
{
    Periox periodique
    Perioz periodique
    Bas Paroi
    Haut Paroi
}
    parametre_equation parametre_implicite
{
    resolution_explicie
}
    conditions_initiales { k_Eps Champ_Uniforme 2 64. 1.4e6 }
}
    turbulence_paroi loi_standard_hydr dt_impr_ustar 0.001
}
}
Convection_Diffusion_Temperature_turbulent
{
    diffusion { }
    convection { EF_stab { alpha 0.2 } }
    boundary_conditions
{
    Periox periodique
    Perioz periodique
    Bas paroi_temperature_imposee Champ_Front_Uniforme 1 673.
    Haut paroi_temperature_imposee Champ_Front_Uniforme 1 680.
}
    conditions_initiales { Temperature Champ_fonc_xyz dom 1 1750.*y+673. }
    Modele_turbulence Prandtl
{
    Turbulence_paroi loi_standard_hydr_scalaire
dt_impr_nusselt 0.001
}
}
}
Postraitemet
{
    Sondes
    {
        sonde_pression      pression      periode 0.0001 segment 50
0.00025 0.0 0.00025 0.00025 0.004 0.00025
        sonde_vitesse      nodes vitesse      periode 0.0001 segment 50
0.00025 0.0 0.00025 0.00025 0.004 0.00025
        sonde_temperature  nodes temperature      periode 0.0001 segment 50
0.00025 0.0 0.00025 0.00025 0.004 0.00025
        sonde_y_plus       nodes y_plus      periode 0.0001 segment 50
0.00025 0.0 0.00025 0.00025 0.004 0.00025
        sonde_k            nodes k          periode 0.0001 segment 50 0.00025 0.0 0.00025 0.00025 0.004 0.000
        sonde_eps           nodes eps          periode 0.0001 segment 50
0.00025 0.0 0.00025 0.00025 0.004 0.00025
        sonde_visco_turb   nodes viscosite_turbulente      periode 0.0001 segment 50
0.00025 0.0 0.00025 0.00025 0.004 0.00025
    }
    format lata Champs dt_post 0.01
{
    pression      elem
    pression      som
    vitesse      elem
}

```

```
vitesse      som
temperature    elem
temperature    som
y_plus        elem
y_plus        som
Viscosite_turbulente elem
Viscosite_turbulente som
k            elem
k            som
eps          elem
eps          som
}
}
}
Solve pb
End
```

## VII. Two-phase Flows with Front-Tracking

**I**N this last part, the test cases correspond to two-phase flows at local scale. Direct numerical simulations of such flows consist in modeling two incompressible and immiscible fluids separated by a mobile interface. The mass and impulsion balance equations hold for each bulk phase with the viscosity and density of each fluid. The temperature equation is neglected as well as phase change but the gravity is considered. In such an approach, bubbles or drops are described individually with their surface tension and the main difficulty is to follow accurately interfaces that evolve in space and time. Several numerical methods are dedicated to such interface tracking. They can be gathered into two main families: “diffuse interface method” and “sharp interface method”. In **TrioCFD**, interfaces are tracked by “Front-Tracking”, a sharp interface method, for which the surface of separation between both fluids is discretized by an additional lagrangian mesh. A re-meshing is required during the calculation with a fine adjustment of numerical parameters. In this part, the method is used for simulating problems of **oscillating bubble** and **hanging drop**.



## Oscillation of a bubble

### 1.1 Purpose

The following study consists to validate the behavior of the Front Tracking algorithm implemented in TrioCFD code. The aim of this test is to check the capability of this algorithm to describe the oscillations of the interface between an air bubble and the surrounding water, so to check if the code ensures a good coupling between the surface tensions and the inertia. This two-phase flow configuration is based on a return to equilibrium of an initial deformed bubble via capillary oscillations .This test is validated by comparing the frequencies of oscillation and the rate of damping with analytical solutions.

By version v1.8.4, validation will be redone on this sheet in order to:

- Validate the code by comparing the frequencies of oscillation and the rate of damping with analytical solutions,
- Quantify the dissipation of the numerical,
- Identify the criteria of stability on the time step according to the Lagrangian mesh at the interface according to physical parameters of fluids: density, viscosity and Surface tension.

Validation made by : A DJEMA.

Report generated 12/06/2023.

### 1.2 Problem Description

The test deals with the presence of a bubble in a box filled of liquid. Initially, the liquid is at rest. No gravity forces are taken into account. In the calculation, the initial shape of the bubble is slightly an ellipsoidal one (a deformed bubble with mode n=2).It makes it be out of equilibrium, its free surface is subject to oscillations. We expect to observe damped oscillations between a prolate form and an oblate schape.To investigate their frequencies, the analytical results to be used as reference are relative to inviscid fluids. Therefore. In addition, since the analytical results are non-dissipative, this test-case provides a tool to estimate the rate of the energy dissipation due to the modeling method. This is connected to the problem of numerical diffusion.

In this two-fluid problem, the following notations are introduced to describe the fluids and interface physical and transport properties. The two fluids are considered as non-miscible. The inclusion equivalent diameter is defined as the diameter of the sphere which volume is equal to that of the actual inclusion. Let  $D$  be this diameter and  $R$  the corresponding radius. The test makes sense if the physical properties correspond roughly to an inertia dominated flow with a very low viscosity for the gas and the liquid. This means that the capillary numbers based on the physical properties of each phase are very small. They are defined by:

$$C_{a_k} = \frac{\rho_k}{\mu_k} \sqrt{\frac{D\sigma}{\rho_k}}$$

where the subscript k = l;g denotes respectively the liquid or the gas phase,  $\rho_k$  ,  $\mu_k$  is the dynamical viscosity and  $\sigma$  is the surface tension between the gas and the liquid. Therefore, it is assumed that viscosity effects vanish when the following condition is fulfilled:

$$C_{a_k} \gg 1$$

#### Analytique validaton

To validate the simulations, we will estimate the frequency of oscillations and the damping rates. These parameters will be analyzed and compared to the analytical models from the literature given by Lamb [1]

who derived the frequency of oscillations of such an inclusion. This derivation is based on the potential flow theory and is valid for any arbitrary inner and outer values of the density. This is shown for example by Lamb [1], (p. 475, equation 10). The angular frequency of the oscillations is obtained for each mode by using the linearized momentum jump at the interface; it is given by:

$$\omega_n^2 = \frac{n(n+1)(n-2)(n+2)}{(n+1)\rho_g + n\rho_i} \frac{\sigma}{R^3}$$

The oscillation frequency [Hz] is given by :

$$f_n = \frac{\omega_n}{2\pi}$$

The rate of damping [s] is given by:

$$\tau = \frac{1}{(n-1)(2n+1)} \frac{r^2 \rho_g}{\mu_g}$$

We focus on the main oscillation mode  $n = 2$ , which correspond to the slowest dissipation of kinetic energy (the mode with the lowest frequency). It leads to the theoretical value of 50 Hz, for the interface oscillation. Two calculations are made in this sheet. The differences between these 2 calculations relate only to the parameters of meshing used which will be explained in the paragraph **Mesh**.

Numerically, the oscillation frequencies of the bubble will be determined by estimating its discrete area at any time during the simulation. So, the amplitudes will correspond to the surface of the bubble. Initially this surface corresponds to a scalene ellipsoid surface (half-axes of ellipsoid are different). This surface was estimated analytically by Knud Thomsen, it's given by:

$$S = 4\pi \left( \frac{a^p b^a + a^p c^p + b^p c^p}{3} \right)^{\frac{1}{p}}$$

Where : a,b and c are the half-axes of the ellipsoide as  $c \prec b \prec a$  et  $p = 1.6075$

This result will be used as an analytical criterion to validate the initial amplitude of the numerical frequency.

The numerical pressure differencing  $\Delta P$  between the two phases at the interface will also be determined and compared with the analytical solution of Laplace, for the case of an undeformed sphere, it's given by :

$$\Delta P = \sigma \left( \frac{1}{R_1} + \frac{1}{R_2} \right)$$

Where :  $R_1$  and  $R_2$  are the main radius of curvature of a spherical bubble

This result will be used to determine if the pressure variation at the interface oscillates around this reference value because in our case the bubble is not spherical

The table .. summarizes the analytical validation values obtained for our flow parameters

## Geometry

	analytic values
Frequency f [Hz]	72.056
Rate of damping [s]	12.8
Initial surface of bubble [ $m^2$ ]	3.23e-05
Pressure deflating [Pa]	87.5

Table VII.1.1: Analytic values for validation

The problem is solved in a cubic field of 0.01 meter side. An ellipsoide bubble having an equivalent diameter is of 0.032 m is initially positioned in its center.

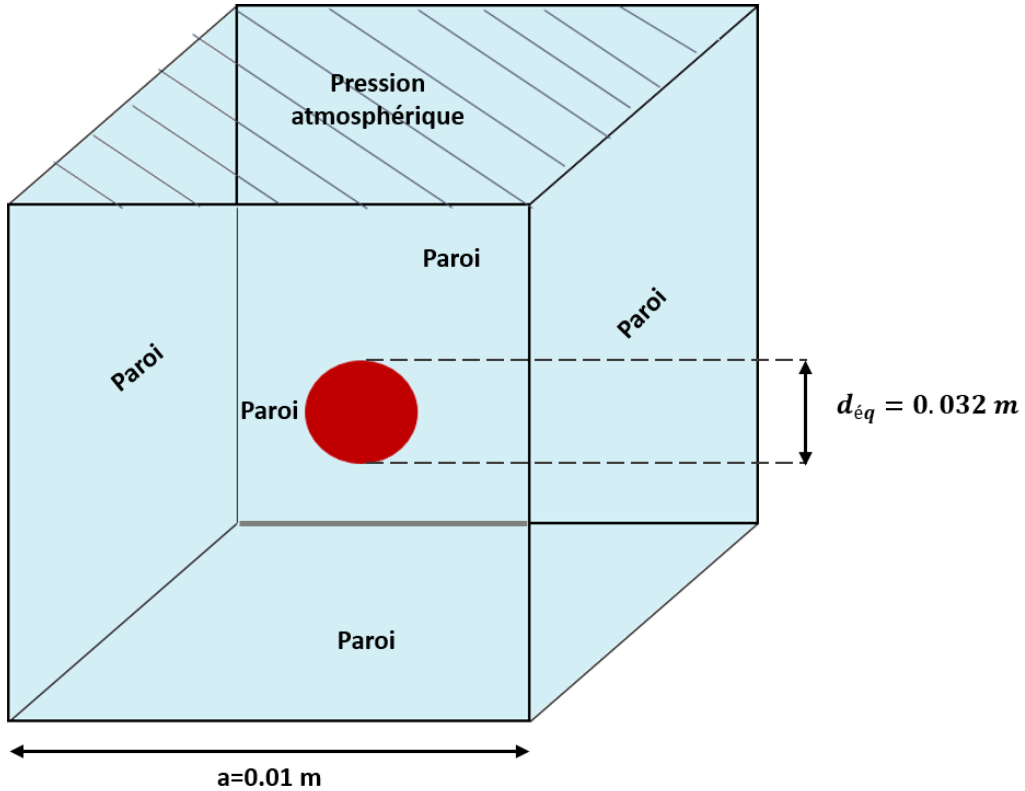


Figure VII.1.1: Geometry

### Initial Conditions and Boundary Conditions

Different initial and boundary conditions are applied between the domain and the water-air interface.

- **For the domain:**

→ *Initial condition:* zero uniform velocity field for the 3 directions (fluid at rest)

→ *Boundary conditions:* at the top of the domain, an outlet boundary condition is defined with an uniform field for  $P/\rho$  equal to 0 ( $\text{Pa}/\text{kg} \cdot \text{m}^3$ ). For the 5 other borders, a situation of adherence is defined.

- **For the interface:**

→ *Initial condition:* the following function is applied to define the initial shape of the bulle :  $0.0016 * 0.0016 - ((x - 0.005) * (x - 0.005) / 2.21 + (y - 0.005) * (y - 0.005) * 2.21 + (z - 0.005) * (z - 0.005))$

→ *Boundary conditions:* a specific boundary condition for discontinuous Front\_Tracking problem is defined *paroi\_ft\_disc* with a symetrie condition.

### Fluid Properties

In order to construct the diphasic fluid, two incompressible fluids, water and air, are defined by the usual. The fluid parameters are presented in the table bellow

	$\rho_g (\text{kg}/\text{m}^3)$	$\mu_g (\text{N}/\text{m}^2/\text{s})$	$\rho_l (\text{kg}/\text{m}^3)$	$\mu_l (\text{N}/\text{m}^2/\text{s})$
Values	1.0	1e-07	1000.0	1e-05

Table VII.1.2: Physical parameters of fluids

### 1.3 Case Setup

#### Grid

The modeling approach here is the Front-Tracking method, so there are two meshes: a fixed hexahedral one in the phases, where are solved the conservation equations and a mobile mesh which follows the interface during its displacement by the moving of markers. In this study

- **Eulerien mesh:**

Five meshes are used, they are defined as follows:

- ⇒ Mesh 1 : 43\*43\*43,
- ⇒ Mesh 2 : 61\*61\*61,
- ⇒ Mesh 3 : 86\*86\*86,
- ⇒ Mesh 4 : 121\*121\*121,
- ⇒ Mesh 5 : 170\*170\*170.

- **Lagrangien mesh in the interface:**

The modeling approach used is the Front-Tracking, so it is essential to re-mesh the interface in order to ensure a good quality of mesh and to conserve the volume. For that, it will be necessary to determine the good parameters to use in the remeshing algorithm.

After a series of tests, two configurations of remeshing parameters were retained. The difference between these two configurations named after case 1 and case 2 is located at the number of Lagrangian markers at the interface and the frequency of the smoothing. The smoothing represents the frequency of diffusion of the curvature per time step during the remeshing process.

The remeshing parameters used in the two cases are illustrated in the data files.

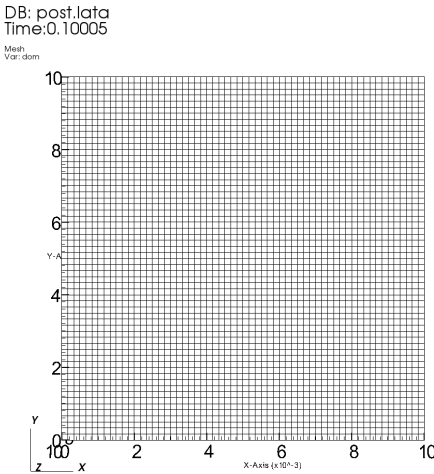


Figure VII.1.2: Illustration of the Eulerien and Lagrangien mesh for 61x61x61 hexaedra

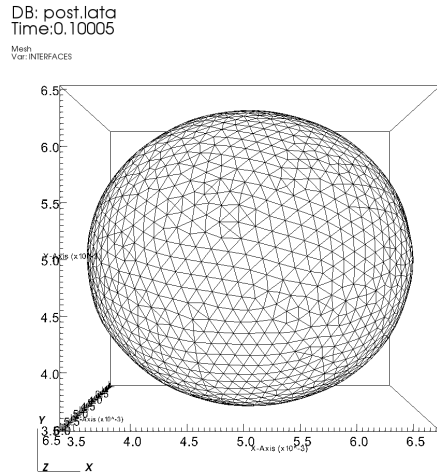


Figure VII.1.3: Cas\_01 : M2 : Bubble in a square box : oscillations of the interface

#### Model Options

Two equations are compulsory : a momentum balance equation (alias Navier-Stokes equation) and an interface tracking equation. The list of equations to be solved is declared in the beginning of the data file. Another difference with more classical TRUST data file, lies in the fluids definition. The two-phase fluid (Fluide\_Diphasique) is made with two usual single-phase fluids (Fluide\_Incompressible). As the list of equations to be solved in the generic Front-Tracking problem is declared in the data file and not predefined in the structure of the problem, each equation has to be distinctively associated with the problem with the Associer keyword.

## Other Options (calculation)

The time scheme defined in this test case is the Explicit Euler scheme and the Rungue Kutta 3 scheme  
The convection schemes defined in this test are : Upwind scheme (decentre amont), central differencing scheme (centre d'ordre 2) and Quick scheme

## 1.4 Results

### Validation Specific Informations

- Version TRUST : 1.9.0
- Type of problem: Front Tracking problem
- Discretization: VDF
- Convection scheme : Schema\_Euler\_explicite
- Type of fluid : air and water
- Location: Front\_tracking\_discontinu/share/Validation/Rapports\_automatiques/FTD\_oscillating\_bubble
- Master Test case: Bulle/FTD\_Oscillation\_Bulle\_3D\_VDF.data
- Generated Test cases :
  - Bulle/Cas\_01/M1/FTD\_Oscillation\_Bulle\_3D\_VDF.data : /\* data file in appendix \*/
  - Bulle/Cas\_01/M2/FTD\_Oscillation\_Bulle\_3D\_VDF.data :
  - Bulle/Cas\_01/M3/FTD\_Oscillation\_Bulle\_3D\_VDF.data :
  - Bulle/Cas\_01/M4/FTD\_Oscillation\_Bulle\_3D\_VDF.data :
  - Bulle/Cas\_02/M1/FTD\_Oscillation\_Bulle\_3D\_VDF.data : /\* data file in appendix \*/
  - Bulle/Cas\_02/M2/FTD\_Oscillation\_Bulle\_3D\_VDF.data :
  - Bulle/Cas\_02/M3/FTD\_Oscillation\_Bulle\_3D\_VDF.data :
  - Bulle/Cas\_02/M4/FTD\_Oscillation\_Bulle\_3D\_VDF.data :
- Performance Chart :

	host	system	Total CPU Time	CPU time/step	number of c
Bulle/Cas_01/M1/FTD_Oscillation_Bulle_3D_VDF	uruk	Linux	193.989	0.800002	74088
Bulle/Cas_01/M2/FTD_Oscillation_Bulle_3D_VDF	uruk	Linux	730.774	1.9231	216000
Bulle/Cas_01/M3/FTD_Oscillation_Bulle_3D_VDF	uruk	Linux	1244.29	1.98737	614125
Bulle/Cas_01/M4/FTD_Oscillation_Bulle_3D_VDF	uruk	Linux	5585.06	4.74404	1728000
Bulle/Cas_02/M1/FTD_Oscillation_Bulle_3D_VDF	uruk	Linux	254.466	0.694837	74088
Bulle/Cas_02/M2/FTD_Oscillation_Bulle_3D_VDF	uruk	Linux	998.766	1.10773	216000
Bulle/Cas_02/M3/FTD_Oscillation_Bulle_3D_VDF	uruk	Linux	2881.92	1.17606	614125
Bulle/Cas_02/M4/FTD_Oscillation_Bulle_3D_VDF	uruk	Linux	25127.7	4.34562	1728000
Total			37017		

Table VII.1.3: Performance Chart

## Plot Data

- Oscillation frequency and pressure difference:

We compare the value of the frequency of the oscillation obtained in the calculation (case 1 and cas 2) to the theoretical one. We can see in the figures below that results are satisfactory. The oscillations of free surface correspond to the theoretical value of 72 Hz. For more details, and at first glance, the oscillation frequencies are double the reference frequency. Indeed, over an analytical period, we have two numerical periods as we can clearly see in the following figure. This is explained by the fact that the initial deformation of the bubble in mode 2 is equivalent to a flattened shape, it will oscillate in order to resume its most stable shape which is the spherical shape, passing through an elongated shape obtained after a first period of oscillation, then it will return to its original flattened shape after a second period of oscillation. It therefore takes two periods for the bubble to resume its initial deformation, and it is this period allowing an initial resumption of shape which is considered as a total period of oscillation as we can see in the second figure.

The pressure difference between inner and outer fluid is also correctly reproduced. The area of the ellipsoide which correspond to the amplitud of the frequency curve at time 0s is well estimated. In the is It seems this result could be considered as a reference calculation. One can see a time damping of oscillations. This effect is due to numerical diffusion due to the utilisation of the upwind scheme.

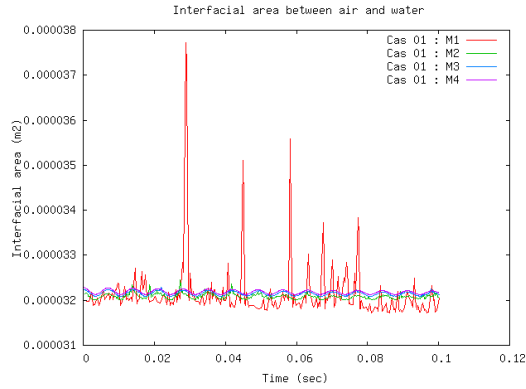


Figure VII.1.4: Interfacial area between air and water

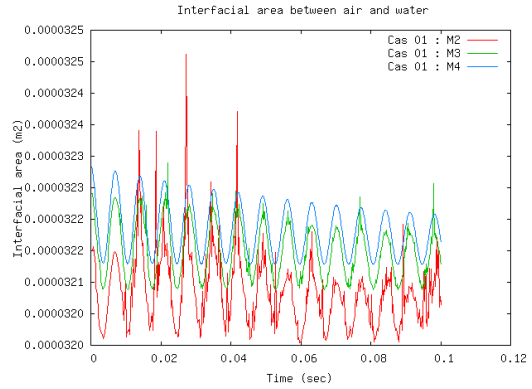


Figure VII.1.5: Interfacial area between air and water

According to the previous figure, the M1 mesh does not correctly deal with the desired problem. Its bad results can come either from an insufficient remeshing or from a too large time step of calculation. We therefore remove it from the previous curve in order to have a finer view of the results obtained with the meshes M2, M3 and M4.

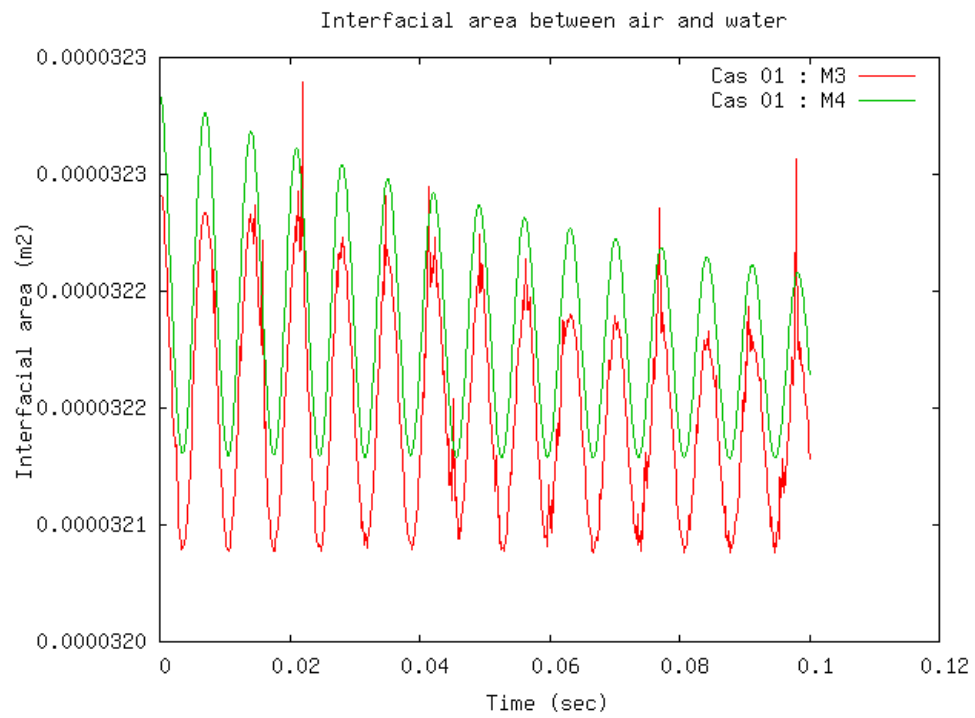


Figure VII.1.6: Interfacial area between air and water

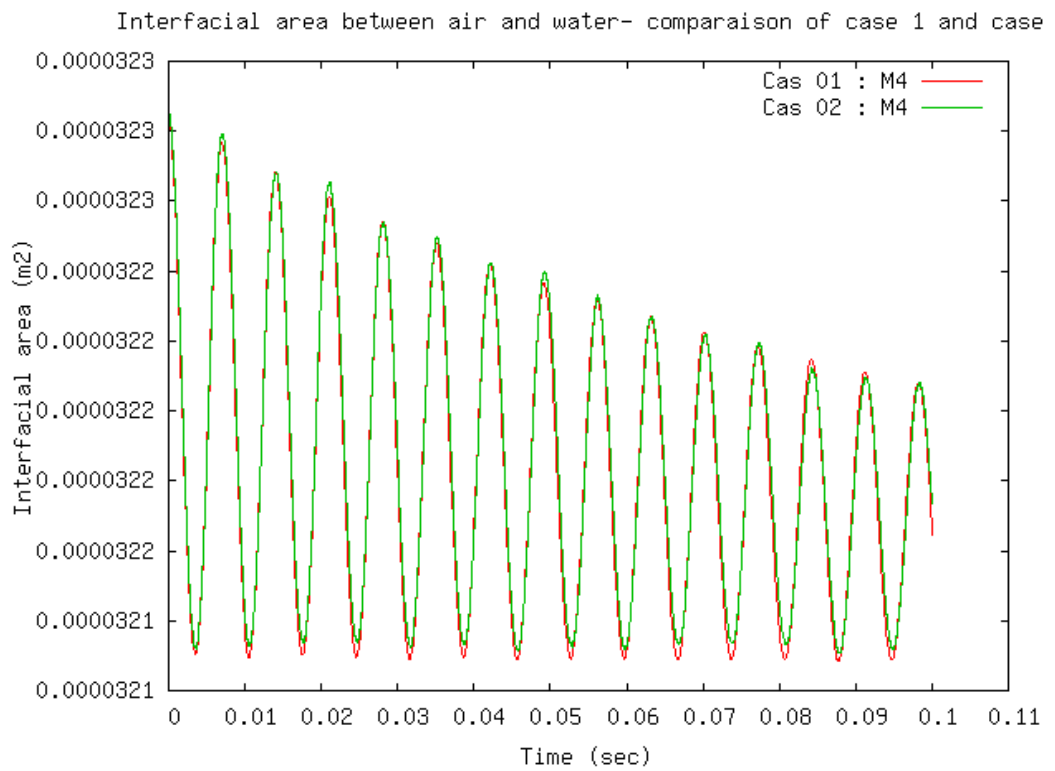


Figure VII.1.7: Interfacial area between air and water- comparaison of case 1 and case 2

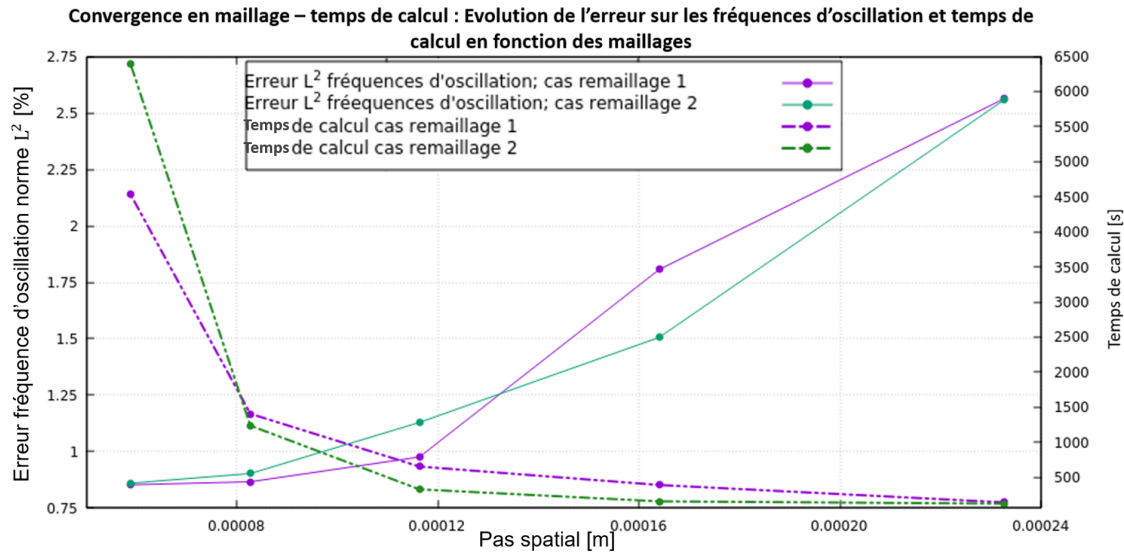


Figure VII.1.8: Mesh convergence : frequency error and time calculation - This curve is not updated when we regenerate the validation sheet

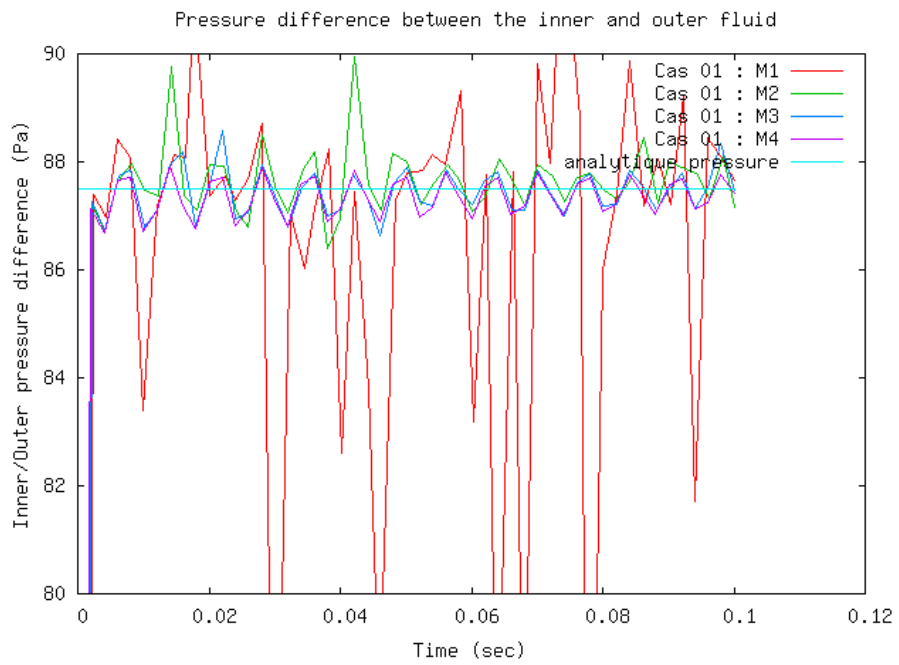


Figure VII.1.9: Pressure difference between the inner and outer fluid

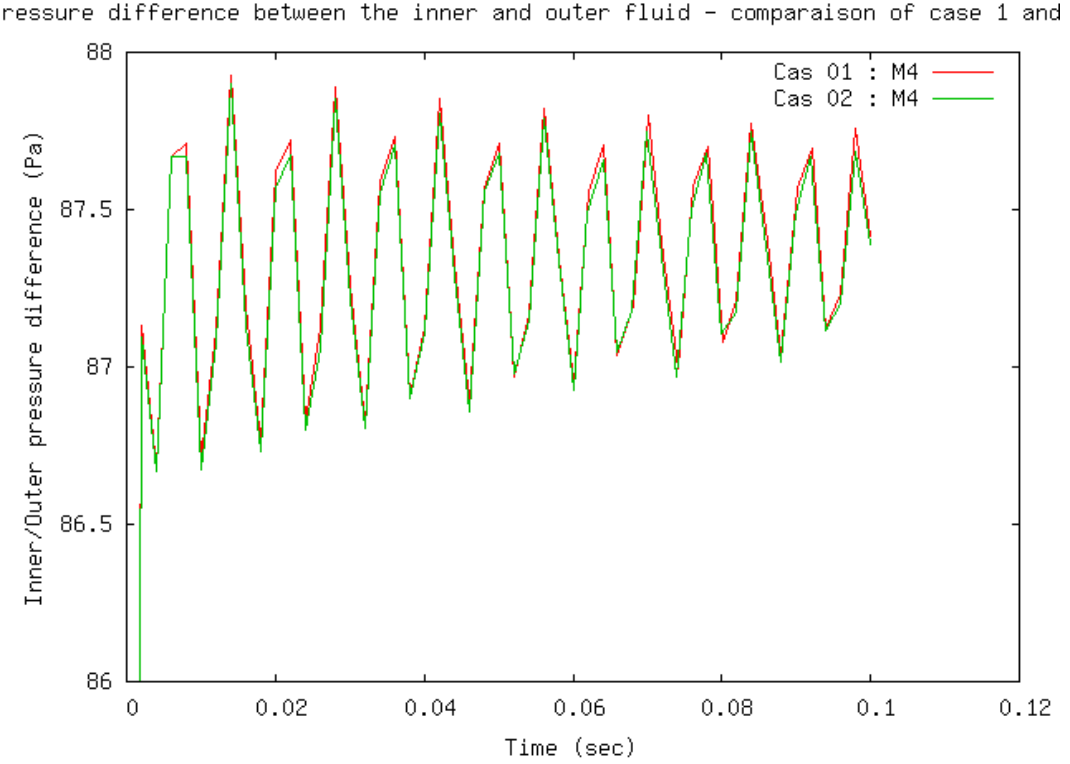


Figure VII.1.10: Pressure difference between the inner and outer fluid - comparaison of case 1 and case 2

- **Damping of oscillations with different numerical schemes:**

Now, we will study the effect of the discretization scheme on the damping of the oscillations. For this, three numerical schemes will be analyzed : the Upwind (primary study), the centered and the Quick. From the figure bellow, it is clear that these three schemes give an identical result for the frequencies of oscillations. But the rate of damping is different, the Upwind scheme dissipates more than the centered and the Quick, because this scheme induces more numerical diffusion unlike the centered and quick schemes which are of higher order and less diffusive.

Regarding the damping rate, it is in order of 0.02 s for the three schemes, so the influence of the numerical scheme is very light. This is due to the remeshing procedure which is more prevalent, inducing surface tensions which modify the shape of the bubble. Its shape will tend to approach the equilibrium shape much faster, so the oscillations are damped.

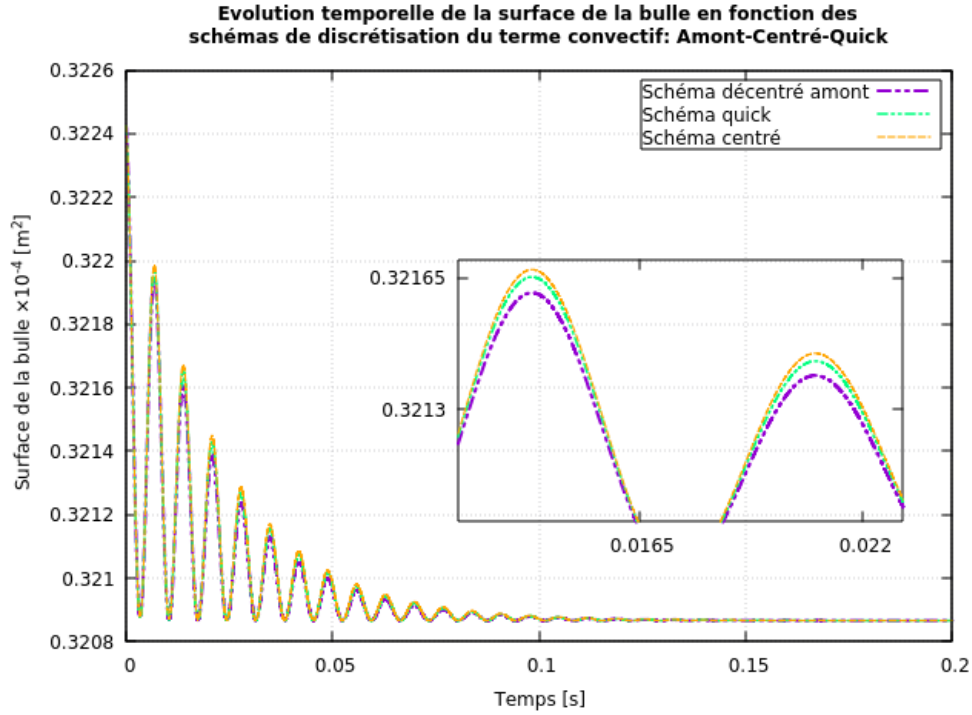


Figure VII.1.11: Damping of oscillation with different numerical schemes - This curve is not updated when we regenerate the validation sheet

As we can see in the figure bellow, the reduction in remeshing and smoothing resulted in a reduction in depreciation. But the dissipation is always present, numerical damping is more accentuated than the analytical predictions.

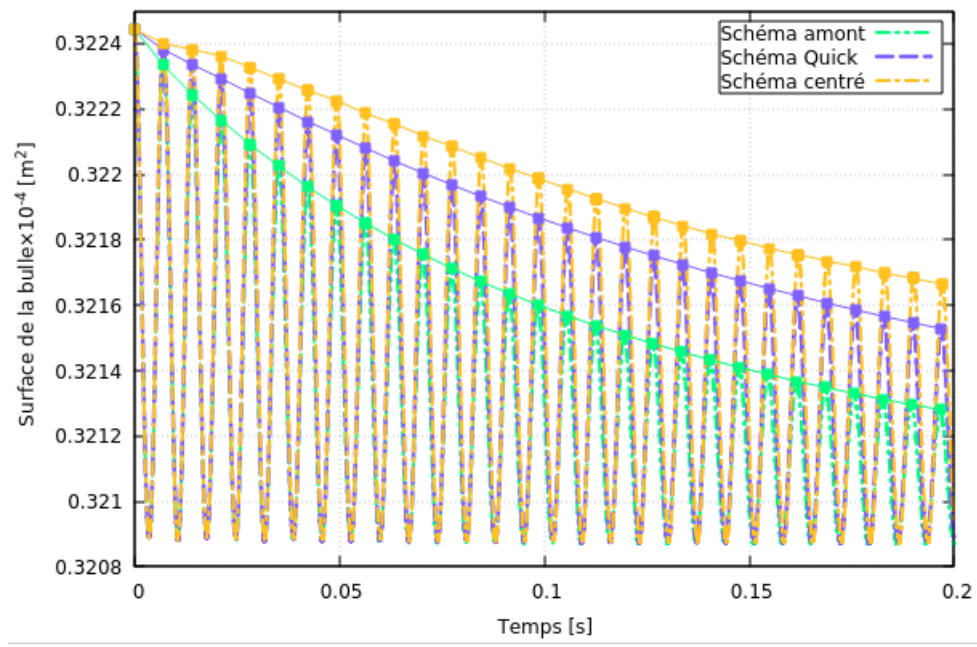


Figure VII.1.12: Damping of oscillation with different numerical shemes after reduction of remeshing - This curve is not updated when we regenerate the validation sheet

- **Comparison of the results given by the two temporal schemes Euler and Runge Kutta 3:**

As we can see in the following figure, temporal schemes (Euler explicite and Runge Kutta 3) give the same result in frequence of oscillation and the damping

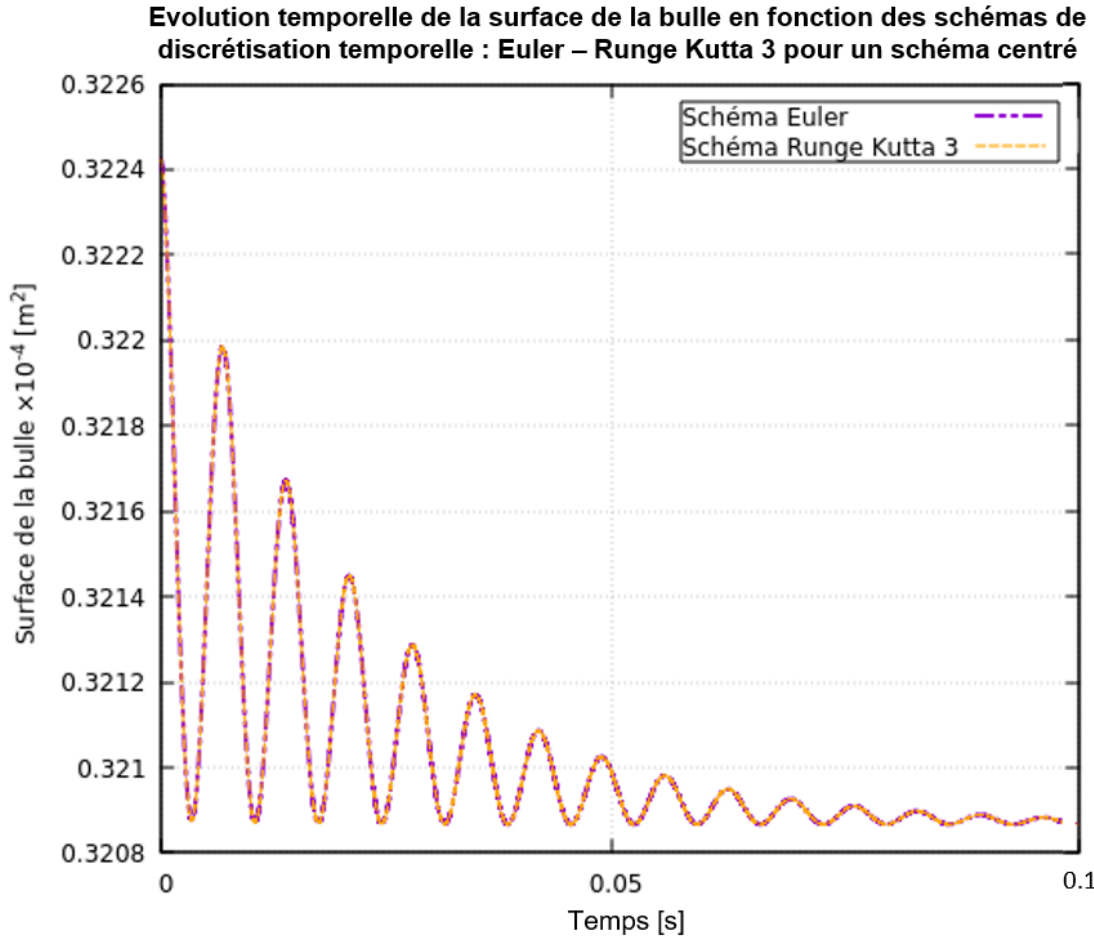


Figure VII.1.13: Comparison of the results given by the two temporal schemes Euler and Runge Kutta 3 - This curve is not updated when we regenerate the validation sheet

- **Study on the limit time step stability in the interface:**

After having validated simulations, we will interest on a very important criterion, it is the time step limit which ensures the stability of computation. It's defined as being the time step of the Navier Stokes equation beyond which the simulation becomes unstable. The added value of this present study is that can be generalized.Indeed, the aim is to find a CFL to integrate into the source code.

We will determine a limit for time step stability in order to find the proportionality factor which links this parameter to the spacing between two markers at the interface.In this study, the two cases of remeshing parameter were tested, in order to see if this proportionality varies according to the type of remeshing.

The results show that the limit time step stability varies linearly with the Lagrangian mesh, with a slope which depends on the parameters used in the algorithm of remeshing.The time step of stability decreases linearly with the refinement of the mesh. The proportionality factor between these two parameters is the slope which have unit of [s / m]. This slope must be dimensioned with a combination of physical parameters of fluids (viscosity, mass volume, surface tension ...).

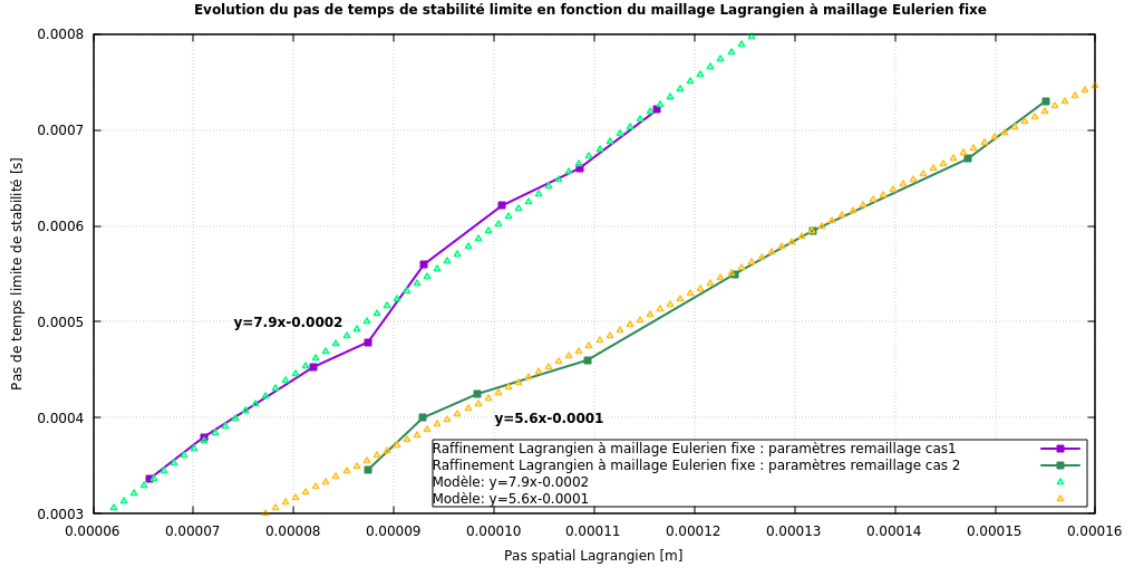


Figure VII.1.14: Limit Time step for stability at the interface - This curve is not updated when we regenerate the validation sheet

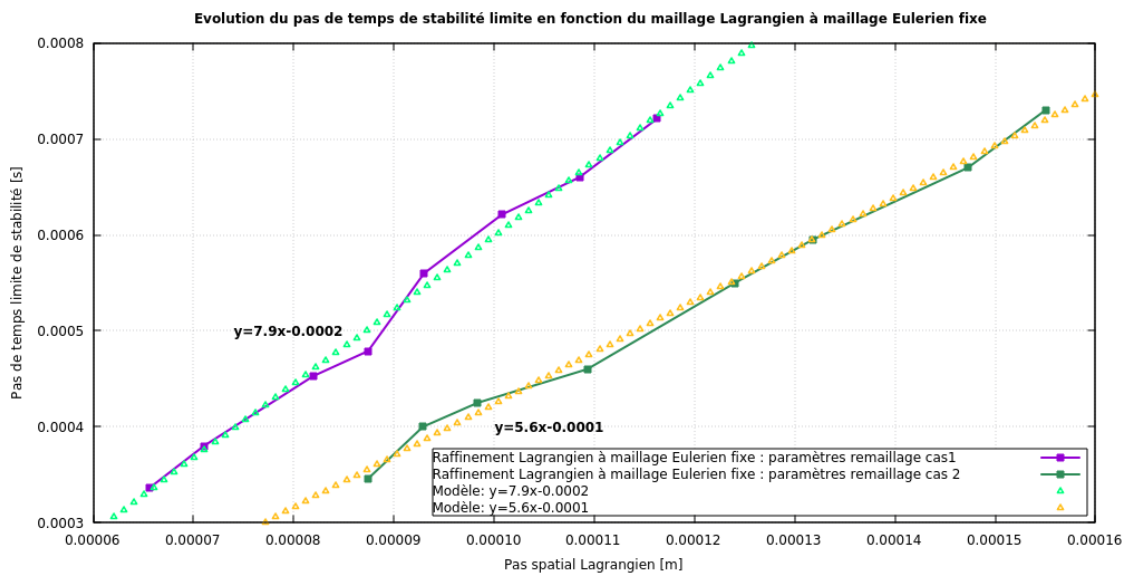


Figure VII.1.15: Limit Time step for stability at the interface - This curve is not updated when we regenerate the validation sheet

- Profiles of the oscillating bubble every 0.002 second:

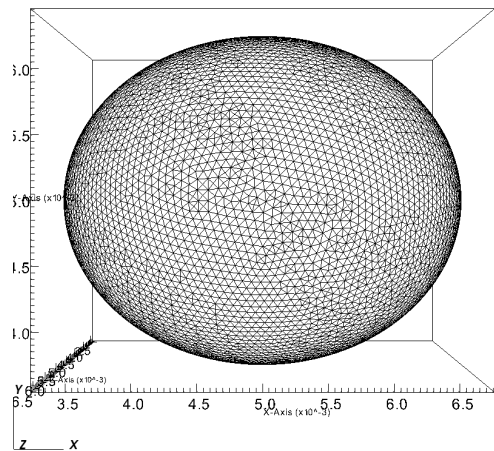
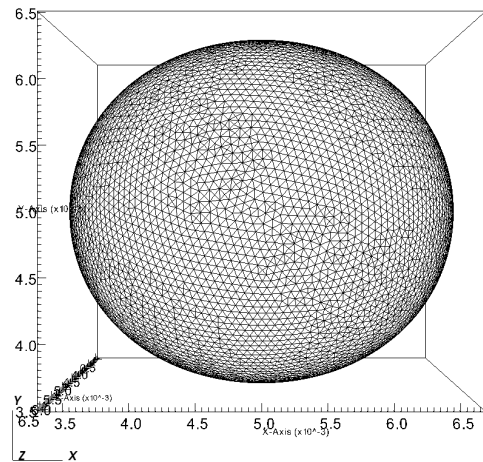
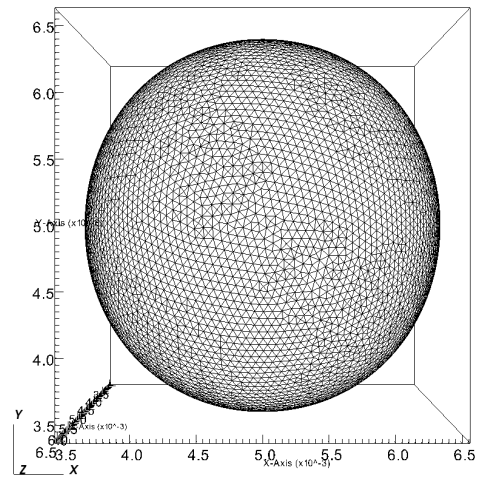
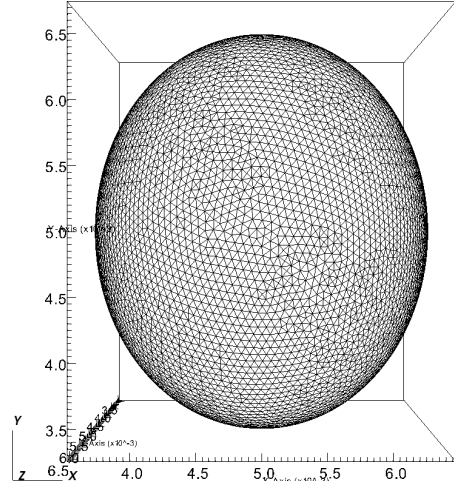
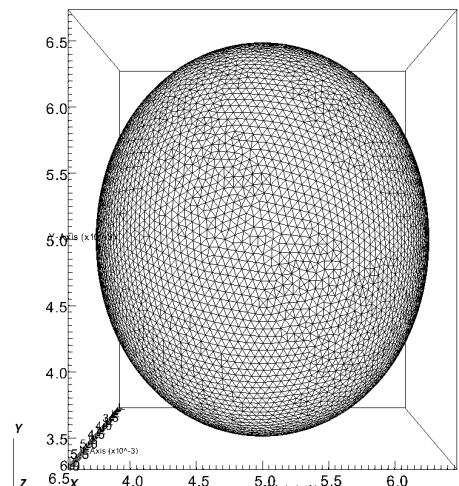
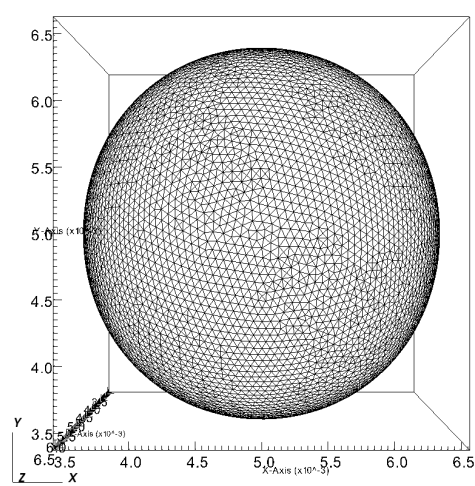
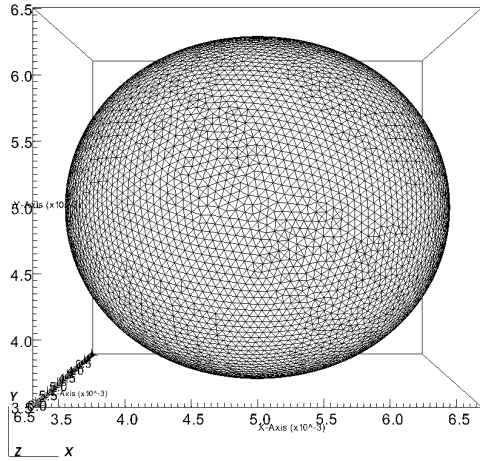
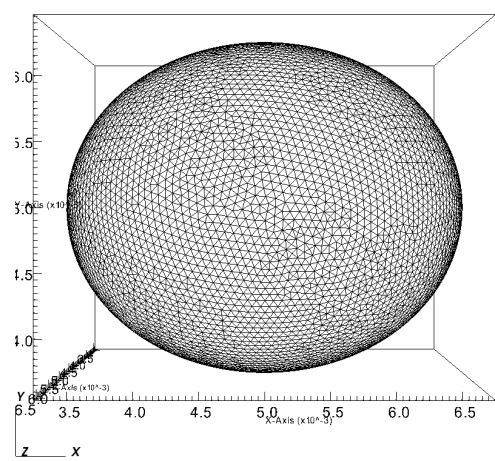


Figure VII.1.16: Initial interface

Figure VII.1.17: Bubble interface at  $t=0.002s$ Figure VII.1.18: Bubble interface at  $t=0.004s$ Figure VII.1.19: Bubble interface at  $t=0.006s$ Figure VII.1.20: Bubble interface at  $t=0.008s$ Figure VII.1.21: Bubble interface at  $t=0.01s$

Figure VII.1.22: Bubble interface at  $t=0.012s$ Figure VII.1.23: Bubble interface at  $t=0.014s$ 

## 1.5 Conclusion

The present work consists of a validation of the Front-Tracking algorithm of TrioCFD on the case of the oscillating bubble. The bubble had good physical behavior during simulations when the interface remeshing parameters were well chosen.

The results converged to the analytical solutions, this test case demonstrates the ability of the TrioCFD code to manage this flow topology. So, the Front-Tracking algorithm has been validated.

## 1.6 References

- [1] Lamb, H.1932 Hydrodynamics. Cambridge University Press.

## 1.7 Data Files

### FTD\_Oscillation\_Bulle\_3D\_VDF

```
# Hydraulique 3D laminaire : schema upwind #
# PARALLEL ONLY 2 #
dimension 3
Probleme_FT_Disc_gen pb
Domaine dom
Scatter dom.Zones dom
VDF dis
Schema_Euler_explicie sch
Read sch
{
  tinit 0.0
  tmax 0.1
  dt_min 1.e-10
  dt_max 9.e-4
  dt_impr 0.2
  dt_sauv 0.1
  seuil_statio -1.e-8
  facsec 0.91
}
Fluide_Incompressible eau
Read eau
{
```

```

mu Champ_Uniforme 1 1.e-5
rho Champ_Uniforme 1 1000.
}
Fluide_Incompressible air
Read air
{
  mu Champ_Uniforme 1 1.e-7
  rho Champ_Uniforme 1 1.
}
Fluide_Diphasique fluide
Read fluide
{
  fluide0 eau
  fluide1 air
  sigma Champ_Uniforme 1 0.07
}
Champ_Uniforme gravite
Read gravite 3 0. 0. 0.
Associate fluide gravite
Navier_Stokes_FT_Disc      hydraulique
Transport_Interfaces_FT_Disc interf
Associate pb hydraulique
Associate pb interf
Associate pb dom
Associate pb sch
Associate pb fluide
System "mkdir -p lata"
Discretize pb dis
Read pb
{
hydraulique
{
  modele_turbulence sous_maille_wale
  {
    Cw          0.
    turbulence_paroi negligable
  }
  solveur_pression GCP { precond ssor { omega 1.6 } seuil 1.e-10 impr }
  convection      { amont }
  diffusion       { }
  conditions_initiales { vitesse champ_uniforme 3 0. 0. 0. }
  equation_interfaces proprietes_fluide interf
  boundary_conditions
  {
    haut Sortie_libre_rho_variable champ_front_uniforme 1 0.
    gauche paroi_fixe
    droite paroi_fixe
    bas paroi_fixe
    devant paroi_fixe
    fond paroi_fixe
  }
  terme_gravite rho_g
}
interf
{
  conditions_initiales {
    fonction 0.0016*0.0016 -((x-0.005)*(x-0.005)/1.21+(y-0.005)*(y-0.005)*1.21+(z-0.005)*(z-0.005))
  }
  methode_transport vitesse_interpolee hydraulique
    # iterations_correction_volume 2 #
  VOFlike_correction_volume 1
}

```

```

nb_lissage_correction_volume 2
    nb_iterations_correction_volume 1 # taken from nb_iter_correction_volume in remaillage
    n_iterations_distance 2
remaillage {
    pas 1e-8
    nb_iter_remaillage 5
    critere_arete 0.35
    critere_remaillage 0.20
    pas_lissage 1e-8
    lissage_courbure_iterations 10
    lissage_courbure_coeff -0.1
    nb_iter_barycentrage 25
    relax_barycentrage 1.
    facteur_longueur_ideale 0.8
    nb_iter_correction_volume 1
    seuil_dvolume_residuel 1e-15
}
boundary_conditions
{
    gauche Paroi_FT_disc symetrie
    droite Paroi_FT_disc symetrie
    haut Paroi_FT_disc symetrie
    bas Paroi_FT_disc symetrie
    devant Paroi_FT_disc symetrie
    fond Paroi_FT_disc symetrie
}
postraitements {
    Sondes
    {
        sonde_pression nodes pression periode 2.e-3 Points 2 0.005 0.005 0.005 0.009 0.009 0.009
    }
    champs dt_post 1. {
        vitesse elem
        indicatrice_interf
    }
}
liste_postraitements {
    postraitements_ft_lata post1 {
        format Lata
        fichier lata/post
        champs dt_post 0.002 {
            indicatrice_interf elem
        }
        interfaces interf {
            courbure som
        }
    }
}
sauvegarde binaire Oscillation_bulle3.rep
}
Solve pb
End
postraitements {
    Sondes
    {
        sonde_vitesse nodes vitesse periode 2.e-3 Segment 51 0. 0.005 0.0025 0.0025
        sonde_pression nodes pression periode 2.e-3 Segment 51 0. 0.005 0.0025 0.0025
        sonde_rho nodes indicatrice_interf periode 2.e-3 Segment 51 0. 0.005 0.0025 0.0025
    }
    champs dt_post 1. {
}

```

```

        vitesse elem
        indicatrice_interf
    }
}
liste_postraitements {
    postraitements_ft_lata post1 {
        format Lata
        fichier lata/post2DVDF
        champs dt_post 0.002 {
            indicatrice_interf elem
            pression som
            vitesse faces
        }
        interfaces interf {
            pe som
            courbure som
        }
    }
}

```

**FTD\_Oscillation\_Bulle\_3D\_VDF**

```

# Hydraulique 3D laminaire : schema upwind #
# PARALLEL ONLY 2 #
dimension 3
Probleme_FT_Disc_gen pb
Domaine dom
Scatter dom.Zones dom
VDF dis
Schema_Euler_explique sch
Read sch
{
    tinit 0.0
    tmax 0.1
    dt_min 1.e-10
    dt_max 9.e-4
    dt_impr 0.2
    dt_sauv 0.1
    seuil_statio -1.e-8
    facsec 0.78
}
Fluide_Incompressible eau
Read eau
{
    mu Champ_Uniforme 1 1.e-5
    rho Champ_Uniforme 1 1000.
}
Fluide_Incompressible air
Read air
{
    mu Champ_Uniforme 1 1.e-7
    rho Champ_Uniforme 1 1.
}
Fluide_Diphasique fluide
Read fluide
{
    fluide0 eau
    fluide1 air
    sigma Champ_Uniforme 1 0.07
}
Champ_Uniforme gravite

```

```

Read gravite 3 0. 0. 0.
Associate fluide gravite
Navier_Stokes_FT_Disc           hydraulique
Transport_Interfaces_FT_Disc     interf
Associate pb hydraulique
Associate pb interf
Associate pb dom
Associate pb sch
Associate pb fluide
System "mkdir -p lata"
Discretize pb dis
Read pb
{
hydraulique
{
    modele_turbulence sous_maille_wale
    {
        Cw          0.
        turbulence_paroi negligable
    }
    solveur_pression GCP { precond ssor { omega 1.6 } seuil 1.e-10 impr }
    convection      { amont }
    diffusion       { }
    conditions_initiales { vitesse champ_uniforme 3 0. 0. 0. }
    equation_interfaces proprietes_fluide interf
    boundary_conditions
    {
        haut Sortie_libre_rho_variable champ_front_uniforme 1 0.
        gauche paroi_fixe
        droite paroi_fixe
        bas paroi_fixe
        devant paroi_fixe
        fond paroi_fixe
    }
    terme_gravite rho_g
}
interf
{
    conditions_initiales {
        fonction 0.0016*0.0016-((x-0.005)*(x-0.005)/1.21+(y-0.005)*(y-0.005)*1.21+(z-0.005)*(z-0.005))
    }
    methode_transport vitesse_interpolee hydraulique
    # iterations_correction_volume 2 #
    VOFlike_correction_volume 1
    nb_lissage_correction_volume 2
    nb_iterations_correction_volume 1 # taken from nb_iter_correction_volume in remaillage
    n_iterations_distance 2
    remaillage {
        pas 1e-8
        nb_iter_remaillage 5
        criterie_arete 0.35
        criterie_remaillage 0.35
        pas_lissage 1e-8
        lissage_courbure_iterations_systematique 1 lissage_courbure_iterations_si_remaillage
        lissage_courbure_coeff -0.05
        nb_iter_barycentrage 25
        relax_barycentrage 1.
        facteur_longueur_ideale 1.
        nb_iter_correction_volume 1
        seuil_dvolume_residuel 1e-15
    }
}

```

```

boundary_conditions
{
    gauche Paroi_FT_disc symetrie
    droite Paroi_FT_disc symetrie
    haut Paroi_FT_disc symetrie
    bas Paroi_FT_disc symetrie
    devant Paroi_FT_disc symetrie
    fond Paroi_FT_disc symetrie
}
}

postraitements {
    Sondes
    {
        sonde_pression nodes pression periode 2.e-3 Points 2 0.005 0.005 0.005 0.009 0.009 0.009
    }
    champs dt_post 1. {
        vitesse elem
        indicatrice_interf
    }
}
liste_postraitements {
    postraitements_ft_lata post1 {
        format Lata
        fichier lata/post
        champs dt_post 0.002 {
            indicatrice_interf elem
        }
        interfaces interf {
            courbure som
        }
    }
}
sauvegarde binaire Oscillation_bulle3.rep
}
Solve pb
End
postraitements {
    Sondes
    {
        sonde_vitesse nodes vitesse
        sonde_pression nodes pression
        sonde_rho nodes indicatrice_interf
    }
    champs dt_post 1. {
        vitesse elem
        indicatrice_interf
    }
}
liste_postraitements {
    postraitements_ft_lata post1 {
        format Lata
        fichier lata/post2DVDF
        champs dt_post 0.002 {
            indicatrice_interf elem
            pression som
            vitesse faces
        }
        interfaces interf {
            pe som
            courbure som
        }
    }
}

```

}  
}

## Drop hanged at the ceiling

### 2.1 Purpose

The aim of this test is to check the capability of the Front Tracking algorithm to model the deformations of the free surface of a drop hanging in the air.

In the current state, this sheet is not really a validation sheet strictly speaking. Indeed, no advanced comparison, whether with other CFD codes or analytical results, is made. Some comparisons are nevertheless made on the evolution of the profile of the drop during the calculation with theoretical values but no reference is given.

By version v1.8.4, validation will be redone on this sheet in order to improve the stability of the test case as well as the validation of this phenomenon with other codes, theoretical and/or analytical results.

Validation made by : S.Pigny.

Report generated 09/06/2023.

### 2.2 Problem Description

A water drop is present at the upper frontier of a closed box. Despite the presence of gravity effects, its position can be maintained hanged close to a solid wall, by the action of surface tension forces. Phenomena related to the contact angle close to the solid wall play an important role. The contact angle is the angle between the surface where is hanged the drop and the tangent at the meridians of the drop close to the solid wall. It is measured on the external face of the drop. Its value leads to the determination of the amount of water that can be present in the drop, before it falls. The present test case is useful to analyse the way the surface tension forces are taken into account in the presence of contact angle. An emphasis is laid on the importance of parasitic currents. During the calculation, the bubble grows due to low velocity water injection. Water is injected at the center of the drop, via a boundary condition located in the wall. The surface involved in the boundary condition is much lower than the surface wetted by the drop. At the beginning of the process, the volume of the drop has a small value. Its shape tends to be a part of a sphere. Thereafter, it changes, due to hydrostatic pressure. The computationally obtained profile of the drop is compared to an analytical reference solution. Its shape is supposed to follow a cylindrical symmetry. It is given by the integration of the following equation :

$$-\frac{\partial \theta}{\partial s} - \frac{\sin \theta}{x} = \frac{g(\rho_l - \rho_g)}{\sigma} (y - y_0)$$

The parameter  $y_0$  is determined so that the contact angle at the top frontier keeps a fixed, constant, given value. The entire profile of the drop is determined via a classical iteration Runge-Kutta method.

In the case modeled here, the following assumptions are taken:

- The drop is hanged close to a solid support;
- The gravity is upwardly oriented;
- The y-axis is the axis of symmetry of the drop.

Solving the integral of the above equation with the previously mentioned hypotheses makes it possible to predict the theoretical profiles of a water drop in air, for different sizes, i.e for different amounts of water involved in it. Different contact angles with solid wall are also presented. Contact angle values are accounted

in the air. The numerical accuracy is satisfactory, since the curvature and the contact angle are second order calculated.

Two calculations are made in this sheet. The differences between them relate only to the contact angle between the tangential curve at the drop close to the wall. In the first case, this one measures 1.5 radian and 2.5 radians in the second case (these values are accounted in the air). This value will be defined in the boundary conditions of the testcase (see sub-section 2.2).

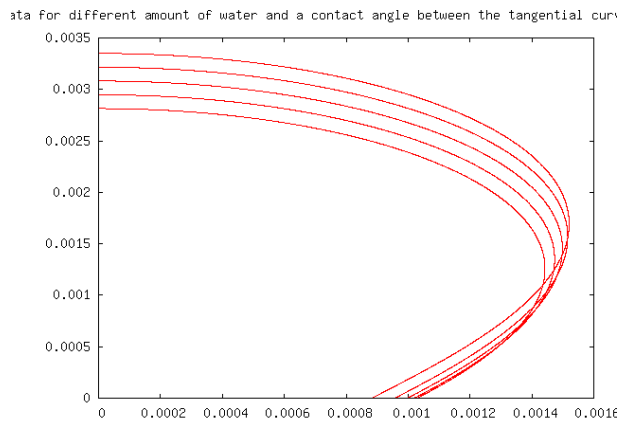


Figure VII.2.1: Profiles of the drop : theoretical data for different amount of water and a contact angle between the tangential curve at the drop close to the wall of 1 radian.

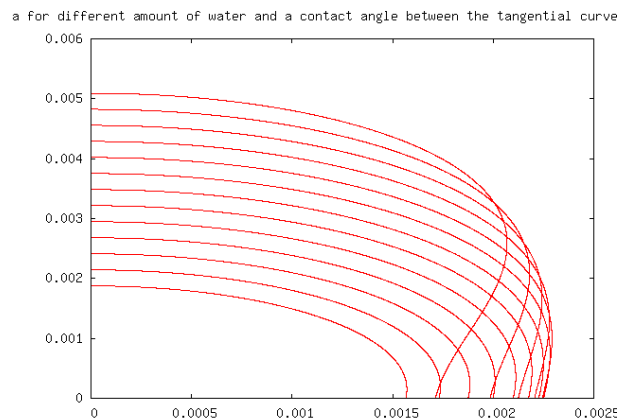


Figure VII.2.2: Profiles of the drop : theoretical data for different amount of water and a contact angle between the tangential curve at the drop close to the wall of 1.5 radian.

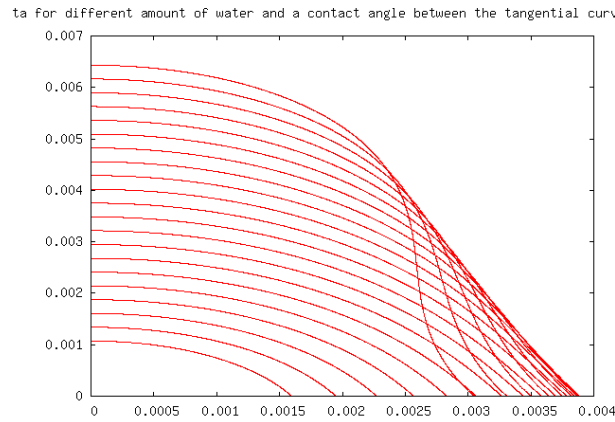


Figure VII.2.3: Profiles of the drop : theoretical data for different amount of water and a contact angle between the tangential curve at the drop close to the wall of 2 radian.

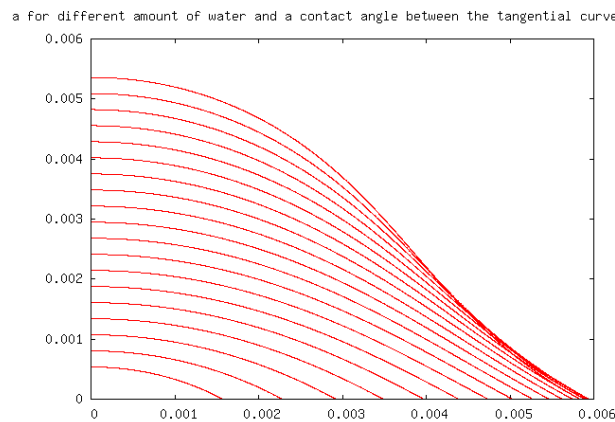


Figure VII.2.4: Profiles of the drop : theoretical data for different amount of water and a contact angle between the tangential curve at the drop close to the wall of 2.5 radian.

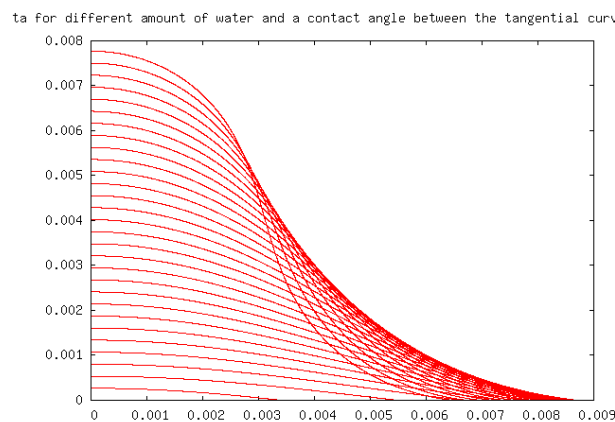


Figure VII.2.5: Profiles of the drop : theoretical data for different amount of water and a contact angle between the tangential curve at the drop close to the wall of 3 radian.

## Geometry

The problem is solved in a cuboid field with dimensions  $0.021 \times 0.012 \times 0.021$  meter according X, Y and Z directions. A drop initially hangs in the center of the top face of the cuboid. The angle formed between the free surface of the drop and the upper face of the domain is 1.5 radian (first case - accounted in the air) or 2.5 radians (second case - accounted in the air).

## Initial Conditions and Boundary Conditions

Different initial and boundary conditions are applied between the domain and the water-air interface.

- **For the domain:**

→ *Initial condition*: zero uniform velocity field for the 3 directions

→ *Boundary conditions*: at the top of the domaine, a velocity boundary condition of  $-0.1\text{m.s}^{-1}$  is applied to give a boost to the drop. At the top of the domain, an outlet boundary condition is defined with an uniform fiefs for  $P/\rho$  equal to 0 ( $\text{Pa/kg.m}^3$ ). For the 4 vertical borders, a situation of adherence is defined.

- **For the interface:**

→ *Initial condition*: the following function is applied to define the initial shape and position of the bubble :  $-(x - 0.0105) * (x - 0.0105) - (z - 0.0105) * (z - 0.0105) - (y - 0.012) * (y - 0.012) + 0.0005 * 0.0005$

→ *Boundary conditions*: a specific boundary condition for discontinuous Front\_Tracking problem is defined *paroi\_ft\_disc* . The boundary condition is used to define the initial contact angle formed by the drop on the upper wall. The defined function is of the form  $\alpha + \sqrt{((x - 0.0105) * (x - 0.0105) + (z - 0.0105) * (z - 0.0105)) * 1000}$ . where  $\alpha$  represents the contact angle on the liquid side. This value of  $\alpha$  will therefore be different for the 2 calculations:  $94^\circ$  in the liquid part to represent 1.5 radians in air (1st case) and  $37^\circ$  in the liquid part to represent 2.5 radians in air (2nd case).

## Fluid Properties

In order to construct the diphasic fluid, two incompressible fluids, water and air, are defined by the usual keyword *Fluide\_Incompressible* . Then, they are associated to create the two-phase fluid via the keyword *Fluide\_Diphasique* .

## 2.3 Case Setup

### Grid

Regarding the interface between air and water (drop surface), a specific mesh adapted to Front-Tracking problem has been defined.

The re-meshing criteria defined to model this phenomenon are relatively high with *lissage\_courbure\_iterations* = 20 , *lissage\_courbure\_coeff* = -0.05 and *facteur\_longueur\_ideale* = 1 .

Indeed, in Front-Tracking calculations, one can notice that the accuracy does not depend on the eulerian mesh only : the equilibrium profile is fully determinated via the geometrical curvature of interfaces and the gravity potentiel, which is evaluated at the interfacial nodes. It does not depend on discretised quantities related to the fixed mesh but to discretized quantities at the interface. Thus, to properly capture the profile of the drop, it is necessary to define an effective remeshing.

In the next version of this sheet, a study will be carried out on these parameters and recommendations adapted to the modeling of this phenomenon will be given to reach a good compromise between the CPU time and the fineness of the results.

### Model Options

This sheet deals with a generic Front-Tracking problem in the discontinuous version. It differs from others TrioCFD test cases : The problem does not state the number of equations that are enclosed in the problem.

Two equations are compulsory : a momentum balance equation (alias Navier-Stokes equation) and an interface tracking equation. The list of equations to be solved is declared in the beginning of the data file. Another difference with more classical TRUST data file, lies in the fluids definition. The two-phase fluid (Fluide\_Diphasique) is made with two usual single-phase fluids (Fluide\_Incompressible). As the list of equations to be solved in the generic Front-Tracking problem is declared in the data file and not predefined in the structure of the problem, each equation has to be distinctively associated with the problem with the Associer keyword.

## 2.4 Results

### Validation Specific Informations

- Version TRUST : 1.6.1
- Type of problem: Front Tracking problem
- Discretization: VDF
- Convection scheme: Schema\_Euler\_explicite
- Type of fluid: air and water at 293K
- Location: Front\_tracking\_discontinu/share/Validation/Rapports\_automatiques/FTD\_hanging\_drop
- Generated Test cases :
  - pendante\_1p5/goutte.data : /\* data file in annex \*/
  - pendante\_2p5/goutte.data : /\* data file in annex \*/
- Performance Chart :

	host	system	Total CPU Time	CPU time/step	number of cell
pendante_1p5/goutte	uruk	Linux	3021.13	0.98608	67240
pendante_2p5/goutte	uruk	Linux	11187.7	1.11624	67240
Total			14208.8		

Table VII.2.1: Performance Chart

### Plot Data

- **First Calculation: contact angle of 1.5 radian between the tangential curve at the drop close to the wall**

The following figures show the growth of the hanging drop at the top of the box for different times.

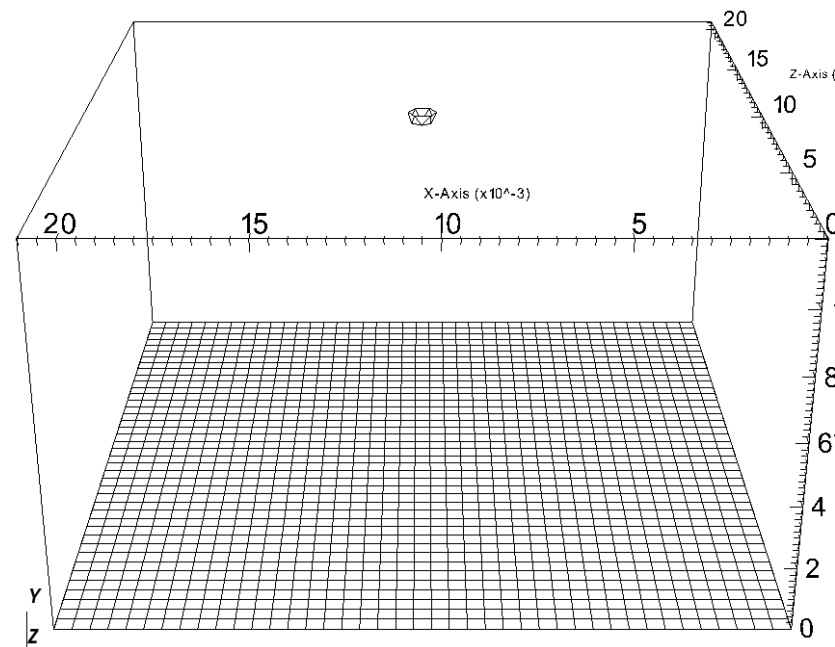


Figure VII.2.6: Drop hanged at the top of the box with a contact angle of 1.5 radian -  $t=0s$

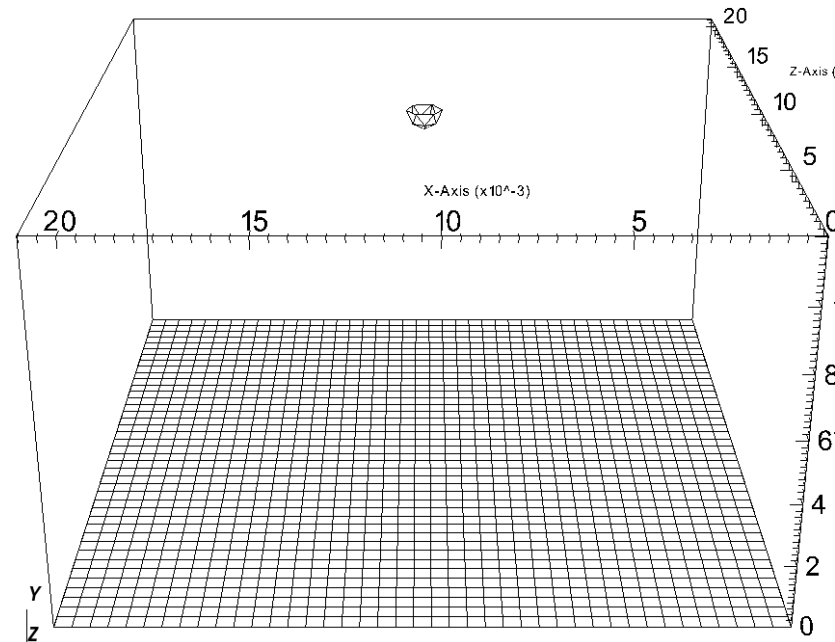


Figure VII.2.7: Drop hanged at the top of the box with a contact angle of 1.5 radian -  $t=0.01s$

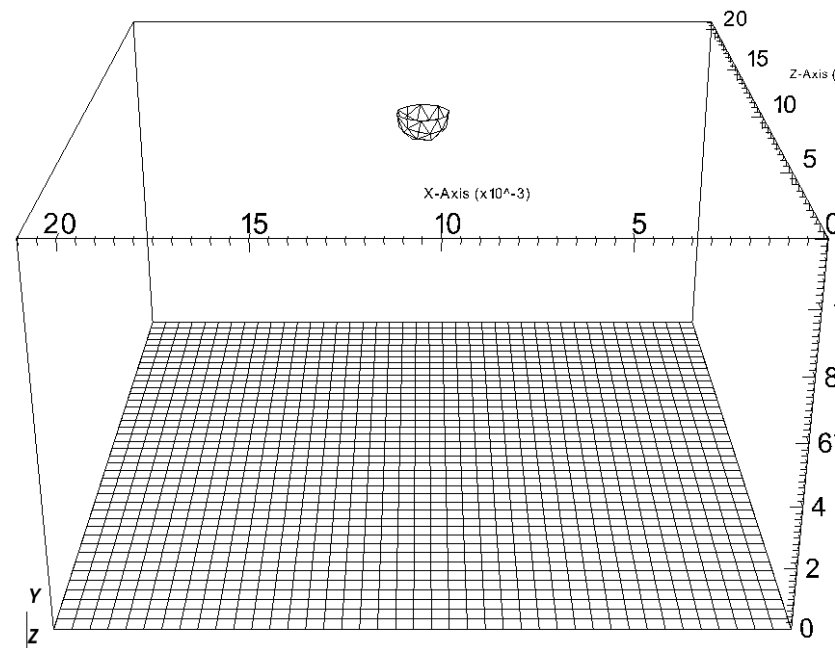


Figure VII.2.8: Drop hanged at the top of the box with a contact angle of 1.5 radian -  $t=0.05s$

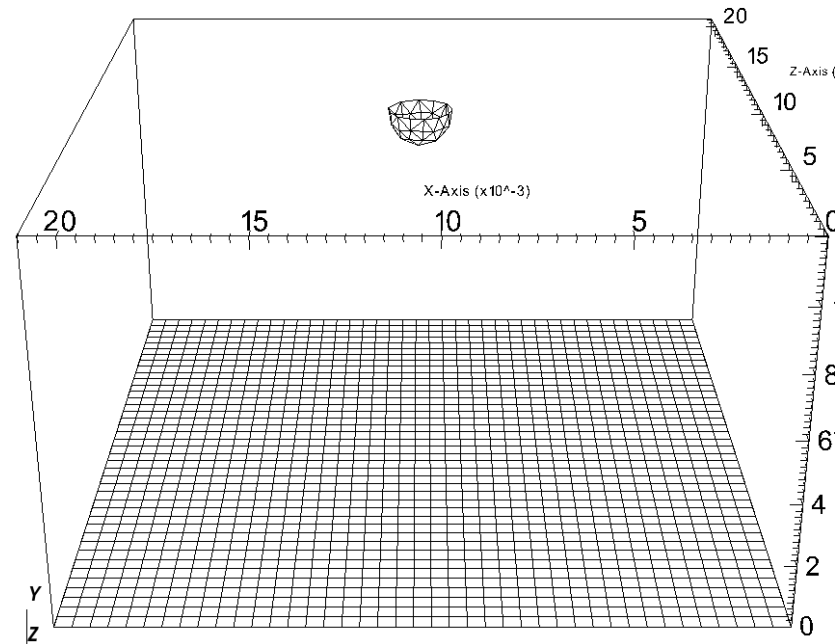


Figure VII.2.9: Drop hanged at the top of the box with a contact angle of 1.5 radian -  $t=0.1s$

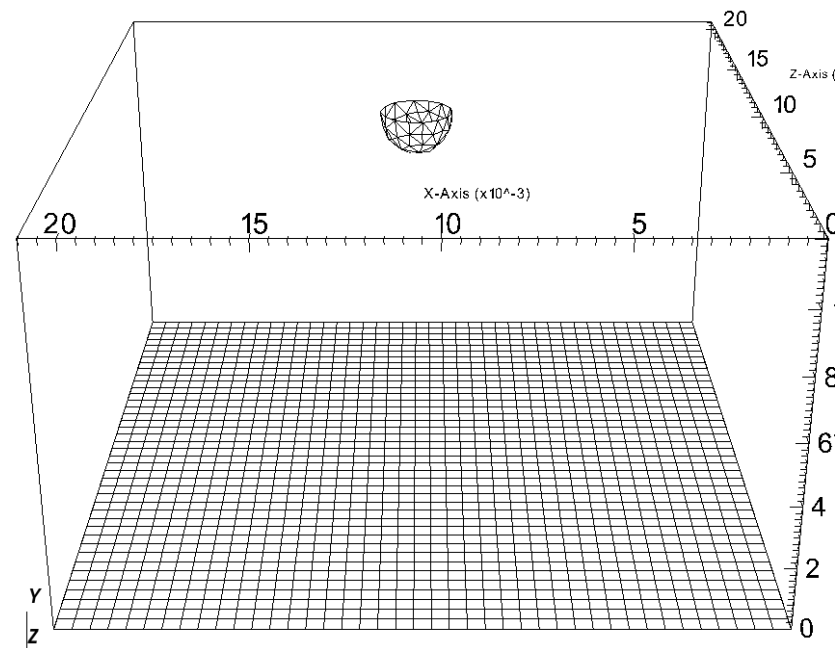


Figure VII.2.10: Drop hanged at the top of the box with a contact angle of 1.5 radian -  $t=0.15s$

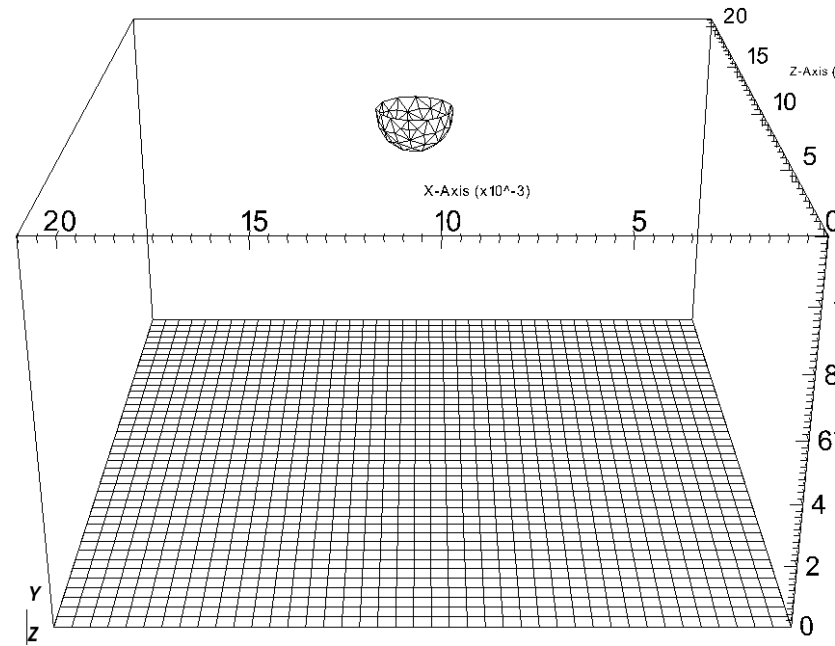


Figure VII.2.11: Drop hanged at the top of the box with a contact angle of 1.5 radian -  $t=0.2s$

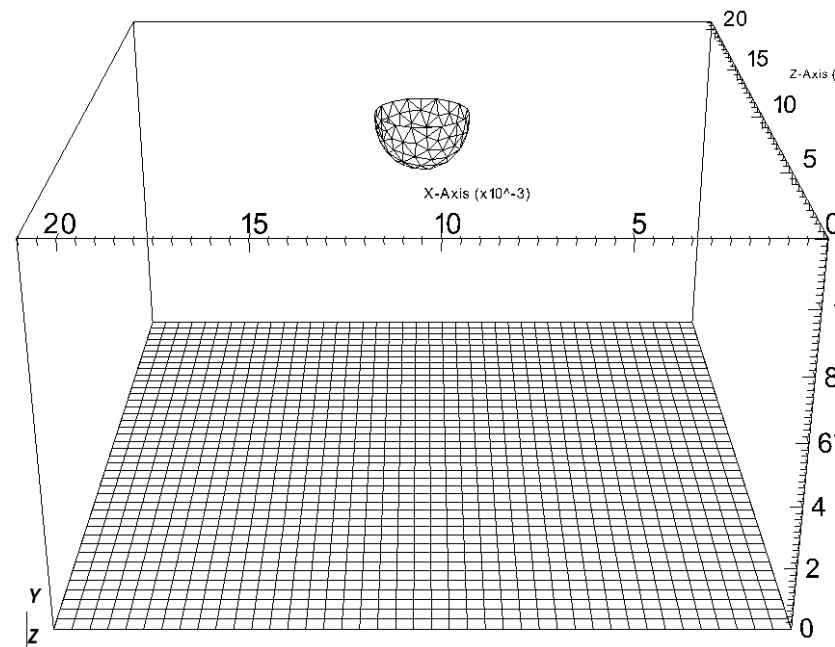


Figure VII.2.12: Drop hanged at the top of the box with a contact angle of 1.5 radian -  $t=0.35s$

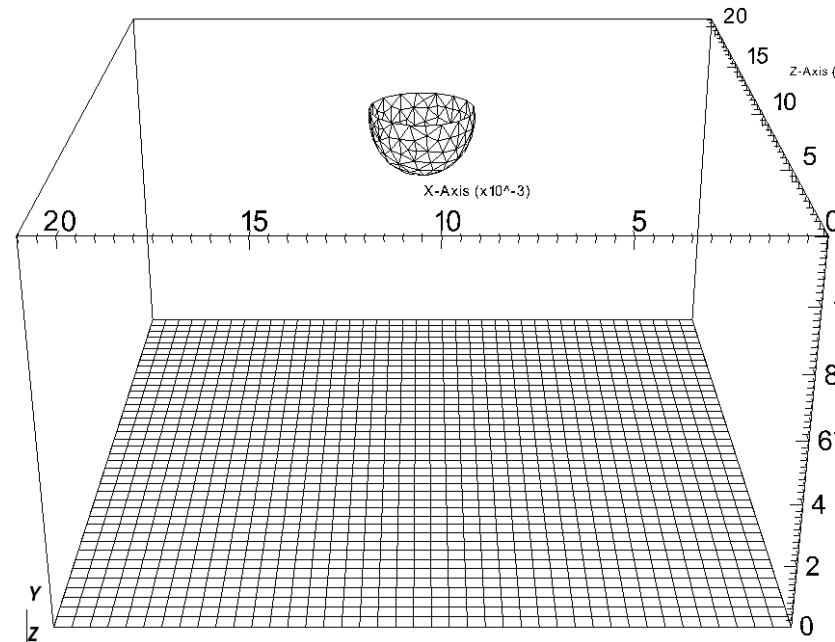


Figure VII.2.13: Drop hanged at the top of the box with a contact angle of 1.5 radian -  $t=0.5s$

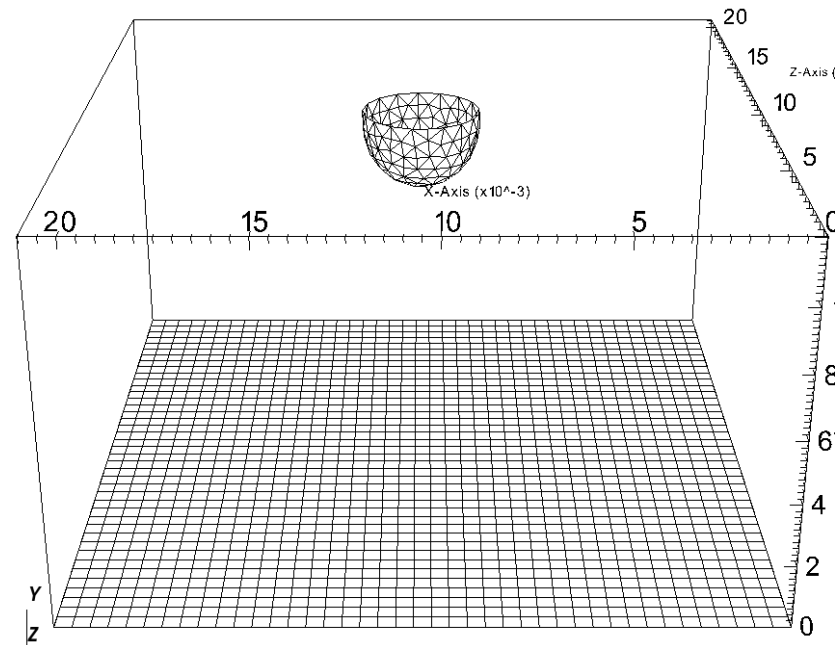


Figure VII.2.14: Drop hanged at the top of the box with a contact angle of 1.5 radian -  $t=0.75\text{s}$

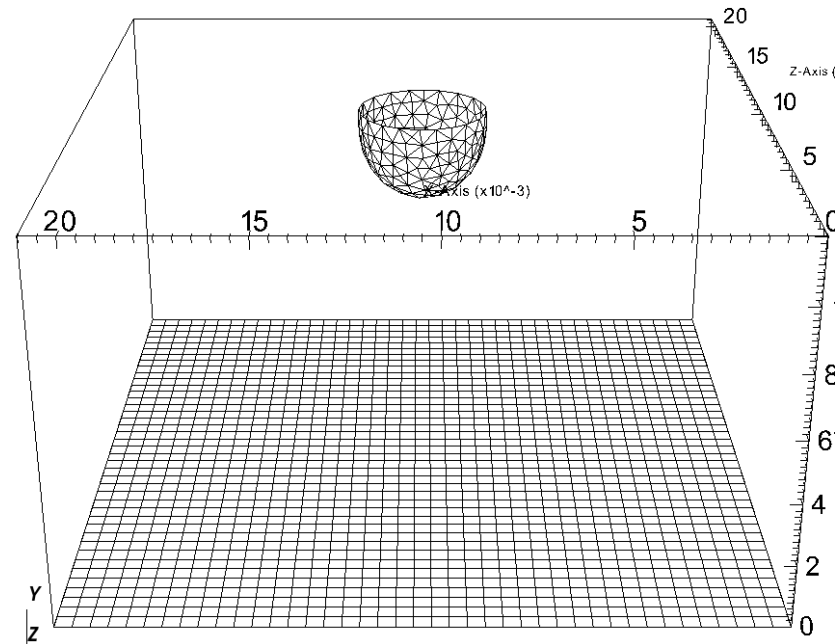


Figure VII.2.15: Drop hanged at the top of the box with a contact angle of 1.5 radian -  $t=1\text{s}$

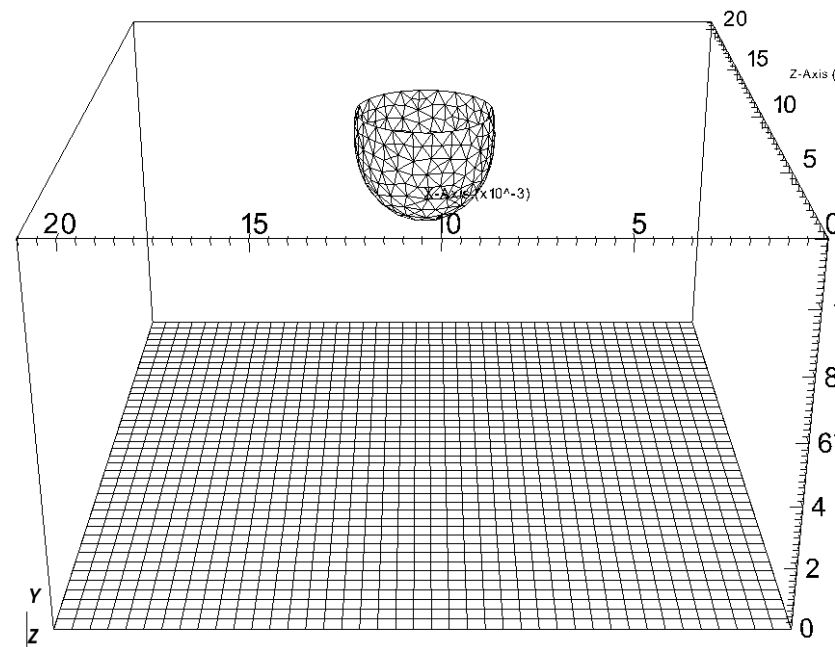


Figure VII.2.16: Drop hanged at the top of the box with a contact angle of 1.5 radian -  $t=1.5\text{s}$

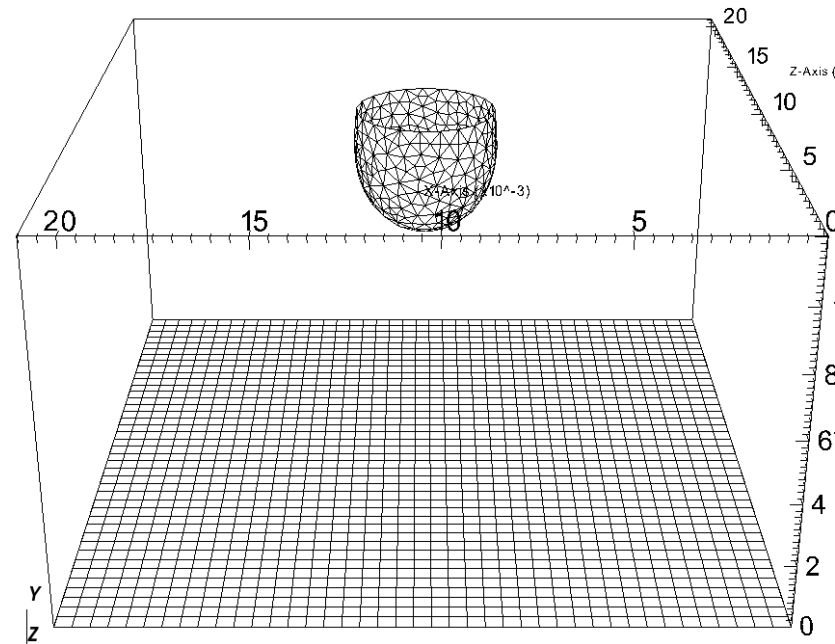


Figure VII.2.17: Drop hanged at the top of the box with a contact angle of 1.5 radian -  $t=2\text{s}$

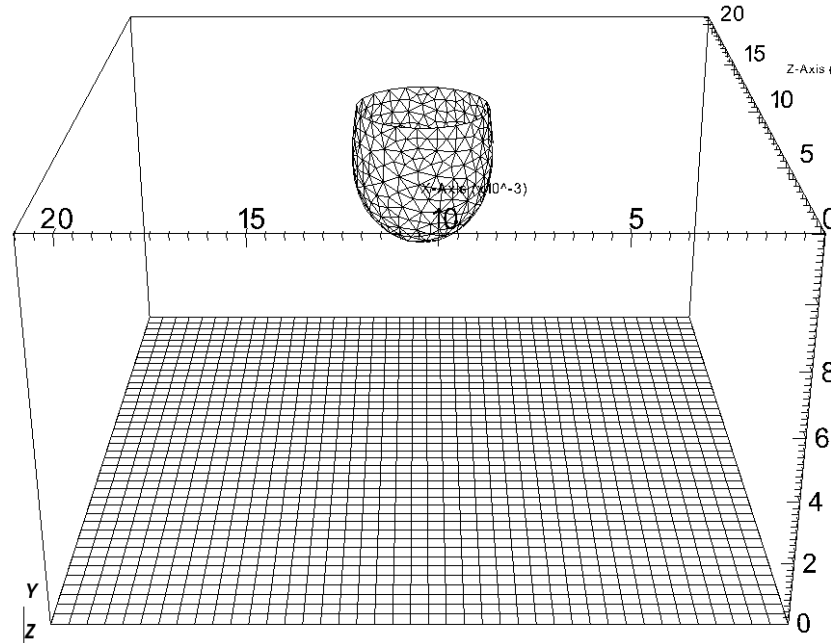


Figure VII.2.18: Drop hanged at the top of the box with a contact angle of 1.5 radian -  $t=2.5\text{s}$

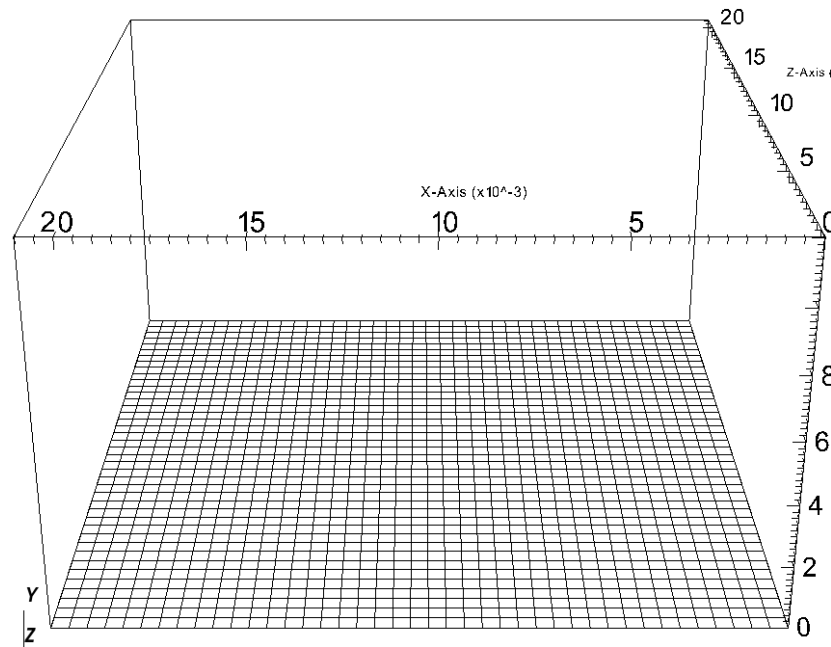


Figure VII.2.19: Drop hanged at the top of the box with a contact angle of 1.5 radian -  $t=3\text{s}$

The following graph represents the profile of the drop at different moment :  $t_1 = 0.45\text{s}$ ,  $t_2 = 1.15\text{s}$  and  $t_3 = 2.05\text{s}$  and comparisions of positions of nodes of lagrangian mesh points and theoretical profiles. The contact angle of the drop become quickly greater than  $90^\circ$  and one can notice that the numerical accuracy degrades for high contact angle values.

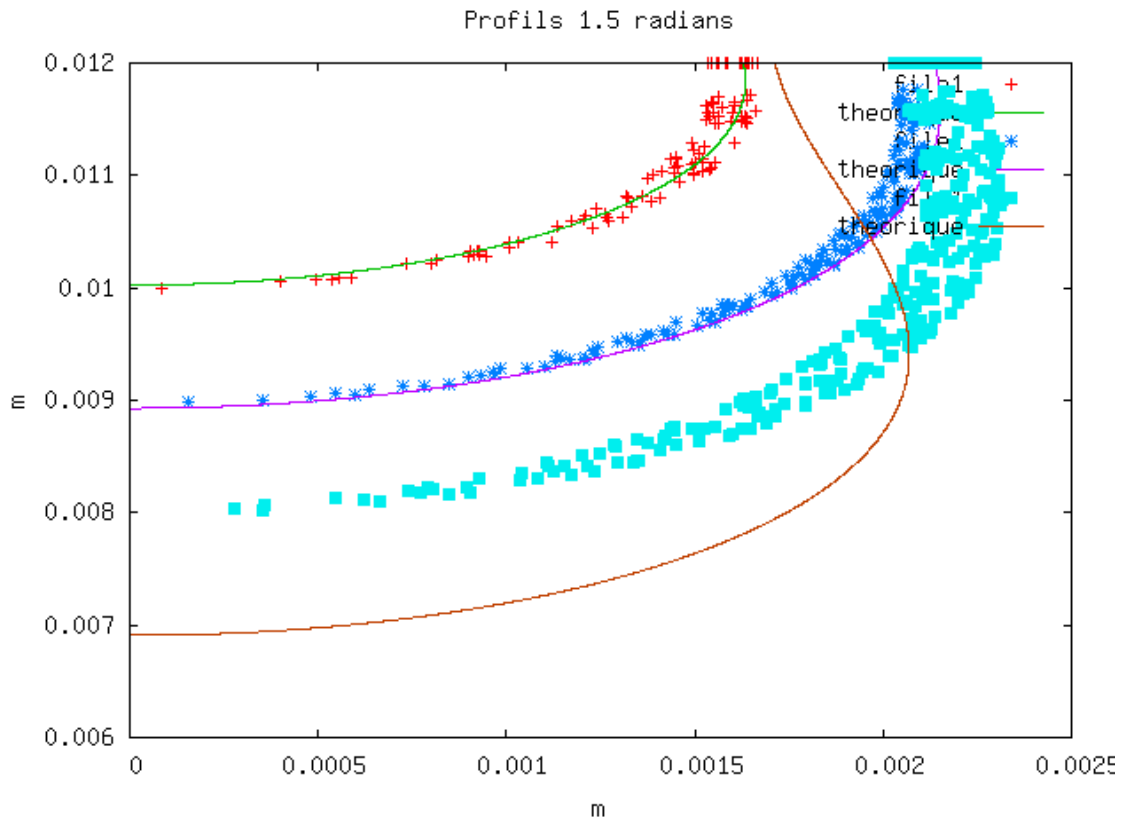


Figure VII.2.20: Profils 1.5 radians

Description des courbes de la figure fic019.png:

- file1 : Trio\_U  
fichier ./pendante\_1p5/profil\_trio\_u\_t1.txt
- theorique : trio\_u  
fichier ./profil/nouv\_1.5\_0.737
- file1 : Trio\_U  
fichier ./pendante\_1p5/profil\_trio\_u\_t2.txt
- theorique : trio\_u  
fichier ./profil/nouv\_1.5\_1.146
- file1 : Trio\_U  
fichier ./pendante\_1p5/profil\_trio\_u\_t3.txt
- theorique : trio\_u  
fichier ./profil/nouv\_1.5\_1.9

- **Second Calculation: contact angle of 2.5 radian between the tangential curve at the drop close to the wall**

The following figures show the growth of the hanging drop at the top of the box for different times.

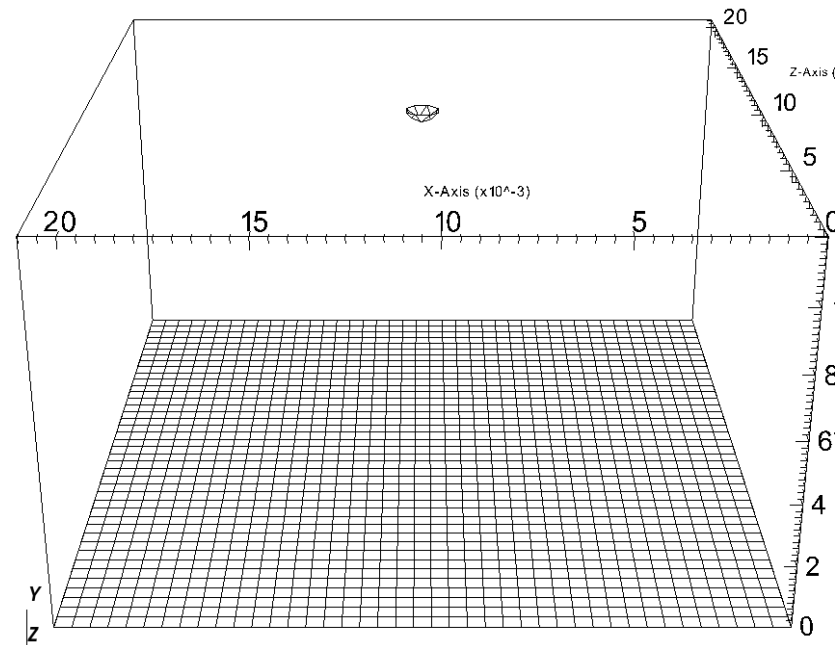


Figure VII.2.21: Drop hanged at the top of the box with a contact angle of 2.5 radian -  $t=0$ s

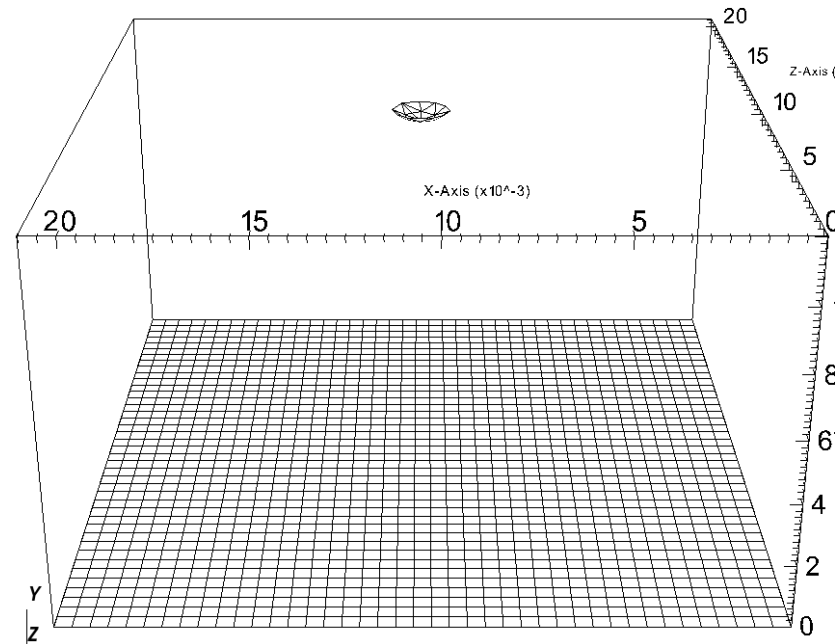


Figure VII.2.22: Drop hanged at the top of the box with a contact angle of 2.5 radian -  $t=0.01$ s

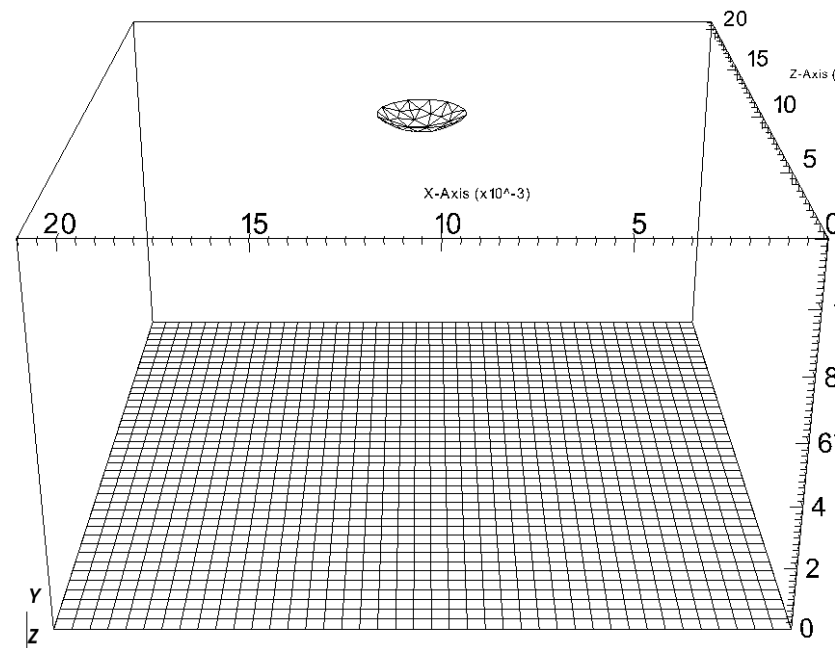


Figure VII.2.23: Drop hanged at the top of the box with a contact angle of 2.5 radian -  $t=0.05s$

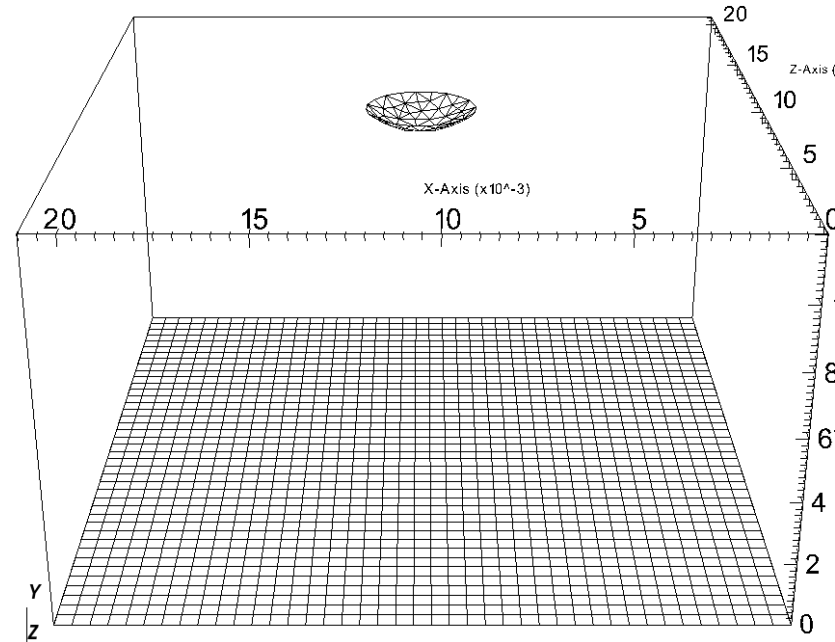


Figure VII.2.24: Drop hanged at the top of the box with a contact angle of 2.5 radian -  $t=0.1s$

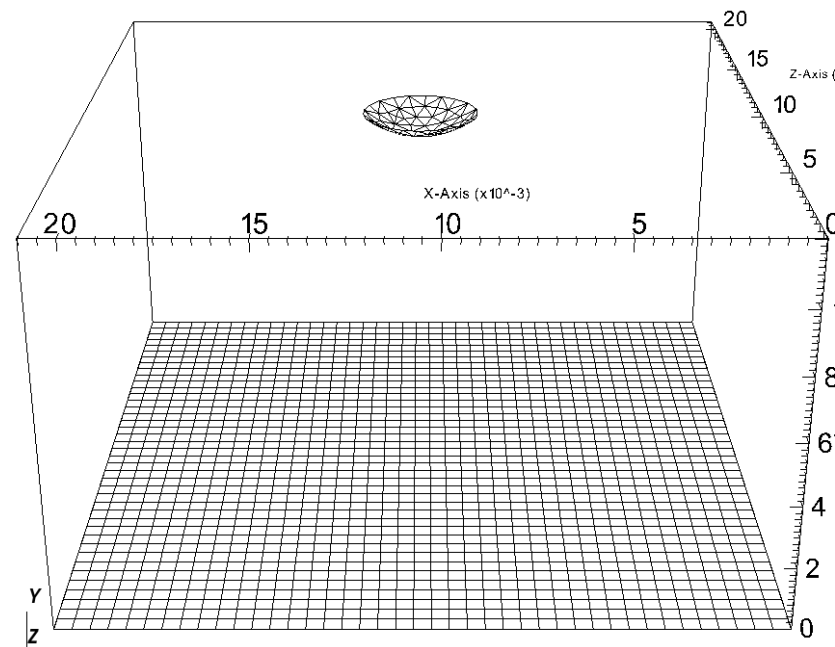


Figure VII.2.25: Drop hanged at the top of the box with a contact angle of 2.5 radian -  $t=0.15s$

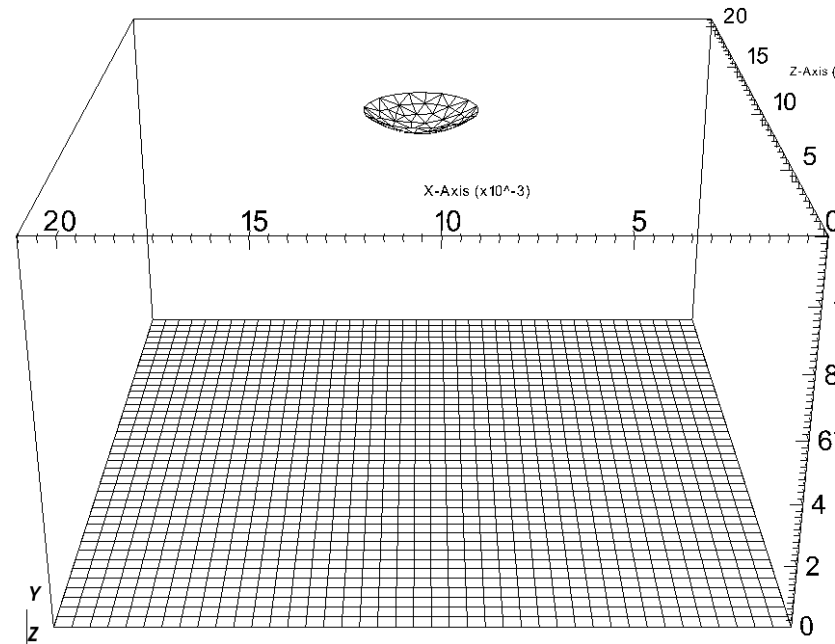


Figure VII.2.26: Drop hanged at the top of the box with a contact angle of 2.5 radian -  $t=0.2s$

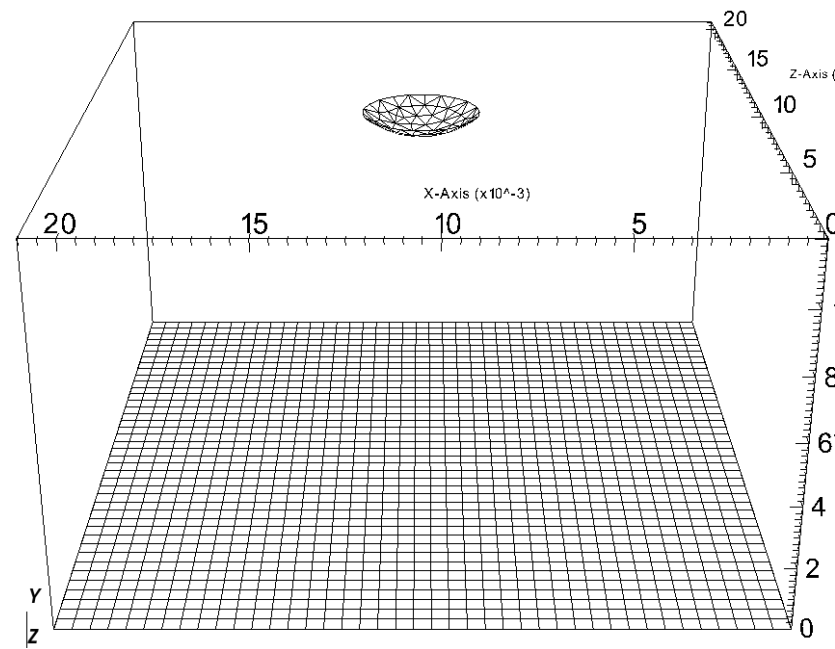


Figure VII.2.27: Drop hanged at the top of the box with a contact angle of 2.5 radian -  $t=0.35s$

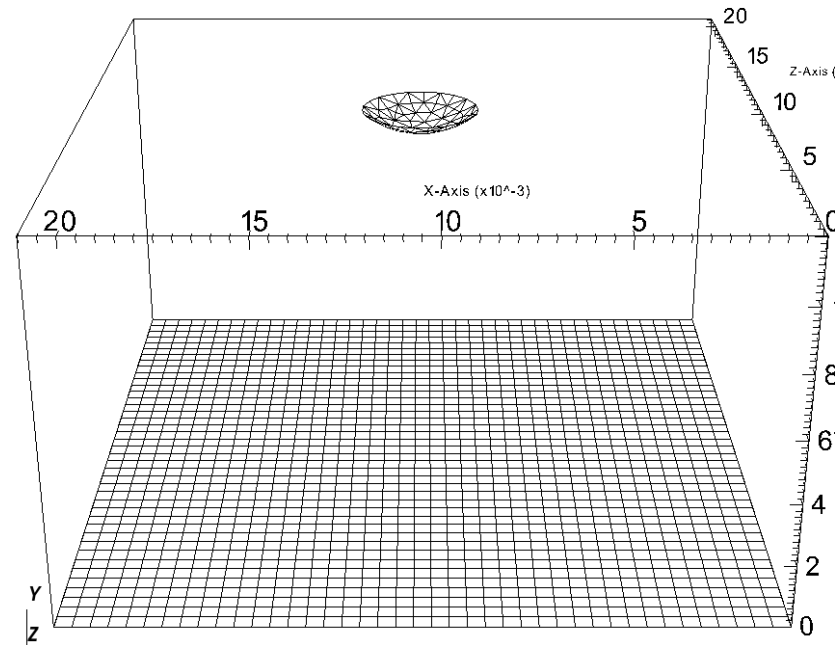


Figure VII.2.28: Drop hanged at the top of the box with a contact angle of 2.5 radian -  $t=0.5s$

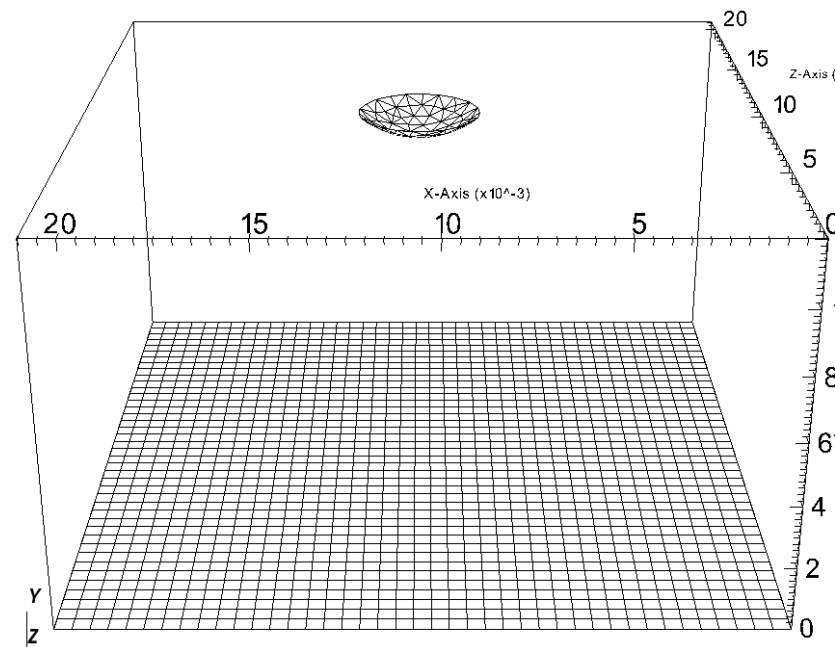


Figure VII.2.29: Drop hanged at the top of the box with a contact angle of 2.5 radian -  $t=0.75s$

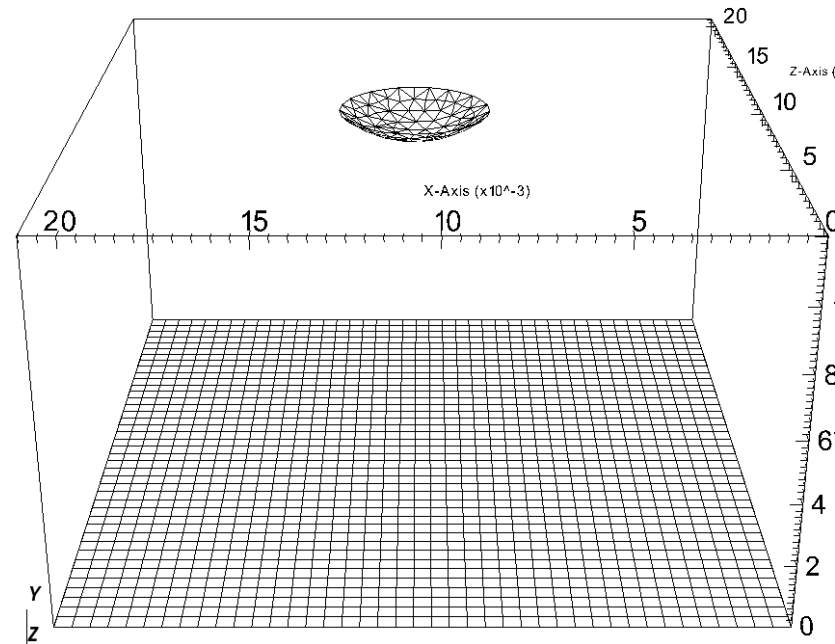


Figure VII.2.30: Drop hanged at the top of the box with a contact angle of 2.5 radian -  $t=1s$

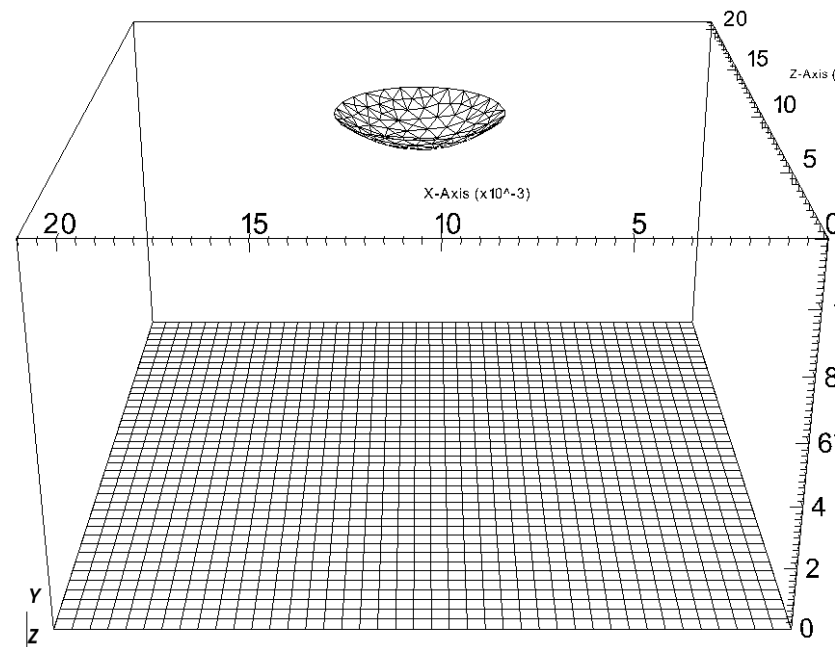


Figure VII.2.31: Drop hanged at the top of the box with a contact angle of 2.5 radian -  $t=1.25s$

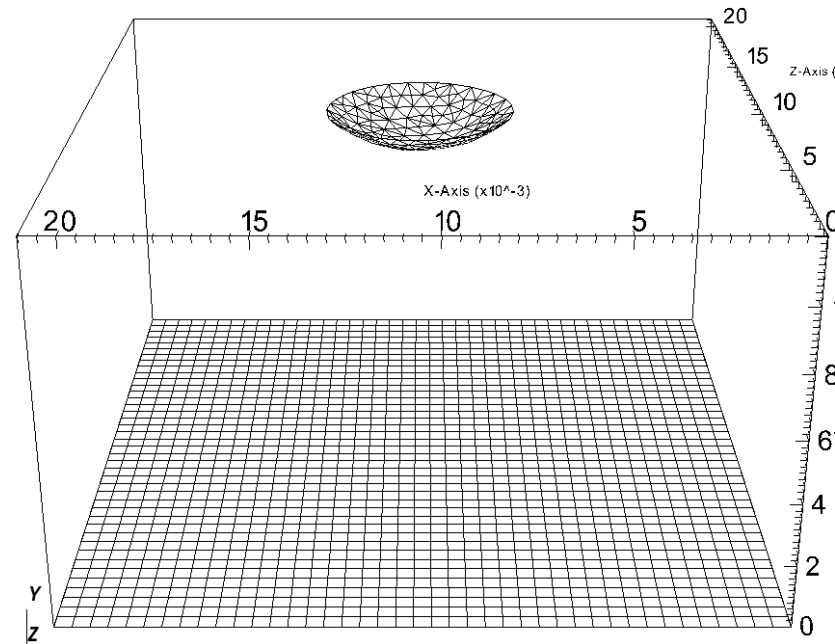


Figure VII.2.32: Drop hanged at the top of the box with a contact angle of 2.5 radian -  $t=1.5s$

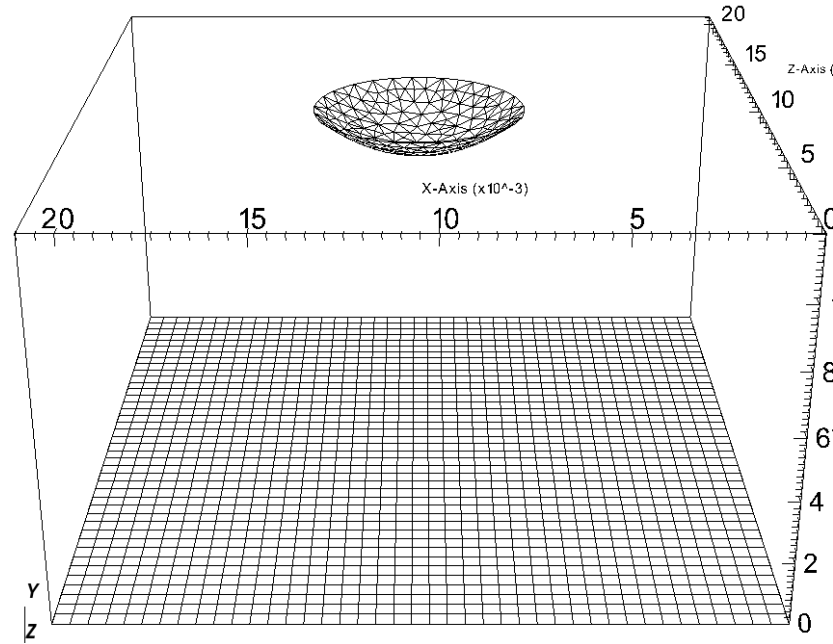


Figure VII.2.33: Drop hanged at the top of the box with a contact angle of 2.5 radian -  $t=1.75s$

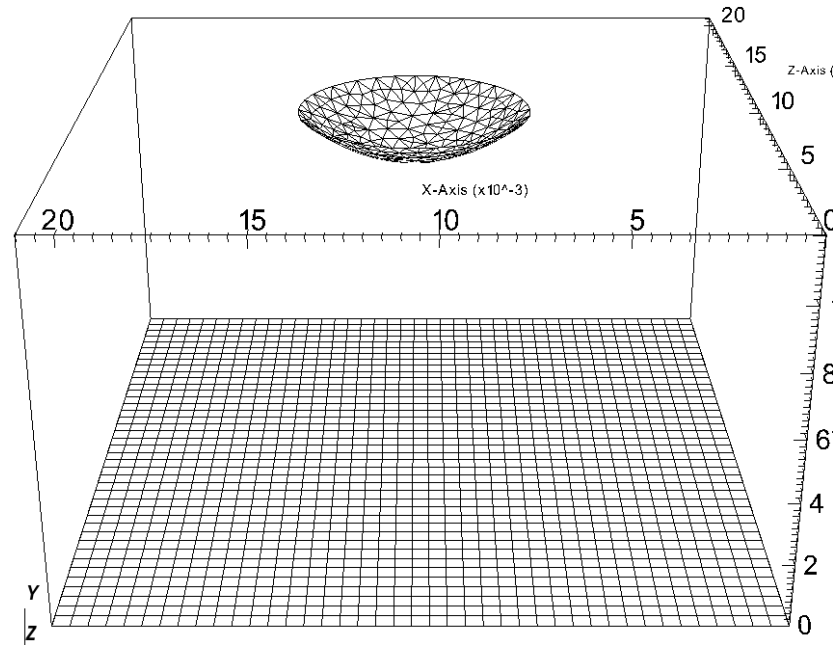


Figure VII.2.34: Drop hanged at the top of the box with a contact angle of 2.5 radian -  $t=2s$

The following graph the profile of the drop at different moment :  $t_1 = 2.4s$ ,  $t_2 = 3.65s$  and  $t_3 = 6.45s$  and comparizons of positions of nodes of lagrangian mesh points and theoretical profiles.  
 Regarding profiles for 1.5 and 2.5 radians, one can notice that for low values of contact angle, the profile is less stable in time. Some spurious oscillations of the interface take place.

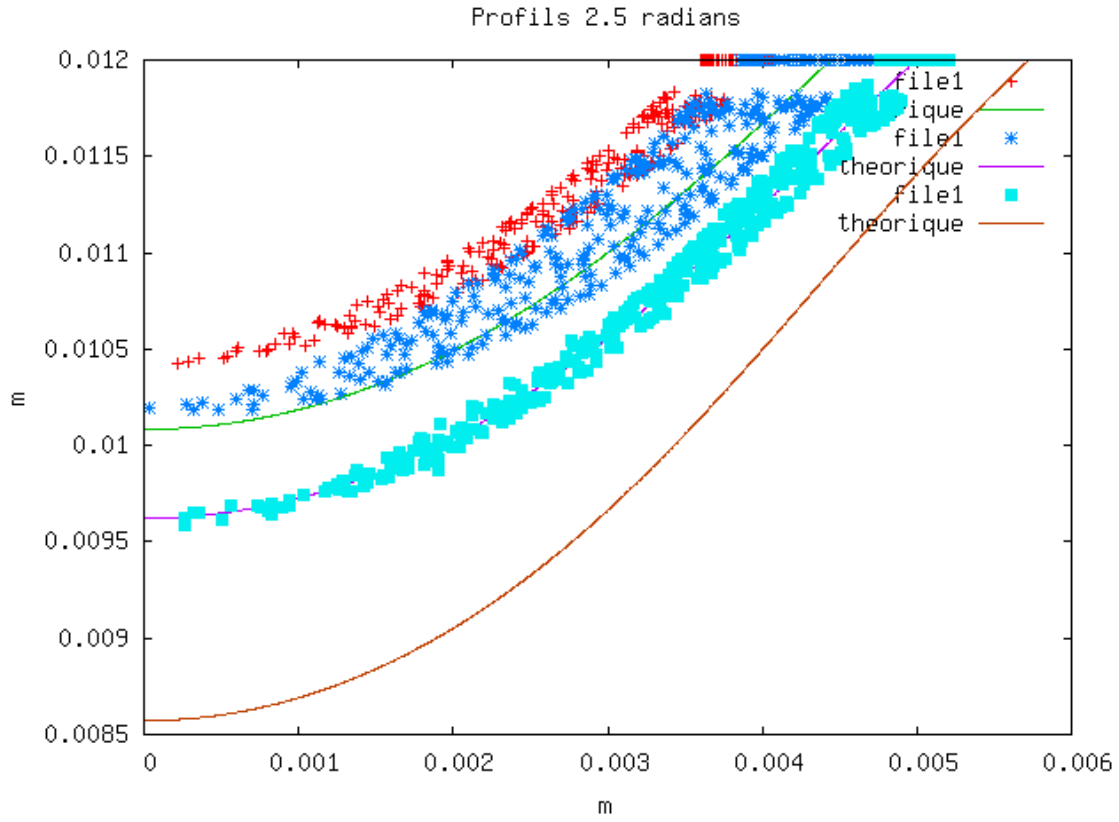


Figure VII.2.35: Profils 2.5 radians

Description des courbes de la figure fic034.png:

- file1 : Trio\_U  
fichier ./pendante\_2p5/profil\_trio\_u\_t1.txt
- theorique : trio\_u  
fichier ./profil/nouv\_2.5\_0.715
- file1 : Trio\_U  
fichier ./pendante\_2p5/profil\_trio\_u\_t2.txt
- theorique : trio\_u  
fichier ./profil/nouv\_2.5\_0.887
- file1 : Trio\_U  
fichier ./pendante\_2p5/profil\_trio\_u\_t3.txt
- theorique : trio\_u  
fichier ./profil/nouv\_2.5\_1.279

## 2.5 Conclusion

This sheet demonstrate the capabilities of TrioCFD for the modeling of this type of phenomenon. A first comparison with the theory shows a good prediction of the shape of the drop over time. However, for drop contact angles greater than  $90^\circ$ , the accuracy is deteriorated. A study will be carried out between now and v1.8.4 in order to understand the origin of these oscillations, reduce them and give recommendations for a good parameterization of Front-Tracking remeshing.

## 2.6 Data Files

**goutte**

```

# Hydraulique 3D laminaire : schema upwind #
dimension 3
Probleme_FT_Disc_gen pb1
Domaine dom_pb1
Read_file dom_pb1 Pb1_44_44_43.geom
VDF dis
schema_euler_explicite sch
Read sch
{
  tinit 0.0
  tmax 3.
  dt_min 1.e-10
  dt_max 0.001
  dt_impr 0.2
  dt_sauv 10.
  seuil_statio -1.e-8
  facsec 1
}
Fluide_Incompressible eau
Read eau
{
  mu Champ_Uniforme 1 2.82e-4
  rho Champ_Uniforme 1 1000.
}
Fluide_Incompressible air
Read air
{
  mu Champ_Uniforme 1 2.82e-5
  rho Champ_Uniforme 1 10.
}
Fluide_Diphasique fluide
Read fluide
{
  fluide0 air
  fluide1 eau
  sigma Champ_Uniforme 1 0.07
}
Champ_Uniforme gravite
Read gravite 3 0. -9.81 0.
Associate fluide gravite
Navier_Stokes_FT_Disc          hydraulique
Transport_Interfaces_FT_Disc    interf
Associate pb1 hydraulique
Associate pb1 interf
Associate pb1 dom_pb1
Associate pb1 sch
Associate pb1 fluide
System "mkdir -p lata"
Discretize pb1 dis
Read pb1
{
hydraulique
{
  modele_turbulence sous_maille_wale
  {
    Cw           0.

```

```

        turbulence_paroi_negligeable
    }
solveur_pression GCP { optimized precond ssor { omega 1.6 } seuil 1.e-11 impr }
convection { quick }
diffusion { }
conditions_initiales { vitesse champ_uniforme 3 0. 0. 0. }
equation_interfaces proprietes_fluide interf
conditions_limites
{
    injection frontiere_ouverte_vitesse_imposee champ_front_uniforme 3 0. -0.1 0.
    paroi paroi_fixe
    ouverte Sortie_libre_rho_variable champ_front_uniforme 1 0.
}
terme_gravite grad_I
}
interf
{
    conditions_initiales {
        fonction
-(x-0.0105)*(x-0.0105)-(z-0.0105)*(z-0.0105)-(y-0.012)*(y-0.012)+0.0005*0.0005
    }
methode_transport vitesse_interpolee hydraulique
    iterations_correction_volume 0
    n_iterations_distance 2
remaillage {
    pas 1.e-4
    nb_iter_remaillage 2
    criterie_arete 0.5
    criterie_remaillage 0.1
    pas_lissage 1.e-5
    lissage_courbure_iterations 20
    lissage_courbure_coeff -0.05
    nb_iter_barycentrage 3
    relax_barycentrage 1.
    facteur_longueur_ideale 1.
    nb_iter_correction_volume 5
    seuil_dvolume_residuel 1e-15
}
collisions {
    active
    juric_pour_tout
    type_remaillage
    Thomas { distance_interface_element_max 1 }
}
conditions_limites
{
# injection Paroi_FT_disc Constant Champ_Front_Uniforme 1 120 #
# Pour un angle de contact de 1 radian compte dans le gaz on a 57
degres_comptes_dans_le_gaz et 123 degres_comptes_dans_le_liquide #
# Pour un angle de contact de 1.5 radian compte dans le gaz on a 86
degres_comptes_dans_le_gaz et 94 degres_comptes_dans_le_liquide #
# Pour un angle de contact de 2 radian compte dans le gaz on a 115 degres_comptes_dans_le_gaz
degres_comptes_dans_le_liquide #
# Pour un angle de contact de 2.5 radian compte dans le gaz on a 143 degres_comptes_dans_le_gaz
degres_comptes_dans_le_liquide #
# Pour un angle de contact de 3 radian compte dans le gaz on a 172 degres_comptes_dans_le_gaz
degres_comptes_dans_le_liquide #
    injection Paroi_FT_disc Constant Champ_Front_Fonc_xyz 1 94.+sqrt(((x-0.0105)*(x-0.0105)+(z-0.0105)*(z-0.0105)))
    paroi Paroi_FT_disc Constant Champ_Front_Fonc_xyz 1 94.+sqrt(((x-0.0105)*(x-0.0105)+(z-0.0105)*(z-0.0105)))
    ouverte Paroi_FT_disc Constant Champ_Front_Fonc_xyz 1 94.+sqrt(((x-0.0105)*(x-0.0105)+(z-0.0105)*(z-0.0105)))
}

```

```

}

postraitements {
    Definition_champs {
        hauteur1 Reduction_0D {
            methode moyenne_ponderee
            source Transformation {
                methode formule
                expression 1 exp(-(x*x+z*z)*1000)*(1-indicatrice_interf_natif_dom_pb1)
                source refChamp { Pb_champ pb1 indicatrice_interf }
            }
        }
        hauteur2 Reduction_0D {
            methode moyenne_ponderee
            source Transformation {
                methode formule
                expression 1 exp(-(x*x+z*z)*10000)*(1-indicatrice_interf_natif_dom_pb1)
                source refChamp { Pb_champ pb1 indicatrice_interf }
            }
        }
        hauteur3 Reduction_0D {
            methode moyenne_ponderee
            source Transformation {
                methode formule
                expression 1 exp(-(x*x+z*z)*100000)*(1-indicatrice_interf_natif_dom_pb1)
                source refChamp { Pb_champ pb1 indicatrice_interf }
            }
        }
    }
    Sondes {
        hauteur1 hauteur1 periode 0.02 points 1 0. 0.1 0.
        hauteur2 hauteur2 periode 0.02 points 1 0. 0.1 0.
        hauteur3 hauteur3 periode 0.02 points 1 0. 0.1 0.
    }
    champs dt_post 1e3
    {
        indicatrice_interf elem
    }
}
liste_postraitements {
    postraitements_ft_lata post1 {
        format Lata
        fichier lata/post
        champs dt_post 0.01 {
            indicatrice_interf elem
            vitesse faces
        }
        interfaces interf {
            courbure som
        }
    }
}
sauvegarde binaire Oscillation_bulle3.rep
}
Solve pb1
Fin

```

**goutte**

```

# Hydraulique 3D laminaire : schema upwind #
dimension 3
Probleme_FT_Disc_gen pb1

```

```

Domaine dom_pb1
Read_file dom_pb1 Pb1_44_44_43.geom
VDF dis
schema_euler_explicode sch
Read sch
{
  tinit 0.0
  tmax 10.
  dt_min 1.e-10
  dt_max 0.001
  dt_impr 0.2
  dt_sauv 10.
  seuil_statio -1.e-8
  facsec 1
}
Fluide_Incompressible eau
Read eau
{
  mu Champ_Uniforme 1 2.82e-4
  rho Champ_Uniforme 1 1000.
}
Fluide_Incompressible air
Read air
{
  mu Champ_Uniforme 1 2.82e-5
  rho Champ_Uniforme 1 10.
}
Fluide_Diphasique fluide
Read fluide
{
  fluide0 air
  fluide1 eau
  sigma Champ_Uniforme 1 0.07
}
Champ_Uniforme gravite
Read gravite 3 0. -9.81 0.
Associate fluide gravite
Navier_Stokes_FT_Disc          hydraulique
Transport_Interfaces_FT_Disc   interf
Associate pb1 hydraulique
Associate pb1 interf
Associate pb1 dom_pb1
Associate pb1 sch
Associate pb1 fluide
System "mkdir -p lata"
Discretize pb1 dis
Read pb1
{
hydraulique
{
  modele_turbulence sous_maille_wale
  {
    Cw           0.
    turbulence_paroi negligable
  }
  solveur_pression GCP { optimized precond ssor { omega 1.6 } seuil 1.e-11 impr }
  convection      { quick }
  diffusion       { }
  conditions_initiales { vitesse champ_uniforme 3 0. 0. 0. }
  equation_interfaces proprietes_fluide interf
  conditions_limites
}

```

```

{
    injection frontiere_ouverte_vitesse_imposee champ_front_uniforme 3 0. -0.1 0.
    paroi paroi_fixe
    ouverte Sortie_libre_rho_variable champ_front_uniforme 1 0.
}
terme_gravite grad_I
}
interf
{
    conditions_initiales {
        fonction
-(x-0.0105)*(x-0.0105)-(z-0.0105)*(z-0.0105)-(y-0.012)*(y-0.012)+0.0005*0.0005
    }
methode_transport vitesse_interpolee hydraulique
    iterations_correction_volume 0
    n_iterations_distance 2
remaillage {
    pas 1.e-4
    nb_iter_remaillage 2
    critere_arete 0.5
    critere_remaillage 0.1
    pas_lissage 1.e-5
    lissage_courbure_iterations 20
    lissage_courbure_coeff -0.05
    nb_iter_barycentrage 3
    relax_barycentrage 1.
    facteur_longueur_ideale 1.
    nb_iter_correction_volume 5
    seuil_dvolume_residuel 1e-15
}
collisions {
    active
    juric_pour_tout
    type_remaillage
    Thomas { distance_interface_element_max 1 }
}
conditions_limites
{
#    injection Paroi_FT_disc Constant Champ_Front_Uniforme 1 120 #
#    Pour un angle de contact de 1 radian compte dans le gaz on a 57
degres compte dans le gaz et 123 degres compte dans le liquide #
#    Pour un angle de contact de 1.5 radian compte dans le gaz on a 86
degres compte dans le gaz et 94 degres compte dans le liquide #
#    Pour un angle de contact de 2 radian compte dans le gaz on a 115 degres compte dans le
degres compte dans le liquide #
#    Pour un angle de contact de 2.5 radian compte dans le gaz on a 143 degres compte dans le
degres compte dans le liquide #
#    Pour un angle de contact de 3 radian compte dans le gaz on a 172 degres compte dans le
degres compte dans le liquide #
    injection Paroi_FT_disc Constant Champ_Front_Fonc_xyz 1 37.+sqrt(((x-0.0105)*(x-0.0105)+(z-
paroi Paroi_FT_disc Constant Champ_Front_Fonc_xyz 1 37.+sqrt(((x-0.0105)*(x-0.0105)+(z-0.0105)*
ouverte Paroi_FT_disc Constant Champ_Front_Fonc_xyz 1 37.+sqrt(((x-0.0105)*(x-0.0105)+(z-0.0105)*
}
postairement {
    Definition_champs {
        hauteur1 Reduction_0D {
            methode moyenne_ponderee
            source Transformation {
                methode formule
                expression 1 exp(-(x*x+z*z)*1000)*(1-indicatrice_interf_natif_dom_pb1)

```

```

        source refChamp { Pb_champ pb1 indicatrice_interf }
    }
    hauteur2 Reduction_0D {
        methode moyenne_ponderee
        source Transformation {
            methode formule
            expression 1 exp(-(x*x+z*z)*10000)*(1-indicatrice_interf_natif_dom_pb1)
            source refChamp { Pb_champ pb1 indicatrice_interf }
        }
    }
    hauteur3 Reduction_0D {
        methode moyenne_ponderee
        source Transformation {
            methode formule
            expression 1 exp(-(x*x+z*z)*100000)*(1-indicatrice_interf_natif_dom_pb1)
            source refChamp { Pb_champ pb1 indicatrice_interf }
        }
    }
}
Sondes {
    hauteur1 hauteur1 periode 0.02 points 1 0. 0.1 0.
    hauteur2 hauteur2 periode 0.02 points 1 0. 0.1 0.
    hauteur3 hauteur3 periode 0.02 points 1 0. 0.1 0.
}
champs dt_post 1e3
{
    indicatrice_interf elem
}
}
liste_postraitements {
    postraitement_ft_lata post1 {
        format Lata
        fichier lata/post
        champs dt_post 0.01 {
            indicatrice_interf elem
            vitesse faces
        }
        interfaces interf {
            courbure som
        }
    }
}
sauvegarde binaire Oscillation_bulle3.rep
}
Solve pb1
Fin

```

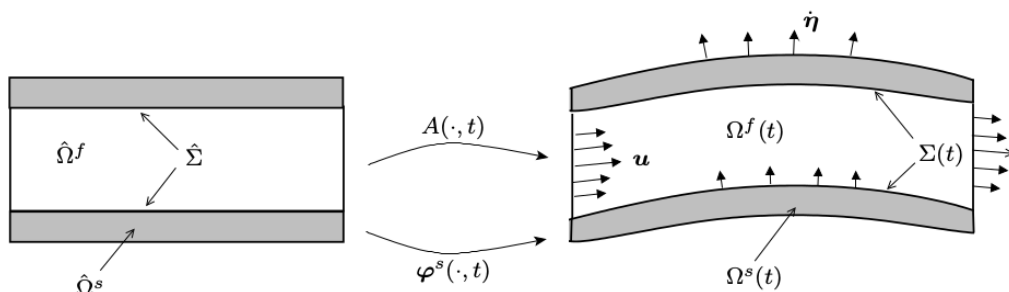
## VIII. Fluid-structure interactions with ALE

To determine the flow of a fluid, it is necessary to describe the kinematics of all its material particles throughout time. To do so, one can adopt either an Euler description of motion, in which a fluid particle is identified by its initial position, or a Lagrange description of motion, in which a fluid particle is identified by its instantaneous position. Both descriptions are totally equivalent, leading to different forms of the Navier-Stokes equations that can be discretized on a stationary mesh grid (Euler) or a mesh grid that follows the motion of the fluid particles (Lagrange). In both cases, the mesh nodes do not account for the motion of the boundaries, which makes the numerical simulations of the related Navier-Stokes equations delicate. To overcome this problem, several approaches, such as the immersed boundary methods, or the Arbitrary Lagrangian-Eulerian (ALE) method have been developed.

Here, we rely on the ALE method. In the ALE approach, the fluid flow is computed in a domain that is deformed in order to follow the movement of the fluid-solid interface. It provides a hybrid description not associated with the fluid particles and the laboratory coordinates. We associate the description with a moving imaginary mesh that follows the fluid domain. The motion of the ALE computational mesh is independent of the material motion, the approach treats the mesh as a frame that moves with an arbitrary velocity. In the Eulerian approach, this velocity is zero, whereas it is equal to the velocity of the fluid particles in the Lagrangian approach. But in the ALE method, this velocity is equal to neither zero nor the velocity of the fluid particles; it varies smoothly and arbitrarily between both of them. This method is a Lagrangian description in zones and directions near a solid interface and Eulerian elsewhere.

In that part, three cases used ALE method are detailed:

- Single-phase flow around a vibrating cylindrical tube
- Hydrodynamic interaction of two cylinders subjected to small oscillations
- Vibrations of a cylinder in a square tube bundle immersed in a viscous fluid (DIVA experiments)



extract from Donea J., Huerta A., Ponthot J. Ph. and Rodriguez-Ferran A., Encyclopedia of Computational Mechanic, American Cancer Society, Arbitrary Lagrangian-Eulerian Methods, 2004

## VIII.1

### Single-phase flow around a vibrating cylindrical tube

#### 1.1 Purpose

A 2D fluid annulus region, confined between an inner wall moving with an harmonic motion and an outer wall fixed, has been numerically simulated.

This validation test case has been created to compare TrioCFD ALE results with the analytical solution of such a problem [1].

We investigate the force exerted by the fluid on the cylindrical tube subjected to a transverse excitation. We will seek, in particular, on the characteristics of the fluid force, represented by the added mass and damping coefficients.

A detailed analysis of the present test case is presented in [2].

Validation made by : M. A. Puscas and D. Panunzio.

Report generated 09/06/2023.

#### 1.2 Problem Description

The domain used for the numerical simulations is the one in Figure 1.

#### Geometry

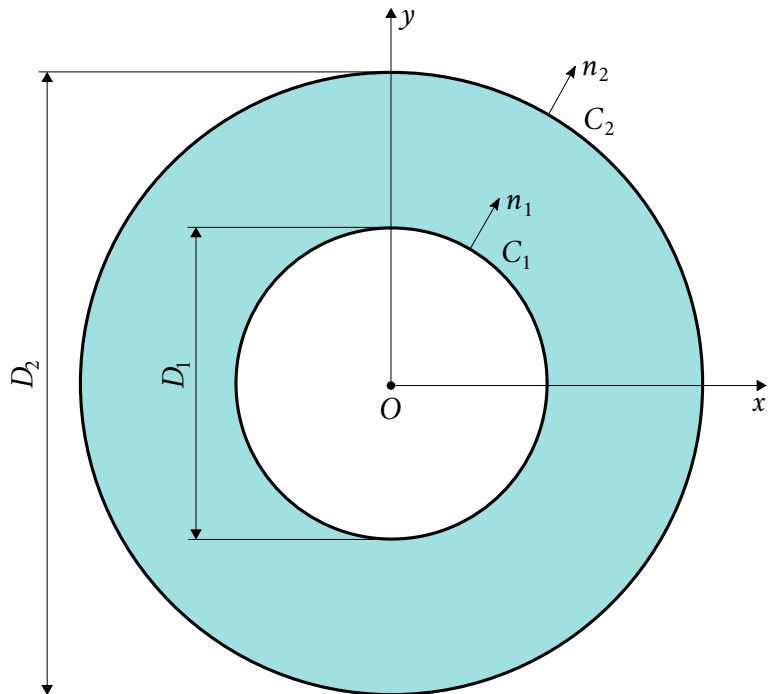


Figure VIII.1.1: The domain

## Initial Conditions and Boundary Conditions

The inner moves with an harmonic motion:  $\mathbf{u} = U * \sin(\omega * t)\mathbf{e}_x$ , where  $U$  : amplitude of displacement and  $\omega$  : angular frequency of displacement.

The outer cylinder fixed.

Initially, the fluid is at rest.

## Fluid Properties

The tube bundle is immersed in a Newtonian and homogeneous fluid, with mass density  $\rho$  ( $1000\text{ Kg/m}^3$ ) and kinematic viscosity  $\nu$  ( $1.007 * 10^{-6}\text{ m}^2/\text{s}$ ). The fluid flow generated by the oscillation of the central cylinder is assumed as incompressible and two-dimensional.

### 1.3 Case Setup

In this section is reported the mesh used during the simulations.

Numerical simulations have been carried out on a set of adaptive meshes. Two local sizes have been defined: a smaller one at the inner wall (min\_size) and a larger one at the outer wall (max\_size). By this way, a refined mesh is used in the regions with large gradient fields whereas a loose mesh is used in the areas with low gradient fields. The main properties are summarized in the table below.

#### Grid

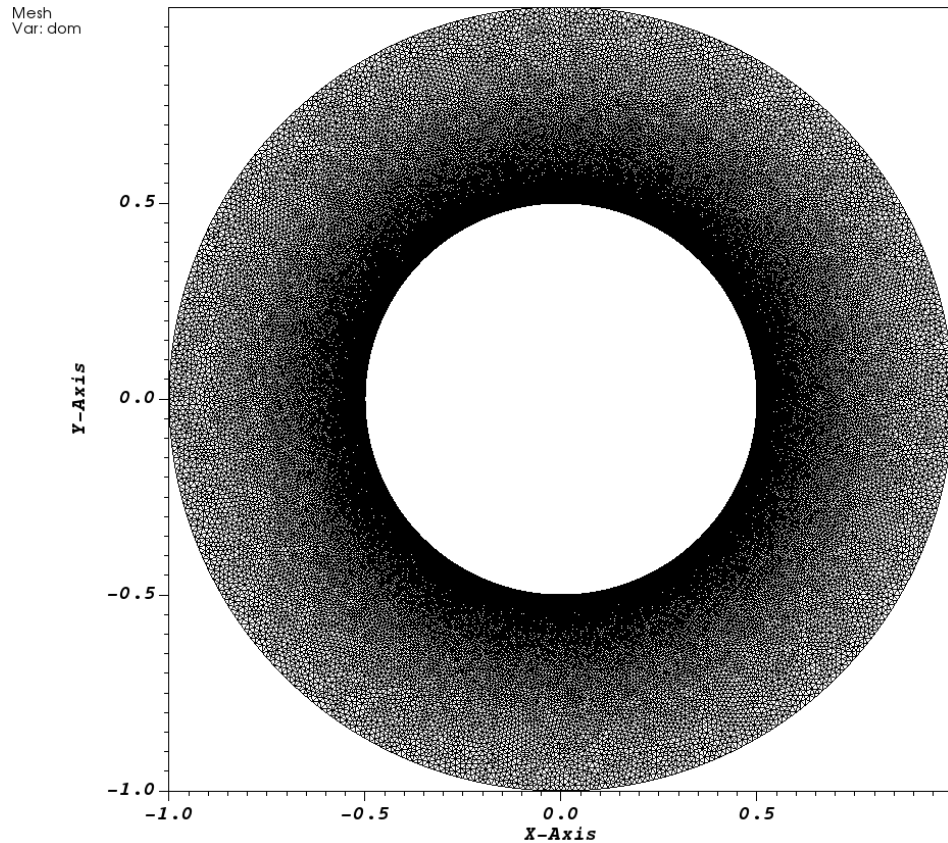


Figure VIII.1.2: Mesh

	Nb_elements	Nb_processors	max_size	min_size
Mesh	110466	4	0.015	0.003

Table VIII.1.1: Meshes properties

## Model Options

The fluid problem with moving boundaries is handled by the Arbitrary Lagrangian-Eulerian (ALE) method. In the ALE approach, the fluid flow is computed in a domain that is deformed in order to follow the movement of the fluid-solid interface. It provides a hybrid description not associated with the fluid particles and the laboratory coordinates. We associate the description with a moving imaginary mesh that follows the fluid domain.

## 1.4 Results

### Validation Specific Informations

- Version TRUST :
- Problem: Pb\_hydraulique\_ALE
- Dimension: 2D
- Domain: Domaine\_ALE
- Pressure solver: Solver\_moving\_mesh\_ALE PETSC Cholesky
- Discretization: VEFPre1B
- Time scheme: Scheme\_euler\_implicit with solver implicite\_ALE GMRES
- Medium: Fluide\_Incompressible
- Hydraulic problem: Navier\_Stokes\_standard\_ALE
- Convection scheme: ALE muscl
- Location: ALE/share/Validation/Rapports\_automatiques/TwoCylindersALE
- Generated Test cases :
  - ./TwoCylinders.data : /\*jdd en annexe\*/
- Performance Chart :

	host	system	Total CPU Time	CPU time/step	number of cell
./TwoCylinders	uruk	Linux	34459.9	6.41835	110466

Table VIII.1.2: Performance Chart

## Plot Data

In this section the analytical solution [1] for the force per unit length exerted by the fluid over the inner cylinder and the added coefficients are compared with the TrioCFD results.

According to Chen et al. [1], the analytical solution of the fluid force per unit length acting on the inner cylinder is:

$$\mathbf{F} = \rho\pi\left(\frac{D_1}{2}\right)^2 u D_1 \omega^2 \left[ m_{self} \sin(\omega t) - c_{self} \cos(\omega t) \right] \mathbf{e}_x \quad (1.1)$$

where  $\rho = 1 \text{ kg/m}^3$ ,  $D_1 = 1 \text{ m}$  (diameter of the inner cylinder),  $u = 10^{-2}$  (dimensionless displacement respect to  $D_1$ ),  $\omega = 0.06327 \text{ rad/s}$  (angular frequency of motion) and  $m_{self}$  and  $c_{self}$  the added mass and damping coefficients, respectively.

The analytical solution (Chen et al. [1]) is here depicted and compared with the numerical one, obtained by the sum of the pressure and viscous force acting on the inner cylinder along x. Simulations have been performed for  $t = [0, 5T]$  where  $T = 2\pi/\omega$ .

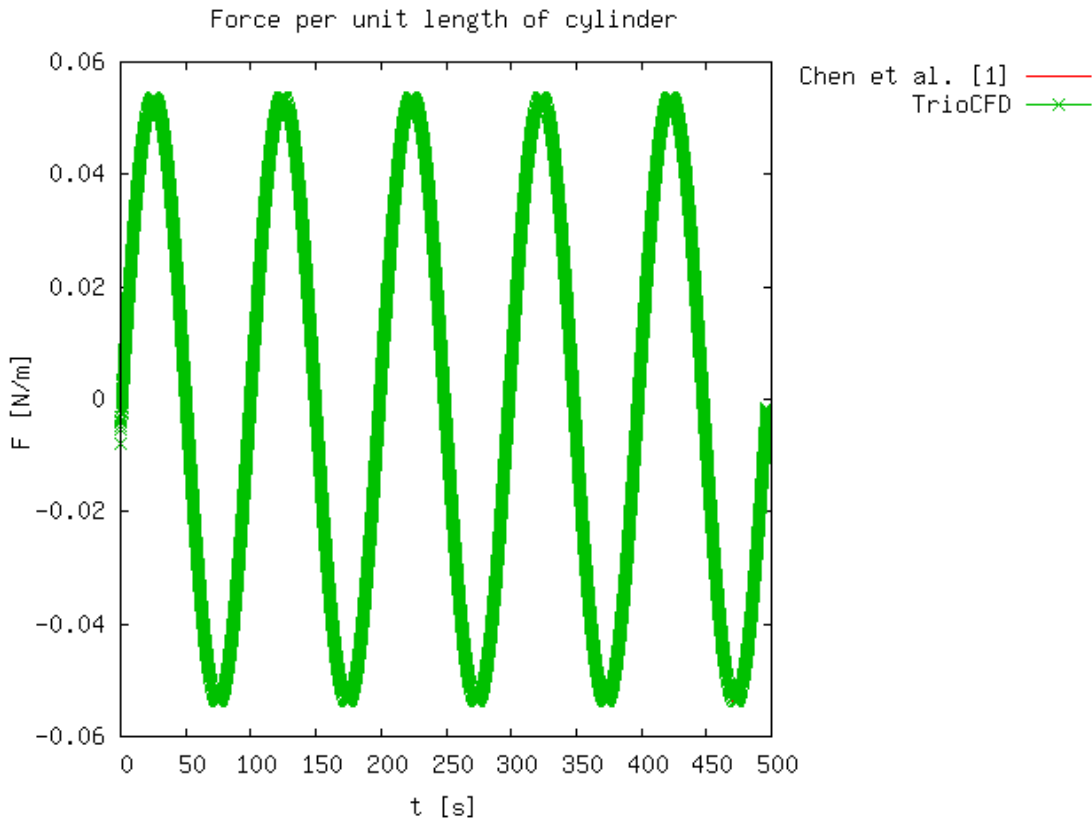


Figure VIII.1.3: Force per unit length of cylinder

For the analytical calculation of the added coefficients, the reader is referred to [1]. Numerically, the added coefficients are computed with a Fourier product as:

$$\begin{aligned} m_{self} &= \frac{\langle \sin(\omega t), F(t) \rangle}{\rho\pi(D_1/2)^2 u D_1 \omega^2} \quad \text{with} \quad \langle \sin(\omega t), F(t) \rangle = \frac{2}{5T} \int_0^{5T} \sin(\omega t) F(t) dt \\ c_{self} &= \frac{\langle \cos(\omega t), F(t) \rangle}{\rho\pi(D_1/2)^2 u D_1 \omega^2} \quad \text{with} \quad \langle \cos(\omega t), F(t) \rangle = \frac{2}{5T} \int_0^{5T} \cos(\omega t) F(t) dt \end{aligned} \quad (1.2)$$

and are reported in the following table:

	$m_{self}$	$c_{self}$
Chen et al. [1]	1.7118	0.046036
TrioCFD	1.708334196728114	0.05154713419757426

Table VIII.1.3: Added mass and damping coefficients

Pressure and velocity fields are reported at final time in order to investigate such distributions. The mesh velocity and the total displacement of the mesh are also plotted.

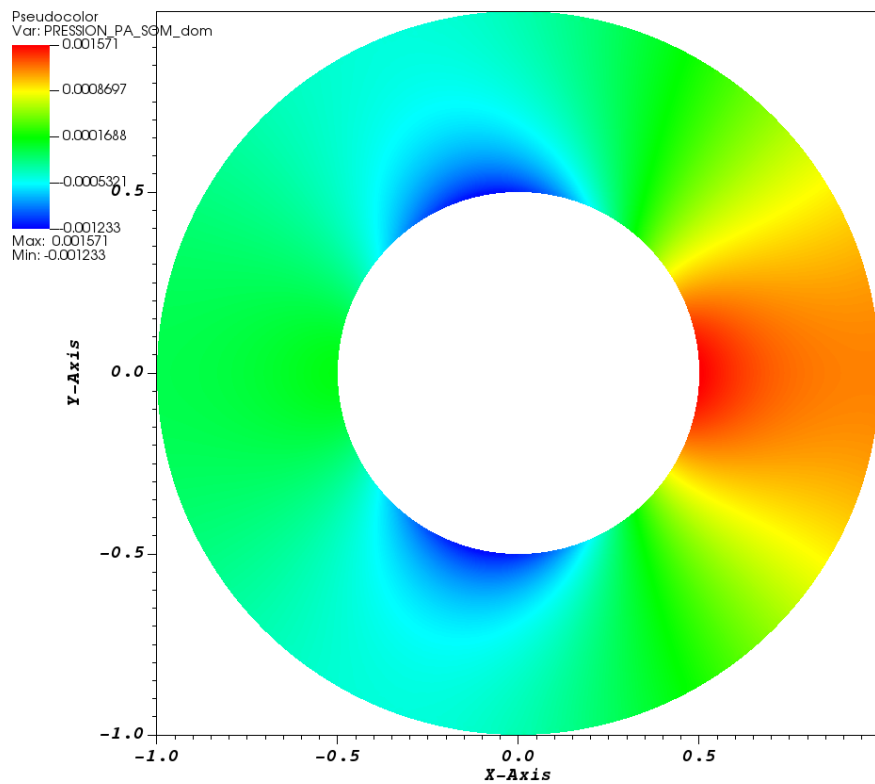


Figure VIII.1.4: TrioCFD PRESSION SOM

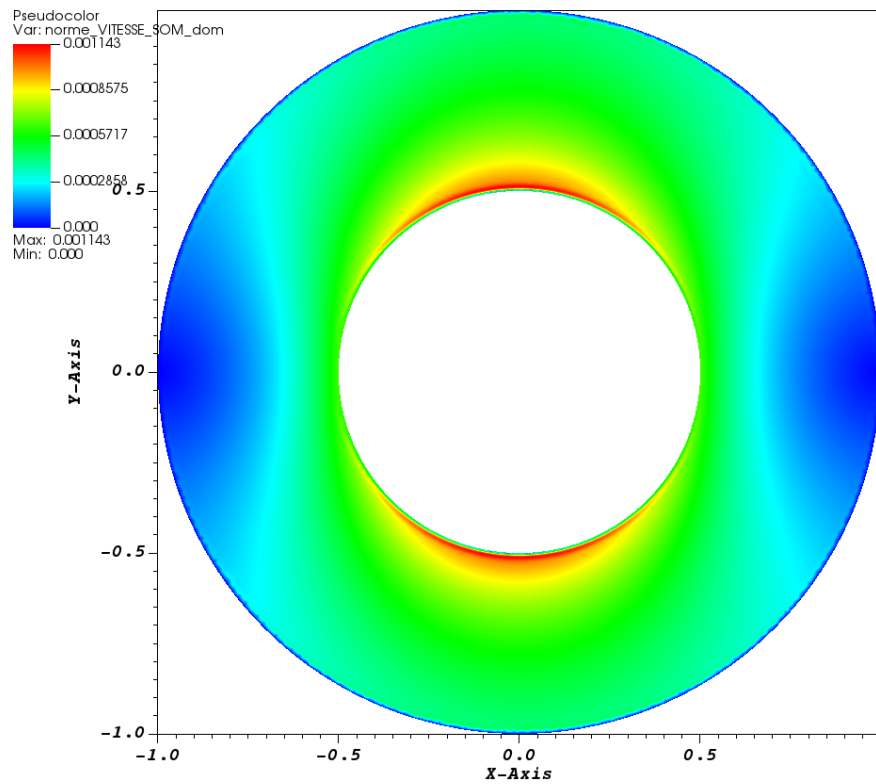


Figure VIII.1.5: TrioCFD VITESSE\_magnitude SOM

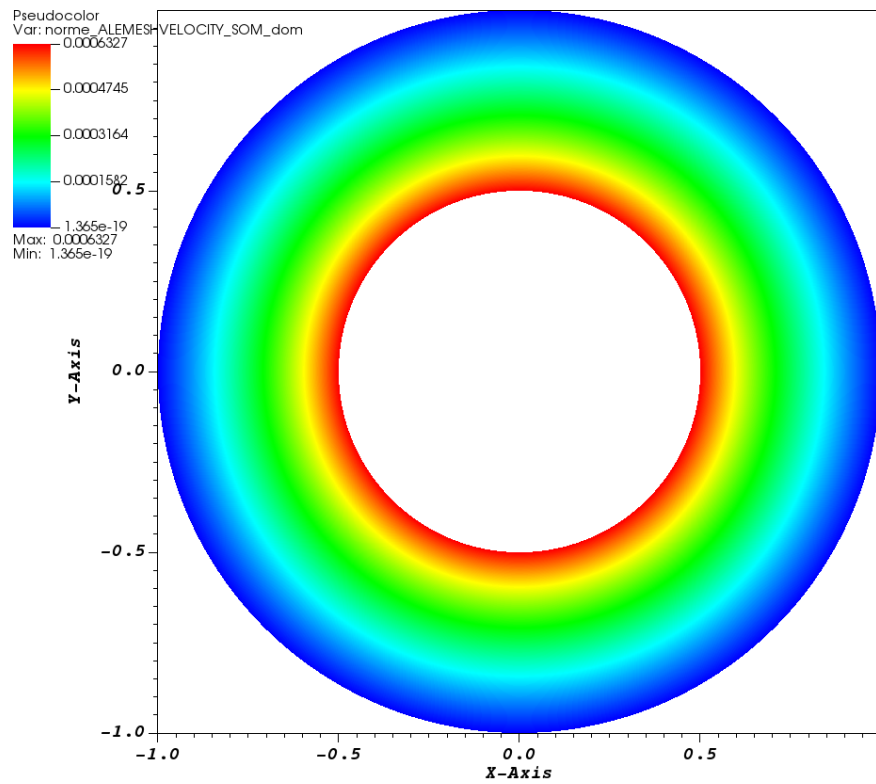


Figure VIII.1.6: TrioCFD Mesh velocity SOM

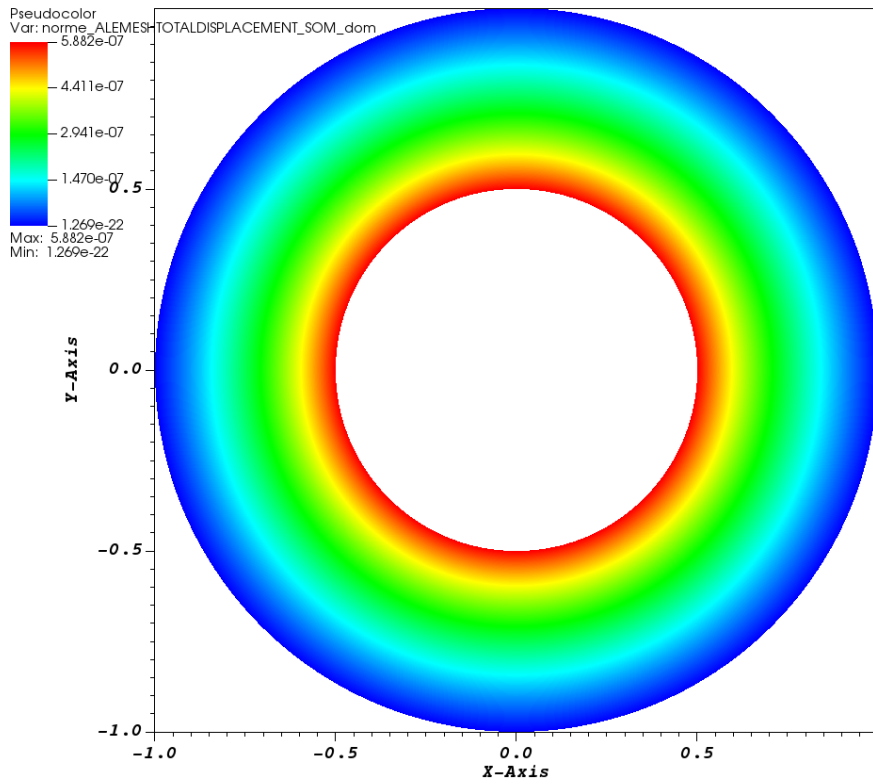


Figure VIII.1.7: TrioCFD Total displacement of the mesh SOM

## 1.5 Conclusion

The harmonic motion of a circular wall in a quiescent viscous fluid, enclosed by a concentric fixed wall, has been numerically simulated. A FEV method is applied to solve such a problem in conjunction with the ALE approach. The numerical results for the fluid force and the added coefficients successfully confirmed the analytical solution [1]. Remark: in order to reduce the numerical error a much more refined mesh must be used!

## 1.6 References

- 1. S. S. Chen, M. W. Wambsganss, and J. A. Jendrzejczyk. Added Mass and Damping of a Vibrating Rod in Confined Viscous Fluids, 1976.
- 2. CFD numerical simulation of a single-phase flow around a vibrating cylindrical tube, D. Panunzio, DES/ISAS/DM2S/SEMT/DYN/RS/2020-67015/A

## 1.7 Data Files

### TwoCylinders

```
# Fluid annulus region confined between an inner wall moving with an harmonic motion and an ou
# Hydraulique 2D laminar with ALE #
# PARALLEL ONLY 4 #
dimension 2
Pb_hydraulique_ALE pb
Domaine_ALE dom
# BEGIN MESH #
```

```

# Read_med family_names_from_group_names dom MeshWithTwoCylinders MeshWithTwoCylinders.med #
# END MESH #
# BEGIN PARTITION
Partition dom
{
    Partition_tool metis { Nb_parts 2 }
    Larg_joint 2
    zones_name DOM
}
End
END PARTITION #
# BEGIN SCATTER #
Scatter DOM.Zones dom
# END SCATTER #
# For the Arbitrary Lagrangian-Eulerian framework: block to indicate the number of mobile
boundaries of the domain and specify the speed that must be imposed on them #
Imposer_vit_bords_ALE dom
{
    1 # number of mobile boundaries #
    CircleA Champ_front_ALE 2 0.01*0.06327167604329844*cos(0.06327167604329844*t) 0.0 # name and
}
# Solver used to solve the system giving the moving mesh velocity #
Solver_moving_mesh_ALE dom { Petsc Cholesky { } }
# I select a discretization #
VEFPreP1B ma_discretisation
# Time scheme, choice between: Euler explicit or implicit, and Adams Bashforth order 2
or order 3 #
Scheme_euler_implicit mon_schema
Read mon_schema
{
    # Time step #
        # Initial time [s] #
        tinit 0.
    # Min time step #
        dt_min 1.e-15
    # Output criteria #
        # .out files printing period #
        dt_impr 5.e-8
    # .sauv files printing period #
        dt_sauv 100.
    # facsec such as dt = facsec * min(dt(CFL),dt_max) ; for explicit scheme facsec <= 1. By defa
    facsec 1
        facsec_max 1
    solveur implicite_ALE
    {
        solveur gmres { diag seuil 1.e-12 nb_it_max 3 }
    }
    # Stop if one of the following criteria is checked: #
        # End time [s] #
    tmax 496.5
    # Max number of time steps #
        # nb_pas_dt_max 2 #
        # Convergence threshold (see .dt_ev file) #
        seuil_statio 1.e-15
    }
    # I define a medium #
    # Gravity vector definition
    Uniform_field my_gravity
    Read my_gravity 2 0.0 0.0 #
    # Association between the different objects #
    Associate pb dom

```

```

Associate pb mon_schema
Discretize pb ma_discretisation
Read pb
{
  fluide_incompressible {
    mu Champ_Uniforme 1 1.007e-3
    rho Champ_Uniforme 1 1000
  }
  Navier_Stokes_standard_ALE
  {
    # Pressure matrix solved with #
    solveur_pression petsc cholesky { }
    # Two operators are defined #
    convection { ALE { muscl } } # A convective scheme for ALE framework. Choice between: among
    diffusion { }
    # Uniform initial condition for velocity #
    initial_conditions {
      vitesse Champ_Uniforme 2 0. 0.
    }
    # Boundary conditions #
    boundary_conditions {
      CircleA frontiere_ouverte_vitesse_imposee Champ_front_ALE 2 0.01*0.06327167604329844*cos
      CircleB paroi_fixe
    }
  }
  Post_processing
  {
    # Fields #
    format lata
    fields dt_post 100
    {
      pression_pa som
      vitesse som
      ALEMeshVelocity som
      ALEMeshTotalDisplacement som
    }
  }
}
# The problem is solved with #
Solve pb
# Not necessary keyword to finish #
End

```

## Hydrodynamic interaction of two cylinders subjected to small oscillations

### 2.1 Purpose

The domain used for the numerical simulations is the one in Figure 1. As we can see from Figure 1., we have a 2-dimensional domain  $\mathcal{D}$ , with arbitrarily large length and width. In this domain, we have a homogeneous Newtonian incompressible fluid at rest, characterized by its volume mass density  $\rho$  and its kinematic viscosity  $\nu$ . In fact, we have two cylinders, with radius  $R_j$  and center  $O_j$ , oscillating at an  $\Omega$  angular frequency.

This validation test case has been created to compare TrioCFD ALE results with the theoretical solution of such a problem [1].

We investigate the force exerted by the fluid on the cylindrical tube subjected to a transverse excitation. We will seek, in particular, on the characteristics of the fluid force, represented by the added mass and damping coefficients.

A detailed analysis of the present test case is presented in [1].

Validation made by : M. A. Puscas.

Report generated 10/06/2023.

### 2.2 Problem Description

The domain used for the numerical simulations is the one in Figure 1.

#### Geometry

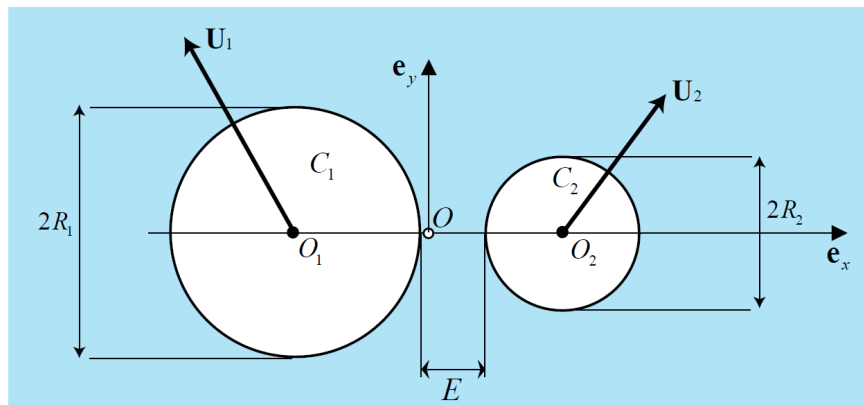


Figure 1. Schematic diagram of the system: two oscillating cylinders  $C_j$  with radii  $R_j$ , centers  $O_j$ , displacement vectors  $\mathbf{U}_j(T)$ , are immersed in a fluid of kinematic viscosity  $\nu$ . The small oscillations of  $C_j$  generate an incompressible fluid flow. The midpoint of  $O_1$  and  $O_2$  is  $O$  and the separation distance is  $E$ .

Figure VIII.2.1: The domain

## Initial Conditions and Boundary Conditions

The left cylinder ( $C_1$ ) is fixed and the right one ( $C_2$ ) moves with an harmonic motion alongside the  $x$ -axis:  $\mathbf{U}_2(T) = u \sin(\omega T) \mathbf{e}_x$ , where  $u = 0.01$ .

The left, right, upper and lower boundaries are fixed.

Initially, the fluid is at rest.

## Fluid Properties

The tube bundle is immersed in a Newtonian and homogeneous fluid, with mass density  $\rho$  ( $1000 \text{ Kg/m}^3$ ) and kinematic viscosity  $\nu$  ( $1.007 * 10^{-6} \text{ m}^2/\text{s}$ ). The fluid flow generated by the oscillation of the right cylinder is assumed as incompressible and two-dimensional.

## 2.3 Case Setup

### Grid

A refined mesh is used in the regions with large gradient fields whereas a loose mesh is used in the areas with low gradient fields.

Calculation has been partitioned on 10 processors, such that each processor worked with 20000-30000 elements.

## Model Options

The fluid problem with moving boundaries is handled by the Arbitrary Lagrangian-Eulerian (ALE) method. In the ALE approach, the fluid flow is computed in a domain that is deformed in order to follow the movement of the fluid-solid interface. It provides a hybrid description not associated with the fluid particles and the laboratory coordinates. We associate the description with a moving imaginary mesh that follows the fluid domain.

## 2.4 Results

### Validation Specific Informations

- Version TRUST : 1.8.2
- Problem: Pb\_hydraulique\_ALE
- Dimension: 2D
- Domain: Domaine\_ALE
- Pressure solver: Solver\_moving\_mesh\_ALE PETSC Cholesky
- Discretization: VEFPre1B
- Time scheme: Scheme\_euler\_implicit with solver implicite\_ALE GMRES
- Medium: Fluide\_Incompressible
- Hydraulic problem: Navier\_Stokes\_standard\_ALE
- Convection scheme: ALE muscl
- Generated Test cases :
  - ./TwoOscillatingCylinders.data : /\*jdd en annexe\*/
- Performance Chart :

	host	system	Total CPU Time	CPU time/step	number of cell
./TwoOscillatingCylinders	uruk	Linux	64679.3	14.5507	241618

Table VIII.2.1: Performance Chart

## Plot Data

In this section the Least Squares (LS) and Collocation (COL) methods (theoretical approximation solutions) presented in [1] for the force per unit length exerted by the fluid over the cylinders and the added coefficients are compared with the TrioCFD results.

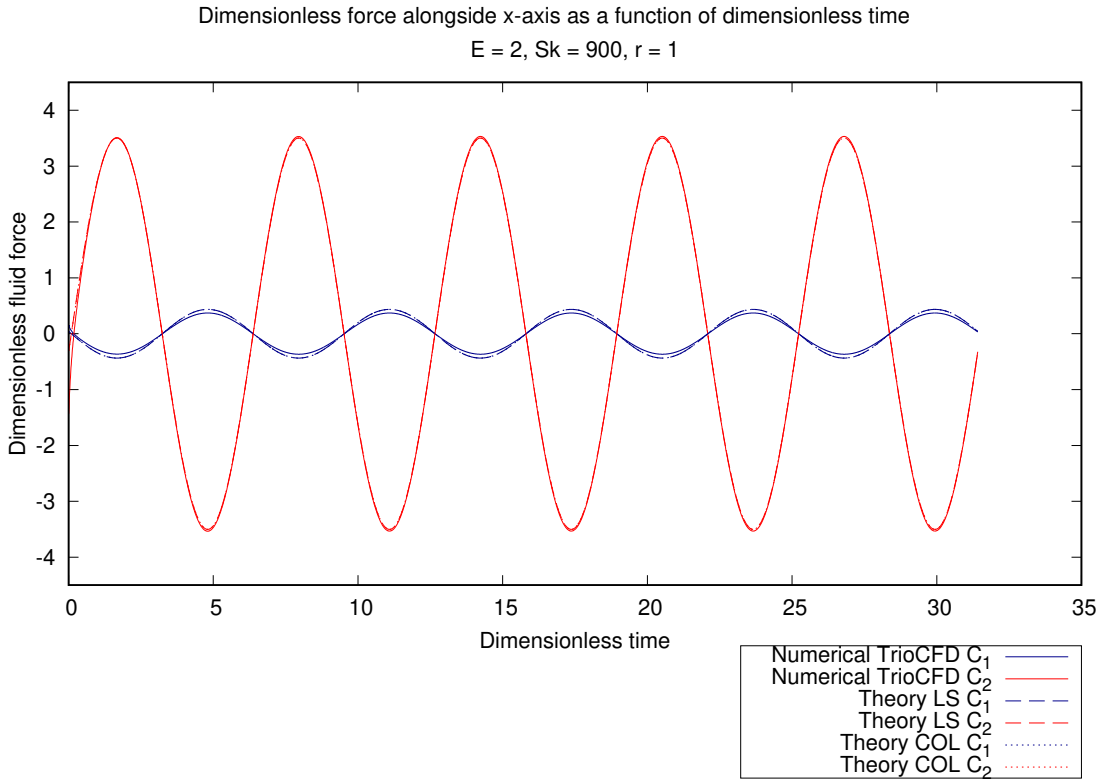


Figure VIII.2.2: Force per unit length of cylinder

For the theoretical calculation of the added coefficients, the reader is referred to [1]. Numerically, the added coefficients are computed with a Fourier product as:

$$\begin{aligned}
 m_{self} &= \frac{\langle \sin(\omega t), F_{C_2}(t) \rangle}{\rho u (R_2)^2 \omega^2} & \text{with} & \quad \langle \sin(\omega t), F_{C_2}(t) \rangle = \frac{2}{5T} \int_0^{5T} \sin(\omega t) F_{C_2}(t) dt \\
 c_{self} &= \frac{\langle \cos(\omega t), F_{C_2}(t) \rangle}{\rho u (R_2)^2 \omega^2} & \text{with} & \quad \langle \cos(\omega t), F_{C_2}(t) \rangle = \frac{2}{5T} \int_0^{5T} \cos(\omega t) F_{C_2}(t) dt \\
 m_{cross} &= \frac{\langle \sin(\omega t), F_{C_1}(t) \rangle}{\rho u (R_2)^2 \omega^2} & \text{with} & \quad \langle \sin(\omega t), F_{C_1}(t) \rangle = \frac{2}{5T} \int_0^{5T} \sin(\omega t) F_{C_1}(t) dt \\
 c_{cross} &= \frac{\langle \cos(\omega t), F_{C_1}(t) \rangle}{\rho u (R_2)^2 \omega^2} & \text{with} & \quad \langle \cos(\omega t), F_{C_1}(t) \rangle = \frac{2}{5T} \int_0^{5T} \cos(\omega t) F_{C_1}(t) dt
 \end{aligned} \tag{2.1}$$

, where  $F_{C_1}$  represents the fluid force acting on the left cylinder (the static one) and  $F_{C_2}$  represents the fluid force acting on the right cylinder (the moving one), and are reported in the following table:

	$m_{self}$	$c_{self}$	$m_{cross}$	$c_{cross}$
COL theory[1]	1.11	0.106	-0.138	-0.0136
LS theory[1]	1.11	0.105	-0.138	-0.0132
TrioCFD	1.1177748565592722	0.10809949093964831	-0.11672369236362198	-0.011730376635105207

Table VIII.2.2: Added mass and damping coefficients

Pressure and velocity fields are reported at final time in order to investigate such distributions. The mesh velocity are also plotted.

DB: TwoOscillatingCylinders.lata  
Time:34664.7

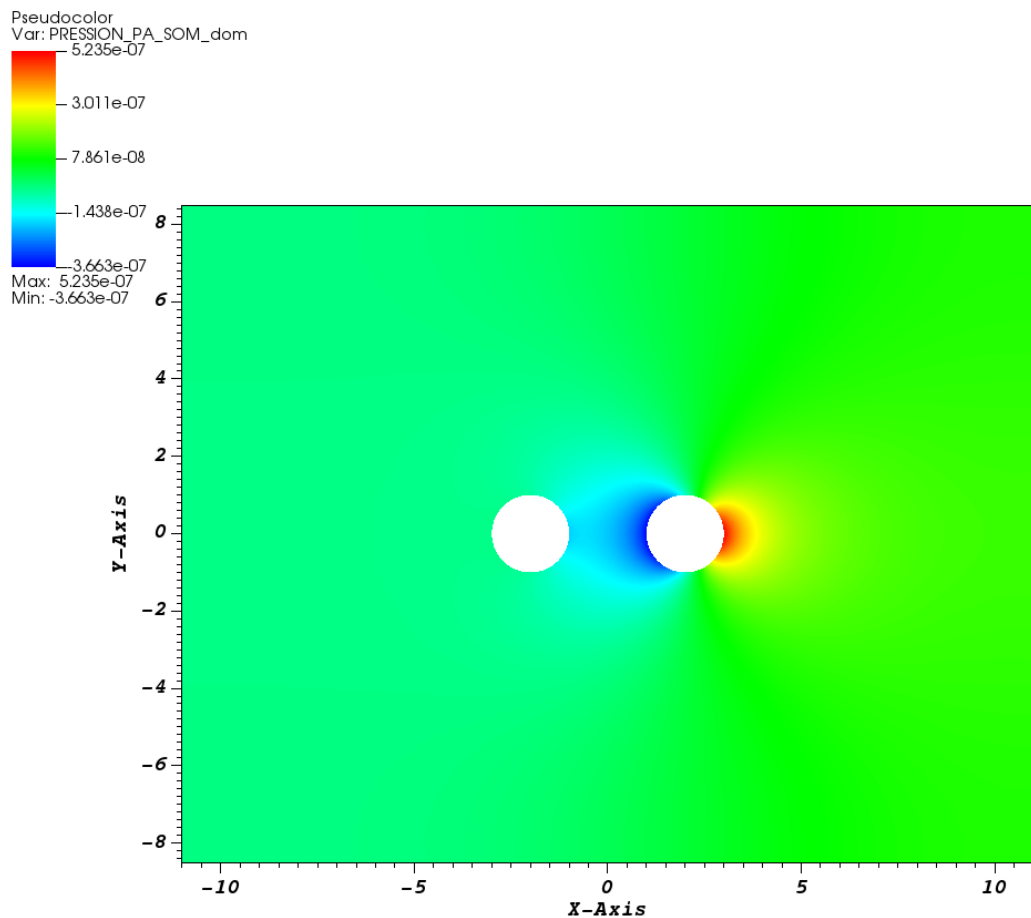


Figure VIII.2.3: TrioCFD PRESSION SOM

DB: TwoOscillatingCylinders.lata  
Time:34664.7

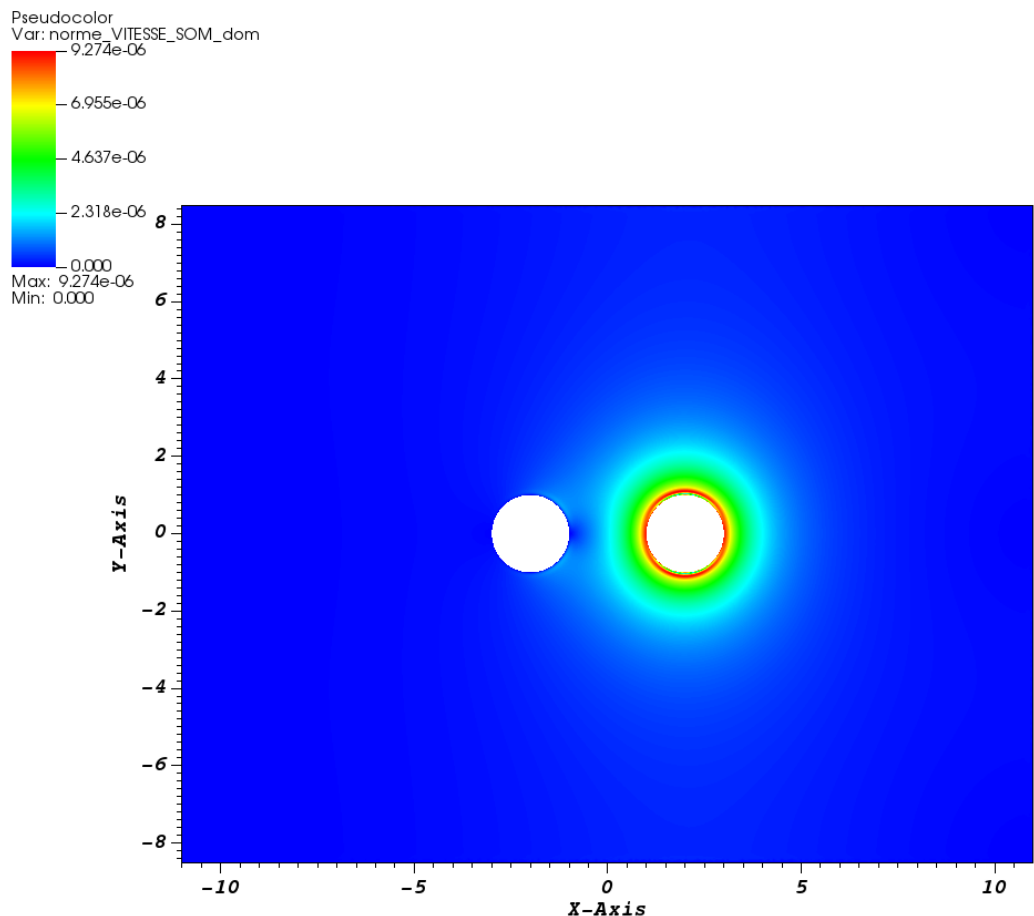


Figure VIII.2.4: TrioCFD VITESSE\_magnitude SOM

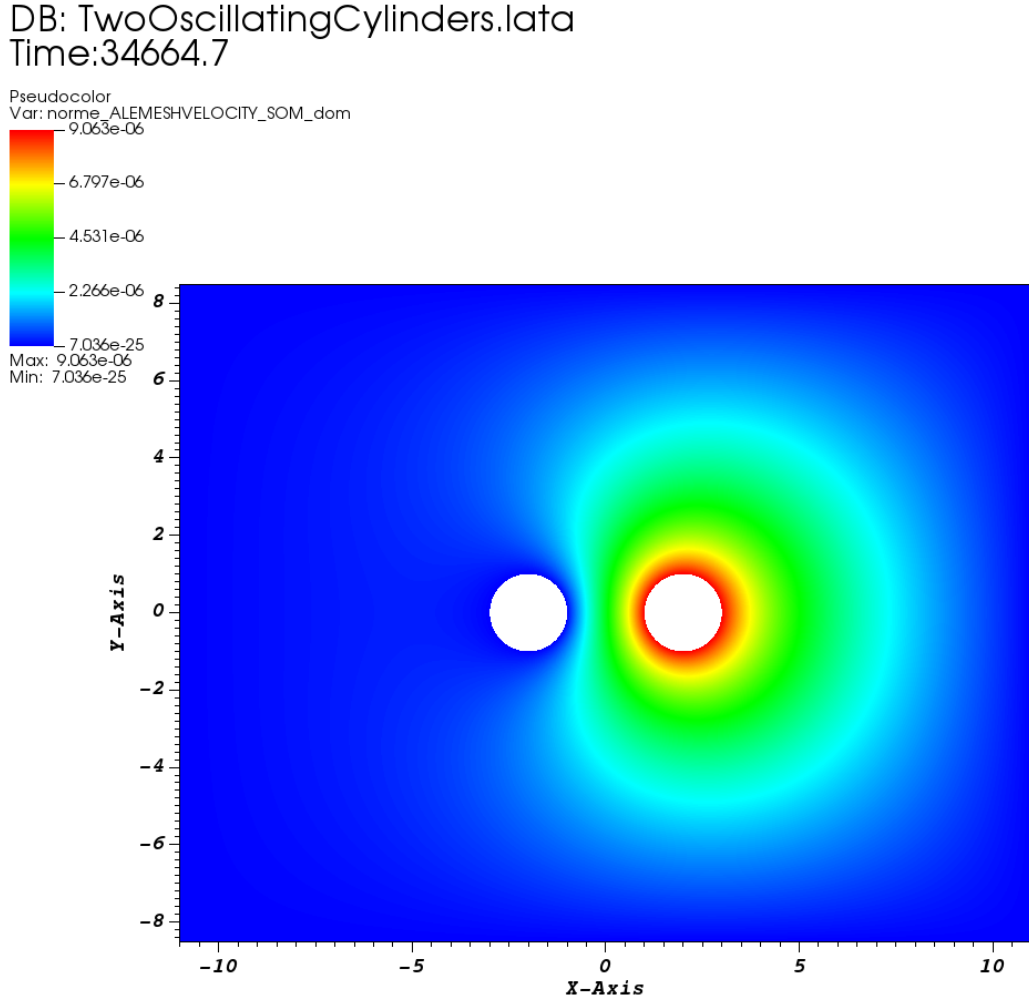


Figure VIII.2.5: TrioCFD Mesh velocity SOM

## 2.5 Conclusion

The harmonic motion of a circular wall in a quiescent viscous fluid, has been numerically simulated. A FEV method is applied to solve such a problem in conjunction with the ALE approach. The numerical results for the fluid force and the added coefficients are in good agreement with the theoretical COL and LS approximation solution [1].

Remark: in order to reduce the numerical error a much more refined mesh must be used!!!

## 2.6 References

- 1. New estimations of the added mass and damping of two cylinders vibrating in a viscous fluid, from theoretical and numerical approaches. R. Lagrange and Y. Fraigneau, Journal of Fluids and Structures, 2020.
- 2. CFD numerical simulation of a single-phase flow around a vibrating cylindrical tube, D. Panunzio, DES/ISAS/DM2S/SEMT/DYN/RS/2020-67015/A

## 2.7 Data Files

### TwoOscillatingCylinders

```

# Hydrodynamic 2D laminar with ALE : interaction of two cylinders subjected to small oscillations
# PARALLEL ONLY 10 #
dimension 2
Pb_hydraulique_ALE pb
Domaine_ALE dom
# BEGIN MESH #
# Read_med family_names_from_group_names dom TwoOscillatingCylinders TwoOscillatingCylinders.med
# END MESH #
# BEGIN PARTITION
Partition dom
{
    Partition_tool metis { Nb_parts 2 }
    Larg_joint 2
    zones_name DOM
}
End
# END PARTITION #
# BEGIN SCATTER #
Scatter DOM.Zones dom
# END SCATTER #
imposer_vit_bords_ale dom
{
    1 # number of mobile boundaries #
    CylinderRight Champ_front_ALE 2 0.01*(9.063e-4)*cos((9.063e-4)*t) 0.0 # name and speed of the
    We have an oscillation position : g(t) = u*sin(OMEGA*t) —> derivative for velocity
#
}
# Solver used in order to solve the system giving the moving mesh velocity #
Solver_moving_mesh_ALE dom { Petsc Cholesky { } }
# I select a discretization #
VFPReP1B ma_discretisation
# Time scheme, choice between: Euler explicit or implicit, and Adams Bashforth order 2
or order 3 #
Scheme_euler_implicit mon_schema
Read mon_schema
{
    # Time step #
    # Initial time [s] #
    tinit 0.
    # Min time step #
    dt_min 1.e-15
    # Output criteria #
    # .out files printing period #
    dt_impr 5.e-6
    # .sauv files printing period #
    # tcpumax 47.5 #
    # .sauv files printing period #
    periode_sauvegarde_securite_en_heures 23
    # facsec such as dt = facsec * min(dt(CFL),dt_max) ; for explicit scheme facsec <= 1. By default
    facsec 1.
    facsec_max 1.
    solveur implicite_ALE
    {
        solveur gmres { diag seuil 1.e-12 nb_it_max 3 }
    }
    # Stop if one of the following criteria is checked: #
}

```

```

# End time [s] ; T = 2*pi/R2*R2*OMEGA = 6933 (period in s) ; 5 periods #
tmax 34664
# Max number of time steps #
# nb_pas_dt_max 2 #
# Convergence threshold (see .dt_ev file) #
seuil_statio 1.e-15
}
# I define a medium #
# Gravity vector definition
Uniform_field my_gravity
Read my_gravity 2 0.0 0.0 #
# Association between the different objects #
Associate pb dom
Associate pb mon_schema
Discretize pb ma_discretisation
Read pb
{
  fluide_incompressible {
    mu Champ_Uniforme 1 1.007e-3
    rho Champ_Uniforme 1 1000
  }
  Navier_Stokes_standard_ALE
{
  # Pressure matrix solved with #
  solveur_pression petsc cholesky { }
  # Two operators are defined #
  convection { ALE { muscl } } # A convective scheme for ALE framework. Choice between: amon
  diffusion { }
  # Uniform initial condition for velocity #
  initial_conditions {
    vitesse Champ_Uniforme 2 0. 0.
  }
  # Boundary conditions #
  boundary_conditions {
    CylinderRight frontiere_ouverte_vitesse_imposee Champ_front_ALE 2 0.01*(9.063e-4)*cos((9
    CylinderLeft paroi_fixe
    RectangularBox paroi_fixe
  }
}
Post_processing
{
  # Fields #
  format lata
  fields dt_post 3000
  {
    pression_pa som
    vitesse som
    ALEMeshVelocity som
  }
}
# resume_last_time binaire TwoOscillatingCylinders_pb.sauv #
}
# The problem is solved with #
Solve pb
# Not necessary keyword to finish #
End

```

## VIII.3

# Vibrations of a cylinder in a square tube bundle immersed in a viscous fluid

### 3.1 Purpose

The importance of fluid-elastic forces in tube bundle vibrations can hardly be over-emphasized, in view of their damaging potential. In the last decades, advanced models for representing fluid-elastic coupling through added-coefficients have therefore been developed by the community of the domain.

In what follows, we aim to determine numerically the fluid added-coefficients (mass and damping), considering the case of a square tube bundle immersed in a viscous fluid at rest.

This validation test case has been created to compare TrioCFD ALE results with the experimental results obtained by the CEA/DYN laboratory for such a problem.

A mesh sensitivity analysis has been carried out, and it is here reported, to detect the best results from both a physical and numerical point of view.

Validation made by : M. A. Puscas and D. Panunzio.  
Report generated 09/06/2023.

### 3.2 Problem Description

A 2D fluid in a set of circular cylinders, arranged in a square configuration (DIVA configuration), has been numerically simulated. Such a pattern is made up of three rows of three cylinders and a set of half cylinders for each square-side. The pitch between the cylinders is  $P = 1.5D$ , for both directions, where  $D$  is the diameter.

## Geometry

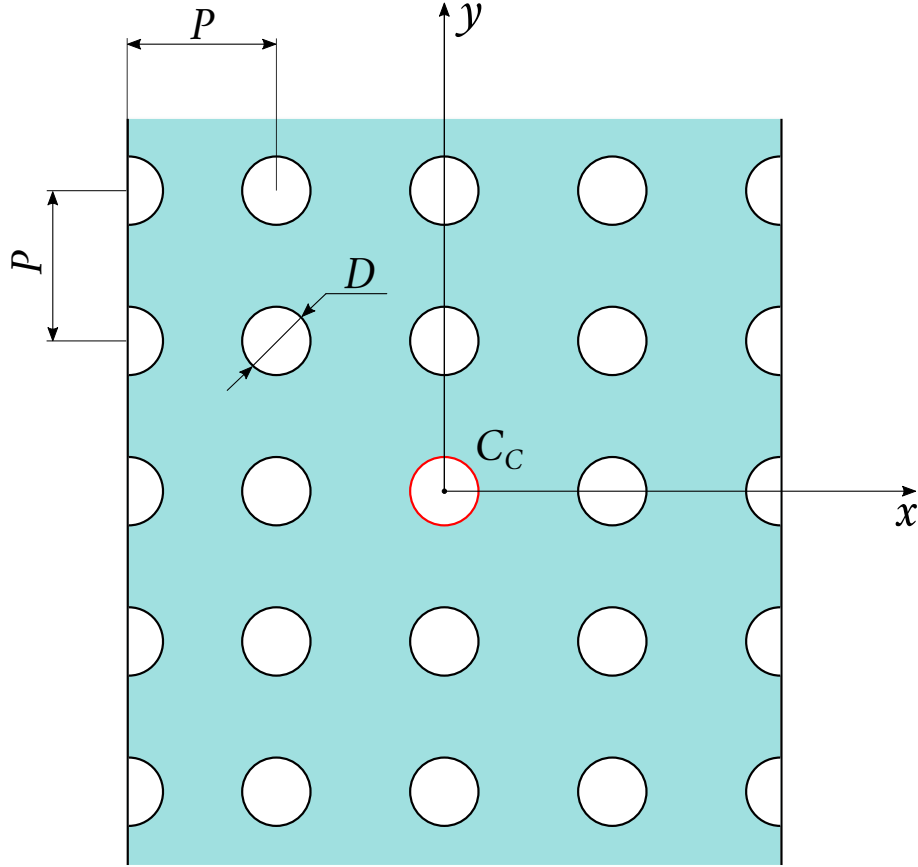


Figure VIII.3.1: DIVA geometry

## Initial Conditions and Boundary Conditions

The central cylinder moves with an harmonic motion:  $\mathbf{u} = U * \sin(\omega * t)\mathbf{e}_x$ , where  $U$  : amplitude of displacement and  $\omega$  : angular frequency of displacement.

The others cylinders (half and quarter cylinders included) are fixed. The left, right, upper and lower boundaries are fixed.

Initially, the fluid is at rest.

## Fluid Properties

The tube bundle is immersed in a Newtonian and homogeneous fluid, with mass density  $\rho$  ( $1000\text{ Kg/m}^3$ ) and kinematic viscosity  $\nu$  ( $1.007 * 10^{-6}\text{ m}^2/\text{s}$ ). The fluid flow generated by the oscillation of the central cylinder is assumed as incompressible and two-dimensional.

### 3.3 Case Setup

In this section are reported the adaptive meshes used during the simulations. Fictitious lines have been added in the design of the geometry of these meshes in order to divide the calculation domain into blocks and ensure a symmetrical discretization by the mesh module MG\_CADSURF of SALOME.

Numerical simulations have been carried out on a set of adaptive meshes. The global size and two local sizes have been defined: a smaller one at the center and immediately adjacent cylinders (min\_local\_size) and a larger one (max\_local\_size) at the other boundaries (right and left walls, upper and lower borders, other cylinders).

By this way, a refined mesh is used in the regions with large gradient fields whereas a loose mesh is used in the areas with low gradient fields.

The main properties are summarized in the table below. Calculation has been partitioned on a number of processors such that each processor worked with 20000-30000 elements.

## Grid

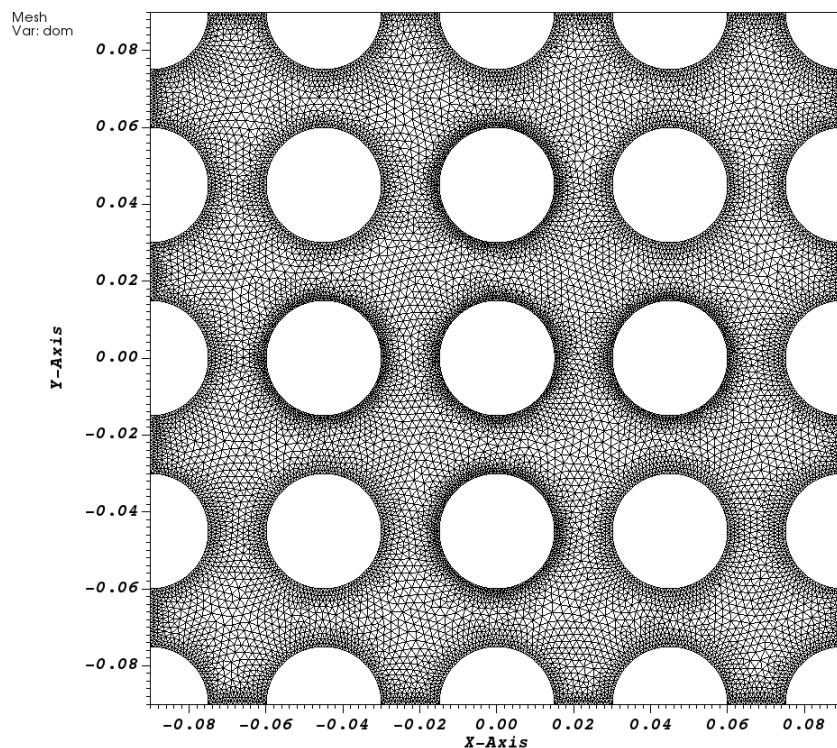


Figure VIII.3.2: Mesh\_1

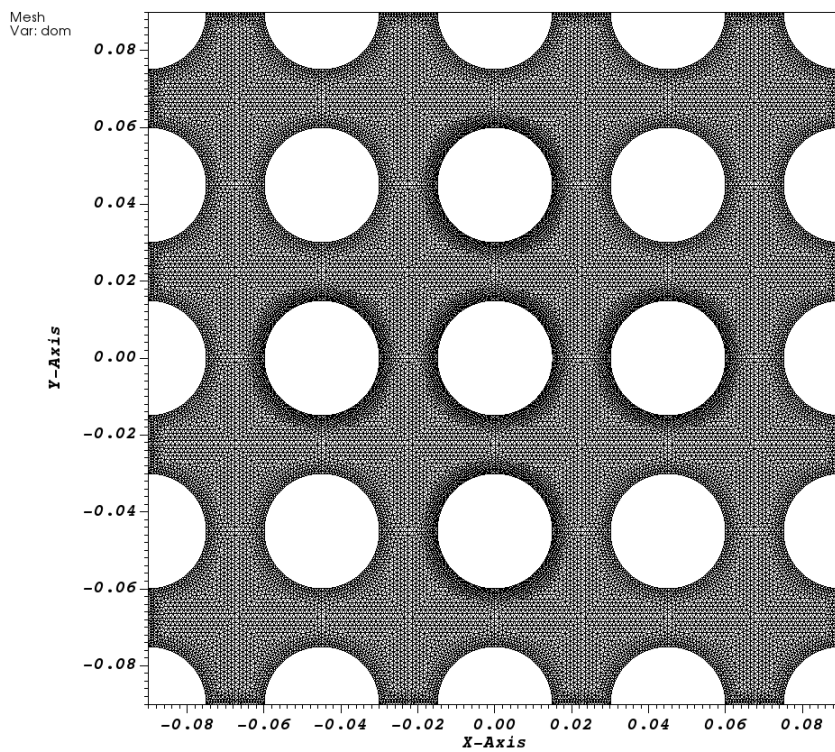


Figure VIII.3.3: Mesh\_2

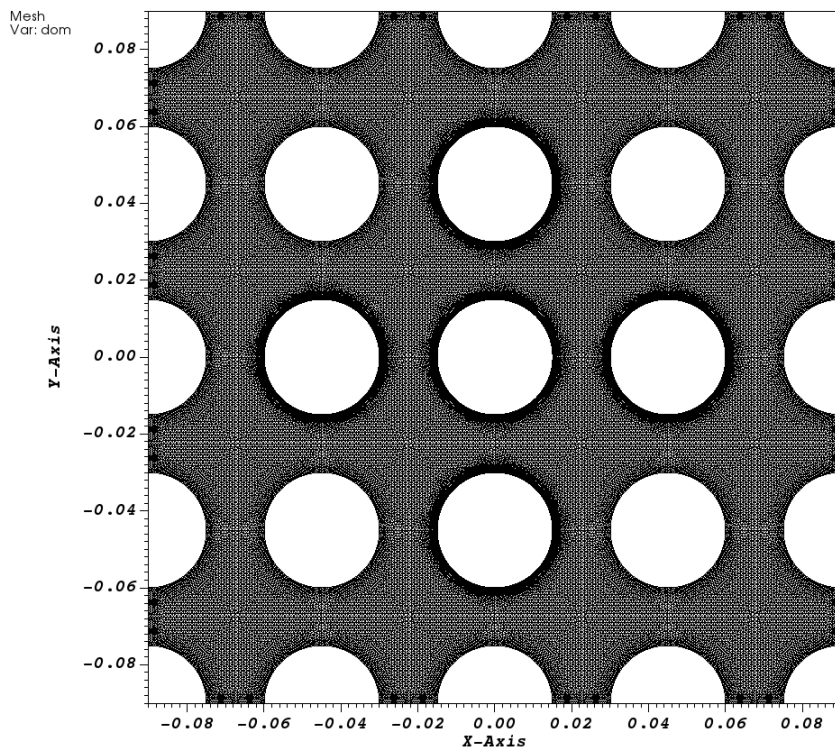


Figure VIII.3.4: Mesh\_3

	Nb_elements	Nb_processors	global_size	max_local_size	min_local_size
Mesh_1	25806	1	0.0012	0.0008	0.0006
Mesh_2	51146	2	0.0011	0.0007	0.00055
Mesh_3	102080	4	0.0008	0.0005	0.0003

Table VIII.3.1: Meshes properties

## Model Options

The fluid problem with moving boundaries is handled by the Arbitrary Lagrangian-Eulerian (ALE) method. In the ALE approach, the fluid flow is computed in a domain that is deformed in order to follow the movement of the fluid-solid interface. It provides a hybrid description not associated with the fluid particles and the laboratory coordinates. We associate the description with a moving imaginary mesh that follows the fluid domain.

## 3.4 Results

### Validation Specific Informations

- Version TRUST : 1.8.2
- Problem: Pb\_hydraulique\_ALE
- Dimension: 2D
- Domain: Domaine\_ALE
- Pressure solver: Solver\_moving\_mesh\_ALE PETSC GCP
- Discretization: VEFPre1B
- Time scheme: Scheme\_euler\_implicit with solver implicite\_ALE GMRES
- Medium: Fluide\_Incompressible
- Hydraulic problem: Navier\_Stokes\_standard\_ALE
- Convection scheme: ALE muscl
- Location: ALE/share/Validation/Rapports\_automatiques/DivaALE
- Generated Test cases :
  - Mesh\_1/DIVA.data : /\*jdd en annexe\*/
  - Mesh\_2/DIVA.data :
  - Mesh\_3/DIVA.data :
- Performance Chart :

	host	system	Total CPU Time	CPU time/step	number of cell
Mesh_1/DIVA	uruk	Linux	6595.04	7.53345	25854
Mesh_2/DIVA	uruk	Linux	9800.27	10.2329	51210
Mesh_3/DIVA	uruk	Linux	25521	14.0779	102144
Total			41916.3		

Table VIII.3.2: Performance Chart

## Plot Data

In this section the experimental results for the force per unit length exerted by the fluid over the center cylinder and the added coefficients are compared with the TrioCFD results. The numerical results are also given for the added coefficients for the North, South, East, West cylinders.

According to Chen [1], the analytical solution of the fluid force per unit length acting on the center cylinder is:

$$\mathbf{F}_x = \rho\pi \left(\frac{D}{2}\right)^2 U\omega^2 \left[ m_{self} \sin(\omega t) - c_{self} \cos(\omega t) \right] \mathbf{e}_x \quad (3.1)$$

where  $\rho = 1 \text{ kg/m}^3$ ,  $D = 0.03 \text{ m}$ ,  $U = 0.003 \text{ m}$  (amplitude of displacement),  $\omega = 125.66 \text{ rad/s}$  (angular frequency of displacement) and  $m_{self}$  and  $c_{self}$  the added mass and damping coefficients, respectively.

The experimental solution is here depicted and compared with the numerical one, obtained by the sum of the pressure and viscous force acting on the center cylinder along x, for the following cases: TrioCFD with Mesh\_1 (TrioCFD Mesh\_1), TrioCFD with Mesh\_2 (TrioCFD Mesh\_2) and TrioCFD with Mesh\_3 (TrioCFD Mesh\_3). Simulations have been performed for  $t = [0, 5T]$  where  $T = 2\pi/\omega$ .

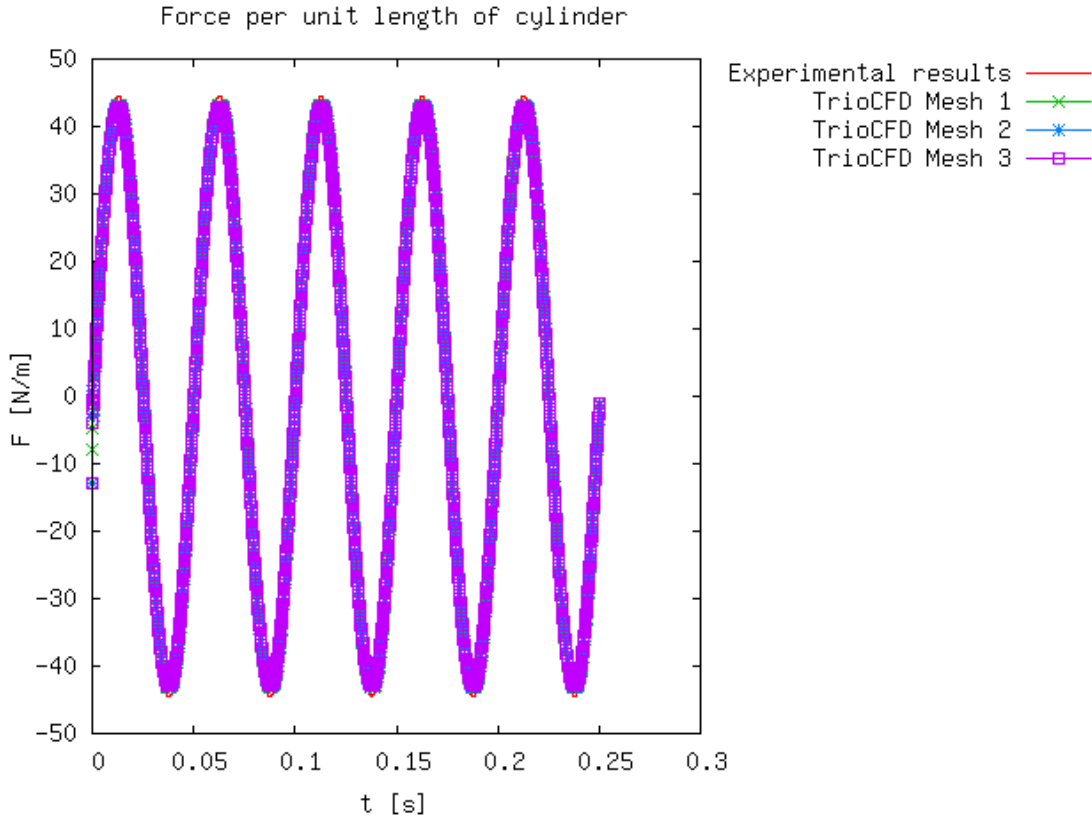


Figure VIII.3.5: Force per unit length of cylinder

The experimental calculation of the coefficients has been carried out on the test bench of the CEA/DYN laboratory. For the Center cylinder, numerically, the added coefficients are computed with a Fourier product

as:

$$\begin{aligned} m_{i,self} &= \frac{\langle \sin(\omega t), F_i(t) \rangle}{\rho\pi(D/2)^2 U \omega^2} & \text{with } \langle \sin(\omega t), F_i(t) \rangle = \frac{2}{5T} \int_0^{5T} \sin(\omega t) F_i(t) dt \\ c_{i,self} &= \frac{\langle \cos(\omega t), F_i(t) \rangle}{\rho\pi(D/2)^2 U \omega^2} & \text{with } \langle \cos(\omega t), F_i(t) \rangle = \frac{2}{5T} \int_0^{5T} \cos(\omega t) F_i(t) dt \end{aligned} \quad (3.2)$$

and are reported in the following tables:

	$m_{x,self}$	$m_{y,self}$
Experimental solution	1.33	0
TrioCFD Mesh_1	1.3019721962306774	-7.606016940201938e-05
TrioCFD Mesh_2	1.2982005623508581	-1.4482147350190461e-05
TrioCFD Mesh_3	1.2863785115141373	3.329069717089464e-06

Table VIII.3.3: Added mass coefficients for the Center cylinder

	$c_{x,self}$	$c_{y,self}$
Experimental solution	0.049	0
TrioCFD Mesh_1	0.06337955444731924	-0.0005286155347936486
TrioCFD Mesh_2	0.0581851918842418	5.556321007087155e-05
TrioCFD Mesh_3	0.04019505704128777	9.949779012241801e-05

Table VIII.3.4: Added damping coefficients for the Center cylinder

For the Nord cylinder, numerically, the added coefficients are computed with a Fourier product as:

$$\begin{aligned} m_{i,cross}^{(N)} &= \frac{\langle \sin(\omega t), F_i^{(N)}(t) \rangle}{\rho\pi(D/2)^2 U \omega^2} & \text{with } \langle \sin(\omega t), F_i^{(N)}(t) \rangle = \frac{2}{5T} \int_0^{5T} \sin(\omega t) F_i^{(N)}(t) dt \\ c_{i,cross}^{(N)} &= \frac{\langle \cos(\omega t), F_i^{(N)}(t) \rangle}{\rho\pi(D/2)^2 U \omega^2} & \text{with } \langle \cos(\omega t), F_i^{(N)}(t) \rangle = \frac{2}{5T} \int_0^{5T} \cos(\omega t) F_i^{(N)}(t) dt \end{aligned} \quad (3.3)$$

and are reported in the following tables:

	$m_{x,cross}^{(N)}$	$m_{y,cross}^{(N)}$
TrioCFD Mesh_1	0.3716451252055933	-0.0006243887366519355
TrioCFD Mesh_2	0.37017776576727224	-0.0006239619823956365
TrioCFD Mesh_3	0.3662295936906056	-0.0003213928829490047

Table VIII.3.5: Added mass coefficients for the Nord cylinder

	$c_{x,cross}^{(N)}$	$c_{y,cross}^{(N)}$
TrioCFD Mesh_1	0.019535840576965315	0.00012168150182348675
TrioCFD Mesh_2	0.01838379470022635	-2.0059304991394714e-05

	$c_{x,cross}^{(N)}$	$c_{y,cross}^{(N)}$
TrioCFD Mesh_3	0.01407069835185018	1.9796695105169396e-05

Table VIII.3.6: Added damping coefficients for the Nord cylinder

For the Sud cylinder, numerically, the added coefficients are computed with a Fourier product as:

$$\begin{aligned} m_{i,cross}^{(S)} &= \frac{\langle \sin(\omega t), F_i^{(S)}(t) \rangle}{\rho\pi(D/2)^2 U \omega^2} \quad \text{with} \quad \langle \sin(\omega t), F_i^{(S)}(t) \rangle = \frac{2}{5T} \int_0^{5T} \sin(\omega t) F_i^{(S)}(t) dt \\ c_{i,cross}^{(S)} &= \frac{\langle \cos(\omega t), F_i^{(S)}(t) \rangle}{\rho\pi(D/2)^2 U \omega^2} \quad \text{with} \quad \langle \cos(\omega t), F_i^{(S)}(t) \rangle = \frac{2}{5T} \int_0^{5T} \cos(\omega t) F_i^{(S)}(t) dt \end{aligned} \quad (3.4)$$

and are reported in the following tables:

	$m_{x,cross}^{(S)}$	$m_{y,cross}^{(S)}$
TrioCFD Mesh_1	0.37163213611538526	0.000626813460606409
TrioCFD Mesh_2	0.37017869763957933	0.0006312439280776619
TrioCFD Mesh_3	0.36622987225305975	0.0003193161614426827

Table VIII.3.7: Added mass coefficients for the Sud cylinder

	$c_{x,cross}^{(S)}$	$c_{y,cross}^{(S)}$
TrioCFD Mesh_1	0.019571856410468817	-4.2085455378056635e-05
TrioCFD Mesh_2	0.018386948600607387	-9.78325420035215e-07
TrioCFD Mesh_3	0.014076780847955658	-2.3179917691895998e-05

Table VIII.3.8: Added damping coefficients for the Sud cylinder

For the Est cylinder, numerically, the added coefficients are computed with a Fourier product as:

$$\begin{aligned} m_{i,cross}^{(E)} &= \frac{\langle \sin(\omega t), F_i^{(E)}(t) \rangle}{\rho\pi(D/2)^2 U \omega^2} \quad \text{with} \quad \langle \sin(\omega t), F_i^{(E)}(t) \rangle = \frac{2}{5T} \int_0^{5T} \sin(\omega t) F_i^{(E)}(t) dt \\ c_{i,cross}^{(E)} &= \frac{\langle \cos(\omega t), F_i^{(E)}(t) \rangle}{\rho\pi(D/2)^2 U \omega^2} \quad \text{with} \quad \langle \cos(\omega t), F_i^{(E)}(t) \rangle = \frac{2}{5T} \int_0^{5T} \cos(\omega t) F_i^{(E)}(t) dt \end{aligned} \quad (3.5)$$

and are reported in the following tables:

	$m_{x,cross}^{(E)}$	$m_{y,cross}^{(E)}$
TrioCFD Mesh_1	-0.16953462106042963	-2.364281092745423e-05
TrioCFD Mesh_2	-0.16899766845061273	-5.568689355258942e-06
TrioCFD Mesh_3	-0.16745690192427068	7.688930257414206e-07

Table VIII.3.9: Added mass coefficients for the Est cylinder

	$c_{x,cross}^{(E)}$	$c_{y,cross}^{(E)}$
TrioCFD Mesh_1	-0.005703524815256174	-7.580610023044735e-05
TrioCFD Mesh_2	-0.005162730897944815	1.344822281622433e-05
TrioCFD Mesh_3	-0.003135412483571656	1.4713389112017475e-05

Table VIII.3.10: Added damping coefficients for the Est cylinder

For the West cylinder, numerically, the added coefficients are computed with a Fourier product as:

$$\begin{aligned} m_{i,cross}^{(W)} &= \frac{\langle \sin(\omega t), F_i^{(W)}(t) \rangle}{\rho\pi(D/2)^2 U \omega^2} \quad \text{with} \quad \langle \sin(\omega t), F_i^{(W)}(t) \rangle = \frac{2}{5T} \int_0^{5T} \sin(\omega t) F_i^{(W)}(t) dt \\ c_{i,cross}^{(W)} &= \frac{\langle \cos(\omega t), F_i^{(W)}(t) \rangle}{\rho\pi(D/2)^2 U \omega^2} \quad \text{with} \quad \langle \cos(\omega t), F_i^{(W)}(t) \rangle = \frac{2}{5T} \int_0^{5T} \cos(\omega t) F_i^{(W)}(t) dt \end{aligned} \quad (3.6)$$

and are reported in the following tables:

	$m_{x,cross}^{(W)}$	$m_{y,cross}^{(W)}$
TrioCFD Mesh_1	-0.17090979461992548	1.9446788113623716e-05
TrioCFD Mesh_2	-0.1702971007077075	-3.857791216136348e-06
TrioCFD Mesh_3	-0.16814290053281405	2.6029590310458798e-08

Table VIII.3.11: Added mass coefficients for the West cylinder

	$c_{x,cross}^{(W)}$	$c_{y,cross}^{(W)}$
TrioCFD Mesh_1	-0.005798410347819413	-9.845552497944854e-05
TrioCFD Mesh_2	-0.005383469037083442	1.7542982598370907e-05
TrioCFD Mesh_3	-0.0033006282850066965	2.522006190186926e-05

Table VIII.3.12: Added damping coefficients for the West cylinder

Pressure and velocity fields are reported at final time in order to investigate such distributions for the following numerical cases: TrioCFD with Mesh\_1 (TrioCFD Mesh\_1), TrioCFD with Mesh\_2 (TrioCFD Mesh\_2) and TrioCFD with Mesh\_3 (TrioCFD Mesh\_3).

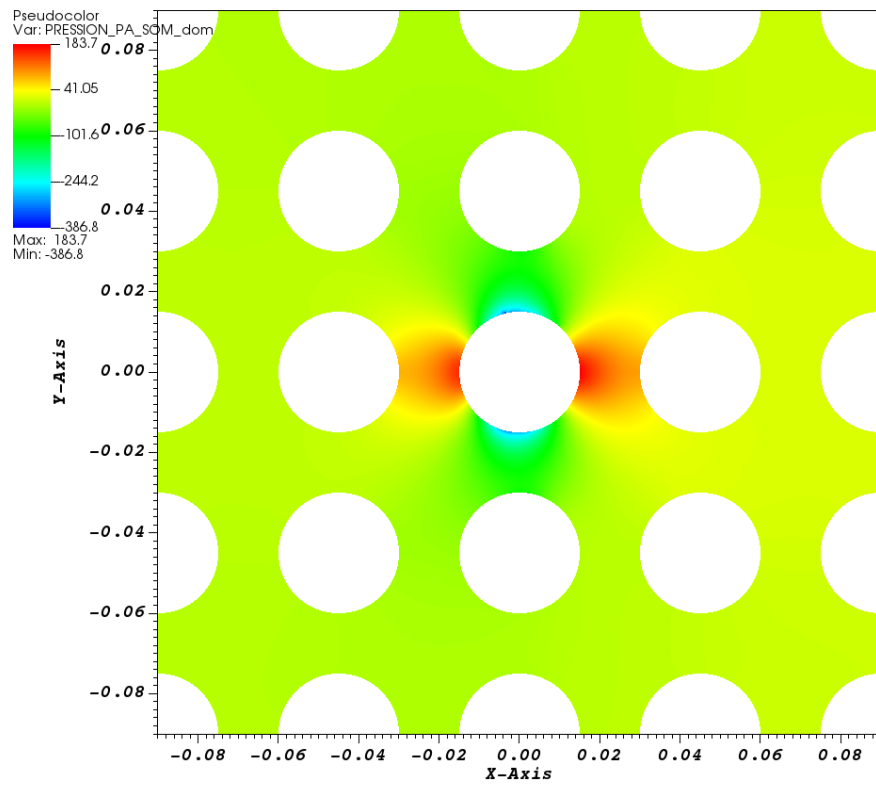


Figure VIII.3.6: TrioCFD Mesh\_1 PRESSION SOM

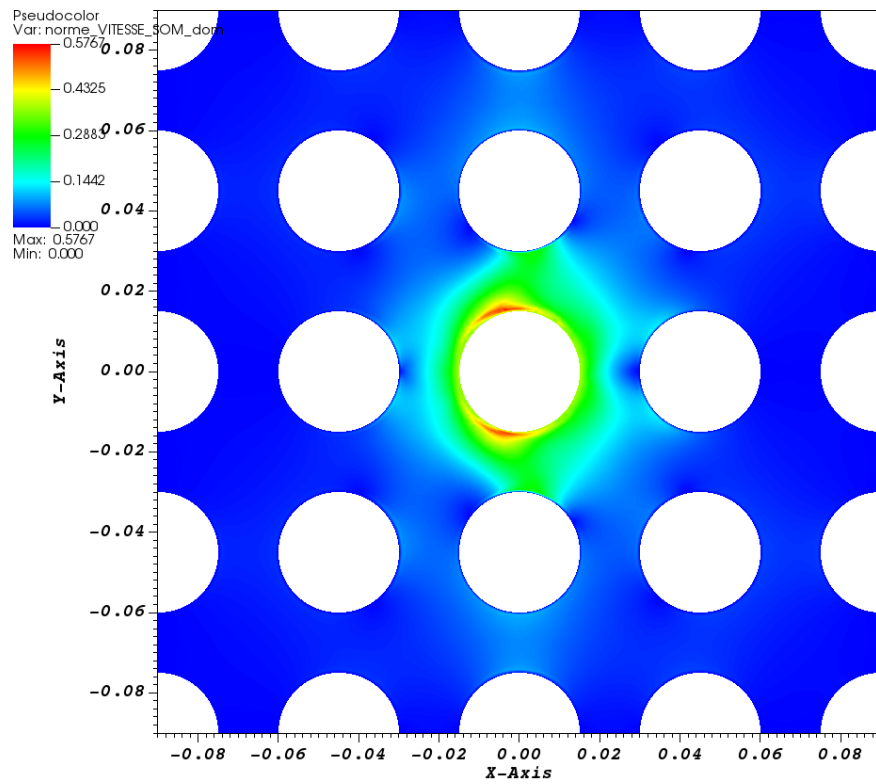


Figure VIII.3.7: TrioCFD Mesh\_1 VITESSE\_magnitude SOM

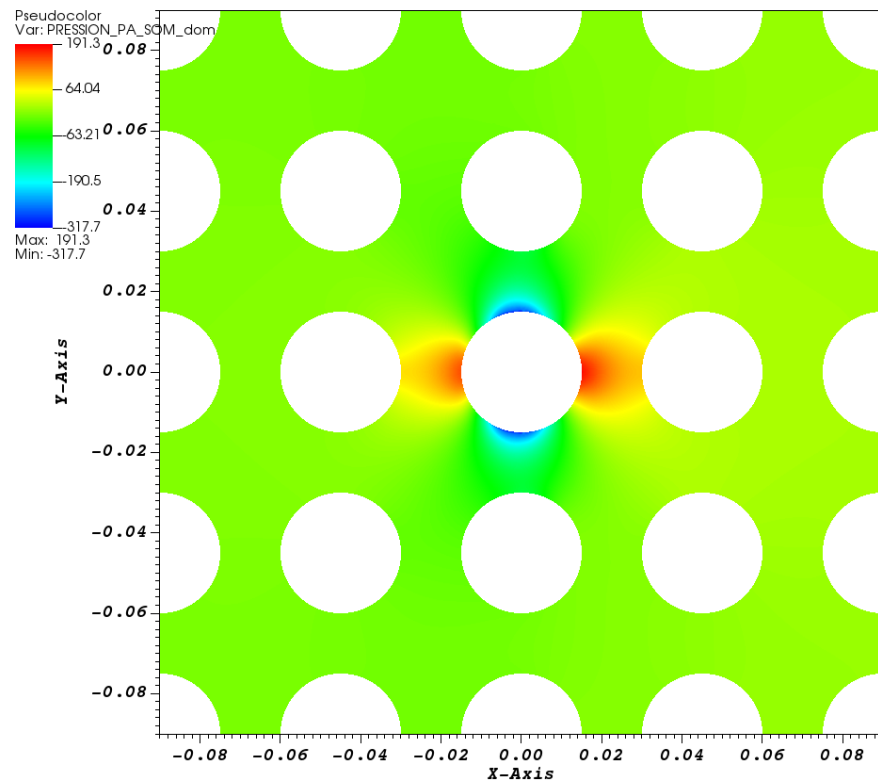


Figure VIII.3.8: TrioCFD Mesh\_2 PRESSION SOM

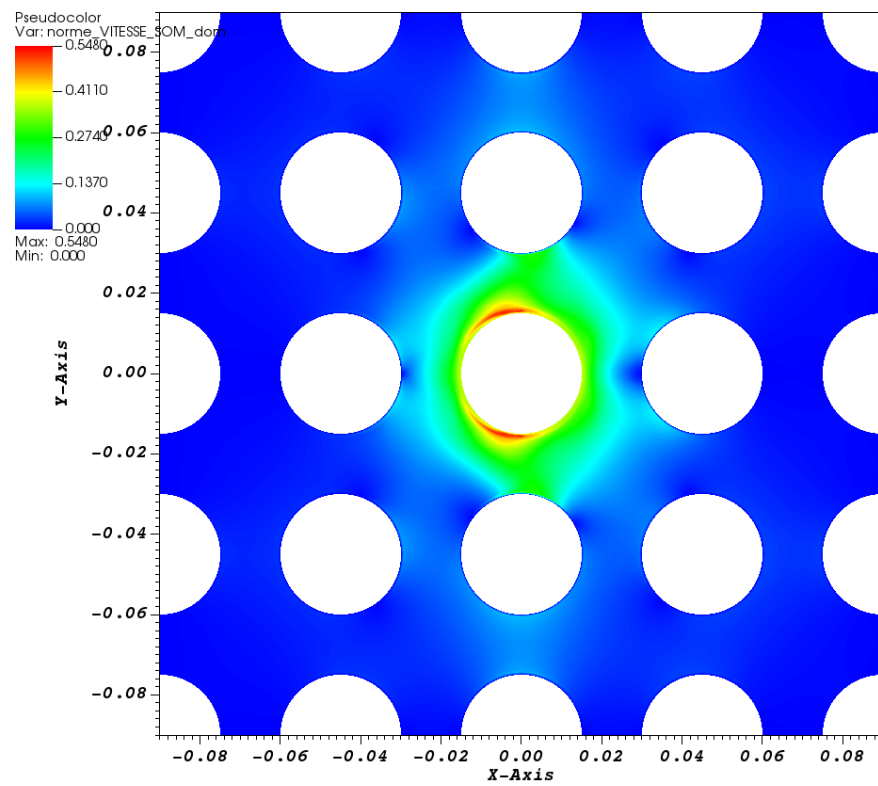


Figure VIII.3.9: TrioCFD Mesh\_2 VITESSE\_magnitude SOM

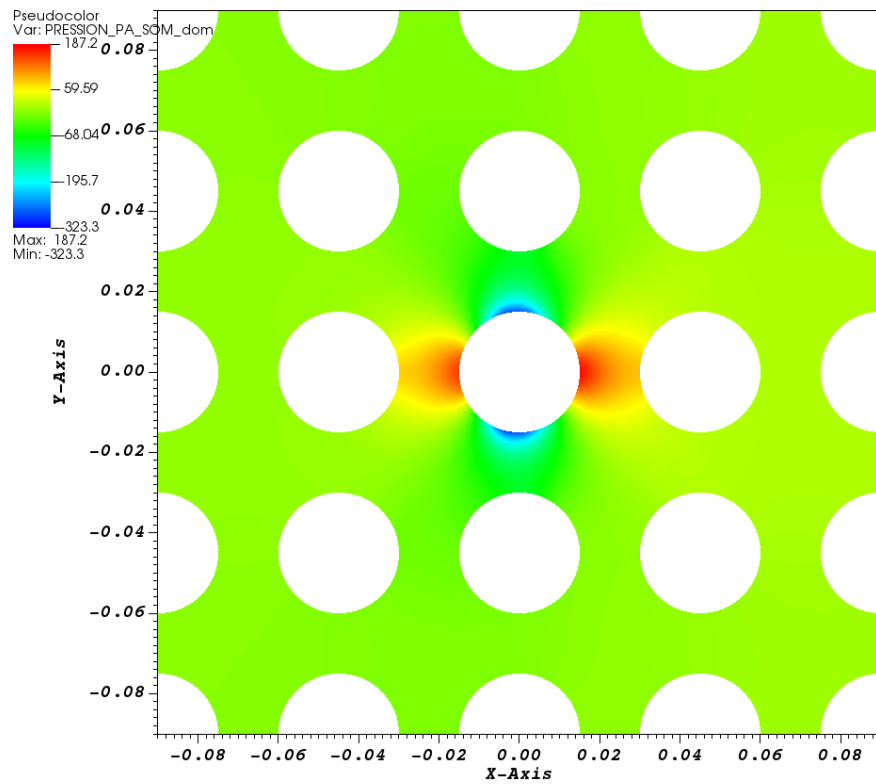


Figure VIII.3.10: TrioCFD Mesh\_3 PRESSION SOM

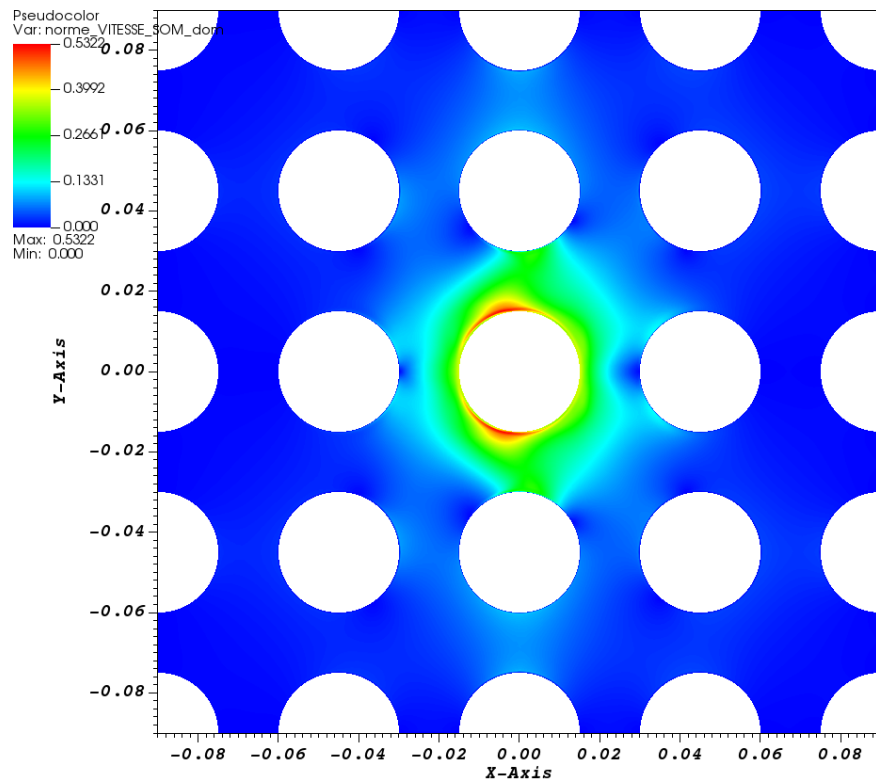


Figure VIII.3.11: TrioCFD Mesh\_3 VITESSE\_magnitude SOM

### 3.5 Conclusion

The harmonic motion of a cylinder in a quiescent viscous fluid, surrounded by a set of cylinders arranged in a square configuration, has been numerically simulated. A FEV method is applied to solve such a problem in conjunction with the ALE scheme. The numerical results for the fluid force and the added coefficients of the center cylinder are in good agreement with the experimental results. As theoretically expected, moreover, the coefficients along the y-axis are zero and the coefficients along x are symmetrical for the North-South and East-West cylinders respectively. This further shows the robustness of our numerical results.

### 3.6 References

- 1. Chen, S S. Flow-induced vibration of circular cylindrical structures, 1987.
- 2. CFD numerical simulation of a single-phase flow around a vibrating cylindrical tube, D. Panunzio, DES/ISAS/DM2S/SEMT/DYN/RS/2020-67015/A

### 3.7 Data Files

#### DIVA

```
# Hydraulique 2D laminar with ALE : DIVA configuration #
# Set of circular cylinders , arranged in a square configuration . The central cylinders moves w#
#
# Moving domain #
# SEQUENTIAL CALCULATION #
dimension 2
Pb_hydraulique_ALE pb
Domaine_ALE dom
# BEGIN MESH #
Lire_MED { domain dom file MeshDIVA_1.med }
# END MESH #
VerifierCoin dom { }
# BEGIN PARTITION
Partition dom
{
    Partition_tool metis { Nb_parts 2 }
    Larg_joint 2
    zones_name dom
}
End
END PARTITION #
# BEGIN SCATTER #
# Scatter DOM. Zones dom #
# END SCATTER #
# For the Arbitrary Lagrangian-Eulerian framework: block to indicate the number of mobile
boundaries of the domain and specify the speed that must be imposed on them #
Imposer_vit_bords_ALE dom
{
    1 # number of mobile boundaries #
    Cylindre_Centre Champ_front_ALE 2 0.003*125.66*cos(125.66*t) 0.0 # name and speed of the boro
}
# Solver used to solve the system giving the moving mesh velocity #
Solver_moving_mesh_ALE dom { PETSC GCP { precond ssor { omega 1.5 } seuil 1e-9 impr } }
# I select a discretization #
VEFPreP1B ma_discretisation
# Lire ma_discretisation { P0 P1 Changement_de_base_P1Bulle 1 Cl_pression_sommet_faible 1 } #
# Time scheme, choice between: Euler explicit or implicit , and Adams Bashforth order 2
or order 3 #
Scheme_euler_implicit mon_schema
```

```

Read mon_schema
{
  # Time step #
    # Initial time [s] #
      tinit 0.
  # Min time step #
    dt_min 1.e-15
  # Output criteria #
    # .out files printing period #
    dt_impr 5.e-6
  # tcpumax 47.5 #
  # .sauv files printing period #
    dt_sauv 100.
  # facsec such as dt = facsec * min(dt(CFL),dt_max) ; for explicit scheme facsec <= 1. By defa
  facsec 1
    facsec_max 1
  solveur implicite_ALE
  {
    solveur gmres { diag seuil 1.e-12 nb_it_max 3 }
  }
  # Stop if one of the following criteria is checked: #
    # End time [s] #
  tmax 0.25
  # Max number of time steps #
    # nb_pas_dt_max 5 #
    # Convergence threshold (see .dt_ev file) #
  seuil_statio 1.e-15
}
# I define a medium #
# Gravity vector definition
Uniform_field my_gravity
Read my_gravity 2 0.0 0.0 #
# Association between the different objects #
Associate pb dom
Associate pb mon_schema
Discretize pb ma_discretisation
Read pb
{
  fluide_incompressible {
    mu Champ_Uniforme 1 1.007e-3
    rho Champ_Uniforme 1 1000
  }
  Navier_Stokes_standard_ALE
  {
    # Pressure matrix solved with #
    solveur_pression PETSC_GCP { precond ssor { omega 1.5 } seuil 1e-9 impr }
    # Two operators are defined #
    convection { ALE { muscl } } # A convective scheme for ALE framework. Choice between: amo
    diffusion { }
    # Uniform initial condition for velocity #
    initial_conditions {
      vitesse Champ_Uniforme 2 0. 0.
    }
  }
  # Boundary conditions #
  boundary_conditions {
    Cylindre_Centre_frontiere_ouverte_vitesse_imposee Champ_front_ALE 2 0.003*125.66*cos(125.
    Cylindre_Nord paroi_fixe
    Cylindre_Sud paroi_fixe
    Cylindre_Est paroi_fixe
    Cylindre_Ouest paroi_fixe
    Paroi_Cylindre paroi_fixe
  }
}

```

```
Paroi_Gauche paroi_fixe
Paroi_Droite paroi_fixe
Periodique_Haut paroi_fixe
Periodique_Bas paroi_fixe
}
}
Post_processing
{
    # Fields #
format lata
fields dt_post 0.025
{
    pression_pa som
    vitesse som
        # vorticite som #
        ALEMeshVelocity som
    # ALEMeshTotalDisplacement som #
}
}
# The problem is solved with #
Solve pb
# Not necessary keyword to finish #
End
```

## IX. Conclusion

THIS document is the first version of a **TrioCFD** validation report resulting of an analysis and a sorting work that have been done on its database. First, an important inventory job was carried out in order to sort the test cases for targeting quickly the use of **TrioCFD** in different CFD configurations. The inventory resulted in a single table with plenty information (LibreOffice format), where the test cases are classified into several subdomains of fluid flows. In this document, some of them have been selected and detailed because 1) they are well-known in the literature, 2) they present comparisons with other academic or commercial CFD codes, 3) they present comparisons with experimental data and 4) they cover an important and representative part of the physics of the code. In this report, the test cases are representative of five subdomains: “Laminar flow” (Part III), “Thermal laminar flow” (Part IV), “Turbulent flow” (Part V), “Thermal turbulent flow” (Part VI), “Front Tracking” (Part VII) and “Fluid/structure interactions with ALE” (Part VIII). The first four parts gather the test cases for single phase flows, coupled or not with turbulence models and thermal effects. Part VII is dedicated to two-phase flows with interface tracking and the last part (VIII) that has been added since the last version of this report focuses on fluid/structure interactions with Arbitrary Lagrangian-Eulerian Method (ALE). The corresponding datafiles were run with the 1.8.3 version of **TrioCFD** to check the achievement of computations. Meanwhile, an important work was carried out to update a new PRM template in order to standardize all validation sheets. For each one of them, let us remind that the PDF file is generated by running a bash script (command `Run_fiche-not_run`) which acts on a PRM file (previously, test cases must have been run). A PRM file is a set of specific instructions for interfacing the L<sup>A</sup>T<sub>E</sub>X commands with the **TrioCFD** results post-processed with **Gnuplot** or **Visit**. Its content can be freely chosen by authors which has the consequence that the number and titles of sections differ from one sheet to another one. The goal of the new PRM template is to harmonize their contents for a more homogeneous rendering of this report. The seven sections of the new PRM template detail the main stages of CFD modeling and describe the comparisons. All validation sheets in this report have been revised and enhanced by taking into account this new PRM template.

### Perspective

Numerous other validation sheets already exist in the **TrioCFD** database and the job must be pursued. Hence, this document does not present an exhaustive list of what **TrioCFD** can do for CFD applications. It can be viewed as a simple “snapshot” that will be gradually improved and increased at each version release. The improvement will be simplified by the methodology and the tools which have been developed for PRM files. After checking and updating the validations sheets, they will be added in the future versions of this report. Among the available test cases, the sort will be pursued to separate those currently “in progress” and the others that lack quantitative comparisons. Multiple variations of the same test case appear in the database (e.g. “Poiseuille flow”). Some of them are simply a 3D extension of the same test case, or an extension with temperature equation or turbulence model. For instance, the laminar test case of “flow with a cylinder” (Chapter III.3) exists in turbulent version in two and three dimensions. Another example is given by the test case named “Backward facing step” which appears in four different versions: the first one is “two-dimensional”, the second one is “implicit”, the third one is “three-dimensional” and the last one is “heated in two dimensions”. More test cases of turbulent flow are also available, such as “Baglietto” and “Flow in curved pipe”. An effort will be done to extend the number of CFD subdomains such as “Quasi-compressible flow”, “Flow in porous media” and “fluid-structure interaction”. Finally several tests are dedicated to the “grid convergence” or “Miscellaneous test” of numerical options.

## Annexe A: List of TrioCFD PRM files

PDF File name	Problem	Dis.	Dim.	Mesh	Nb jdds	Goal of the sheet	State
<b>Laminar Flow</b>							
Channel_lam_pressure_drop	Pb_hydraulique	VDF VEF	3	160 hexa 1920 tetra	21	Convection schemes - Periodic BC fluid : helium	old format
Cir_Cyl_Re100	Pb_hydraulique	VEF	2	9668 triang.	2	Explicit Euler with implicit diffusion - literature comparison	new format report
ConvergenceTaylorGreen	Pb_hydraulique	VEF	2	4 $\Rightarrow$ 256 to 16384 triang.	20	Convergence for different meshes and convection scheme	old format
ConvergenceTaylorGreen WithDiffusion	Pb_hydraulique	VEF	2	3 $\Rightarrow$ 256 to 4096 triang.	54	Convergence for different meshes and time scheme	old format
DirectionalPressureLoss	Pb_hydraulique	VEF	3	3 $\Rightarrow$ 1152, 9216 and 73728 tetra	6	Validation of 64 bits integers possibility to configure	old format
FVCA_test_EF_stab	Pb_hydraulique	VEF	3	7 $\Rightarrow$ 27 to 1728 tetra	70	Convergence orders of the EF_stab convection schemes	old format
FVCAB_Cas_2.2_3D_steady _Stokes_Taylor_Green_vortex	Pb_hydraulique	VEF VDF	3	7 $\Rightarrow$ 215 to 61052 tetra 5 $\Rightarrow$ 8 to 32768 hexa	12	3D Taylor-Green vortex FVCAB experiments	old format
Lid_driven_cavity	Pb_hydraulique	VEF	2	105724 triang.	1	<b>Implicit Euler steady scheme</b> comparison with litterature	new format report
Poiseuilleperio2D	Pb_hydraulique	VEF	2	6 $\Rightarrow$ 6, 24, 96 384, 1536, 6144 triang.	18	Poiseuille comparisons: EF_stab versus Amont schemes	old format
PoiseuillePerio2DVEF _prismes	Pb_hydraulique	VEF	3	2785 triang.	2	EF_stab versus Amont schemes with an ICEM generated VEF mesh	old format
PoiseuillePerio2DVEF _fNcells	Pb_hydraulique	VEF	2	8 $\Rightarrow$ 6 to 98304 triang.	20	EF_stab versus Amont schemes with different mesh sizes	old format
PoiseuillePerio2DVEF _fNcells_prismes	Pb_hydraulique	VEF	2	2785 triang.	3	EF_stab versus Amont schemes with an ICEM generated VEF mesh	old format

PDF File name	Problem	Dis.	Dim.	Mesh	Nb jdds	Goal of the sheet	State
<b>Laminar Flow</b>							
PoiseuillePerio2DVEF _fNcells_trianfin	Pb_hydraulique	VEF	2	6 $\Rightarrow$ 6 to VEF	20	Convection schemes comparison mesh created using trianguler_fin	old format
Poiseuille_flow_2D _VDF_VEF	Pb_hydraulique	VDF	2	200 rect. VEF	5	Validation of the incompressible laminar module with analytical solution	new format report
PoiseuilleInOutVDFVEF	Pb_hydraulique	VDF	2	600 rect. VEF	10	Hydraulic with pressure drop	old format
PoiseuilleInOut2DVDFVEF _trianfin	Pb_hydraulique	VDF	2	600 rect. VEF	10	Hydraulic with pressure drop mesh created using trianguler_fin	old format
PoiseuilleInOut2DVDFVEF _prismes	Pb_hydraulique	VDF	2	600 rect. VEF	10	Hydraulic with pressure drop ICEM generated VEF mesh	old format
poiseuille_3D	Pb_hydraulique	VEF	3	17360 tetra.	5	Hydraulic with pressure drop comparison of 2 convection schemes	old format
PoiseuillePerio3DVDFVEF _fRe	Pb_hydraulique	VDF	3	160 hexa. VEF	28	Validation of convection and time schemes Tetraedrisation for VEF discretization	old format
PoiseuillePerio3DVDFVEF _fRe_tetrafin	Pb_hydraulique	VDF	3	160 hexa. VEF	28	VEF mesh is created using tetraedriser _homogene_fin - improved results	old format
PoiseuillePerio3DVDFVEF _fRe_prismes	Pb_hydraulique	VDF	3	160 hexa. VEF	28	Same as previous with VEF mesh generated with ICEM	old format
Poiseuille_Pipe_Velocity	Pb_hydraulique	VEF	3	126560 tetra	4	Validation of different convection schemes	old format
Diagonale_Cube	<b>Pb_hydraulique</b> <b>_concentration</b>	VEF	3	192000 tetra.	5	Convection schemes recommandations for 3D scalar passive transport	old format
test_div_grad_Prep1b	Pb_hydraulique	VEF	2	1324 tri	5	Laminar flow through a plane channel coding verification	old format
Mixing_Bidim_Axi	<b>Pb_hydraulique</b> <b>_concentration</b>	VDF	2	5 $\Rightarrow$ 5784 to Axi	5	Comparison of the dispersion coefficient with experimental for different meshes	old format

PDF File name	Problem	Dis.	Dim.	Mesh	Nb jdds	Goal of the sheet	State
<b>Laminar Flow</b>							
Turbulence _synthetique	Pb _hydraulique	VDF VEF	3 2	1024 to 65536 hexa 6144 to 16777216 hexa 7 $\Rightarrow$ 16 to 65536 rect 7 $\Rightarrow$ 16 to 65536 quad 6 $\Rightarrow$ 40 to 104420 tri	15 8 40	Generation of isotropic synthetic fluctuations as inlet boundary condition Verification of vorticity and Stream function in a square cavity	new format old format
Vorticite _et _fonction _de _Courant	Pb _hydraulique <b>Pb _conduction</b>	VDF VEF	2	999 tri	1	<b>Implicit_Euler_steady_scheme</b> Numerical Test	old format
2D_VEF_Cylindre _steady	Pb _hydraulique	VEF	2	104420 tri.	8	<b>Implicit_Euler_steady_scheme</b> Numerical: comparison with analytical	old format
Navier_Stokes_2d _steady	Pb _hydraulique	VEF	3	61052 tetra	3	<b>Implicit_Euler_steady_scheme</b> Numerical: comparison with analytical	old format
NoFlow	Pb _hydraulique	VEF <b>P0 RT</b>	2	3 $\Rightarrow$ 242, 1054 & 4262 tri.	24	<b>Validation of the <math>P_0 - RT</math> scheme</b> in case of a $\vec{u} = 0$	old format
StatVortex2D	Pb _hydraulique	VEF <b>P0 RT</b>	2	3 $\Rightarrow$ 242, 1054 & 4262 tri.	24	<b>Validation of the <math>P_0 - RT</math> scheme</b> for a steady state 2D vortex	old format
StatVortex	Pb _hydraulique	VEF <b>P0 RT</b>	3	4 $\Rightarrow$ 215 to 7711 tetra	40	<b>Validation of the <math>P_0 - RT</math> scheme</b> for a steady state 3D vortex	old format
RotFlow	Pb _hydraulique	VEF <b>P0 RT</b>	2	3 $\Rightarrow$ 242, 1054 & 4262 tri.	24	<b>Validation of the <math>P_0 - RT</math> scheme</b> for a rotational velocity	old format

PDF File name	Problem	Dis.	Dim.	Mesh	Nb jdds	Goal of the sheet	State
<b>Thermal Laminar Flow</b>							
Convection_Rotating _Table	Pb_thermohydraulique	VEF	2	6130 tri	28	Laminar advection of temperature fields on a circular rotating table	old format
Convection_Vahl_Davis	Pb_thermohydraulique	VDF	2	4761 rect	10	Validation of the coupling between flow and thermics in laminar condition	new format
		VEF		1444 & 6084 tri			
Oscillating_Flow	Pb_thermohydraulique	VDF	2	2500 rect	5	Natural convection inside a rectangular heated cavity	new format
		VEF		5040 tri			report
Pb_couple_2D	Pb_thermohydraulique	VDF	2	36 rect	2	Laminar heat exchange through a plane channel with wall conduction	old format
	<b>Pb_conduction</b>	VEF		64 tri			
PorousWithPLoss _VEF	Pb_thermohydraulique	VEF	2	84 tri	4	Laminar flow in a channel with porous media and pressure loss	old format
		VEF	3	486 tetra			
VAHL_DAVIS_impl	Pb_thermohydraulique	VDF	2	10000 rect	22	Comparison of velocity and temperature profiles using explicit or implicit algo	old format
		VEF		6400 tri			
therm_stratif _water_tank	Pb_thermohydraulique	VDF	2	39402 rect	2	Vertical flat heated plate	
		VDF	3	86246 hexa	2	immersed in pool of water	old format
		VEF	2	18816 tri	2	open to atmosphere	
		VEF	3	86400 tetra	2		
ThHyd_3D_VEF _steady	Pb_thermohydraulique	VEF	3	1270 tetra	1	<b>Implicit_Euler _steady_scheme</b>	old format
<b>Numerical Test</b>							
Radiation		VDF	2	20+25 and 100 rect		Coupling between radiation,	
	Pb_Thermohydraulique	VEF	2	80+40 and 1600 tri		Conduction and natural convection	
	<b>Pb_conduction</b>	VDF	3	100+125 and 125 hexa	10	inside a 2D or 3D channel	old format
	<b>Pb_Couple_Rayonnement</b>	VEF	3	1958+1220 to 5884 tetra		<b>Radiation in transparent medium</b>	
		VDF	Axi	100 rect		<b>Pb_Couple_Rayonnement</b>	

PDF File name	Problem	Dis.	Dim.	Mesh	Nb jdds	Goal of the sheet	State
<b>Turbulent Flow</b>							
Backward_Facing_StepImpl	Pb_hydraulique_Turbulent	VEF	2	2944 tri	11	Turbulent channel air flow with backward step - $\kappa - \epsilon + \text{loi}$ standard hydr	old format
Backward_Facing_Step3D	Pb_hydraulique_Turbulent	VDF VEF	3	28620 rect 366230 tri	2	Turbulent channel air flow with backward step - $\kappa - \epsilon + \text{loi}$ standard hydr	old format
Backward_Facing_Step	Pb_hydraulique_Turbulent	VDF VEF	2	3228 rect 2944 tri	6	$\kappa - \epsilon + \text{loi}$ standard hydr or $\text{loi}$ expert hydr	old format
ChannelPerio2D_VEF_fNy	Pb_hydraulique_Turbulent	VEF	3	4 $\Rightarrow$ 80 $\rightarrow$ 640 tri	8	Longueur_Melange + $\text{loi}$ standard hydr	old format
Turbulent_perio_2D_channel	Pb_hydraulique_Turbulent	VEF	2	6 $\Rightarrow$ 6 $\rightarrow$ 6144 tri	24	Comparison of convection schemes - Longueur_Melange+ $\text{loi}$ standard hydr	old format
ChannelML3DVDF_fNydxdz	Pb_hydraulique_Turbulent	VDF	3	3 $\Rightarrow$ 684 to 10516 hexa	19	Longueur_Melange + $\text{loi}$ standard hydr	old format
ChannelML3DVEF_fNydxz	Pb_hydraulique_Turbulent	VEF	3	960 & 3840 tetra 2348 $\rightarrow$ 47405 tetra	24	Longueur_Melange + $\text{loi}$ expert hydr	old format
ChannelMLPerio3D_VEF_fRe	Pb_hydraulique_Turbulent	VEF	3	480 tetra	12	Turbulent helium flow through a periodic plane channel	old format
ChannelMLPerio3D_VEF_fRe_tetrafin	Pb_hydraulique_Turbulent	VEF	3	3840 tetra	12	Same than previous with mesh refinement - better results for high Re	old format

PDF File name	Problem	Dis.	Dim.	Mesh	Nb jdds	Goal of the sheet	State
<b>Turbulent Flow</b>							
KEps_Meshing _VEF	Pb_hydraulique_Turbulent	VEF	3	960 & 3840 tetra 11735 → 16551 tetra	23	Meshing tests for 3D VEF-plane channel with $\kappa - \epsilon$ model	old format
ChannelkepsPerio 3DVEF_fRe	Pb_hydraulique_Turbulent	VEF	3	480 tetra	12	Pressure drop in a 3D periodic turbulent flow in a plane channel	old format
ChannelkepsPerio 3DVEF_fRe_tetrafin	Pb_hydraulique_Turbulent	VEF	3	3840 tetra	12	Same than previous with mesh refinement - $\kappa - \epsilon + \text{loi\_expert\_hydr}$	old format
Channelkeps 3DVDF_fNydxdz	Pb_hydraulique_Turbulent	VDF	3	3 ⇒ 684, 2332 & 10516 hexa	18	Meshing tests for 3D VDF plane channel with $\kappa - \epsilon$ model	old format
Channelkeps 3DVEF_fNydxdz	Pb_hydraulique_Turbulent	VEF	3	960 & 3840 tetra 5 ⇒ 2348 → 47405	24	Meshing tests for 3D VEF plane channel with $\kappa - \epsilon$ model	old format
ChannelKEps_CLboite Perio_entree	Pb_hydraulique_Turbulent	VEF	3	13552 tetra	1	Periodic box on a turbulent flow in a plane channel with $\kappa - \epsilon$ model	old format
k_eps_vef _perio	Pb_hydraulique_Turbulent	VEF	3	1152 tetra	1	Verification of friction velocity in a periodic plane channel with $\kappa - \epsilon$ model	old format
Canal_plan_VDF_VEF _k_eps_standard _bicephale	Pb_hydraulique_Turbulent	VDF	2	276 rect	2	Comparaison of the coupled and decoupled methods for solving	new format
		VEF	2	172 tri	2	the $\kappa - \epsilon$ transport equations	
		VDF	3	828 hexa	2		
		VEF	3	1982 tetra	2	k_epsilon_bicephale	

PDF File name	Problem	Dis.	Dim.	Mesh	Nb jdds	Goal of the sheet	State
<b>Turbulent Flow</b>							
expansion_2D_axi_3D _VEF_circular	Pb_hydraulique_Turbulent	VDF VEF	Axi 3	5577 rect 65923 tetra	5 5	Expanding turbulent flow with various inlet velocities	old format
expansion_3D _VDF_VEF	Pb_hydraulique_Turbulent	VDF VEF	3	48400 hexa 51840 tetra	5 5	Same than previous in 3D with VDF and VEF mesh	old format
Mixing_length _VEF_WF	Pb_hydraulique_Turbulent	VEF VEF	2 3	7 $\Rightarrow$ 80 to 7680 tetra	14	Mixing length in 2D and 3D VEF-plane channel	new format report
OBI_diffuser_VEF _k_eps	Pb_hydraulique_Turbulent	VEF	2	36644 tetra	2	Turbulent flow in a 2D diffuser with the $\kappa - \epsilon$ model	new format report
Tube_turb_perio _EF_stab	Pb_hydraulique_Turbulent	VEF	3	78576 tetra	1	Fully developed turbulent flow in circular tube	old format
Tube_turb_perio _muscl	Pb_hydraulique_Turbulent	VEF	3	78576 tetra	1	Same than previous with muscl scheme better prediction of turbulent viscosity	old format
EsthairNoWire	Pb_hydraulique_Turbulent	VEF	3	3 $\Rightarrow$ 3114 to 11829 tetra	5	Esthair calculations of a 19 rods sub-assembly without space wire	old format
ContractionTurbFlow _3D_VEF	Pb_hydraulique_Turbulent	VEF	3	684 & 1260 29011 & 107842	6	Pressure loss through a sudden contraction	old format
Cube_Atmo	Pb_hydraulique_Turbulent	VEF	3	2 $\Rightarrow$ 42964 and 55183 hexa	4	Atmospheric flow around a cube	old format
Couche_Limite _Atmospherique	Pb_hydraulique_Turbulent	VEF	3	27727 tetra	3	Simulation of the atmospheric boundary layer - Source_Transport_K_Eps	old format
Loi_paroi_3D_VEF	Pb_hydraulique_Turbulent	VEF	3	9 $\Rightarrow$ 288 to 9216 tetra	24	Validate behaviour of VEF/Nicholson/ $\lambda u'$ approach - Source_Qdm_lambdaup	old format
Watlon_k_eps	Pb_hydraulique_Turbulent	VEF	3	661632 tetra	6	Watlon experiment: fluid mixing in T-pipe with long cycle fluctuations	old format skip
Flow_in_curved_pipe	skip Pb_Hydraulique_Turbulent	VEF	3	463259 tetra	2	Swirling turbulent flow through a curved pipe	old format skip

PDF File name	Problem	Dis.	Dim.	Mesh	Nb jdds	Goal of the sheet	State
<b>Turbulent Flow</b>							
Fiche_validation_Re590	Pb_hydraulique_Turbulent	VDF VEF	3	62370 hexa 61440 tetra	4	New wall law treatment for the LES of turbulent heat transfer in a periodic channel	old format
CHANNEL_LES_VEF _RE_TAU_1110	Pb_hydraulique_Turbulent	VEF	3	65856 tetra	4	Channel LES VEF $Re_\tau = 1110$ with EF_STAB scheme	old format
les THI_qdm_ReInf_VEF	Pb_hydraulique_Turbulent	VDF VEF	3	195112 hexa 196608 tetra	12	LES: Isotropic homogeneous turbulence in a periodic cube	old format exclu_nr
Channel_VEFLES_Hyd _WF_Pressure_drop	Pb_hydraulique_Turbulent	VEF	3	4800 tetra	12	Pressure drop in a 3D periodic turbulent flow in a plane channel	old format
Loi_paroi2D_VEF	Pb_hydraulique_Turbulent	VEF	2	5 $\Rightarrow$ 80 to 1280 tetra	24	Validation of a Crank-Nicholson time scheme - stabilization with a source term $\lambda u'$	old format
Baglietto	Pb_hydraulique_Turbulent	VEF	2	162 tri	6	Study of non-linear Baglietto $\kappa - \epsilon$ model for low Reynolds number	old format
Low_Reynolds	Pb_hydraulique_Turbulent	VDF VEF	3	1192 hexa mesh	7	Validation of Launder-Sharma, Jones-Launder and Lam-Bremhorst for low Reynolds	old format
Verification_k_epsilon _transport_equation	Pb_hydraulique_Turbulent	VDF VEF	3	$10^6$ hexa $7.5 \cdot 10^5$ tetra	4	Check the post-processing of the convective, diffusive and source terms of the $k - \epsilon$ model	new format
decroissance_keps	Pb_hydraulique_Turbulent	VDF	2	1 rect	2	Decreasing turbulence in a plane channel - Coding verification	old format
Marche_incline	Pb_hydraulique_Turbulent	VEF	2	200 tria	3	Turbulent channel flow with backward step - Coding verification	old format
Test_ghost_visit	Pb_hydraulique_Turbulent	VDF	3	300 rect	1	Test of visualisation mors specially with ghost - Coding verification	old format
2D_Cyl_Re20000	Pb_hydraulique_Turbulent	VEF	2	3 $\Rightarrow$ 9034 to 32032 tetra	18	2D cylinder in turbulent oscillating cross water flow	old format skip
Drag	Pb_hydraulique_Turbulent	VEF	2	6 $\Rightarrow$ 920 to 1123 tri	24	Obstacles of different shapes in turbulent air flow	old format
3D_Cyl_Re20000	Pb_hydraulique_Turbulent	VEF	3	458802 tetra	6	3D cylinder in turbulent oscillating cross water flow	old format skip

PDF File name	Problem	Dis.	Dim.	Mesh	Nb jdds	Goal of the sheet	State
<b>Turbulent Flow</b>							
Turbulent_Simple_water_jet	Pb_hydraulique_Concentration_Turbulent	VEF	3	72692 tetra	4	Turbulent water jet with concentration in a box	old format
Turbulent_Simple_water_jet_refined	Pb_hydraulique_Concentration_Turbulent	VEF	3	283772 tetra	8	Turbulent simple water jet with refined mesh	old format skip
Marche_SKE_steady	Pb_hydraulique_Turbulent	VEF	2	45489 tri	1	Steady 2D Turbulent $k - \epsilon$ : Marche_SKE Implicit_Euler_steady_scheme	old format
Diffuseur_SKE_steady	Pb_hydraulique_Turbulent	VEF	2	47940 tri	1	Steady 2D Turbulent $k - \epsilon$ : Diffuseur_SKE Implicit_Euler_steady_scheme	old format
Verification_CEG	Pb_hydraulique_Turbulent	VEF	3	3 $\Rightarrow$ 3465 to 15628 tetra	3	Vortices detection and calculation of gas entrainment criterias - CEG	old format

PDF File name	Problem	Dis.	Dim.	Mesh	Nb jdds	Goal of the sheet	State
<b>Thermal Turbulent Flow</b>							
Channel_T1_T2 _incompressible	Pb_thermohydraulique _turbulent	VEF	3	5 ⇒ 1536 to 5184 tetra	5	$\kappa - \epsilon + \text{loi\_standard\_hydr}$ Prandtl + loi_standard_hydr_scalaire	new format report
Channel_ML_Thydr _TBLE_VEF_ReT7200	Pb_thermohydraulique _turbulent	VEF	3	2880 tetra + 4 TBLE 1D mesh	7	Turbulent heat exchange through a periodic plane channel	old format
Conv_Heated_pipe _wall_temp	Pb_thermohydraulique _turbulent	VEF	3	5 ⇒ 576 to 3308 tetra	14	Forced convection with imposed wall heat flux	old format
Conv_Pipe_Perio _Expl	Pb_thermohydraulique _turbulent	VEF	3	2160 tetra	3	Forced convection with EF_stab scheme in explicit time scheme	old format
Conv_Pipe_Perio _Impl	Pb_thermohydraulique _turbulent	VEF	3	2160 tetra	3	Forced convection with EF_stab scheme in implicit time scheme	old format
Conv_Pipe_InOut	Pb_thermohydraulique _turbulent	VEF	3	97200 tetra	3	Forced convection with EF_stab scheme Inlet/Outlet BC	old format
Heated_floor _k_eps	Pb_thermohydraulique _turbulent	VDF VEF	2	7784 rect 11385 tri	3	Turbulent flow above a heated floor: $k - \epsilon$ modeling	old format
Heated_Backward _Facing_Step_2D	Pb_thermohydraulique _turbulent	VDF VEF	2	4134 rect 10855 tri	3	Turbulent flow above a heated backward facing step: $k - \epsilon$ modeling	old format

PDF File name	Problem	Dis.	Dim.	Mesh	Nb jdds	Goal of the sheet	State
<b>Thermal Turbulent Flow</b>							
Jet_impingement_on_a_hot_flat_plate	Pb_thermohydraulique turbulent	VEF	3	116356 tetra	3	Turbulent heated air jet impacting an isothermal plane wall	old format
Thermal_stratification_flow	Pb_thermohydraulique turbulent	VEF	2	2968 tri	4	Thermal stratification in a cooled plenum	new format report
Two_Layers_Stratif	Pb_thermohydraulique turbulent	VDF	2	7000 rect	6	Turbulent mixing layers at different velocities and temperatures	old format
Two_Layers_Stratif_impl	Pb_thermohydraulique turbulent	VEF	2	7200 tetra	20	Same as previous with implicite time scheme - with different algorithms	old format
Turb_coupled_pipeFlow	Pb_thermohydraulique turbulent	VEF	3	Fluid: 3304 tetra Solid: 2543 tetra	15	Turbulent heat exchange through a periodic circular pipe coupled with wall conduction	old format
<b>Pb_conduction</b>							
PeriodicBox	Pb_thermohydraulique turbulent	VEF	3	463259 tetra	4	Flow in a curved pipe with RANS and LES model Re=50000	old format
wl_vef_laminar	Pb_thermohydraulique turbulent	VEF	3	2400 tetra	4	Wall law validation for VEF discretization	old format
wl_vef_analytic	Pb_thermohydraulique turbulent	VEF	3	3 $\Rightarrow$ 1200 to 28800 tetra	6	Same than previous with comparison between with and whitout wall laws	old format
wl_vef_correlation	Pb_thermohydraulique turbulent	VEF	3	2400 tetra	5	Same than previous with $k - \epsilon + \text{loi\_standard\_hydr}$	old format
wl_vef_coupling	Pb_thermohydraulique turbulent	VEF	3	2400 hexa + 2400 in wall	4	Turbulent heat exchange through a periodic plane channel coupled with wall conduction	old format
<b>Pb_conduction</b>							
Uniform_keps_front_field_from_ud	Pb_thermohydraulique turbulent	VDF	2	781 rect			
		VEF	2	3124 tri	8	Check Champ_front_normal fields	old format
		VDF	3	700 hexa		Coding verification	excl_nr
		VEF	3	16800 tetra			
Boussinesq_VEF	Pb_thermohydraulique turbulent	VEF	3	34992 tetra	8	Check Boussinesq source term in VEF for LES - Schema_Predictor_Corrector	old format

PDF File name	Problem	Dis.	Dim.	Mesh	Nb jdds	Goal of the sheet	State
<b>Thermal Turbulent Flow</b>							
Channel_LES_Re_tau405_Pr071_T0Q	Pb_thermohydraulique turbulent	VDF	3	8192 hexa 24192 & 65856	3	Channel LES T0-Q $Re_\tau = 405$ with VEF - EF_STAB Scheme - logarithmic standard wall law	old format
les_Re395Pr0025_T0Q	Pb_thermohydraulique turbulent	VDF	3	8192 hexa 32928 & 67362	6	Turbulence (LES) and Heat transport (Heat Flux) in a channel flow $Re_\tau = 395$ - $Pr = 0.025$	old format
les_Re395Pr0025_ToQ_couple	Pb_thermohydraulique turbulent	VDF	3	8192 hexa 12960 tetra	4	Turbulence (LES) and Heat transport (coupling with solid walls - thermal activity ratio $K=0.28$ ) in a channel flow $Re_\tau = 395$ - $Pr = 0.025$	old format
les_Re395Pr071_T0Q	Pb_thermohydraulique turbulent	VDF	3	8192 hexa 22176 & 67362	5	Turbulence (LES) and Heat transport (Heat Flux) in a channel flow $Re_\tau = 395$ - $Pr = 0.71$	old format
les_Re180Pr071_T0Q	Pb_thermohydraulique turbulent	VDF	3	67392 hexa 134640 tetra	3	Turbulence (LES) and Heat transport (Heat Flux) in a channel flow $Re_\tau = 180$ - $Pr = 0.71$	old format
Fiche_validation_Re395_Pr0.71	Pb_thermohydraulique turbulent	VDF	3	18216 hexa 22176 tetra	4	New wall law treatment for the LES of turbulent heat transfer in a periodic channel $Re_\tau = 395$ and $Pr = 0.71$	old format
Fiche_validation_Re180_Pr0.025	Pb_thermohydraulique turbulent	VDF	3	1920 hexa 2880 tetra	4	New wall law treatment for the LES of turbulent heat transfer in a periodic channel $Re_\tau = 180$ and $Pr = 0.025$	old format
Fiche_validation_Re180_Pr0.71	Pb_thermohydraulique turbulent	VDF	3	1920 hexa 2880 tetra	4	New wall law treatment for the LES of turbulent heat transfer in a periodic channel $Re_\tau = 180$ and $Pr = 0.71$	old format
Comp_conv	Pb_thermohydraulique turbulent	VEF	2	628 tri 40320 tetra	26 24	Temperature convection as a passive scalar	old format
Test_tparoi	Pb_thermohydraulique turbulent	VEF	2	4 tri	3	Coding verification of the Tparoi post treatment	old format
Verification_flux_implicite	Pb_thermohydraulique turbulent	VEF	2	fluid : 16 solid : 16	28	Coding verification of the heat balance: compensation between the flow from solid to liquid and the flow from liquid to solid	old format
Poreux_VEF	Pb_thermohydraulique turbulent	VEF	2	2968 tri	6	Verification case of the flow in a porous channel	old format
Nusselt_Correlation_2D	Pb_thermohydraulique turbulent	VDF	2	10 rect 24 tri	2	1D flow using a Nusselt number correlation in a Forced convection regime	old format

PDF File name	Problem	Dis.	Dim.	Mesh	Nb jdds	Goal of the sheet	State
<b>Thermal Turbulent Flow</b>							
Nusselt_Correlation _Coupling_Pb	Pb_thermohydraulique _turbulent	VDF VEF	3	100 hexa 222 tetra	2 2	1D flow using a Nusselt number correlation, coupled to a conduction problem ; forced convection	old format
<b>Pb_conduction</b>							
EFstab_Muscl_and _Limiters_VEF	Pb_thermohydraulique _turbulent	VEF VEF	2 3	900 & 6130 tri 6000 tetra	20	Evaluation of EF_stab an Muscl convective schemes in simple VEF-configurations	old format
T_paroi	Pb_thermohydraulique _turbulent	VEF	2	144 tri	3	Wall temperature verification in VEF discretisation with Neumann conditions	old format
GR16_k_eps	Pb_thermohydraulique _turbulent	VEF	3	2851995 tetra	4	Validation of heat exchange in tube bundles without spacer wire on sodium heat exchangers	old format skip
ThermalCoupling_TurbulentFlow_VEF	Pb_thermohydraulique _turbulent	VEF VEF	3	864 + 432 (Trio) 1578 (ICEM)	2	Thermal coupling between a fluid and a solid domains for a turbulent flow	old format
<b>Pb_conduction</b>							
Couplage_Implicite _Instationnaire	Pb_thermohydraulique _turbulent	VEF	3	160 tetra	1	Coupled pipe flow with non stationnary conduction solved by an implicit scheme	old format
<b>Pb_conduction</b>							
Marche_k_eps_T _steady	Pb_thermohydraulique _turbulent	VEF	2	365 tri	1	Steady Themohydraulique 2D Turbulent K-Eps VEF Numerical test	old format
les THI_T _scalaire_VEF	Pb_thermohydraulique _turbulent	VEF	3	196608 tetra	2	Isotropic homogeneous turbulence in a periodic cube	old format exclu_nr

PDF File name	Problem	Dis.	Dim.	Mesh	Nb jdds	Goal of the sheet	State
<b>Two-phase Flows with Front-Tracking</b>							
Bullage_Huile_Creuset_Froid	Probleme_FT_Disc_gen	VEF	3	52920 hexa	2	Rapport on IBC with interfaces	old format
Chimie_FT	Probleme_FT_Disc_gen	VDF VEF	2	1 rect 4 tri	5	Test of chemical reactions in Front-Tracking <b>Chimie, reactions</b>	old format
ellipsoid_vdf_therm	Probleme_FT_Disc_gen	VDF	3	18000 hexa	2	Influence of thermal penalization in Front-Tracking in 3D molten glass bath reactor with stirrer + thermal	old format
ftd_gravite	Probleme_FT_Disc_gen	VEF	3	5239 tetra	1	Free fall of a drop	old format
FTD_hanging_drop	Probleme_FT_Disc_gen	VDF	3	67240 hexa	2	Drop hanging to a solid wall	new format report
FTD_hysteresis	Probleme_FT_Disc_gen	VDF	3	72000 hexa	38	Contact line treatment with contact angle hysteresis	old format
FTD_oscillating_bubble	Probleme_FT_Disc_gen	VDF	3	216000 hexa	2	Bubble in surrounding fluid with a free surface subject to oscillations	new format report
FTD_particles_coupling	Probleme_FT_Disc_gen	VDF VEF	3	20000 hexa 1600 or 20000 tet	7	Account for fluid effects on a particle in a column and for reaction effect and two way coupling	old format
FTD_particles_transfo	Probleme_FT_Disc_gen	VDF VEF	3	200096 hexa 72000 tetra	2	Transformation of gas bubbles into particles and vanishing of particles entering into the gas	old format
FTD_PhaseChange_1D	Probleme_FT_Disc_gen	VDF	3	720 hexa	4	Validation Test for the Interface Movement and the Diphasic Heating	old format
ftd_remaillage	Probleme_FT_Disc_gen	VDF VEF	3	1500 hexa 5239 tetra	4	Test of the volume and surface conservation during the remeshing	old format
ftd_remesh_bidim_axi	Probleme_FT_Disc_gen						old format

PDF File name	Problem	Dis.	Dim.	Mesh	Nb jdds	Goal of the sheet	State
<b>Two-phase Flows with Front-Tracking</b>							
FTD_solid_particle _fall_viscosity	Probleme_FT_Disc_gen	VDF	3	20000 hexa	3	Fall of a solid particle in viscous fluid followed by FTD	old format
FTD_TCL _boling_bubble	Probleme_FT_Disc_gen						old format
FTD_TCL_imposed _constant_growth	Probleme_FT_Disc_gen						old format
FTD_TCL _Qmicro	Probleme_FT_Disc_gen						old format
FTD_TCL_static _thermal_wedge	Probleme_FT_Disc_gen						old format
IBC_penalisation _poiseuille	Probleme_FT_Disc_gen	VDF	2	902 rect	2	Influence of penalization in Front-Tracking in 2D verification test	old format
ibc_refroidi	Probleme_FT_Disc_gen	VDF	2	2400 rect	2	Influence of thermal penalization in Front-Tracking	old format
iodure-iodate-melange	Probleme_FT_Disc_gen	VEF	2	4 tri	17	Checking for competing reactions	old format
iodure-iodate	Probleme_FT_Disc_gen	VEF	2	4 tri	7	Verification of competing reactions	old format
PB_FT	Probleme_FT_Disc_gen	VDF	2	7200, 8800 and 21600 rect	3	Influence of the mesh and its discontinuity on the behavior of a bubble - verification test	old format
pena_couette	Probleme_FT_Disc_gen	VDF	2	961 rect	2	Interpolation method test on a Taylor-Couette flow Fluid flow between two counter-rotating cylinders	old format
pena_ellipsoide	Probleme_FT_Disc_gen	VDF	3	2250 hexa	2	Influence of penalization in Front-Tracking in 3D Molten glass bath reactor with stirrer	old format
tubeY	Probleme_FT_Disc_gen	VDF VEF	2	1088 rect 1088 tri	2	Checking for competing reactions	old format

PDF File name	Problem	Dis.	Dim.	Mesh	Nb jdds	Goal of the sheet	State
Two-phase Flows with Front-Tracking IJK							
bulle_oscillante							old format
channel_swarm_fixed							old format
compaTrioCFD_and_CPU							old format
conservation_volume							old format
creeping_flow							old format
energie_bulle_seule							old format
follow_color							old format
interfacial_temperature_and_flux							old format
reprise_xyz_ijk							old format
repulsion							old format

PDF File name	Problem	Dis.	Dim.	Mesh	Nb jdds	Goal of the sheet	State
Two-phase Flows with Front-Tracking IJK							
schemas_temps							old format
shear_boundary_conditions							old format
stat_diph_gradUP							old format
stat_temperature							old format
taylor_green_vortices_3D							old format
temperature_bulle_conv							old format
temperature_canal_bulles_symetrique							old format
temperature_canal_poiseuille_source							old format
temperature_channel_swarm_fixed							old format
temperature_monop							old format

PDF File name	Problem	Dis.	Dim.	Mesh	Nb jdds	Goal of the sheet	State
Two-phase Flows with Front-Tracking IJK							
temperature_stat							old format
temperature_test_pb_reprise							old format
test_sigma							old format
tests_schemas_monophasique							old format

PDF File name	Problem	Dis.	Dim.	Mesh	Nb jdds	Goal of the sheet	State
<b>Two-phase Flows with CMFD</b>							
Verification_k_tau_ transport_equation	Pb_Multiphase	PolyMAC	3	8000	2	verification of velocity gradient and vorticity	Jupyter
Verification_wall_law	Pb_Multiphase	PolyMAC	3	18000	2	Coding verification of CMFD turbulent wall laws	Jupyter
canal_plan	Pb_Multiphase	PolyMAC	2	81 $\Rightarrow$ 5 to 7500	1	Verification of adaptive wall laws in a 2D plane channel	Jupyter
decroissance_ktau	Pb_Multiphase	PolyMAC	2	4 tetra	2	Verification of velocity gradient and vorticity coding	Jupyter
expansion_NO_MASS	Pb_HEM	PolyMAC	2	4999	1	Validation of the Homogeneous Equilibrium Model coupled with Stiffened Gaz on an expansion tube	new format
expansion_WITH_MASS	Pb_HEM	PolyMAC	2	4999	1	Validation of the Homogeneous Equilibrium Model with mass transfert on an expansion tube	new format skip_prm
shock_dodecane	Pb_HEM	PolyMAC	2	10000	1	Validation of the Homogeneous Equilibrium Model on a two-phase shock tube	new format

PDF File name	Problem	Dis.	Dim.	Mesh	Nb jdds	Goal of the sheet	State
<b>Fluid-structure interactions with ALE</b>							
3dOscillatingBeam	Pb_hydraulique_ALE VEF	3	1454267 tetra	1	3D oscillating cylindrical beam into a confined space		new format
DivaALE	Pb_hydraulique_ALE VEF	2	25806, 51146 & 102080 tri	3	Vibrations of a cylinder in a square tube bundle immersed in a viscous fluid		new format
RotationALE	Pb_hydraulique_ALE VEF	2	30000 tri	1	2D annulus with the inner wall turning with a constant angular velocity and outer wall fixed was chosen		new format
SquareObstacleALE	Pb_hydraulique_ALE VEF	2	51700 tri	3	Flow across a horizontally moving square in a tank		new format
TwoCylindersALE	Pb_hydraulique_ALE VEF	2	110466 tri	1	2D fluid annulus region confined between an inner wall moving with an harmonic motion and an outer wall fixed		new format
TwoOscillatingCylindersALE	Pb_hydraulique_ALE VEF	2	241618 tri	1	Hydrodynamic interaction of two cylinders subjected to small oscillations		new format

PDF File name	Problem	Dis.	Dim.	Mesh	Nb jdds	Goal of the sheet	State
<b>Dilatable Fluids</b>							
Channel_T1_T2_QC	Pb_Thermohydraulique _Turbulent_QC	VEF	3	2214 tetra with 3 stretching	3	Quasi-compressible turbulent heat exchange through a plane channel	old format
ConvectionJuarez	Pb_Thermohydraulique _QC	VDF	2	3 ⇒ 2974, 12344 & 50284 rect	5	Heat transfer calculations in an open cavity considering natural convection and temperature- dependent fluid properties	old format
Convection_kEps_QC	Pb_Thermohydraulique _Turbulent_QC	VEF	2	4752 rect 4752 tri	5	Thermohydraulic and turbulent flow in a heated square cavity Quasi Compressible fluid at low Mach	old format
Coupled_plane_channel_VEF	Pb_Thermohydraulique _Turbulent_QC	VEF	3	Fluid: 2598 tetra Solid: 5355 tetra	1	Simulation of a 3D VEF plane chanel in quasi-compressible thermohydraulics coupled to a solid with power output	old format excl_nr
INEEL_VDF_QC_1D_2D	Pb_Thermohydraulique _QC	VDF	3	400 & 6400 hexa	3	Laminar flow in a heated pipe with a volumetric power in a rectangular cavity	old format
INEEL_VEF_QC	Pb_Thermohydraulique _QC	VDF	3	6400 hexa 19200 tetra	8	Laminar flow heated either with a volumetric power or a wall heat flux Analytical valid. with INEEL exp	old format
NoFlow-lami-espece	Pb_Thermohydraulique _Especes_QC	VDF	3	4000 hexa 24000 tetra	2	Mixing of species without chemical reactions	new format
laminar_flow_vertical_plate	Pb_Thermohydraulique _QC	VEF	3	4800 hexa 3 ⇒ 9600 to 19200	27	Free and mixed convection along a vertical hot plate	old format

PDF File name	Problem	Dis.	Dim.	Mesh	Nb jdds	Goal of the sheet	State
<b>Sensitivity Analysis</b>							
Sensitivity_analysis_for Pb_Thermohydraulique _Steady_Obstacle	Pb_Hydraulique_ sensibility	VEF	2	91829 triang.	1	<b>Sensitivity equation method</b> for the Navier-Stokes : Estimation of the variance	new format
Sensitivity_analysis_for Pb_Thermohydraulique _Vahl_Davis	Pb_Hydraulique_ sensibility	VEF	2	98635 triang.	5	<b>Sensitivity equation method</b> for the Navier-Stokes : applied on the benchmark problem of natural convection	new format
<b>Other applications</b>							
conduction_T_ oscillant	Pb_conduction	VEF	3	4 $\Rightarrow$ 576 to 129600 tetra	7	VEF calculation of Conduction in a wall through a rectangular box	old format